Western Graduate&PostdoctoralStudies

Western University
Scholarship@Western

Electronic Thesis and Dissertation Repository

6-8-2017 12:00 AM

Predictive Shutdown Systems for Nuclear Power Plants

Drew J. Rankin
The University of Western Ontario

Supervisor
Dr. Jin Jiang
The University of Western Ontario

Graduate Program in Electrical and Computer Engineering
A thesis submitted in partial fulfillment of the requirements for the degree in Doctor of Philosophy
© Drew J. Rankin 2017

Follow this and additional works at: https://ir.lib.uwo.ca/etd

Part of the Signal Processing Commons

Recommended Citation

Rankin, Drew J., "Predictive Shutdown Systems for Nuclear Power Plants" (2017). *Electronic Thesis and Dissertation Repository*. 4635.
https://ir.lib.uwo.ca/etd/4635

This Dissertation/Thesis is brought to you for free and open access by Scholarship@Western. It has been accepted for inclusion in Electronic Thesis and Dissertation Repository by an authorized administrator of Scholarship@Western. For more information, please contact wlswadmin@uwo.ca.

Abstract

This dissertation investigates the use of a Kalman filter (KF) to predict, within the shutdown system (SDS) of a nuclear power plant (NPP), whether a safety parameter measurement will reach a corresponding trip set-point (TSP). The proposed predictive SDS (PSDS) designs aim to initiate shutdown actions at a time which is earlier than conventional shutdown initiation. These early detections are, in turn, expected to improve safety and productivity margins within the NPP.

The KF-based point-PSDS design utilizes a linear time-varying (LTV) system model to predict mean safety parameter measurements for comparison against the TSP. The KF considers noise covariances that either have assumed predetermined values, or are estimated online using an adaptive limited memory filter (ALMF). The PSDS is enhanced to consider, by recursive least squares (RLS) estimation, conditions that are uncertain with respect to the assumed system model and noise properties. The result is a KF/RLS-based PSDS that compensates for prediction error by RLS-based estimation of deterministic disturbances to the system state and measurement. The PSDS is further enhanced to calculate confidence intervals for the predictions as a function of the propagated error covariance. This enhancement results in interval-PSDS designs that consider confidence in an impending condition by comparing predetermined confidence interval bounds against the TSP. Finally, an optimal-PSDS design is formulated to adapt the effective prediction, e.g. horizon or bias, by limiting and minimizing the probability of missed and false trip

occurrences respectively using hypothesis testing methods and optimal alarm theory. In this manner, the optimal-PSDS is made aware of the quality of past predictions.

The PSDS designs are compared, through simulation and experiment, against a conventional SDS in terms of response time or time-to-trip for the steam generator level low (SGLL) safety parameter under various conditions of uncertainty, e.g. parameter error or unmeasurable signals. MATLAB-based simulations demonstrate that the PSDS designs are able to reduce time-to-trip. The PSDS designs are then implemented within a Tricon v9 safety-PLC with a scan time that adheres to current nuclear industry regulations. The experimental results reveal that a reduced time-to-trip can be achieved for a real-world system with unknown system-model mismatch.

Keywords: prediction, Kalman filtering, uncertainty, optimal alarm, safety instrumented systems

This dissertation is dedicated to my beautiful wife Cara.

It is her love, support, encouragement, and understanding

that has made this research possible,

and that makes this life complete.

Acknowledgements

Thank you to my adviser Dr. Jin Jiang for ensuring that my doctoral studies were productive, stimulating, and relevant, yet challenging. This research would not have been possible without his continued support. I am very thankful for the freedom he has provided me in taking on this research. It has been an honour to be his student.

This research would not have been possible without the assistance of my valued colleagues in the Control, Instrumentation, and Electrical Systems (CIES) research group. Thank you to Dr. Xinhong Huang for helping me to develop both personally and professionally. Thank you also to Dr. Sungwhan Cho and Dr. Ataul Bari for sharing your experience and knowledge. My time here at Western was made more enjoyable in large part due to the colleagues turned friends that have become an important part of my life. Most importantly, Dr. Lingzhi Xia and Dr. Jianping Ma have provided me with insightful dialog and cultural experiences since the early days of my studies. They have also helped me to focus on the positive aspects of research life and to strive for excellence as well as completion. Thank you both. Thank you also to Dr. Jingke She, Dr. Hisham Mahmood, Michael Gverzdys, Dennis Michaelson, Andrew Moore, Elizabeth Tomaszewski, Mahmood Akkawi, Syed Ahmed Raza, and Kyle VanHoof for our many collaborative research endeavours and impromptu discussions at the door of our adjoined labs.

In regards to this dissertation, thank you to the members of my doctoral examination committee, Dr. Ilia Polushin, Dr. Vijay Parsa, Dr. Han-Ping Hong, and Dr. Jamie Coble, for taking the time to review my research and for providing insightful comments that

have helped to strengthen this work. In addition, I am grateful for the funding and equipment that have made this doctoral research possible. Specifically, financial support from the Natural Sciences and Engineering Research Council of Canada (NSERC) and the University Network of Excellence in Nuclear Engineering (UNENE) as well as equipment made available by Invensys/Schneider and Ontario Power Generation (OPG). I am also honoured to have received an Ontario Graduate Scholarship in Science and Technology (OGSST) and an NSERC Postgraduate Scholarship-Doctoral (PGS-D).

Many thanks must be given to those friends that have helped me throughout these many years of research. I am thankful to have a great group of friends that have provided me with all forms of social support as well as regular escapes from the confines of research, if only for moments at a time. You have each, in your own way, contributed to the success of this work. Thank you specifically to Michael Fallaise for being my right hand man and for challenging me to avoid complacency. Thank you also to the Pageau clan for letting me be a part of your family and for taking interest in all that I do.

Lastly, thank you to my family for their love and encouragement. Thank you to my parents Jan and Gary who encouraged me to be inquisitive, to love science and engineering, and to pursue a life filled with learning. Thank you to my brothers Aric and Bryce and their families for helping me to escape the madness that is doctoral research, to have fun, to take adventures, and to sing well into the evening. Thank you also to my Carson family for taking interest in my work and for never waning in your support of this endeavour. Most of all, thank you to my loving, supportive, encouraging, and patient wife Cara whose support throughout the course of my doctoral studies is appreciated beyond words. It is because of her that I have seen further.

Contents

Abstract **ii**

Dedication **iv**

Acknowledgements **v**

Table of Contents **vii**

List of Figures **xi**

List of Tables **xvii**

List of Algorithms **xviii**

List of Appendices **xix**

List of Abbreviations, Symbols, Nomenclature **xx**

Acronyms and Initialisms xx

Mathematical Notations xxi

Roman Symbols xxii

Greek Symbols xxv

1 Introduction **1**

1.1 Background and Motivation 4

1.2 Problem Statements, Objectives, and Scope 13

1.2.1 Shutdown system enhancement and reduction of time-to-trip . . . 14

1.2.2 Predictive shutdown concept 17

1.2.3 Prediction of abnormal conditions under uncertainty 19

1.2.4 Objectives 25

1.2.5 Scope 26

1.2.5.1 Methodology 27

1.2.5.2 Experimental verification 33
1.3 Contributions 35
1.4 Organization 37

2 Literature Review **39**
2.1 Time-series Prediction 40
2.1.1 Filtering and estimation 40
2.1.2 Kalman-filter-based prediction 50
2.1.3 Prediction under uncertainty 56
2.2 Safety Instrumented and Shutdown Systems 66
2.2.1 Regulations and standards 67
2.2.2 CANDU shutdown systems 69
2.2.3 Time-to-trip and shutdown system response time 75
2.2.4 Optimal alarms 78

3 Prediction under Uncertainty for Linear-Time-Varying Systems **81**
3.1 State-space Modelling, Prediction, and Uncertainty 84
3.2 Kalman-Filter-Based State Estimation 93
3.2.1 The Kalman filter 96
3.2.2 Related equations 101
3.2.3 Initial conditions, convergence, model selection, and bumpless transfer 104
3.3 Kalman-filter-based point-prediction 109
3.4 Confidence and prediction intervals 116
3.5 Kalman-filter-based measurement interval-prediction 123
3.6 Noise covariances and uncertainty 132
3.7 Monitoring for nonconvergence and divergence 147
3.8 Summary 150

4 Estimation of Disturbance Inputs for Prediction Error Compensation **152**
4.1 Least-Squares-based Estimation of Disturbance Inputs 156
4.1.1 Estimation and estimation error compensation 160
4.1.2 Prediction error compensation 171
4.2 Recursive Least Squares Formulation of Disturbance Estimation and Prediction Error Compensation 179
4.2.1 Disturbance to the measurement 181
4.2.2 Disturbance to the state 188

4.2.3 Disturbances to both the measurement and state 195
4.2.4 Resetting the disturbance and RLS covariance 200
4.2.5 Adaptive-limited-memory-filter-based noise covariance estimation 204
4.3 Summary 207

5 Predictive Shutdown and Assessment of Prediction Quality 209
5.1 A Conventional Shutdown System Design 214
5.2 Predictive Shutdown System Designs 217
5.2.1 Point-PSDS: point-predictive shutdown system 220
5.2.2 Interval-PSDS: interval-predictive shutdown system 223
5.3 Prediction Quality Assessment 228
5.3.1 Hypothesis testing 232
5.3.1.1 Innovation bound or Z test 237
5.3.1.2 Normalized innovations squared or chi-squared χ^2 test . 239
5.3.1.3 Innovation whiteness or autocovariance test 242
5.3.2 Optimal alarms 244
5.3.3 Optimal-PSDS: optimal predictive shutdown system 251
5.4 Summary 255

6 Experimental Setup 257
6.1 Physical System 263
6.2 The Scaled-Irving Model 266
6.3 Closed-loop Control 271
6.4 Operating Modes 273
6.5 Postulated Initiating Event 276
6.6 Shutdown Systems 278
6.6.1 Predictive shutdown, the Kalman filter, and point-prediction . . . 280
6.6.2 Noise covariances, stochastic uncertainty, and the adaptive limited memory filter 284
6.6.3 Disturbance inputs, deterministic uncertainty, and the recursive least squared filter 287
6.6.4 Point-, interval- and optimal-predictive shutdown system designs . 289
6.7 Summary 292

7 Results and Analysis 294
7.1 Simulation Results 295
7.1.1 Benchmark: Conventional shutdown 299

7.1.2 PSDS Case 1: Reduced-order multi-model 301
7.1.2.1 Case 1a: KF-based point-predictive shutdown 302
7.1.2.2 Case 1b: KF-based interval-predictive shutdown without ALMF 308
7.1.2.3 Case 1c: KF-based interval-predictive shutdown with ALMF 314
7.1.2.4 Case 1d: KF-based optimal-predictive shutdown 317
7.1.3 PSDS Case 2: Reduced-order multi-model with parameter error . 320
7.1.3.1 Case 2a: KF-based point-predictive shutdown 321
7.1.3.2 Case 2b: KF/RLS-based point-predictive shutdown . . . 324
7.1.3.3 Case 2c: KF/RLS-based interval-predictive shutdown . . 326
7.1.3.4 Case 2d: KF/RLS-based optimal-predictive shutdown . . 327
7.1.4 Summary 329
7.2 Experimental Results 332
7.2.1 Benchmark: Conventional shutdown 333
7.2.2 PSDS Case 1: Reduced-order multi-model with measured PIE . . 335
7.2.2.1 Case 1a: KF/RLS$_y$-based point-predictive shutdown . . 335
7.2.2.2 Case 1b: KF/RLS$_y$-based interval-predictive shutdown with ALMF 337
7.2.2.3 Case 1c: KF/RLS$_y$-based optimal-predictive shutdown . 339
7.2.3 PSDS Case 2: Reduced-order multi-model with unmeasured PIE . 340
7.2.3.1 Case 2a: KF/RLS$_y$-based point-predictive shutdown . . 341
7.2.3.2 Case 2b: KF/RLS$_y$-based interval-predictive shutdown with ALMF 343
7.2.3.3 Case 2c: KF/RLS$_y$-based optimal-predictive shutdown . 344
7.2.4 Summary 345

8 Conclusions and Recommendations **348**
8.1 Recommended future work 352

Bibliography **354**

Appendices **366**

Curriculum Vitae **367**

List of Figures

1.1 Operating conditions/modes, set-points/thresholds/limits, and conceptual events and system transients, trajectories, or paths of operation. 6
1.2 Improvement of a) conventional trip in terms of b) safety and c) productivity margins as a conceptual result of predictive trip. 9
1.3 Sample trip sequence and time-to-trip measure for SDS1 of the CANDU NPP. Unless stated otherwise, time-to-trip is the total amount of time of these time components. 10
1.4 The concept of predictive shutdown, or predictive trip, for a single safety parameter with a predictive trip occurring at time-step k. 18

2.1 The conventional SDS trip logic within the context of safety instrumented systems (SISs). 70
2.2 CANDU SDS1 safety parameters and related subsystems. 73

3.1 Combined state and measurement equations in (3.1) and (3.2) respectively. 86
3.2 Combined stochastic state and measurement equations in (3.9) and (3.10). 91
3.3 Connectivity between the system and a state observer, which may be KF-based, within the context of state estimation. 93
3.4 Combined *a posteriori* and *a priori* state estimation equations in (3.16) and (3.18) respectively; the angled arrow indicates an adaptive parameter, in this case $K[k]$. 98
3.5 Combined Kalman gain equation in (3.15) as well as the *a posteriori* and *a priori* state estimation equations in (3.17) and (3.19) respectively; ($\bullet$) indicates where the input variable is substituted within the equation of the corresponding block. 99
3.6 Connectivity between the system and the KF-based state estimation procedure of Algorithm 3.1. 100
3.7 The *a priori* state estimate equation in (3.18) under the assumption that the future model parameters and system inputs have the same values as for current time-step, k. 111

3.8 Connectivity between the system and the KF-based measurement prediction procedure of Algorithm 3.2. 112
3.9 Confidence intervals of significance levels $\alpha \approx 0.023$ and $\alpha = 0.159$ for the a) respective outer and inner bounds of a sequence of measurement errors, $\tilde{y}$, and corresponding b) one-tailed bound as well as, c) two-tailed bound including probability density function (PDF). 117
3.10 The *a priori* state error covariance equation in (3.19) under the assumption that the future model parameters and system inputs remain at the same values as for current time-step, k. 125
3.11 Connectivity between the KF-based measurement prediction as well as confidence interval calculation procedures of Algorithm 3.3. 126
3.12 Confidence interval of significance level $\underline{\alpha} = 0.0004$ and level of confidence equal to 99.96% for the a) bounds of a sequence of measurement errors, $\tilde{y}$, and corresponding b) two-tailed predictive decision problem including probability density function (PDF) and the value of the cumulative probability outside of the bounds. 129
3.13 Confidence interval of one-tailed significance level $\underline{\alpha} = 0.0002$ and level of confidence equal to 99.98% for the a) bounds of a sequence of measurement errors, $\tilde{y}$, and corresponding b) one-tailed lower bound, as well as c) one-tailed upper bound including probability density function (PDF) and values of the cumulative probability within and outside of the bounds. . . 130
3.14 Connectivity between KF-based state estimation and the error covariance procedures of Algorithm 3.5. 145

4.1 Disturbance estimation and prediction error compensation to complement the KF-based measurement prediction algorithms of Chapter 3. 154
4.2 Connectivity between KF-based measurement prediction and the measurement disturbance estimation and prediction error compensation procedure of Algorithm 4.1. 188
4.3 Connectivity between KF-based measurement prediction and the measurement disturbance estimation and prediction error compensation procedure of Algorithm 4.1. 194
4.4 Connectivity between KF-based measurement prediction and the measurement disturbance estimation procedure of Algorithm 4.1. 207

5.1 Modular modification of a) conventional SDS logic to include the following capabilities b) prediction quality assessment and alarm/trip optimization, c) safety parameter prediction, d) uncertainty or noise covariance estimation, and c) prediction error compensation, all within the context of safety instrumented systems (SISs). 211
5.2 Conventional shutdown system (SDS) in the context of safety instrumented systems (SISs). 214
5.3 KF/RLS-based point-predictive shutdown system (point-PSDS) in the context of safety instrumented systems (SISs) with the option for activating RLS or ALMF algorithms. 221
5.4 KF/RLS-based interval-predictive shutdown system (interval-PSDS) in the context of safety instrumented systems (SISs) with the option for activating RLS or ALMF algorithms. 224
5.5 IB or Z test statistics and critical values for unbiased prediction error as well as positive and negative biases that are introduced at time-step 250. 239
5.6 NIS or χ^2 test statistics and critical values for unbiased prediction error as well as positive and negative biases, and over and underestimated error covariances that are introduced at time-step 250. 242
5.7 Receiver operating characteristic (ROC) space. 245
5.8 Constrained region and optimal behaviour of the optimal alarm within the receiver operating characteristic (ROC) space. 250
5.9 KF/RLS-based optimal-predictive shutdown system (optimal-PSDS) in the context of safety instrumented systems (SISs) with the option for activating RLS or ALMF algorithms. 252

6.1 U-tube steam generator with admissible range, y_R. 258
6.2 The a) simulation and b) experimental platforms. 261
6.3 Functional diagram of the physical plate level system (PLS) in the a) nominal and b) compensated, or modified, form. 264
6.4 Open-loop response of the scaled-Irving model to a 10kg/s step increase in a) feedwater flow-rate, $\underline{q}_e$, and b) steam flow-rate, q_v. 269
6.5 Swell-based set-point function, steam generator level low (SGLL) trip set-point and level high (SGLH) alarm threshold. 273
6.6 Steam generator water level responses to power transients a) step-wise power increase (SWPI) from 5% to 40%, and b) power ramp down (PRD) from 30% to 5% initiated at 10s. 275

6.7 Steam generator water level response to an unanticipated step change in water level set-point at a power level of 30% with set-point made equal to 29.1% at 10s. This is the nontrip-SPD transient. 276

7.1 Benchmark: simulated conventional SGLL trip occurrences due to loss of feedwater flow PIE during a) SWPI and b) PRD power transients. 298
7.2 Benchmark: simulated conventional SGLL trip occurrences due to a disturbance in the water level set-point from a normal value of 62.24% to an anomalous value of 29.0%. 299
7.3 Benchmark: time-steps surrounding conventional SGLL trip occurrences plotted for a) SWPI as in Figure 7.1a), b) PRD as in Figure 7.1b), and c) trip-SPD as in Figure 7.2. 300
7.4 Case 1a: simulated KF-based point-predictive SGLL trip occurrences due to loss of feedwater flow PIE during a) SWPI and b) PRD power transients under multi-model matching conditions. 304
7.5 Case 1a: simulated KF-based point-predictive SGLL trip occurrences due to a disturbance in the water level set-point from a normal value of 62.24% to disturbed values of a) 29.0%, and b) 29.1% under multi-model matching conditions. 305
7.6 Case 1a: time-steps surrounding the simulated KF-based point-predictive SGLL trip occurrences for a) SWPI, b) PRD, c) trip-SPD, and d) nontrip-SPD under multi-model matching conditions. 306
7.7 Case 1a: KF-based point-predictions being propagated over the prediction window, $i = 0, \ldots, 3$, while approaching the SGLL trip occurrence during a) SWPI, b) PRD, and c) trip-SPD transients under multi-model matching conditions. 308
7.8 Case 1b: time-steps surrounding the simulated KF-based interval-predictive SGLL trip occurrences due to a loss of feedwater flow PIE during a) SWPI and b) PRD, c) trip-SPD, and d) nontrip-SPD transients under multi-model matching conditions without ALMF-based noise covariance estimation. 311
7.9 Case 1b: KF-based point-predictions being propagated over the prediction window, $i = 0, \ldots, 3$, while approaching the SGLL trip occurrence during a) SWPI, and b) PRD power transients under multi-model matching conditions without ALMF-based noise covariance estimation. 312

7.10 Case 1b: KF-based point-predictions being propagated over the prediction window, $i = 0, \ldots, 3$, while approaching the SGLL trip occurrence during an SWPI power transient with assumed state noise covariances of a) $\hat{R}_x = \text{diag}\,(0.1)$, and b) $\hat{R}_x = \text{diag}\,(3120.0)$. 313
7.11 Case 1c: simulation of KF-based interval-predictive SGLL trip occurrences due to a loss of feedwater flow PIE during a) SWPI, b) PRD, c) trip-SPD, and d) nontrip-SPD transients under multi-model matching conditions with ALMF-based noise covariance estimation. 315
7.12 Case 1c: examples of the KF-based interval-predictions iterating over the entire prediction time-interval, $i = 0, \ldots, 3$, while approaching the SGLL trip occurrence during a) SWPI and b) PRD power transients under multi-model matching conditions with ALMF-based noise covariance estimation. 316
7.13 Case 1d: simulation of KF-based optimal-predictive SGLL trip occurrences due to a loss of feedwater flow PIE during a) SWPI, b) PRD, c) trip-SPD, and d) nontrip-SPD transients under multi-model matching conditions. . 319
7.14 Case 2a: time-steps surrounding the simulated KF-based point-predictive SGLL trip occurrences for a) SWPI, b) PRD, c) trip-SPD, and d) nontrip-SPD under the model parameter error condition. 322
7.15 Case 2a: time-steps surrounding the simulated KF-based point-predictive SGLL trip occurrences for a) SWPI and c) trip-SPD under the model parameter error condition with only ALMF-based state noise covariance estimation and constant measurement noise covariance, $\hat{R}_y = 6.24$. 323
7.16 Case 2b: time-steps surrounding the simulated KF/RLS-based point-predictive SGLL trip occurrences for a) SWPI and b) PRD under the model parameter error condition. 324
7.17 Case 2b: simulated KF/RLS-based point-predictive SGLL missed-trip occurrence during the trip-SPD transient under the model parameter error condition. 325
7.18 Case 2c: time-steps surrounding the simulated KF/RLS-based interval-predictive SGLL trip occurrences for a) SWPI and b) PRD under the model parameter error condition. 326
7.19 Case 2d: time-steps surrounding the simulated KF/RLS-based optimal-predictive SGLL trip occurrences for a) SWPI, b) PRD, and, c) trip-SPD under the model parameter error condition. 327

7.20 Case 2d: time-steps surrounding the simulated KF/RLS-based optimal-predictive SGLL trip occurrences for a) SWPI, b) PRD, and, c) trip-SPD under the model parameter error condition. 329
7.21 Benchmark: experimental conventional SGLL trip occurrences due to loss of feedwater flow PIE during a) SWPI and b) PRD power transients. . . 334
7.22 Case 1a: experimental point-predictive trip due to SGLL during power transients a) SWPI and b) PRD under model mismatch. 337
7.23 Case 1b: interval-predictive trip due to SGLL during power transients a) SWPI and b) PRD under model mismatch. 338
7.24 Case 1c: optimal-predictive trip due to SGLL during power transients a) SWPI and b) PRD under model mismatch. 340
7.25 Case 1c: interval-predictive trip due to SGLL during power transients a) SWPI and b) PRD under model mismatch. 341
7.26 Case 2a: point-predictive trip due to SGLL during power transients a) SWPI and b) PRD under model mismatch and unmeasured initiating event. 342
7.27 Case 2b: interval-predictive trip due to SGLL during power transients a) SWPI and b) PRD under model mismatch and unmeasured initiating event. 344
7.28 Case 2c: optimal-predictive trip due to SGLL during power transients a) SWPI and b) PRD under some model mismatch and unmeasured initiating event. 345

List of Tables

5.1 Error matrix. 233
5.2 Condition table for combination IB and NIS tests. 243

6.1 Irving model parameters, steam flow-rates as well as control intervals, and controller gains at specific power levels. 267
6.2 Control intervals, and controller gains for the discretized controller within power level operating ranges. 272
6.3 State noise covariance estimates for use without ALMF. 286

7.1 Summary of the PSDS methods that are investigated within each simulation case. * indicates both with and without the ALMF 297
7.2 Power level selection by steam flow-rate to determine the active scaled-Irving parameters within the KF of the PSDS. 302
7.3 Summary of simulation time-to-trip, k_c or k_p, and effective prediction horizon, N_{p_e}, results.
* - a false trip occurs for nontrip-SPD 330
7.4 Summary of experimental time-to-trip and effective prediction horizon results. 346

List of Algorithms

3.1 Kalman-filter-based (KF) state estimation, KF_e. 100
3.2 Kalman-filter-based (KF) state and measurement point-prediction, KF_p, under the assumption that the future model parameters and system inputs remain at the same values as for current time-step, k. 113
3.3 Kalman-filter-based (KF) measurement interval-prediction, KF_{ip}, under the assumption that the future model parameters and system inputs have the same values as for the current time-step, k. 127
3.4 Adaptive-limited-memory-filter-based (ALMF) measurement $ALMF_y$ and state $ALMF_x$ noise covariance estimation 143
3.5 Initialization of the noise covariance estimation subroutines using adaptive limited memory filter (ALMF) 144
3.6 ALMF/KF-based state estimation 146
4.1 Update and predict stages of the recursive least squares (RLS) measurement disturbance input estimation and prediction error compensation procedure, $RLS_{y,ip}$. 187
4.2 Update and predict stages of the recursive least squares (RLS) state disturbance input estimation and prediction error compensation procedure $RLS_{x,ip}$. 193
4.3 RLS/KF-based measurement interval-prediction with combined measurement and state disturbance input estimation and prediction error compensation where the measurement disturbance is considered primary. 201
4.4 RLS/KF-based measurement interval-prediction with ALMF noise covariance estimation, dual combined measurement and state disturbance input estimation and prediction error compensation where the measurement disturbance is considered primary 205

List of Appendices

Appendix A: Copyright permissions 366

List of Abbreviations, Symbols, Nomenclature

Acronyms and Initialisms

2oo3	Two out of three	72
ALMF	Adaptive limited memory filter	28
AOO	Anticipated operational occurrence	5
BDBA	Beyond design basis accident	6
CANDU	Canadian Deuterium Uranium	10
CDF	Cumulative distribution function	116
CNSC	Canadian Nuclear Safety Commission	70
CP-1	Chicago Pile number 1	4
CPU	Central processing unit	8
DBA	Design basis accident	6
DCS	Distributed control system	7
EKF	Extended Kalman filter	44
EnKF	Ensemble Kalman filter	46
EPS	Emergency protection system	4
FNR	False negative rate	33
FPGA	Field programmable gate array	8
FPR	False positive rate	33
IAEA	International Atomic Energy Agency	4
IB	Innovation bound	32
IEC	International Electrotechnical Commission	67
IW	Innovation whiteness	32
KF	Kalman filter	11
LOCA	Loss of coolant accident	34
LPV	Linear parameter varying	86

LS	Least squares	11
LSSS	Limiting safety system setting	7
LTI	Linear time-invariant	28
LTV	Linear-time-varying	28
μC	Micro-controller	265
MPC	Model predictive control	20
MWe	Megawatts electric	2
NIS	Normalized innovations squared	32
NPP	Nuclear power plant	1
NPV	Negative preditive value	234
OPG	Ontario Power Generation	279
OPL	Operations per loop	98
PI	Proportional integral	260
PIE	Postulated initiating event	5
PLC	Programmable logic controller	7
PLS	Plate level system	260
PDF	Probability density function	116
PSDS	Predictive shutdown system	11
RLS	Recursive least squares	22
ROC	Receiver operating characteristic	78
RPS	Reactor protection system	4
RRS	Reactor regulating system	15
RTS	Reactor trip system	4
SCRAM	Safety control rod axe man	4
SDS	Shutdown system	4
SDS1	Shutdown system number one	10
SGLL	Steam generator level low	34
SIF	Safety instrumented function	67
SIS	Safety instrumented system	3
SPD	Set-point disturbance	274
SVD	Singular value decomposition	119
TPR	True positive rate	33
TSP	Trip set-point	7
UKF	Unscented Kalman filter	45
US-NRC	United States Nuclear Regulatory Commission	4
V&V	Verification and validation	75

Mathematical Notations

$\bullet$	Symbol placeholder; represents any symbol that satisfies the accompanying context, or; the placement of an input variable within the block of a block diagram 99
$\triangleq$	Defined to be equal to 86
$\|$	A value or event that is conditional given the occurrance of the respective time-step or event that is to the right of the operator 95
$\in$	Belongs to, or is within the set of 85
q^{-1}	Backward time-shift, or delay, operator; operates on an element of a time-series to produce the previous element within the time-series 85
$\Pr(\bullet)$	Probability of a specified event occurring 117
$S(\bullet)$	LS objective function 160
$\text{diag}(\bullet)$	A matrix of diagonal elements equal to $\bullet$ and off-diagonal elements equal to zero 310
$\text{erf}^{-1}(\bullet)$	Inverse Gaussian error function 120
$E\{\bullet\}$	Expectation of a signal/sequence of samples 94
$\bullet[k]$	Primary representation of time-dependency 85
$\bar{\bullet}$	The true value of a parameter or signal, vector, or matrix that is the exact representation of the actual system 93
$\hat{\bullet}$	Estimate or approximation of a vector 89
$\bullet_k$	Alternative representation of time-dependency 100
$\bullet^{n\times n}$	An n by n vector/matrix of $\bullet$ elements 105
$\bullet'$	The transpose of a matrix, or vector 94
$(\bullet)^{\underline{2}}$	Square of a value, vector, or matrix, calculated as $(\bullet)^{\underline{2}} = (\bullet)(\bullet)'$ 105
$\tilde{\bullet}$	Error between the estimated and true values of a vector or matrix 95
$\underline{\bullet}$	Symbol modifier that indicates an alternate interpretation of a variable 105
$\bullet_w$	A vector/matrix that is associated with the least squares estimation of prediction error 157

Roman Symbols

$\underline{A}_x$	Combined KF update and propagation matrices for additive disturbance to state equation 167
$\underline{A}_y$	Combined KF update and propagation matrices for additive disturbance to measurement equation 161
$\arg\min_{\bullet}$	Determines the value of $\bullet$ at which a given function attains a minimum

	value 162
A, B, C, D	State, input-to-state, state-to-measurement, and feed-through matrices; together referred to as the system matrices 85
F_e, F_v	Digital filters for open-loop compensation of the feedwater and steam flow-rate signals 265
FN	False negative 232
FP	False positive 232
τ_1, τ_2	Irving steam generator model parameters 267
G_1, G_2, G_3	Irving steam generator model gain parameters 267
$h^{y,\bullet}$	Half-width of measurement confidence interval for corresponding significance level $\bullet$ 125
H_0	Null hypothesis 232
H_1	Alternate hypothesis 232
H_{PLS}	Continuous time transfer function of the nominal plate level system 268
$\mathbb{I}$	Identity matrix of appropriate dimension 97
$j_\bullet$	Indices of time-steps within a sequence, window, range of time-steps; usually within a series summation or product 88
$\mathcal{K}$	RLS gain matrix 180
KF_e	Standard Kalman filter (KF) state estimation algorithm 105
KF_e	Standard Kalman filter (KF) state estimation algorithm 101
KF_{ip}	Kalman filter (KF) measurement interval-prediction algorithm 126
KF_p	Kalman filter (KF) measurement point-prediction algorithm 112
K	Kalman gain matrix 96
k	Current time-step; number of time-steps that have passed since the onset of the simulation or experiment, t/T_s 17
K_f, K_m	Frequency and magnitude scaling parameters for the scaled-Irving steam generator model 267
K_{CO}	Common gain for the level error within the three element proportional integral controller 272
K_C	Common gain within the three element proportional integral controller 272
k_c	Time-step of conventional trip 17
k_d	Time-step of detecting an abnormal condition 297
k_e	Time-step of initiating the postulated initiating event (PIE) 297
K_{IO}	Interval gain for the level error within the three element proportional integral controller 272

K_I	Interval gain within the proportional integral controller 272
k_p	Time-step of predictive trip 17
N	Positive integer representing a number of time-steps 17
n	Dimension of a matrix/vector 85
$N_{\mathcal{O}}$	Length of window over which detectability or observability is calculated 89
N_p	Length of window over which predictions are calculated 17
N_p	Length of window over which predictions are calculated 297
N_v	Length of window over which state error covariances are calculated . 139
$\mathcal{O}$	Observability matrix 89
O	Big O notation for computational complexity 101
$\mathscr{P}$	Covariance of the RLS disturbance estimate 181
$P_{\bullet_1,\bullet_2}$	Cross-covariance between the signals included in the subscript 165
$P_{\bullet}$	Covariance of the signal included in subscript 95
$\underline{Q}_e, Q_v$	Steam generator feedwater and steam flow-rates within the s-domain 267
q_e, q_v	Feedwater and steam flow-rate signals 266
$\mathbb{R}^{n\times n}$	An n by n matrix/vector of real-valued elements 85
$\mathscr{R}$	Steam generator water level set-point within the s-domain 271
r	Steam generator water level set-point 273
r_x	Initial state covariance scaling parameter within the Kalman filter .. 107
R_x, R_y	State and measurement noise covariance matrices 93
$RLS_{x,ip}$	Recursive least squares (RLS) state disturbance input estimation ... 194
$RLS_{y,ip}$	Recursive least squares (RLS) measurement disturbance input estimation 188
s	Complex laplace variable and frequency parameter 267
Θ	Precentage reactor power level 268
Υ	Irving steam generator model parameter 267
t	Relative time; the amount of time that has passed since the onset of the simulation or experiment 85
T_{CI}	Control interval within the process controller 271
T_s	Sampling interval; the amount of time between the samples at subsequent discrete time-steps within the process controller as well as the shutdown system 17
TN	True negative 233
TP	True positive 232
v_u	Input noise vector/signal 90

v_x, v_y State and measurement noise vectors/signals 90

$w_{x,\bullet}, w_{y,\bullet}$ Disturbance inputs to the individual components of the state and measurement disturbance models 158

w_x, w_y State and measurement disturbance inputs 157

x, y, u System state, system measurement, and system input signals 85

x_R Magnitude of the admissible range with the domain of the state 106

$\hat{y}^{u,\underline{\alpha}}, \hat{y}^{l,\underline{\alpha}}$ Upper and lower limits of significance level $\underline{\alpha}$ 120

Y Steam generator water level within the s-domain 267

y_{sim}, y_{exp} Simulated and experimental water levels, when included in the same plot 274

y_R Admissible range within the assumed Irving steam generator model 258

$y_{R,\text{PLS}}$ Admissible range within the plate level system 268

$\mathbb{Z}^{n\times n}$ An n by n matrix/vector of integer-valued elements 85

$z_\bullet$ Statistical score associated with a specified significance level 117

Greek Symbols

α One-sided significance level 116

$\underline{\alpha}$ Two-sided significance level 118

$\Gamma_{x,\bullet}, \Gamma_{y,\bullet}$ Equivalent state matrices for the individual components of the state and measurement disturbance profiles 158

$\gamma_{x,\bullet}, \gamma_{y,\bullet}$ Individual components of the state and measurement disturbance profiles 158

Γ_x, Γ_y Dynamic profiles of the state and measurement disturbances 157

$\underline{\Gamma}_{x,\bullet}, \underline{\Gamma}_{y,\bullet}$ Equivalent state-to-measurement matrices for the individual components of the state and measurement disturbance profiles 158

Λ_x Matrix of forgetting factors for least squares estimation of an additive state disturbance 169

λ_x Scalar forgetting factor for least squares estimation of an additive state disturbance 169

Λ_y Matrix of forgetting factors for least squares estimation of an additive measurement disturbance 163

λ_y Scalar forgetting factor for least squares estimation of an additive measurement disturbance 163

$\underline{\lambda}_\bullet$ Scalar forgetting factor for each time-step within the least squares estimation of an additive state disturbance 168

ψ_x Pseudo cumulative effect of state disturbance profile, Γ_x, on measurement

	estimate 189
ψ_y	Pseudo cumulative effect of measurement disturbance profile, Γ_y, on measurement estimate 182
ρ_x, ρ_y	Effect of state and measurement disturbances on measuremnt estimate 160
$\underline{\rho}_x$	Cumulative effect of state disturbance model, Γ_x, on measurement estimate 167
$\underline{\rho}_y$	Cumulative effect of measurement disturbance model, Γ_y, on measurement estimate 161
$\underline{\underline{\rho}}_x$	Cumulative effect of state disturbance model, Γ_x, on state estimate . 167
$\sigma_\bullet$	Standard deviation of $\bullet$ 107
Θ	Switching function for the alternating disturbance estimation procedure 203
θ	Parameter vector 86
ξ	Conventional trip signal that contains a set of high and low trip signals, ξ_h and ξ_l 215
ξ_p	Predictive trip signal that contains a set of high and low predictive trip signals, $\xi_{p,h}$ and $\xi_{p,l}$ 221
Ξ_c, Ξ_p	Effective conventional and predictive trip set-point 18
Ξ_l	Steam generator level low trip set-point 273
ζ	An arbitrary matrix 105

Chapter 1

Introduction

In general, an unsafe system has the potential for an uncontrolled release of large amounts of energy. In contrast, a safely operating nuclear power plant (NPP) releases energy in a controlled manner. Within an NPP, nuclear energy is first converted into thermal energy within the reactor core by means of fissile material undergoing fission reactions. All NPP designs utilize nuclear energy to produce electrical power. Within pressurized water reactor and pressurized heavy water reactor NPP designs, the thermal energy is transferred between the coolants of one or more subsequent heat transport loops to a subsystem known as the steam generator or boiler. As thermal energy accumulates in the secondary-side coolant of the steam generator, the coolant boils and the resulting steam is piped out of the top of the steam generator. For electrical power generation, and within all NPPs, the net positive kinetic energy of some flowing material is then made to rotate a set of turbines that are affixed to the rotor of an electrical generator. This rotation results in the kinetic energy being converted into electrical energy. Finally, electrical power is output from the generator to a switch-yard where a small portion of the total power is returned to the station as auxiliary power and the remainder is made available to the grid for transmission,

distribution, and consumption.

The thermodynamic efficiency of the a nuclear power generating system increases in proportion to the nominal operating thermal power of the reactor core. This nominal amount of thermal power, in turn, determines the amount of electrical power that is output by the electrical generator. Thus, in order to improve thermodynamic efficiency, the electrical power output of a single NPP unit is usually rather large, ranging from hundreds to thousands of megawatts electric (MWe). Large amounts of energy therefore flow between, and are stored throughout, the subsystems of an NPP. These large amounts of energy increase the potential for accidents involving uncontrolled releases of energy to occur. In addition, NPPs utilize a radioactive primary fuel source that, if affected, may significantly increase the severity of such accidents. NPP designs therefore undergo continual enhancement to include measures that aid in preventing and mitigating the consequences of severe accidents, i.e. accidents that involve significant core degradation. These enhanced measures aim to protect workers, the public, and the environment from the harmful effects of the ionizing radiation that is produced as a result of fission reactions and is to be contained during a severe accident [1]. The development of these enhanced measures is essential in reducing the likelihood of future severe accidents like those that have occurred at Three Mile Island NPP Unit 2 in 1979, Chernobyl NPP Unit 4 in 1986, and Fukushima Daiichi NPP Units 1, 2, 3, and 4 in 2011.

In line with the concepts of prevention, mitigation, and protection, this dissertation aims to enhance the decision-making mechanism or logic solver within a shutdown type of NPP automatic protection system by including the capability of predicting an impending abnormal condition. This enhancement presents a paradigm shift from the like-for-like

functional replacements that have historically been performed when replacing existing protection systems with modern computer-based technologies. The predictive shutdown methods of this dissertation take advantage of increases in computational power and advanced functional capabilities that are common to modern industrial computerized technologies. These methods are, at the same time, constrained by the capabilities of these technologies when compared against cutting edge computer processors and supercomputers.

In achieving the above aim, it is expected that abnormal conditions will be predicted at a time which is earlier than conventional shutdown detection. This early detection is essentially a reduction in the amount of time between a trip inducing fault, failure, or initiating event and the activation of sufficient protective actions within the reactor core. It is expected that this reduction in time will, in turn, result in increased margins of safety between peak surges in energy, inventory, pressure, temperature, and flow, and the physical limits of the subsystems and components within the NPP. Moreover, these increased margins of safety are also expected to reduce the likelihood of the NPP dynamics reaching unsafe, or accident conditions. The predictive decision-making methods developed herein are also not limited to shutdown applications or the NPP systems. These methods may therefore be applied within the logic solvers of a safety instrumented system (SIS) for a variety of generic applications in order to make early decisions regarding impending safety-related conditions.

The remainder of this chapter is organized as follows. Section 1.1 introduces industry specific terminology, establishes context regarding the enhancement of NPP automatic protection systems, and provides a brief introduction to the prediction methods. Section 1.1 also presents the rationale for enhancing automatic protection systems in order to

reduce protection system response time and to achieve earlier activations of the related safety function. Section 1.2 elaborates on the two high-level problems that are investigated within this dissertation, conceptualizes a predictive shutdown sequence, and segments the two problems into a list of objectives. Section 1.2 also states the scope of this research, including high level limitations and assumptions. Section 1.3 describes the main theoretical and practical contributions, and deliverables that are the result of this study. Finally, the organization of this dissertation is outlined in Section 1.4.

1.1 Background and Motivation

According to the United States Nuclear Regulatory Commission (US-NRC), shutdown is a decrease in the rate of fission and heat or thermal energy production within a reactor [2]. Shutdown may also be referred to as: trip, i.e. the activation of a mechanism, or safety control rod axe man (SCRAM)[1], as used during the first controlled release of energy by nuclear fission at Chicago Pile number 1 (CP-1) [5,6]. The components within an NPP that are responsible for shutdown are commonly referred to as a shutdown system (SDS) while reactor protection system (RPS), reactor trip system (RTS), and emergency protection system (EPS) may also be used [7, 8].

The International Atomic Energy Agency (IAEA) categorizes SDSs within a sub-category of safety systems known as protection systems. According to the IAEA, a protection system *"encompasses all electrical and mechanical devices and circuitry, from and including the sensors up to the input terminals of the safety actuation systems and the*

[1]the exact terms used within the scram acronym are often contested [3, 4]

safety system support features, involved in generating the signals associated with the protective tasks" [9]. Further, the IAEA states that the purpose of a protection system within an NPP is to *"monitor the operation of a reactor and which, on sensing an abnormal condition, automatically initiate actions to prevent unsafe conditions"* [10]. An SDS is therefore a collection of electrical and mechanical devices and circuitry that monitor the operation of a reactor as well as supporting subsystems and, upon sensing an abnormal condition, automatically initiates actions to decrease the rate of fission and heat or thermal energy production within the reactor core. Each subsystem is referred to individually as a system being protected when it is necessary to discern the system that is being protected from an otherwise unprotected system.

The subsystems of an NPP operate within one of many different operating modes or conditions; normal, abnormal, unsafe, and emergency or accident. These conditions are illustrated in Figure 1.1 along with the thresholds that are the boundaries or limits between the conditions. This conceptual illustration includes conditions that are two-dimensional, y_1 and y_2, although the conditions may also be single dimensional or have greater than two dimensions.

The operation of the various systems may follow any of the numbered paths or transients as provided in Figure 1.1. For example, the system may deviate from (1) an anticipated operational occurrence (AOO) as the result of a postulated initiating event (PIE) and approach abnormal (2) and then unsafe (5) conditions. PIEs are those events are are anticipated to cause a safety parameter to operate outside of the normal operating conditions. Alternatively, a trip occurrence activates a safety function in order to prevent the system from reaching unsafe conditions (3). The system may then be returned to a normal oper-

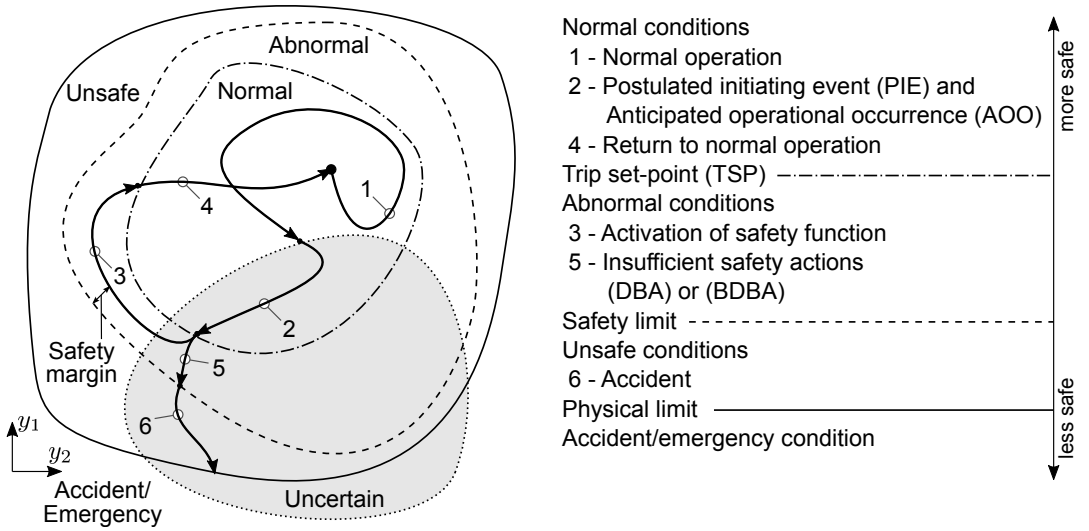

Figure 1.1: Operating conditions/modes, set-points/thresholds/limits, and conceptual events and system transients, trajectories, or paths of operation.

ating condition, and possibly the original operating point by means of start-up procedures (4). It is therefore assumed, that a system operating beyond normal conditions will not recover from the abnormal conditions without some form of safety action being performed.

The system may also exhibit unanticipated behaviours while operating under any on the conditions as is indicated by the uncertain region of Figure 1.1.In Figure 1.1, the numbered paths do not correspond with the uncertain condition. It is convenient to consider, however, that a PIE causes the system behaviour to become uncertain as illustrated in Figure 1.1. Moreover, paths (5) and (6) may correspond with either a design basis accident (DBA) or a beyond design basis accident (BDBA) within the nuclear industry. These are postulated accidents which have respectively been considered and are beyond consideration during the design of the NPP according to established design criteria [10].

The first shutdown type of nuclear-related automatic protection system was that of CP-1. This first protection system was responsible for releasing neutron absorbing rods when signals from ion chambers, a type of sensor to measure nuclear fission reactions,

exceeded a predetermined trip set-point (TSP) which may also be referred to as a limiting safety system setting (LSSS) [11]. Upon release, the shut-off rods were pulled into the reactor pile by a 100lbs weight. The instrumentation for this and other early SDSs was composed of simple amplifier circuits made up of triodes, diodes, and resistors, as well as magnetic amplifiers and electro-mechanical relays. In addition, the TSPs for these SDSs were calibrated to release safety actuators at predetermined values corresponding to physical properties of the actuating devices, e.g. current to an electromagnet or position of a solenoid catch mechanism [12]. More generally, the TSPs are the thresholds against which safety parameters are compared within a protection system in order to detect abnormal conditions. The TSP is therefore the boundary between normal and abnormal conditions of Figure 1.1.

Since the days of CP-1, SDS instrumentation has undergone various functional and technological enhancements. Although the main functionality of SDSs remains as it was in CP-1, SDSs now include coincidence voting, hysteresis, and seal-in logic, as well as TSPs that may vary as a function of major system parameters. These enhancements have resulted in the rewriting of standards, regulations, and best practices, e.g. the extensive review of software by formal methods [13]. Further, many safety concepts, including defence in depth, diversity, redundancy, and other best-practices are now formally defined in a vast number of safety reports and guides [14, 15]. Technologically, SDSs have evolved from a basic electrical, electro-mechanical, direct wired, analog signal form through an electronic, solid-state form, to in some cases, an electronically programmable, fully computerized, digital form within a safety-rated distributed control system (DCS) or programmable logic controller (PLC). Moreover, within the last decade there has been growing interest in replacing the

software and central processing unit (CPU) of these fully computerized SDSs with an electronically programmable hardware implementation known as a field programmable gate array (FPGA) [16, 17, 18].

Given proper safety and hazard analysis and selection of protective actions, enhancements to protection systems are primarily concerned with: true and spurious trip; safety variables, sensors, and TSPs; response time; environmental and power conditions; and system reliability [19]. In fact, these design bases are the safety principles for automatic protection system development and, in some cases, are a means of measuring system performance, i.e. response time, reliability, independence, availability, simplicity, and conformance to environmental, power, and various other conditions [14, 20].

In general, protection system enhancements aim to improve either safety or productivity and to maintain a balance between the two. For example, TSPs can be improved by considering beyond design basis events [21]. In fact, it is common for nuclear utilities to develop enhancements that reduce margins of uncertainty while maintaining or improving margins of safety in order to utilize excess electrical generating capacity that was previously unavailable [22]. For example, an increase in safety sensor accuracy may allow for an increase in a TSP and subsequent increases in the nominal operating power of the reactor as well as the electrical power generated by the NPP. The end result is a balanced increase in safety and productivity, or alternatively, an increase in production while maintaining safety margins. These two competing results are compared in Figure 1.2 for conventional and conceptual predictive trip occurrences. The predictive trip of Figure 1.2 results in an effective TSP that is a time-varying value or threshold equal to the safety parameter measurement at the time the trip action is initiated. This effective TSP varies with the

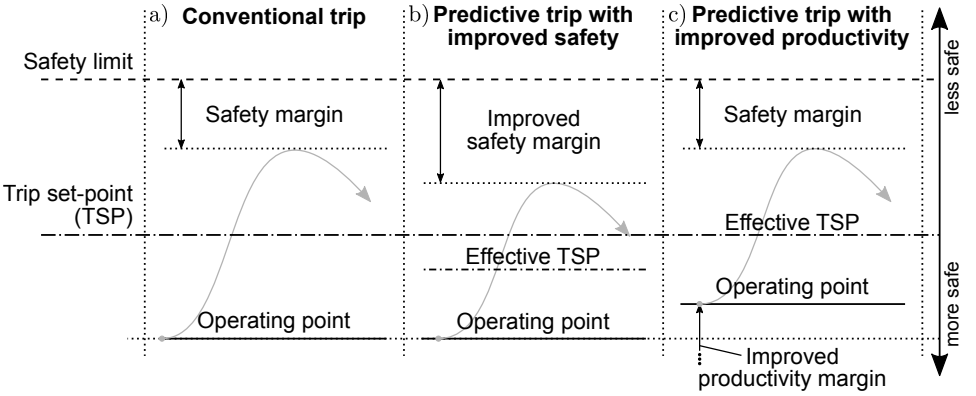

Figure 1.2: Improvement of a) conventional trip in terms of b) safety and c) productivity margins as a conceptual result of predictive trip.

quality of the predictions as well as the length of the forecast window or prediction horizon.

The nuclear power generating industry is very conservative with respect to the conceptual modified operations of Figure 1.2 where rigorous analyses of any and all modifications to protection systems are required to ensure identification and mitigation of any possible negative impacts on safety [22]. For example, delaying the response time of the SDS may result in a reduction in the number of spurious protective actions, otherwise known as spurious or false trips. Reductions in spurious trips, in turn, increase the availability of the NPP unit to generate electrical power. In this inadvisable example, the NPP has improved production, or capacity factor, at the cost of reducing margins of safety since the delayed SDS activation results the peak response of the safety parameter transients being closer to the established safety limits; see (3) in Figure 1.1.

As previously stated, this dissertation aims to improve safety by detecting abnormal conditions at a time that is earlier than is possible when using conventional SDSs. More specifically, this research aims to reduce the amount of time between the occurrence of

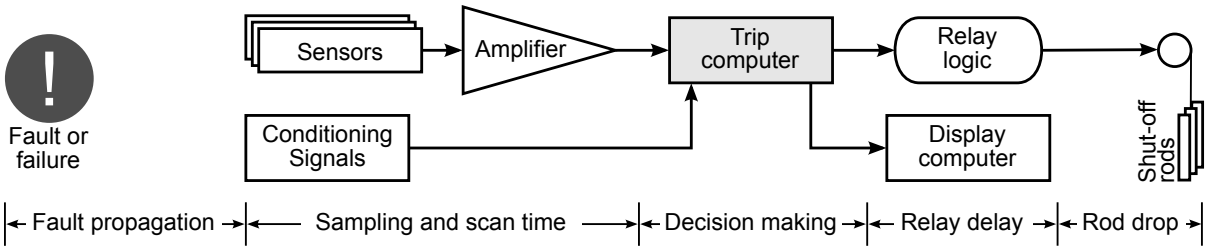

Figure 1.3: Sample trip sequence and time-to-trip measure for SDS1 of the CANDU NPP. Unless stated otherwise, time-to-trip is the total amount of time of these time components.

a trip inducing fault or failure and the insertion of sufficient negative reactivity into the reactor core without causing a reduction in the margins of safety. This amount of time is also referred to as time-to-trip, and includes the response time of the trip computer or logic solver within the SDS. A sample trip sequence and time-to-trip measure are provided in Figure 1.3 for the Canadian Deuterium Uranium (CANDU) shutdown system number one (SDS1) design. The proposed SDS modifications, and more specifically the early detections, are expected to provide the advantage of reducing the maximum values of the peak surges in the parameters of the safety related subsystems as illustrated in Figure 1.2.

In terms of time-to-trip, conventional SDSs have the fundamental limit of, at best, initiating the insertion of negative reactivity into the reactor core at the instant a safety parameter reaches a TSP. Moreover, conventional SDSs are increasingly being implemented within trip computers that are modern industrial computers, programmable electronic systems, safety DCSs, PLCs, and even FPGAs. These modern platforms, however, are generally underutilized in terms of computational power due to the relatively simple functionality required by protection systems when compared against advanced control system algorithms. This research therefore overcomes the fundamental limit of conventional shutdown by predicting the future behaviour of the monitored subsystems and associated safety parameter

values and making anticipatory, or predictive trip decisions, i.e. a predictive shutdown system (PSDS).

Prediction and forecasting dates back to over two millennia ago with the rudimentary prediction of celestial body movements and a growing interest in the field of astronomy [23]. The mathematical methods that form the foundation of optimal prediction were not established, however, until 1632 when Galileo investigated the minimization of various functions of error to help explain his experimental celestial observations [24]. Another century and a half would pass before the first complete theory of linear estimation, known as the method of least squares (LS), was formulated by Gauss in 1795. This achievement in forecasting also centred around the study of celestial body movements, as reported and independently formulated by Legendre in 1805 [24,25,26]. More recently, modern predictive algorithms incorporate system models and also account for uncertainty in the model and signals. For example, the stochastic state-space model assumed within the Kalman filter (KF) published by Kalman in 1960 [27]. Nowadays, prediction algorithms have even been used within NPP controls systems [28].

In utilizing a prediction algorithm for shutdown, it is expected that a PSDS will be able to initiate shutdown actions at the instant a fault, failure, or initiating event is predicted to result in an abnormal condition. At this limit, anticipatory or predictive shutdown is conceptually similar to fault detection [29], a field which has numerous applications within NPP systems [30,31]. Moreover, given the well-established literature regarding prediction of dynamical systems as well as the availability of capable industrial computer technologies, it seems natural to investigate the development of a predictive automatic protection system. It is expected that the predictive protection system will be able to make confident, high

quality decisions at a time which is earlier than the conventional case without reducing margins of safety or productivity. It is further expected that these algorithms can be implemented within modern safety-critical industrial computer platforms given limited processing and memory resources.

In addition to reducing time-to-trip, the proposed SDS modifications deviate from the historical practice of like-for-like functional transfer of SDS logic from existing to newly commissioned technologies by developing, in an evolutionary manner, an advanced safety-critical decision-making algorithm. Within the nuclear industry, plant life extensions and related refurbishments have resulted in the replacement of antiquated and obsolescent industrial computers, programmable digital comparators, analog circuitry, and relay logic with modern industrial computer technologies [8,32,33]. These platforms are capable of executing advanced functional, mathematical, and logical capabilities that enable a broader set of decision-making algorithms to be implemented. Moreover, these algorithms include well-established filtering and modelling methods that allow for control and protection systems to consider a larger set of prior knowledge regarding the system being controlled or protected. For example, the automotive industry has recently developed and implemented collision avoidance systems and automatic predictive braking within a variety of automobiles [34].

Finally, this work considers the consequences of implementing advanced decision-making algorithms within safety-critical industrial computers. For example, a given algorithm may require additional execution time that may result in delayed decisions. The advanced algorithms investigated herein are therefore designed to anticipate, or predict, impending conditions. Forecasting and prediction does, however, introduce a new form of uncertainty

within the safety-critical shutdown task. Thus, in predicting the future behaviour of a system being protected, the effects of uncertainty and the complexity of the prediction algorithm on SDS performance, e.g. spurious trip rate, must also be well understood and taken into consideration within the predictive trip detection mechanism.

1.2 Problem Statements, Objectives, and Scope

Two major problems are investigated within this dissertation. The main problem is the enhancement of NPP SDSs to utilize the increased computational power as well as functional capabilities of modern industrial computers in an effort to reduce the amount of time required to activate a safety function. This primary problem is expected to be resolved by incorporating a prediction algorithm within the SDS. In investigating this main problem, a secondary problem is encountered. The secondary problem is the development of a prediction algorithm that considers a larger set of prior information or knowledge to accurately predict impending abnormal conditions even when the dynamic process is operating under uncertain conditions. In addition, the functionality of the prediction algorithm is modified to consider the quality of previously calculated multi-step-ahead predictions. These two problems are expected to be resolved by incorporating prediction error compensation and statistical quality assessment routines within the SDS.

1.2.1 Shutdown system enhancement and reduction of time-to-trip

The primary problem that is addressed within this dissertation is the enhancement of SDS functionality in an effort to reduce time-to-trip. Within the nuclear power industry, SDS enhancements are most often performed to address hardware obsolescence. These enhancements may also, however, be performed to address insufficient electrical energy production and safety margins. Of these enhancements, those that are due to obsolescence result in the replacement of existing SDS components with new or more advanced technologies while trip logic functionality remains largely unchanged. In contrast, those enhancements that aim to improve energy production or safety generally focus on improving SDS reliability, independence, availability, simplicity, or conformance to government regulations and international standards rather than SDS response time.

The problem is not that these existing and upgraded SDS designs fail to meet regulatory requirements for response times which are typically less than a few hundred of milliseconds in length. The problem is instead that conventional SDSs at best initiate shutdown actions at the instant a safety parameter is determined to have reached a TSP. Thus, SDSs currently utilize comparator-based trip functionality even though modern technologies are capable of executing increasingly advanced model- and data-based prediction, detection, and decision-making algorithms, many of which are straightforward, well-established and have been proven through use. There is therefore an opportunity to detect in advance, with predetermined confidence and without reducing safety or productivity margins, that a system is approaching an abnormal condition. There are also significant safety, energy

production, and economic benefits that may be realized by reducing time-to-trip. These benefits are due to the nominal operating thermal power as well as the electrical power output of a given NPP unit being functions of SDS response time. More precisely, it may be possible to increase the operating power and electrical power output of the NPP as a result of reducing time-to-trip.

A reduction in time-to-trip reduces the magnitude of fault-induced high power surge, and in turn, the temperature within the reactor core and the potential for critical components to be damaged [35]. Achieving near-immediate time-to-trip is essential during operating conditions when fission reactions within the reactor core may be beyond the control of the reactor regulating system (RRS) and the heat energy accumulating within the reactor core may increase exponentially leading to unsafe operation, or even accident conditions. For these reasons, a reduction in time-to-trip results in increased margins of safety [36]. In addition, for existing NPPs where increased margins of safety can be guaranteed, it may be possible to take advantage of additional electrical power generating capacity by undertaking power up-rating initiatives [22]. That said, the current state-of-the-art in terms of SDS functionality is to use an FPGA to compare trip parameter measurements against a TSP that is most often a constant value, and is at most a function of some major safety-related system parameter.

By continuing along the path of like-for-like functional replacement of SDS decision-making algorithms, it is expected that the ability of automatic protection systems to meet the safety demands of increasingly complex and challenging engineering problems will be hindered both within and beyond the nuclear power generating industry. In addition, it is becoming necessary to consider the consequences that proactive, prognostic, and predictive

decisions have on safety and operability given that these strategies are now being implemented within the monitoring and supporting controllers of potentially hazardous systems. By considering the effects of predictive functions from the perspective of a safety-critical system, it is expected that there will be a reduced likelihood of safety being compromised in order to attain an increase in production value whether within the nuclear power industry or otherwise. In addition, a paradigm shift to a continuing evolutionary enhancement of automatic protection system algorithms will bring about improvements to safety and production margins, the efficiency of existing NPP units, and the economic performance of nuclear power generation in general. More specifically, a reduction in time-to-trip leads to increased productivity as a direct result of increased margins of safety as illustrated in Figure 1.2. In one report, it is stated that each additional percentage of increased operating trip margin increases revenue by a present value of 20 to 40 million dollars per reactor unit [37].

In response to the SDS enhancement and reduction of time-to-trip problem, Chapter 3 investigates various theoretical methods for advanced and intelligent but well-established prediction algorithms. These prediction algorithms are utilized to calculate predictions of the safety parameter measurements that are available within conventional SDSs. Chapter 5 constructs various modular PSDS designs that each aim to reduce time-to-trip. The predictions are then compared against a corresponding TSP to determine whether a trip condition is imminent. This TSP is also referred to as an alarm threshold, and the trip occurrence as a threshold-crossing event. Chapter 5 also aims to re-frame SDS enhancement and safety-critical decision-making in general, by making accurate predictive decisions while at the same time considering the computational power of modern industrial safety

controllers. These considerations are essential for implementation of the PSDS designs within the Tricon v9 safety-PLC of the experimental platform presented in Chapter 6. By performing these enhancements in an evolutionary manner, it is expected that the proposed PSDS designs will maintain the reliability of the existing conventional SDSs.

1.2.2 Predictive shutdown concept

A conceptual predictive shutdown occurrence is illustrated in Figure 1.4. This figure illustrates for a single safety parameter the measurement, corresponding TSP, as well as past, present, and future safety parameter predictions. In Figure 1.4, discrete time index k denotes the current, or present, time-step with units equal to seconds over the sampling interval T_s, or s/T_s. Time-steps that have values less than k have occurred in the past and time-steps that have values greater than k are yet to occur in the future. At each time-step, the prediction algorithm propagates the safety parameter predictions to a prediction horizon N_p time-steps into the future. The predictions are then compared against a corresponding TSP. A predictive trip is initiated if any of the predictions within the prediction window have reached the TSP. Thus, in the example sequence of Figure 1.4, a predictive trip occurs at time-step k due to the predicted safety parameter measurements, propagated to prediction horizon $(k + N_p)$, having reached the TSP. Predictive trip therefore results in a reduction in time-to-trip when compared against a conventional shutdown that occurs at some future time-step. For example, a reduction in time-to-trip of N_p time-steps would result for a hypothetical conventional shutdown occurring at time-step $(k + N_p)$.

Predictive shutdown has the potential for improving two performance margins when

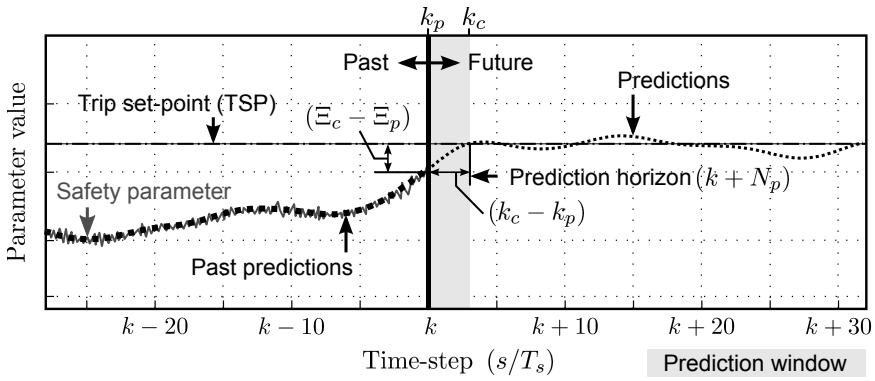

Figure 1.4: The concept of predictive shutdown, or predictive trip, for a single safety parameter with a predictive trip occurring at time-step k.

compared against conventional shutdown. These margins are illustrated in Figure 1.4 with respect to a hypothetical conventional trip occurring at the prediction horizon. The first margin coincides with the main objective of reducing time-to-trip, where time-to-trip has been reduced by $(k_p - k_c)$ time-steps. This is the difference in time between the predictive, k_p, and conventional, k_c, times-to-trip. The second margin is the indirect advantage of an $(\Xi_p - \Xi_c)$ increase in the effective TSP that is an approximation of the change to the safety margin as a result of the reduction in time-to-trip. The effective TSPs are the values of the safety parameter measurement at the time of trip. These changes to safety and production margins are similar to those presented in Figure 1.2b).

Within the nuclear industry, margin of safety is defined as the minimum difference in measurement between a predetermined physical safety limit and the safety parameter measurements during the process fluctuations that follow a trip occurrence [36]. An example of this is the conceptual safety margin of Figure 1.1. When compared to the case of conventional trip, the predictive trip occurs: i) at a time which is earlier, and ii) where safety parameter measurements are a greater distance from the physical safety limits. Where increased safety margin can be guaranteed, one of two benefits may result. Either i) the

operating power of the NPP remains at the pre-enhancement level with improved safety, or alternatively, ii) the productivity of the NPP is increased through an increase in electrical power output and the safety margins are returned to the pre-enhancement margins as illustrated in Figure 1.2.

1.2.3 Prediction of abnormal conditions under uncertainty

A supporting problem that was identified in the course of this dissertation work is the accurate prediction abnormal conditions under uncertainty. The topics of linear and adaptive prediction are thoroughly covered in the existing literature which includes model- and data-based prediction algorithms. These algorithms provide solutions to the prediction problem for models that i) possess some inherent randomness and are considered stochastic, ii) are fully determined by parameter values as well as initial conditions and are therefore deterministic, or iii) are a mix of stochastic and deterministic components.

Those algorithms that consider stochastic models are preferred since NPP subsystems are designed to match within some degree of uncertainty the real-world dynamic response to a dynamic model. In this form, the calculated predictions are defined over a probability space that, at specific points within the measurement domain, can be interpreted as levels of confidence with respect to the predicted measurement. More specifically, in the case of KF-based prediction, the system model is assumed to be linear and the uncertainty in this model is assumed to be additive white Gaussian noise. The predictions that are plotted in the conceptual predictive trip of Figure 1.4 may therefore be calculated through the use of a KF predictor given an assumed model and statistical noise properties or uncertainty

descriptions.

KFs are often implemented as estimators and predictors with little attention given to the effect that various uncertainties have on prediction accuracy and the quality of the calculated prediction probability distributions. Although the standard KF can be incorporated as the prediction algorithm within an SDS, a more advanced KF-based prediction algorithm is investigated herein in order to make increasingly accurate predictions under a variety of operational and uncertain conditions.

The problem of predicting an impending abnormal condition becomes more difficult when the dynamic process changes and the statistical properties that are assumed within the prediction algorithm no longer represent the true uncertainty. In addition, when making safety-critical predictive decisions, the prediction algorithm should consider the possibility that the system is operating under uncertain conditions. The prediction algorithm should also be aware of the quality or accuracy of past predictions. The standard KF does not, however, include either of these features.

Uncertainties or discrepancies between the prior knowledge regarding the system model and signals may arise as a result of a fault, failure or initiating event during the transient towards the TSP. Under uncertain conditions, the predictions as well as the probability distributions that describe uncertainty in the predictions may be erroneous. For example, the assumption of additive white Gaussian noise may no longer hold, or the system may be being affected by a more deterministic fault, failure, or disturbance. Thus, it is necessary to compensate for prediction error within the prediction algorithm. The presence of uncertainty and error is addressed by robust prediction algorithms including model predictive control (MPC) and fault prognostic applications.

Robust prediction algorithms, however, often require complex application-specific solutions. These algorithms also generally ignore the quality of multi-step-ahead predictions. It is therefore necessary to develop a relatively simple yet robust prediction algorithm that includes a mechanism for monitoring the accuracy and quality of the calculated predictions. With respect to making the KF more robust, the offline estimation of noise covariance is often left to best practices that are not very well defined. Moreover, it may be beneficial to modify a KF-based prediction algorithm to adapt the prediction metrics over the given prediction window since KF predictors do not inherently take into consideration multi-step-ahead prediction error.

Without compensating for prediction error, the predictive decision-making algorithm will not be able to accurately predict the behaviour of the system under uncertain conditions. Moreover, without assessing prediction quality, the decision-making algorithm will not be aware of whether or not previously predicted safety parameter values are, in fact, valid. These two factors may result in an impending abnormal condition being missed, i.e. a missed trip, and the usefulness of the prediction algorithm being degraded. Missed trips occur when a trip sequence is not initiated but the system has reached an abnormal condition. In contrast, reductions in time-to-trip by erroneous predictions may result in an increased number of spurious or false trip occurrences. Spurious trips occur when a trip sequence is initiated but the system has not truly reached an abnormal condition. For example, a measurement sample that initiates shutdown may be erroneous due to improper calibration, sensor degradation, electromagnetic interference, etc. These spurious trip occurrences reduce NPP revenue by at least 50 thousand dollars per hour per non-operational unit for the CANDU SDS1 design [38]. In one case time-delay functions have

been included within the logic solver of an SDS to reduce the number of spurious trip occurrences [39]. These spurious and missed trip occurrences must be well understood and taken into consideration within the modified SDS designs.

This research work combines methods from a set of existing publications regarding prediction under uncertainty within Chapter 3, prediction of abnormal conditions in Chapter 4, and the assessment of prediction quality within Chapter 5. The improvement of performance margins by predictive trip requires accurate and high quality predictions. In practice, however, there may be mismatch between the model used within the KF and the true model of the physical system. There may also be disturbances within the signals of the system. KF-based predictors consider these uncertainties in the form of covariances that allow the estimates to be weighted more heavily either towards measurement, i.e. the output of the system, or the system model.

In safety system applications with redundant sensors there is usually a high degree of sensor measurement accuracy. KF-based predictions are propagated, however, using the model as there are no future measurements on which to correct the predictions. Thus, in certain cases of system-model mismatch, the predictions diverge from the true future measurement with each time-step into the future. For this reason, LS estimation is used to correct the multi-step ahead predictions by estimating a model-based disturbance in the measurement as presented in Chapter 4. In addition, a recursive form of the LS solutions known as the recursive least squares (RLS) filter is also formulated in Chapter 4. This estimation of disturbance inputs provides the added benefit of indicating that the system response is deviating from that of the model. The result of this LS estimation is a KF/ RLS-based prediction algorithm.

The statistical assumptions within the KF also allow for the incorporation of statistical and hypothesis testing methods to assess the quality of the calculated predictions. These testing methods also close the loop with respect to the multi-step-ahead KF-based predictions and provide a mechanism by which to adapt the effective prediction horizon or mean prediction error. Hypothesis testing methods can then be used to assess the potential for impending spurious trip and also missed trip occurrences as these two occurrences correspond to false positive and negative hypotheses. Finally, optimal alarm theory may be used to optimize the predictive activation of trip. By enhancing the SDS to calculate accurate and high quality predictions of impending abnormal conditions, it is expected that predictive shutdown will achieve reduced time-to-trip while maintaining existing margins of safety and productivity even when the system is operating under uncertain conditions.

In general, the above-mentioned reductions in time-to-trip are achieved by methods that do not involve the modification of safety system functionality. In fact, the task of modifying the software within an SDS requires a significant amount of resources in order to ensure that the software does not infringe upon the safe operation of the NPP. Thus, it is important to consider that the addition of predictive trip detection may affect safety. It is also the case that the predictive shutdown will provide various model- and data-based metrics and time-series that may be useful in alarm management and operator indication although these aspects of prediction are considered beyond the scope of this dissertation work.

Although the KF is a popular tool for model-based prediction and prognostics, the research presented herein encompasses the first known effort to combine a prediction algorithm with an NPP automatic protection system. In addition, there are only a limited

number of existing publications that combine prediction with protective functions for dynamical systems. A study by Juricek *et al.* relates closely to the proposed concept of predictive shutdown wherein a KF is used for predictive monitoring of abnormal situation management for a mixing or stirring application [40]. In addition, Juricek *et al.* also consider uncertainty and accuracy in the predictions through the use of confidence intervals and statistical testing as well as LS estimation to compensate for prediction error caused by a disturbance to the system state. This solution presented herein, however, formulates the recursive solution to the RLS problem, and investigates disturbance within both the system state and measurement.

During preliminary development of an initial KF-based PSDS design, the ability of the KF to calculate accurate predictions for time-varying systems under uncertainty became of concern. An extended literature review brought forward an algorithm for noise covariance estimation, as well as one particular study by Martin combines KF-based prediction with optimal alarm theory [41]. Martin formulates a probabilistic solution for the prediction of a two-sided symmetric threshold crossing event over the entire prediction window while assuming a steady state solution for the Kalman gain. In contrast, the solution presented herein considers each time-step within the prediction window individually. Moreover, the abnormal conditions are one-sided and are not symmetric. The optimization of an alarm threshold within this dissertation does not therefore produce an explicit solution to the alarm region problem as presented by Martin [41]. The solution presented in this work instead selected a prediction from within a set of predictions that has the maximal probability of an abnormal condition given a trip, which in this context may be referred to as an alarm.

1.2.4 Objectives

This work investigates the reduction of SDS response time through the use of model-based prediction algorithms. These prediction algorithms are required, however, to be accurate under operating conditions that may be uncertain with respect to an assumed model and signal parameters or properties, and of reasonable computational complexity for implementation within a commercial off the shelf industry-standard safety-PLC. The proposed PSDS designs are therefore made to compensate for prediction error, to asses the accuracy of previous predictions, and to adapt the current predictions accordingly. Given these criteria, the objectives of this research are as follows:

1. Review the state-of-the-art literature regarding NPP shutdown and reactor trip, prediction of abnormal conditions under uncertainty, and methods of assessing prediction quality
2. Develop an initial PSDS design
   (a) predict future safety parameter measurements
   (b) adapt the uncertainty descriptions that are provided to the prediction algorithm
   (c) compensate for prediction error
   (d) combine prediction algorithm with conventional SDS logic
3. Enhance the PSDS design to consider prediction uncertainty
   (a) calculate confidence intervals for the predicted safety parameters
   (b) select bound of confidence interval for comparison against TSP
4. Enhance the PSDS design to consider prediction quality
   (a) evaluate prediction consistency to assess prediction quality

(b) reduce Type I and (II) errors, i.e. inactivation (activation) of a safety function when the potentially hazardous system is actually operating abnormally (normally), i.e. missed and false trip occurrences

(c) select or adapt optimal effective prediction metrics, e.g. prediction horizon, as a function of the above statistical measures, for comparison against TSP

5. Implement the SDS and PSDS designs for a single safety parameter within the Tricon v9 safety-PLC

(a) adhere to functional scan time requirement of 100ms; report PLC scan time

In support of the methods used to achieve the above objectives, this thesis provides comparisons of performance, benefits, and drawbacks between the developed PSDS designs and a conventional SDS through both simulation and experiment. These objectives ultimately aim to improve upon the state-of-the-art regarding the design of NPP protection systems, the prediction of abnormal conditions, and prediction under uncertainty in general.

1.2.5 Scope

The scope of this research is segmented into two main categories: those of the methods, and those of the experimental application. The methods include the fundamental theories behind the prediction, error compensation, prediction quality assessment, optimal alarm algorithms, as well as the strategies for enhancing the SDS designs. Review of the history and state-of-the-art for these methods are included primarily within Section 2.1. In contrast, SDS enhancement and the quality assessment strategies are discussed in Section 2.2. The assessment of prediction quality and optimal alarm theory are included within this

second section since these methods related to decision rather than prediction theory. The experimental application includes the development of a predictive shutdown logic solver based on the CANDU SDS1 design with state-of-the-art for SDS development reported in Section 2.2. In addition, discussion regarding international standards and national regulations including the more general design of an SIS as well as the industrial design of CANDU SDS1 are included within Section 2.2. For a more detailed description of assumptions that relate to the experimental setup refer to Chapter 6.

1.2.5.1 Methodology

The methodologies of this work are divided into four main topics: prediction under uncertainty, prediction of abnormal conditions, safety system enhancement, and the assessment of prediction quality.

Prediction under uncertainty: This dissertation investigates time-series prediction methods that support short-term prediction horizons, are computationally simple, and are relatively well-established within the literature and industrial application. The prediction methods are to be executed online in real-time for discrete-time linear time-varying dynamic processes with partially documented models that include some uncertainty and are therefore stochastic and potentially nonstationary. In contrast, this thesis does not investigate whether the system, model, or data are natural or synthetic, univariate or multivariate, and clean or noisy.

There are many algorithms that allow for the calculation of predictions, however, this dissertation only considers those that are based on the KF. The system and uncertainty

descriptions are therefore limited to those that are considered within the definition of the standard KF equations, i.e. stochastic state-space model with assumed additive white Gaussian noise uncertainties in the state and measurement equations. The KF-based predictor utilizes the error covariances that are calculated within the KF to, in turn, calculate confidence intervals for the predictions. The distribution of the resulting predictions is also assumed to be Gaussian. The KF-based predictor therefore considers uncertainties that can be represented using a Gaussian distribution in order to calculate probability distributions for the predictions that are also Gaussian. The KF investigated in this work is not the steady state KF that is common to linear time-invariant (LTI) systems. The KF is the standard recursive form discrete-time KF including update and predict stages. This work does not consider nonlinear or non-Gaussian implementations of the KF. The KF-based predictor is, however, modified to consider a linear-time-varying (LTV) system with potentially linear time-varying statistical noise descriptions. In order to achieve the second of these objectives, an adaptive limited memory filter (ALMF) is incorporated into the KF state estimation procedure. Moreover, since the model is assumed to be time-varying, the future values of the parameters are assumed to be known within the current time-step to allow for the calculation of predictions. This is also true with respect to the values of the system input and output signals and other related signals.

Prediction of abnormal conditions: Prediction of abnormal conditions refers, within this work, to the early detection of a threshold crossing event by an estimate of a future safety parameter measurement where the alarm threshold is a constant TSP. It is naive to assume that the system model will match exactly the true conditions of the subsystem when

the dynamic response of the subsystem is approaching a TSP. Thus, this work investigates the prediction of abnormal conditions, i.e. reaching a TSP, under the uncertain condition of either system-model mismatch or disturbances within the system signals. In either case, the uncertainty is modelled as a sustained additive disturbance to either the state or measurement equation of the state-space model for the subsystem. Within this work, the disturbance model is limited to represent a ramp or an offset to either the state and/ or measurement equations. Moreover, the estimation of these disturbances are limited to LS-based algorithms. The LS filter is selected as it allows for a deterministic model of the disturbance to be considered. The deterministic representation of disturbances complements that of the stochastic assumptions regarding the state and measurement equations within the KF. In contrast to the work of Juricek *et al.* [40], the disturbance estimation procedure assumes that the time-step of disturbance initiation is unknown. The initiating time of the disturbance is instead reset or updated at regular intervals during the course of operation. This work does not investigate the robustness of the LS filter or the recursive implementation of the LS filter to the selection of the disturbance model. The disturbances are assumed to be significant and consistent, e.g. a step or ramp change in input.

Enhancement of shutdown: The enhancement of the SDS is performed in an effort to reduce time-to-trip. It is expected that this reduction can be achieved by implementing the aforementioned KF-based prediction algorithm. The resulting PSDS algorithms are limited to the advanced functionalities that are available in modern programmable electronic systems. In terms of performance, this dissertation aims to achieve high accuracy

with low computational complexity. High accuracy is necessary due to the safety-critical nature of the application whereas reduced computational complexity is required due to the processing power of the available programmable electronic systems that are qualified for safety-critical applications within NPPs, e.g. the Tricon v9 safety-PLC.

The proposed PSDS designs are restricted in terms of complexity to be within reasonable execution intervals or scan times, although these scan times are insignificant in comparison to the prediction horizons, e.g. a 100ms scan time against a 2000ms prediction horizon. It is expected that the effective prediction horizon can be adapted so that high accuracy short-term predictions of 300 or 400ms may even be utilized within the predictive trip decision-making process. It is also possible to use KF-based measurement estimations to make trip decisions. The use of estimates would not, however, result in a reduction in time-to-trip. In fact, due to the time required to execute the KF algorithm, the use of filtered measurement estimates may actually delay the trip decision and increase the time-to-trip.

The purpose of developing the PSDS methods is to prototype the predictive shutdown concept and to better understand the ability of relatively simple prediction algorithms to predict impending abnormal conditions. These methods are not, however, developed in an attempt to qualify for regulatory approval. That said, the complexity of the PSDS is limited so as to satisfy the scan time functional requirement of CANDU SDS1. The inclusion of a prediction algorithm within the SDS is expected to benefit existing SDS implementations. For this reason, the signals that are required by the developed prediction algorithm are assumed to already be monitored within the target NPP SDS. In this way, no new cabling or sensors need to be installed. In addition, this research does not investigate the recalculation of either the safety limit or TSP for the chosen safety parameter. These

two calculations are complex tasks that involve specific safety analysis codes and thorough uncertainty analysis with respect to a given set of PIEs.

The PSDS is designed as an evolution of the conventional SDS. Moreover, the conventional SDS logic remains active within all of the proposed PSDS designs. This backup conventional logic is strongly recommended for real-world PSDS implementations so that the PSDS does not perform worse, with respect to response time, than the conventional SDS. These conventional mechanisms are, however, disabled within the simulations and experiments of Chapter 7. Although the main aim of this research is to reduce time-to-trip, significant effort is made to prevent these reductions from resulting in increased spurious, unnecessary or false trip, as well as increased occurrences of missed trip. Thus, beyond the simple addition of an "open loop" prediction algorithm, this research also investigates various statistical techniques that are able to assess the quality of the predicted future safety parameter values. This research does not, however, attempt to cover all possible impacts on safety that result from either the inclusion of the prediction algorithm or the reduction in time-to-trip.

Assessing prediction quality: This research is primarily concerned with the calculation of accurate predictions. In order to achieve this objective, it is expected that KF-based prediction needs to be "closed-loop" with respect to multi-step-ahead predictions. This research does not, however, attempt to close this loop within the standard KF algorithm and equations. This research instead considers the statistical assumptions regarding the stochastic variables of the KF equations. More specifically, this research investigates the use of statistical and hypothesis testing methods that are able to quantify the quality of

previously calculated multi-step-ahead KF-based predictions.

Although various statistical tests may be applied to the quality assessment problem, this research makes use of three statistical testing methods that are specifically related to Gaussian probability distributions. The three tests are selected based on the assumption within the KF that the additive noise terms of the state and measurement equations and therefore the resulting state and measurement signals being Gaussian. The first test is referred to as the innovation bound (IB) or Z test. The IB metric assesses whether the prediction error is bounded within a predetermined interval of the Gaussian probability distribution. This research also makes use of the one-tailed Z test that is more conducive to the one-sided threshold-crossing problem of optimal alarm theory. The second test is the square of the normalized prediction error, normalized innovations squared (NIS), or chi-square (χ^2) test. The NIS metric transforms the Gaussian distribution of the measurement space into the chi-square distribution with a specified number of degrees of freedom. For an uncorrelated sequence of samples, the number of degrees of freedom is equal to the length of the sequence. The third test is referred to as innovation whiteness (IW) and is a measure of correlation between the prediction errors of different time-steps. This measure is calculated by taking the convolution of the prediction errors and comparing these convolutions against an acceptance gate. These three tests assess whether there is any bias within the calculated predictions, and also whether the calculated uncertainty in the predictions is either wide or narrow with respect to the standard deviation of the error covariance. These statistical tests are not, however, intended to test whether the distribution of prediction errors actually belongs to the Gaussian distribution rather than an alternate probability distribution.

The above tests are utilized in hypothesis testing to investigate the occurrence of true

and false positive and negative decisions. These concepts are shared with those of optimal alarm theory where the probability of an impending abnormal condition is optimized for the expected probability of an alarm given the calculated predictions. The research of this dissertation, instead, considers the performance of past predictions of the current measurement with respect to the value of the current measurement. The effective prediction horizon is then selected by optimizing the probability of an impending trip condition given that a predictive trip occurs, e.g. the true positive rate (TPR) and false positive rate (FPR). Hypothesis testing therefore provides measures that are related to the spurious and missed trip occurrences that are to be minimized within the design of NPP SDSs since these two event occurrences correspond directly with false positive and false negative detections, FPR and false negative rate (FNR) respectively. This research does not investigate whether the addition of hypothesis testing or optimal alarm methods actually reduces spurious or missed trip rates under all conditions. The results of this research do, however, demonstrate that a prediction algorithm can be made aware of the quality of past predictions, and can adapt current decisions as a function of prediction quality.

1.2.5.2 Experimental verification

This dissertation studies a portion of CANDU SDS1 as an example to demonstrate that KF-based prediction can improve time-to-trip within CANDU NPPs. This investigation is limited, however, to a single safety parameter being considered within the SDS and PSDS designs. In contrast, the full SDS1 implementation considers between ten and twelve signals, as discussed in Section 2.2. Moreover, the input signals for the model of the selected system are also assumed to be available to, and measured by, the SDS. These

signals are not measured within the current implementation of CANDU SDS1; however, it is anticipated that the necessary system inputs could be estimated given models of related NPP subsystems as well as the other existing safety parameter signals.

The safety parameter of interest is the steam generator level and the steam generator level low (SGLL) TSP. The model provided to the KF is therefore the open-loop discrete-time state-space representation of the steam generator water level dynamic. Although the steam generator level has a relatively slow dynamic, the complex inverse response characteristic of the steam generator water level provides an interesting case for the predictive trip problem. In other words, the dynamic of the steam generator level is rather complex in that it has an initial response that opposes the manoeuvre made by the manipulating variable. This dynamic is discussed in more detail within Chapter 6. In contrast, SDS enhancements are usually studied with respect to the faster dynamics of the neutronic trip parameters and corresponding PIE known as the loss of coolant accident (LOCA). It is expected that the nonlinear model of the neutronics within the reactor core may be more suited to an advanced form of the KF as discussed in Section 2.1, but these aspects are beyond the scope of the current work.

The experiments of this dissertation examine only a single initiating event otherwise referred to as a PIE. This PIE is, however, investigated for varying degrees of uncertainty both between the true system and the model and also within the signals that are made available to the SDS. The specific PIE studied within this work is the loss of secondary side coolant. The PIE is studied within two normal operating manoeuvres that are referred to as power transients. This research also considers an unanticipated change or disturbance in the water level set-point for the steam generator. In terms of uncertain conditions, the

simulations and experiments of Chapter 7 investigate parameter error or model mismatch between the true system and the assumed model provided to the KF. Moreover, an undetectable fault in the manipulated variable of the steam generator is also investigated within the experimental results.

1.3 Contributions

The main contributions of the research performed within this dissertation are summarized as follows:

1. Application, analysis, and evaluation of the KF towards reducing the time-to-trip within the SDS of a NPP by predicting the future behaviour of safety parameter measurements related to a system being protected.
2. Analysis and evaluation of the effect of uncertainty, in the form of noise and error in the signals and parameters of a stochastic state-space model, on the performance of the KF-based prediction algorithms.
3. Application of confidence intervals to the safety parameter prediction problem to achieve an increased level of confidence in the predicted impending conditions.
4. Derivation, application, analysis, and evaluation of KF/RLS-based prediction algorithms towards improving prediction performance by compensating for prediction error within the KF-based predictions when the system is operating under uncertain conditions.
5. Integration of the KF and RLS algorithms as well as the confidence-based decision-making into the conventional SDS structure, i.e. a point-PSDS design and an interval-

PSDS design, while adhering to technological and timing constraints as well as industry standards.

6. Derivation, application, analysis, and evaluation of three separate statistical tests towards assessing the quality of the KF-based predictions given the assumed stochastic state-space model of the system as well as additive noise characteristics.
7. Application, analysis, and evaluation of hypothesis testing towards quantifying the quality of the calculated predictions against the eventual measurements.
8. Derivation of an adaptive decision-making algorithm towards limiting and minimizing respectively the probability of spurious and missed trip occurrences by combining statistical and hypothesis testing with optimal alarm theory.
9. Integration of the optimal decision-making algorithm into the PSDS structure, i.e. optimal-PSDS, again while adhering to technological constraints and industry standards.
10. Comparison, analysis, and evaluation, through simulation and experimentation, of the developed PSDS algorithms as well as a conventional SDS implementation in terms of time-to-trip and computational complexity.

In addition to the above contributions, the various other deliverables that have been developed or implemented over the course of this study are summarized as follow:

1. Implementation of the three-element PI controller within a Siemens S7-400 DCS using the Simatic engineering workstation software and modification of the existing experimental platform to interface in real-time with various external control systems.
2. Identification of the model for an existing experimental platform.

3. Application, analysis, and evaluation of the use of a digital filter within a Microchip PIC micro-controller to analytically compensate the dynamics of the existing experimental platform towards matching the dynamic behaviour of the steam generator level.
4. Implementation of the digital filter within the Microchip PIC micro-controller using the MPLAB integrated development environment and modification of the existing experimental platform by analytical compensation so that the behaviour of the platform mimics that of the steam generator water level dynamics.
5. Construction of a simulation platform for the conventional and predictive shutdown algorithms using MATLAB.
6. Implementation of the conventional and predictive shutdown algorithms within the Invensys Triconex Tricon v9 safety-PLC using the Tristation engineering workstation software.
7. Application, analysis, and evaluation of the operating conditions and initiating events associated with NPP accident, shutdown, or trip conditions and construction of a simulation environment for these conditions and events in MATLAB.
8. Development of various other software for data collection and hardware interfacing.

1.4 Organization

Chapter 2 includes a literature review that covers prediction theory, prediction under uncertainty, NPP safety and shutdown, and optimal alarm theory. KF-based prediction is then investigated in Chapter 3 where ALMF-based noise covariance estimation, and confidence-

based predictive decision-making are combined within KF-based state and measurement prediction algorithms. The recursive solution to the LS disturbance estimation problem is then formulated in Chapter 4 and is also combined with the KF-based prediction algorithm. The prediction algorithms are then incorporated within the PSDS designs through the modular modification of a conventional SDS design in Chapter 5. These modular modifications result in two PSDS designs referred to as point-PSDS and interval-PSDS whereby predictive trip decisions are made by comparing either the mean or bound of a confidence interval against the corresponding TSP. In addition, Chapter 5 formulates methods for assessing prediction accuracy using various statistical tests for hypothesis testing, as well as minimization of erroneous predictive decisions. These developments result in an enhanced PSDS design known as the optimal-PSDS. Chapter 6 describes the experimental setup including the dynamic response of steam generator water level. The steam generator is the target system being protected that is studied within Chapter 7. Chapter 6 also reveals the similarities and differences between the simulation and experimental platforms. The simulation and experimental results are then presented in Chapter 7 where the three PSDS routines are compared against a benchmark conventional SDS. Finally, Chapter 8 concludes the thesis and recommends potential extensions of this thesis work.

Chapter 2

Literature Review

This chapter includes two sections; one for each of the two problems stated in Section 1.2. The publications that are reviewed within these sections form a foundation for the contributions outlined in Section 1.3.

Individually, Section 2.1 establishes the framework for linear, nonlinear, and adaptive time-series estimation and prediction of dynamic processes or systems. Section 2.1 also reviews KF-based prediction methods that consider prediction error and prediction reliability. Section 2.1 then concludes with publications that are directly related to the prediction problem addressed by this dissertation work, i.e. the early detection of abnormal conditions under uncertainty.

In contrast to prediction, Section 2.2 establishes the framework for safety instrumented systems as well as safety systems. Section 2.2 also reviews publications that are related to the enhancement of SDSs, including reductions in time-to-trip, and the development of computerized safety systems. Section 2.2 includes an overview of one specific NPP

safety system: CANDU SDS1. This chapter then concludes by connecting safety system enhancement with the design of optimal alarm systems.

2.1 Time-series Prediction

The following review of prediction methodology includes three sections. Section 2.1.1 presents a background of linear, nonlinear, and adaptive estimation and prediction theory with a particular focus on the KF. Section 2.1.2 reviews publications that investigate or advance KF-based prediction methods. Finally, Section 2.1.3 reviews publications that go beyond KF-based prediction to determine or compensate for prediction error and reliability.

2.1.1 Filtering and estimation

Prediction theory is composed of the fields of linear prediction and adaptive prediction. Linear and adaptive prediction are in turn specializations within the fields of linear and adaptive estimation. In the context of linear and adaptive estimation, the term estimation refers to the extraction of information about a quantity of interest from noisy data [24]. Moreover, estimations are produced by functions that are referred to as estimators. These estimators are also referred to as filters in reference to the filtering of noise from a signal. The term adaptive specifies that the algorithms, estimators, or filters include parameters that are adapted or adjusted as a function of the data that is input to the algorithm. In other words, standard estimation algorithms calculate optimal approximations of either unknown parameters or signal values whereas adaptive estimation algorithms update the unknown parameters while at the same time approximating the signal values.

Since the onset of estimation and prediction theory, many methods have been investigated for predicting the future behaviour of a dynamic process. The main purpose for developing these new methods is to improve prediction algorithms with respect to:

- misadjustment or accuracy,
- rate of convergence,
- tracking for nonstationary processes,
- robustness,
- computational requirements,
- structure, or
- numerical properties

within the context of a given application [24]. Moreover, prediction methods can be categorized by the following attributes of the dynamic process for which the predictions are to be made:

- short/long prediction horizon,
- deterministic/stochastic,
- if stochastic:

  stationary/nonstationary,
- continuous/discrete-time,
- linear/non-linear,
- time-invariant/time-varying
- documented/structured/blind,

  i.e. white-/grey-/black-box,
- univariate/multivariate,
- natural/synthetic system,
- clean/noisy signal,
- one/multiple trial(s),

as well as the computational complexity of the algorithm, and whether or not the prediction algorithm is required to be implemented online in real-time or supports offline execution. These attributes are an extension of the list discussed in [42].

Although there are a vast number of textbooks covering estimation, filtering, and pre-

diction, the citations and work within this dissertation often refer back to a few well known texts. These texts are, in no particular order, summarized as follows. The first is by Goodwin and Sin and presents adaptive filtering, prediction, and control methods for deterministic and stochastic processes in two separate parts [43]. The next text is by Haykin and focuses on adaptive filter theory but dedicates an entire chapter each to the topics of linear prediction as well as the KF [24]. Haykin also presents an extensive summary of the history of linear estimation and adaptive filtering theory. The third is by Anderson and Moore and presents optimal filtering including a chapter dedicated to the discrete-time KF [44].

In addition to the above three texts, Sayed presents the fundamentals of adaptive filtering in [45]. Brown and Hwang cover various practical aspects of the KF including applications in MATLAB [46]. These concepts are also presented by Grewal and Andrews where KF theory is applied within MATLAB [47]. These last two texts are at the center of the KF-based prediction methodology presented in Chapter 3.

Linear estimation

Following the work of Gauss, early contributions to linear estimation theory include the minimum mean-square estimation of stochastic processes that was performed throughout the 1930's and 1940's by Kolmogorov and Krein [48,49], and independently by Wiener [50], Wiener and Hopf [51], and Levinson [52]. More specifically, Kolmogorov, having been inspired by the work of Wold [53], developed a solution for the linear prediction of discrete-time stochastic processes with Krein extending the work of Kolmogorov to derive the continuous-time filter. In the meantime, Wiener and Hopf had derived an explicit formula,

known as the Wiener-Hopf equation, for the optimum predictor of the continuous-time linear prediction problem and had also considered the problem of filtering a process that was corrupted by additive noise [50]. The discrete-time solution for the Wiener-Hopf equation was subsequently derived by Levinson in 1946 [52].

The next major contribution to linear estimation and prediction theory occurred in the late 1950's when Kalman solved Wiener's interpretation of the linear estimation problem and developed what is now referred to as the Kalman filter (KF). To solve Wiener's problem, Kalman used a well-known method from probability theory for optimal estimation and orthogonal projection and then modified the representation of the process to be in the state-space form in order to solve the linear estimation problem for growing and infinite memory filters with stationary and nonstationary statistics [27]. The result is a minimum mean squared error one step-ahead predictor for linear systems affected by additive white Gaussian noise. As a filter, the KF calculates the mean and error covariance of the state vector under the assumption that the state vector has a Gaussian distribution. This assumption can, in general, satisfied as a result of the central limit theorem and can be verified by analyzing the probability distribution of the corresponding signal or residual. The continuous-time domain treatment of the KF was performed by Kalman and Bucy and is sometimes referred to as the Kalman-Bucy filter [54].

In the decade that followed Kalman's original publication, it became common practice for the state vector to be augmented to include model parameters that are then estimated along with the state [55]. Although the augmented state vector results in a nonlinear filtering problem, it allows for the estimation of unknown or time-varying parameters as a function of assumed additive white Gaussian noise. In addition, the KF was reformulated

by Kailath *et al.* [56, 57, 58] in the late 1960s using an innovations approach introduced by Kolgomorov [48] as well as Bode and Shannon [59]. In Kailath's approach, the KF is a causal and causally invertible filter with a white-noise process as input and a stochastic process as output. Here the term innovation refers to the white-noise input providing new information to the estimation problem where the input is statistically independent of, or uncorrelated with, the filter output [24]. Kailath's method isolates the predictable or deterministic part of the filter from the new statistical information provided by the current measurements.

Nonlinear dynamic processes

The KF is an extremely useful tool for many real-world prediction applications due to the accuracy of the calculated estimations and relative ease in design and programming [60]. For some applications, however, computation of the state error covariance may not be feasible due to a model that is of high dimension. In contrast, accuracy may be poor due to nonlinearities from real-world dynamic processes or the assumption of an augmented state vector. Thus, various extensions to the KF have been proposed to address the nonlinear filtering problem.

The first modifications to the KF that considered nonlinearities were introduced within years of Kalman's original publication. The most prominent of these early modifications is the class of filters known as the extended Kalman filter (EKF). The EKF propagates state estimates using given nonlinear system functions in the same manner as the standard KF. State error covariances, however, are propagated using matrices of time-varying parameters that are approximated by first- or second-order Taylor series evaluated at the

current estimate of the state vector. Early contributions to the EKF are often credited to multiple authors including Smith *et al.* [61], Kopp and Orford [62], and Cox [63] with the second-order EKF being credited to Athans *et al.* [64]. There are now many different interpretations of the EKF for various applications as discussed in [60] and [65]. No matter the interpretation, the appeal of the EKF is that, given a nonlinear mathematical abstraction of system behaviour, it is simple to use a linear approximation to calculate the state error covariance. Caveats of the EKF, however, include the online calculation of the state-dependent matrix Riccati equation as opposed to offline calculation for steady state KF gains, and large errors due to linearization that sometimes cause the filter to diverge [65].

Possible divergence of the EKF has more recently lead to the development of a sampling approach for propagating the state error covariance where the probability distribution of the state estimate, with state error assumed to be Gaussian, is approximated using a mathematical function known as the unscented transform. This approach is included in an extension to the KF known as the unscented Kalman filter (UKF). The UKF propagates state estimates in the same manner as for the EKF, however, the state error covariance is propagated using the given nonlinear system functions as well as a set of carefully chosen sample points representing the moments of the probability distribution for the state vector. The UKF was first proposed by Julier and Uhlmann [66]. The appeal of the UKF is that the state and state error covariance estimates are accurate to the third-order Taylor series expansion for any nonlinear model representation [65]. Thus, the UKF achieves superior performance compared to the, at most, second-order accuracy of the EKF. In addition, the computational complexity of the UKF is roughly the same as for the first-order EKF [60]. Thus, the UKF has better accuracy than the most accurate EKF and

requires less computational complexity than the least complex EKF.

Another extension to the KF is the ensemble Kalman filter (EnKF). The purpose of the EnKF is to avoid calculating and propagating the state error covariance for high-dimensional processes where the state error is assumed to have a Gaussian probability distribution. The EnKF instead propagates the state error covariance using the given non-linear system functions as well as an ensemble set of sample points that then represent the probability distribution of the state vector. This is similar to the UKF concept except that in the case of the EnKF the sample points are randomly calculated and are not specifically the moments of the probability distribution. Calculation of state estimates, however, remains the same as for the EKF and UKF. The EnKF was first proposed by Evensen [67] and Burgers *et al.* [68]. The appeal of the EnKF over the EKF is that, like the UKF, the third- and higher-order moments of the error covariance are not discarded. In addition, for high-dimensional processes, e.g. those found in meteorology and oceanography, the sample mean and covariance is calculated from the propagated ensemble sample points. This results in a reduction in computational complexity to be a function of the number of ensemble sample points rather than the order of the process [69].

Non-Gaussian probability distributions

For some applications, estimation accuracy may be poor due to the assumption that the additive noise is white and Gaussian and that the state vector is a Gaussian random variable. For problems of this type, there exist two additional extensions to the KF. The first utilizes a Gaussian mixture model or a weighted sum of Gaussian probability density functions to approximate the true state error probability distribution. Essentially, a bank of KFs

operate in parallel to obtain a suboptimal estimate of the state error covariance. This method was developed by Alspach and Sorenson for both linear and nonlinear dynamic processes [70, 71]. The second extension is referred to as a particle filter and is similar to the EKF in that there exist many different interpretations of the filter. In general, the particle filter approximates the non-Gaussian probability density of the state vector using sample points as in the UKF and EnKF where the sample points, or particles, are propagated using the given linear or nonlinear system functions. For the particle filter, however, the sample points are selected in an efficient manner according to weights that are calculated from an approximation of the state estimate probability distribution known as a proposal distribution [72]. This sampling within the particle filter takes the form of a sequential Monte Carlo approach. The particle filter is attributed to the work of Gordon *et al.* [73]. For a more thorough review of particle filter development in relation to the KF refer to Chen [72]. Although these two methods are the focus of current research efforts, the Gaussian mixture model or particle filter algorithms are generally more computationally complex than the previously discussed algorithms that assume a Gaussian probability distribution for the state error. These methods therefore require more computationally powerful controllers and computer platforms in order to be implemented.

Adaptive filtering

The theory of adaptive filtering or adaptive estimation developed alongside that of linear and nonlinear estimation. The difference between linear and adaptive filters is that the latter are said to be self-designing through recursive updating of parameter estimates. This feature is necessary where prior knowledge of the underlying dynamic process is incomplete.

Although the parameter update mechanism results in adaptive filters being nonlinear, adaptive filters are classified as linear if the input-output relationship obeys the principle of superposition while the parameters are held constant. In contrast, if the linear input-output relationship is not satisfied then the adaptive filter is classified as nonlinear [24].

In general, there are two primary methods of adaptive filtering. The first is the stochastic gradient approach that includes the least mean square and gradient adaptive lattice algorithms. These two algorithms are relatively simple and effective for adapting transversal and lattice-based filters respectively. In addition, these algorithms are independent of the process model, as opposed to the KF that relies on a given model of the process. The least mean square algorithm was first proposed by Widrow and Hoff in the late 1950s [74, 75] whereas the gradient adaptive lattice algorithm was introduced by Griffiths in the 1970s [76, 77]. The function of these two algorithms is to recursively iterate the parameters or weights of the filter in the direction of the gradient of the mean squared magnitude of error between the desired response and the filter output as a function of the current parameters. In other words, the parameters are adapted so as to follow an error-performance surface, e.g. a paraboloid, toward the optimum Wiener solution that is the minimum point of the surface. Least mean square adaptation is made possible through an iterative procedure based on the method of steepest descent to solve the Wiener-Hopf equations. Basically, the updated parameters are equal to the previous parameters summed with the product of a learning-rate or step-size parameter, an error signal, and the input to the filter. The appeal of the least mean square algorithm is that it is simple. The least mean square algorithm does, however, suffer from a relatively slow rate of convergence and sensitivity to the correlation matrix. These factors result in the least mean square

algorithm being unsuitable for use with nonstationary, time-varying processes, unless the input data vary slowly relative to the learning rate of the algorithm [24].

The second well-known adaptive filtering approach is based on the method of least squares (LS). This approach provides a solution to adapting traversal filters that includes both a block and a recursive formulation, i.e. the RLS filter. The recursive form of LS filter is more common as it requires less memory and computational power. The RLS method is model dependent and is therefore a special case of the KF. The RLS filter was originally reported by Plackett in 1950 [78] although the algorithm was not popularized until the work of Godard in 1974 [79]. The RLS filter recursively minimizes the sum of the weighted squared error between the desired response and the filter output. It is assumed that the filter weights can be estimated through recursive estimation whereby the updated parameters are equal to the previous parameters, or weights, summed with the product of cost minimizing gain vector and the error between the desired response and the filter output.

The RLS algorithm is more computationally complex than the least mean square algorithm. Various efforts have been made to reduce complexity and improve robustness of the RLS filter and to relate the RLS algorithm to the KF. Reduction in complexity originated with the work of Morf and the so-called fast RLS algorithm in 1974 [80]. These fast algorithms take advantage of redundancy in the structure of the input data matrix. Further, a numerically robust RLS algorithm was achieved through the use of QR-decomposition for matrix algebra by Gentleman and Kung in 1982 [81]. These filters are also referred to as square-root adaptive filters as they are the square-root form of the standard RLS algorithm. Finally, in 1994 Sayed and Kailath [82] investigated the use of KF theory toward the

adaptive filtering problem by demonstrating that the QR-decomposition and fast KF algorithms are special cases of the KF. The RLS algorithm is appealing due to it corresponding with KF theory and having faster convergence when the process model matches the actual process behaviour. In contrast, model mismatch within the RLS filter may result in poorer tracking performance when compared against the least mean square filter [24].

2.1.2 Kalman-filter-based prediction

Linear and adaptive estimation cover three major problem types: filtering, smoothing, and prediction. Filtering is the calculation of estimates for the current time-step, smoothing is the calculation of estimates for past time-steps, and prediction is the calculation of estimates for future time-steps, i.e. forecasting. It is therefore natural for the estimation methods of Section 2.1.1 to be extended to the prediction problem. When applied within engineering problems, these three forms of estimation are assumed to be causal. In other words, the filter output is a function of past and current but not future inputs.

The most simple form of linear prediction involves the use of model parameters that have been optimized for predicting the future behaviour of a process given an assumed or derived model structure, as well as, if necessary, future excitation signals. For systems and signals that are completely documented with precisely known parameters, i.e. deterministic, the resulting predictions are exact. In contrast, the prediction mechanism that is inherent to the structure of the KF algorithm [27] accounts for non-determinism in a stochastic framework through a measure of uncertainty in the initial state conditions, the model parameters, and the input and output signals of the system. To calculate predictions, the KF propagates

estimates of the state vector and error covariance into the future given assumed uncertainty in the model and signals in addition to the assumptions as described above for the case of linear prediction. State error covariance is a matrix representation of the multidimensional variance for the state error including correlations between the variances along the multiple dimensions. By propagating the state vector and covariance, the KF has a benefit over deterministic prediction in that it can calculate point-predictions as well as a measure of uncertainty or confidence interval in the point-predictions as a function of the calculated standard deviation.

For both the exact and inexact KF-based prediction methods, parameter optimization is assumed to be performed off-line by linear regression for a model that is at least partially documented. Thus, neither of prediction method is considered to be adaptive [54]. There are, however, many adaptive prediction methods that build upon the KF algorithm. This subsection reviews and categorizes a small subset of related works from the vast number of publications related to KF-based prediction in order to better understand how KFs may be used to solve prediction problems.

Linear and nonlinear prediction

An obvious extension of the KF and also the state equation within the state-space model of a system is to propagate the state vector beyond one time-step. In [27], Kalman states that his solution to the Wiener problem may be applied to filtering or estimation as well as smoothing and prediction problems. Kalman does not, however, include specific procedures or equations for propagating the state error covariance within the KF. The following are example applications of varying complexity that utilize the KF to solve a prediction

problem. The accuracy of the KF-based predictions are provided for those publications that quantify error or performance.

One of the earliest uses of the KF for prediction was by Toyoda *et al.* [83] to calculate short-term predictions of the future load behaviour for on-line and real-time control of complex power systems. This use of a KF for multi-step ahead prediction, in turn, cites the work of Sorenson [84]. More specifically, Sorenson provides an extensive discussion regarding Kalman filter theory as well as techniques for space navigation problems. In addition, within the same text, Schmidt discusses prediction within the navigation problem whereby error between the propagated future state and an impending reference trajectory determines whether any control actions are required at present [85]. These publications do not, however, state explicitly the multi-step-ahead prediction problem. At around the same time as Toyoda *et al.*, Galiana [86] also uses the KF for forecasting the future behaviour of electric load. Thus, although the trajectories of celestial bodies and space travel may have motivated solutions to the estimation and prediction problems, these solutions were soon after adapted to various other applications.

To aid in the landing of aircraft while at sea, Sidar and Doolin [87] design a KF-based predictor to predict in real-time the motion of an aircraft carrier. The study cites both Sorenson [84] as well as Kalman and Bucy [54] for the multi-step ahead prediction method. The strategy is reported to achieve reasonable error bounds of less than 60cm over a time interval of up to 20s. Prediction quality is assessed by calculating the amount of time that the actual ship movement differs in sign from that of the prediction. This amount of time is reported to differ for less than 0.5s over an interval of 60s.

Chung *et al.* [88] use the KF to estimate a wave-excitation forcing input function in

order to predict ship motion. Estimation of the forcing input function allows for future values of the input to be predicted. The predictions are then input to the ship-motion dynamic model to predict the motion of the ship for exact as well as uncertain parameters. This method of prediction is referred to as prediction of state via input excitation and is compared against predictions calculated using a standard KF. A comparison with standard KF-based predictions reveals that the proposed input prediction method achieves mean squared errors that are between 50 and 70% of the KF results at prediction horizons of up to 20s.

Ten Brummelhuis *et al.* [89] use the EKF for online prediction of the water levels in tidal estuaries. The EKF is implemented to linearize the model against a discrete reference state trajectory for errors in the deterministic model. Linearization is performed at every time-step. The EKF also simultaneously calculates parameter estimates and is therefore essentially a dual-EKF. The performance of the dual-EKF implementation is not quantitatively analyzed, although visual inspection of the included plots indicate a maximum prediction error of under 50cm for peak to peak tides of 400cm.

Chen *et al.* [90] propose a particle predictor for nonlinear time-varying systems. The task of fault prediction differs from fault detection in that the former predicts whether a fault is going to occur at some time in the future whereas the latter detects whether a fault has already occurred. The particle predictor utilizes sampling importance resampling which is also known as Bayesian bootstrap filtering. In this manner, the predictor is able to represent uncertainty in the predictions as a non-Gaussian probability density function. This representation is achieved using a sequential Monte Carlo technique.

Moradkhani *et al.* use a dual state-parameter EnKF to estimate and predict streamflow

given a documented hyrdological rainfall-runoff model [91]. The dual state-parameter algorithm estimates both the states of the system as well as the parameters of the model. The study discusses the identification of perturbation factors for ensemble generation and for selection of ensemble size. The confidence interval for parameter-state estimation can then be calculated at each time-step.

Mastali *et al.* [92] use an EKF as well as a dual EKF to estimate and predict the state of charge for various battery types and configurations within the battery management system of a hybrid vehicle. In addition, the dual EKF also estimates the parameters of the battery management system. It is argued that the KF is necessary since the batteries experience a dynamic operational environment, i.e. time-varying model parameters. The study incorporates three competing models into the EKFs, the best of which achieves an agreement of less than 4% error between the predictions and the experimental data.

Adaptive prediction

Alternatively, the KF can also be used to estimate the parameters and structure of an assumed model to improve prediction quality rather than, or in addition to, propagating the states of a state-space model. These strategies differ from those above in that the KF adapts the model parameters and not a non-KF-based supporting parameter estimation routine.

Sriyananda and Towill [93] augment the state vector within a standard KF to estimate unknown parameters as well as to predict the future performance of a human operator. The proposed KF predictor demonstrates that it is possible to calculate accurate predictions for both time-invariant and time-varying model parameters. In the time-varying case, the

parameters change in an infrequent and abrupt manner. It is found that large errors due to erroneous initial conditions rapidly decrease as more data becomes available. The study also suggests that improved estimations can be calculated through the use of parameter smoothing. For the time-invariant case, an approximate error of 5% is observed in the forecast performed on day 17 for day 70. For the time-varying case, there is said to be a 20 day period for readjusting the parameters before the predictions are considered to have reasonable accuracy.

Heath [94] uses an autoregressive model to predict future heart inter-beat interval and heart-rate observations with the parameters of the autoregressive model estimated by a KF. The one-step ahead predictions are reported to have a mean squared error of 39.02ms over a peak to peak range of approximately 70ms within an unspecified number of samples. In addition, a change detection algorithm is presented. The detection algorithm is a function of prediction error and the chi-squared distribution and is able to detect nonlinearities in the autoregressive model following changes in a stimulus.

Mizumura and Chiu [95] use an autoregressive moving average model of various orders to predict snow melt runoff. The snow melt predictions are calculated for prediction horizons of one and two time-steps using the optimal parameters as calculated by the KF. It is stated that the predictions are effective although quantitative analysis of error is not included in the article.

Hawthorne [96] uses a moving average propagation model to predict the future properties of an 800 megahertz radio signal for a mobile receiver. The prediction error for the received signal is reported to have zero mean and a standard deviation of 5.08dB. These statistics were determined to indicate good agreement between the model and the measured

propagation losses.

Melgaard *et al.* [97] aim to calculate a maximum likelihood estimate of the system parameters for a continuous-time model of a four-stroke spark ignition engine for the purpose of predicting engine dynamics. A KF calculates the conditional mean and variance of the one-step ahead predicted observations for both maximum likelihood estimation of the model parameters as well as for forecasting the engine dynamics. Although no quantitative analysis of prediction error is given, the prediction error is stated as well as demonstrated through a plot to show good agreement with future observations.

2.1.3 Prediction under uncertainty

The above-mentioned publications aim to calculate predictions through the use of a KF. These predictions may be inaccurate, however, when the model parameters or structure that is provided to, or calculated by, the KF does not match that of the true system being modelled, e.g. the system is experiencing uncertain conditions with respect to the nominal model. Moreover, these uncertainties may lead to, or indicate, impending abnormal, unsafe, or even emergency conditions. According to Nimmo [98], industrial systems operate in one of three modes: normal, abnormal, or emergency. The boundaries between these modes are respectively referred to as alarm and emergency thresholds within a system being protected, and more specifically within the nuclear power generating industry as included in Figure 1.1. A system being protected is one that is monitored by a protection system. Upon detecting an abnormal condition, a protection system activates a sequence of events that prevent an unsafe or hazardous condition from occurring. In some industries, additional

protection or mitigation actions may also occur upon detection of unsafe or emergency conditions.

In the following discussion, the terms abnormal and emergency conditions are not necessarily interchangeable yet it is possible to predict either an abnormal or an emergency condition given either threshold. The difference between the two detections being that the prediction of an abnormal condition can only occur during normal operation whereas the prediction of an emergency condition may occur within either normal or abnormal operation. In the context of NPP shutdown, the trip event is initiated as the result of an abnormal condition being detected. It is imperative, throughout the development of a predictive safety or protection system, that an impending emergency condition be predicted whether the system is operating within or beyond the normal operating mode, including operation under uncertainty conditions. Thus, the effectiveness of the protection system can only be ensured if the predictions remain accurate while the system is operating under uncertainty.

Of the publications that address KF-based prediction of abnormal conditions under uncertainty, that of Juricek *et al.* [40] is the most similar to the concepts covered within this dissertation. In fact, the work of Juricek *et al.* is the foundation for the development of the KF/LS-based prediction algorithms that are developed within Chapter 4. This is especially true regarding the consideration of uncertainty due to the presence of abnormal conditions. Juricek *et al.* [40] suggest that the following topics are related to the prediction under uncertain conditions problem: fault detection and diagnosis based on linear process models; and MPC methods that utilize state estimation and are concerned with assessing prediction accuracy.

MPC algorithms are able to optimize control inputs based on predictions of the future dynamic response and control inputs of the system. These optimizations are performed over predetermined intervals of time, known as horizons, extending from the present into the future [99]. KFs have been investigated for use in fault detection algorithms within the reactor regulating system of an NPP [100] as well as various other applications including tracking, navigation, and environmental prediction [47]. The KF has therefore been extensively studied and proven through use in a predictive application that resembles the predictive shutdown problem, i.e. the model predictive portion of MPC.

In relating MPC to the prediction under uncertain conditions, Juricek *et al.* [40] state that the concept of predicting abnormal conditions could be considered model predictive monitoring. The prediction under uncertainty problem is therefore addressed through various robust MPC strategies. That said, MPC has the added benefit of being closed loop with respect to the system being protected. These methods are often not applicable within protection systems. For more information regarding MPC refer to [99, 101].

The other suggested topic of fault diagnosis can be extended to fault prognosis given the predictive nature of the current problem, e.g. early fault detection or predictive diagnostics. In general, diagnostics and prognostics differ in that the former are performed posterior to the occurrence of an event while the latter are performed prior to occurrence of the event. More specifically, diagnostic methods are utilized to classify and possibly isolate faults whereas prognostic methods predict future conditions and remaining useful life. For predictive shutdown within an NPP, the prediction under uncertainty problem is concerned with the detection of an impending emergency condition given the potential presence of an abnormal condition. Thus, both prognostic and diagnostic methods are related to

the current problem. In other words, prognosis of the impending condition is considered necessary to achieve an earlier time of detection. The initiating event, however, may have occurred at some time-step previous to the time of detection, hence diagnostics. An overview of prognostics is provided at the end of this section.

Prediction and abnormal conditions

In practice, inaccurate predictions result from the inability to obtain an exact model of the system and environmental conditions, and also from assumptions made during the modelling and system identification process. These assumptions affect the accuracy of, and sometimes define, the statistical properties related to the system and signals. More specifically, inaccurate predictions may be caused by:

1. disturbances in system input, output, and state signals;
2. system-model mismatch due to unanticipated operating conditions, unmodelled dynamics, linearization, nonlinearities, aging, degradation, etc.; or
3. erroneous initial conditions or anticipated future signal values.

Each of these causes may be more prominent during abnormal conditions. To improve prediction accuracy, robust prediction algorithms include mechanisms which compensate for prediction error or calculate a bounds within which the predictions are expected to occur.

Juricek *et al.* [40] state that the following two issues are important when calculating predictions under uncertain conditions:

- interpreting the predictions with respect to decision-making; and

- assessing the reliability, herein referred to as quality, of the predictions.

Here, interpretation of the predictions refers to obtaining an understanding of how and why an individual prediction can be used to make a decision. In addition, quality refers to both the overall consistency as well as the accuracy of the predictions with respect to the eventual parameter, measurement, or signal of interest. Having considered the above-listed issues, Juricek *et al.* combine a steady state KF with an LS filter to calculate predictions for a linear stochastic state-space model. The purpose of the KF is to propagate the state estimates over a prediction horizon, and the purpose of the LS filter is to estimate an unknown disturbance input that is referred to as a pseudo-disturbance. The resulting predictions provide a means to determine whether an emergency limit will be violated within the prediction horizon.

The work of Juricek *et al.* [40] aims to predict whether future process variables will reach a predetermined emergency threshold. Predictions are calculated using a KF as well as a model of the process or system. Prediction accuracy is improved through LS estimation of an unmeasured disturbance input as a function of prediction error using a modified form of a fault detection method developed by Basseville and Nikiforov [102]. More specifically, the LS estimation algorithm is a component of the generalized likelihood ratio method of Basseville and Nikiforov [102]. This LS method differs from conventional LS methods in that it considers the effect of the disturbance input on the dynamics of both the system response and the KF-based predictions. LS estimation of the disturbance inputs accounts for nonrandom bias as has also been investigated in [55,103]. The LS filter is preferred over utilizing an EKF and augmenting the state vector due to the augmented state

vector requiring that fictitious statistical noise descriptions be specified for an otherwise deterministic disturbance. A preliminary investigation of the augmented state form of KF estimation of the disturbance revealed that the predicted outputs were sensitive to the selected values of uncertainty, or fictitious noise [40].

Regarding the implementation of LS estimation, Juricek *et al.* [40] state that it is more important to predict accurate future measurements than to estimate the true disturbance. The result is a modified set of KF mean and covariance equations which account for the estimated disturbance input. The bounds or limits of the confidence interval for the prediction are compared against the emergency threshold. Finally, an emergency condition is detected when both the upper and the lower bounds of the confidence interval reach the emergency threshold.

The following conditions, assumptions, and constraints apply to the research presented in [40]. Predictions are calculated after a fault or abnormal situation has been detected. Prediction error compensation only considers large sustained disturbances, e.g. ramp and step, as input to the state equation. The use of two forms of disturbances is justified since they are more likely to cause an emergency limit to be reached. The process is assumed to be described by a linear stochastic state-space model. Additive noise terms are assumed to be white and Gaussian. The state vector is assumed to be observable. The future inputs are assumed to be known and the disturbance estimate is assumed to be constant over the prediction window. The steady state implementation allows for the LS parameters to be computed offline. The LS estimation results in more accurate predictions. In simulation, the initial time-step of the fault is assumed to be known.

The simulation results presented by Juricek *et al.* [40] indicate, for a process that can be described by a linear model, that the combined LS/KF method provides good predictions under the condition that the model and the noise statistics are known and there is sufficient data for accurate estimation of the pseudo-disturbance. In contrast, the presence of process nonlinearities, model mismatch, and nonstationary disturbances may result in erroneous predictions. Thus, a mechanism for detecting erroneous predictions is developed. Juricek *et al.* evaluate the accuracy of previously performed predictions through the T^2 statistic. This statistic determines if the residual is zero mean under the assumption that the covariance matrix is correct. The T^2 statistic is then compared against a confidence bound for the T-squared distribution. Predictions are ignored if the prediction accuracy is determined not to be suitable. Other statistical tests regarding the forecasting problem are described in [104]. Although the strategy proposed by Juricek *et al.* is not suitable for complex processes with time-varying disturbances, it is suitable for those that are locally linear and are subject to sustained disturbances, the strategy is useful as long as prediction error and quality are monitored.

Other related works

The research presented in [105] is a minor extension to the work of [40]. Predictions are calculated using an EKF as well as a nonlinear model of the process instead of a KF and a linear model of the process. The first time-step of the unmeasured disturbance input is then calculated by comparing the covariance of the compensated residual against the scaled covariance matrices of the additive noise terms. The EKF method is only partially presented. The LS estimation is derived for a steady state KF and does not consider

process nonlinearities. Moreover, a measure of prediction reliability is not considered. This thesis does not consider the extensions presented in [105] since they are not as thoroughly developed as those of [40].

Lagarias and Aminzadeh [106] solve a linear quadratic Gaussian control problem for multi-stage planning processes through the use of multi-step ahead KF prediction. The proposed strategy differs from the linear quadratic Gaussian problem through the use of matrix weighted linear combinations of KF estimates where the weights account for both prediction accuracy as well as stability. In other words, the method penalizes forecasts for a particular instant in time that vary significantly between successive time-steps.

Yang *et al.* [107] present a predictive maintenance strategy for a DC motor whereby time of failure is predicted using a KF. The proposed strategy propagates predictions over a prediction horizon of one and two time-steps with a sampling interval of one hour. Alarm signals are generated when the KF-based predictions indicate the speed of the DC motor has reached the predetermined failure threshold. The study finds that there should be some margin between the failure threshold and the nominal value of the process. Further, the study finds that the sampling interval should be as short as possible in order to react to abrupt disturbances. Otherwise, the study determines that the observed prediction errors are acceptable by comparing the mean prediction error interval for a specific level of confidence against the prediction horizon.

Prognostics

With respect to prognostics, Juricek *et al.* cite Nomikos and MacGregor [108] for performing predictive monitoring of a batch process using multiway principal component analysis.

A similar strategy is employed for continuous processes by Chen and McAvoy [109]. The purpose of the multiway principal component analysis method is to detect and eliminate faults from progressing and to achieve a more consistent production quality. First, the algorithm extracts information from all historical process variable signals and projects this information onto a lower-dimensional space composed of principal components. Then, as in statistical process control, the future behaviour of the process is monitored by comparing it against limits obtained from past batches that are known to have performed well. This form of multiway principal component analysis is a data-driven prediction technique that requires the batch process to have comparable runs and the detected events to be observable. The multiway principal component analysis method does not, however, calculate time-series predictions of impending conditions in real-time. Moreover, although labelled as such by Juricek *et al.,* the multiway principal component analysis method is not strictly a prognostic method since neither the probability of failure or the remaining useful life are calculated.

More broadly, prognostic methods for dynamic systems are either classified into three major types: experience-based; data-driven; and model-based, or are a hybrid of two or more of the listed types [110,111]. With the exception of the research performed by Nomikos as well as MacGregor and Frank, Juricek *et al.* also cite various publications related to diagnostics rather than prognostics. A better understanding of the state-of-the-art in prognostics is obtained in the survey performed by Jardine [29] and the literature review performed by Butler [110].

Jardine presents a thorough review of machinery diagnostics and prognostics [29]. Jardine states that predictive maintenance decisions are based on one of two measures: remain-

ing useful life, or probability of operating without a failure over some prediction horizon. The majority of prognostic papers cited by Jardine relate to measuring remaining useful life. Further, Jardine categorizes prognostic methods into three categories: statistical, artificial intelligence, and model-based.

Butler presents a thorough background on condition-based maintenance and prognostic methods [110]. In condition-based maintenance, maintenance activities are only performed when there is objective evidence of an impending fault or failure condition. Further, condition-based maintenance takes into consideration safety, reliability, and cost. Condition-based maintenance may incorporate diagnostic and/or prognostic strategies and often employ some form of remaining useful life estimation. Thus, as in [29], Butler also focuses on remaining useful life rather than probability of operating within a safe operating region. Butler discusses the requirement for prognostics incorporating "real" predictions that describe the evolution of either a signal of interest or a fault indicator. Butler states that uncertainty is the primary difficulty for calculating predictions. Moreover, there are two issues when considering uncertainty: representation and management. Representation is the ability to model uncertainty in various forms from various sources whereas management is the ability to shrink the uncertainty bounds as a fault evolves [111].

As with Jardine, Butler categorizes prognostic methods into three categories by citing Vachtsevanos *et al.* [111]: experience-based, data-driven, and model-based approaches. These categories parallel those listed in Jardine with the artificial intelligence category of Jardine including hybrid methods that are both data-driven and model-based. Finally, Butler lists three metrics for comparing the performance of prognostic algorithms as: prognostic horizon, relative accuracy, and Alpha-Lambda performance, i.e. a measure that

evaluates whether the algorithms remain within the desired performance levels relative to the actual remaining useful life.

2.2 Safety Instrumented and Shutdown Systems

Within the nuclear industry, safety systems are responsible for:

- ensuring the return to a safe state of a potentially hazardous system;
- removing residual energy from a potentially hazardous system; or
- limiting the consequences of anticipated operational occurrences (AOOs) and design basis accidents (DBAs) [10].

In other words, safety systems are responsible for actuating fail-safe components that conform to the "Control, Cool and Contain" principle: control the reactor power level, cool the residual heat produced by the fission chain reactions, and contain the radioactivity.

Safety systems can be grouped into those that are for protection, actuation, and support. Protections systems, as introduced in Section 1.1, are those systems that monitor the operation of the reactor, and, upon detecting abnormal conditions, automatically initiate actions to prevent unsafe conditions from occurring [10]. In general, protection systems utilize simple algorithms or functions when making safety-critical decisions, e.g. threshold-crossing events [112]. That said, the complex task of designing a protection system must not be understated. Although the functionality within the protection system is simple, protection system design takes into consideration a variety of other safety-related criteria, including those of defence in depth. Moreover, the calculation, or best estimate, of thresholds for the detection of abnormal and accident conditions involves complex safety analysis

code, including thermal-hydraulic and neutron-kinetics codes, as well as uncertainty analysis [113].

One of the primary objectives of this research is to investigate the functional enhancement of protection systems that are responsible for shutdown. This section presents a review of literature related to nuclear safety, regulations and standards, the enhancement of SDSs with respect to response time, and the development and design of CANDU SDS1 protection systems. This section also introduces literature related to optimal alarms, as these methods can be utilized to assess and improve upon the quality of safety-related decisions. This material is an extension of the background included in Section 1.1, e.g. the concepts of safety margins, TSPs, safety limits, and operating conditions.

2.2.1 Regulations and standards

Protections systems can be considered as a form of SIS. These SISs are prominent in the transportation, energy, aerospace, medicine, and defence industries. An SIS is defined as *"implementation of one or more safety instrumented functions. An SIS is composed of any combination of sensor(s), logic solver(s), and final element(s) [114]."* This definition is consistent with that of International Electrotechnical Commission (IEC) standard IEC61508 and IEC61511, with IEC61508 providing general requirements for functional safety whereas IEC61511 focuses on SISs for the process industry sector [115, 116]. The definition of SISs is more complete alongside the definition of a safety instrumented function (SIF). An SIF is defined as *"a safety function with a specified safety integrity level which is necessary to achieve functional safety [114]."* Moreover, a safety function is defined

as *"a function to be implemented by an SIS, other technology safety-related system, or external risk reduction facilities which is intended to achieve or maintain a safe state for the process with respect to a specific hazardous event [114]."* It is further stated within IEC61508 that the logic solver of an SDS may include software and is assumed to be either electrical, electronic, or programmable electronic. IEC61508 also provides guidance regarding the life-cycle requirements for hardware and software of the logic solver, e.g. risk analysis and system realization.

In addition to the above IEC standards, there exist two standards that are more specific to the nuclear industry: IEC61513 and IEC62138 [117,118]. IEC61513 provides general requirements for instrumentation and control systems that are important to safety within the NPP. This standard covers systems that may include hard-wired electro-mechanical, solid-state, or even computer-based equipment. Moreover, IEC61513 includes requirements that range from broad recommendations to component level specifications. IEC62138 instead focuses on the software aspects of computer-based systems that may perform SIFs within NPPs. More precisely, IEC62138 provides requirements for software that is considered either category B or C as per IEC62304, i.e. systems for which non-serious injury, serious injury, or death is possible. These software aspects relate to IEC61513 in the same manner as the third section of IEC61508 relates to the first section of IEC61508.

Another somewhat related IEC standard is IEC61131 since it specifies requirements for programmable controllers, including programming languages and functional safety [119]. Although IEC61131 is a more general standard, it is the standard for the programming languages that are available within the Tricon v9 PLC that is utilized within the experiments of this dissertation. Thee above IEC standards are generally well agreed upon through-

out the international nuclear power generating community. The standards are therefore often reinterpreted within the country-specific regulations and guidelines for NPP design, development, research, and operation.

The IAEA also provides a number of publications that are specific to the nuclear industry with application to power generation as well as medical isotope production. A variety of power generation related IAEA publications are cited in Section 1.1. These publications explicitly define, describe, and discuss all matters related to the appropriate use of nuclear energy. The publications also include country-specific cases, and experience with all aspects of design, development, and operation. For example, safety related instrumentation is discussed in [9], modernization of instrumentation and control system is covered in [32,33], the calculation of safety margins in [120], and a glossary of safety definitions is even provided in [10]. Although there are no technical documents related to the use of prediction algorithms in SDSs, numerous documents guide the development of instrumentation and control systems that are important to safety including [121] and one report addresses the problem of prognostics with respect to structures, systems, and components [31].

2.2.2 CANDU shutdown systems

Within an NPP, control systems may provide some degree of safety protection since these systems are responsible for maintaining the operation of the plant. Special safety systems, however, are more specifically defined as systems that implement one or more SIFs and are composed of a combination of sensors, logic solvers, and final elements, i.e. an SIS as illustrated in the conventional shutdown logic of Figure 2.1 [7]. There are two shutdown-

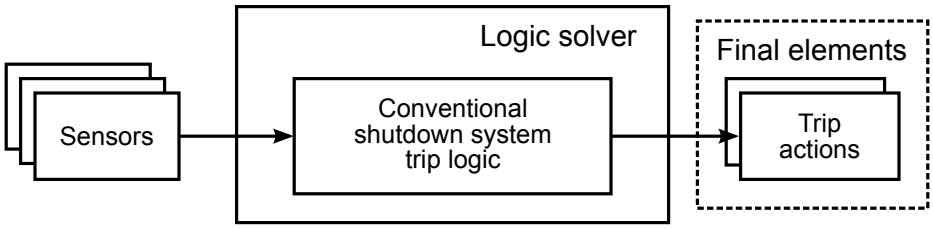

Figure 2.1: The conventional SDS trip logic within the context of safety instrumented systems (SISs).

related SISs in CANDU NPPs. The primary system, SDS1, consists of mechanical shut-off rods while the secondary system, SDS2, injects a neutron absorbing solution into the moderator via liquid poison injection system. Each SDS monitors a set of safety parameters that include neutronic as well as process signals. Further, either system is capable of shutting down the reactor and maintaining shut down for all design basis events [7].

The two shutdown systems, SDS1 and SDS2, of CANDU NPPs are designed in compliance with Canadian Nuclear Safety Commission (CNSC) regulations. General performance and design requirements state that the two SDSs are to [7]:

- be independent, diverse, redundant, and testable;
- incorporate diverse, physical and operational independence;
- demonstrate a target unavailability of less than 10^{-3} years per year including availability, testing, and maintenance;
- provide shutdown capabilities regardless of electrical power supply condition;
- have consistent safety capabilities in all operating and failure modes, i.e. failed components must fail to a safe state;
- prevent disabling of manual operator shutdown capabilities, and respond to redundant and remote location manual shutdown; and

- be effective and independent of normal process, safety, or special safety systems.

Acting alone, each SDS ensures that: the reactor is rendered and maintained sub-critical; the reference dose limits are not exceeded; and a loss of primary heat transport system integrity shall not result from any fuel failure mechanism, in the event prompt shutdown is required. In addition, shaking due to a design basis earthquake must not prevent nor slow shutdown system actuation beyond predetermined safety analysis limits. This shaking is not, however, monitored as a safety parameter within the CANDU SDS [122].

SDS1 is the primary method of terminating reactor operation when specific safety parameters are detected to have reached an abnormal condition. SDS1 reduces the capability of nuclear fission reactions within the core through the release of spring-assisted gravity-drop shut-off rods [7]. The shut-off rods are composed of the neutron absorbing material cadmium. SDS1 has three independent channels designated D, E and F. Each channel is responsible for detecting an abnormal condition given a predetermined set of safety parameters. In addition, each channel is responsible for de-energizing a set of relays that control direct current clutches for the release the shut-off rods into the reactor core. This triplicated design ensures that a trip occurs even when a component from a single channel or a power supply fails. By these means, a single failure can not incapacitate or spuriously initiate shutdown actions. Moreover, the triplicated design allows for periodic testing of the individual channels [7].

The redundant outputs of the SDS are generally combined using either local or general coincidence voting. These two voting configurations differ in that k-out-of-n, abbreviated $koon$, channels of the SDS must trip via either: k of the same safety parameters; or a

combination of any k safety parameters, over the n channels respectively for the local and general configurations. In referring to coincidence trip logic, the variables k and n are separate from the definitions provided in the nomenclature. The logic for CANDU SDS1 operates using general coincidence. General coincidence logic requires, prior to initiating the shutdown procedure, that two out of three (2oo3) channels have detected an abnormal condition. Moreover, the detected abnormal conditions are not required to occur for the same safety parameter over the two channels. Thus, if any two parameters are beyond the corresponding TSPs, SDS1 initiates the shutdown procedure [7]. SDS1 and SDS2 operations differ when more than one trip parameter is beyond normal operating range. Although both SDS1 and SDS2 use a 2oo3 voting mechanism, SDS2 requires that the two parameters that indicate and abnormal condition be produced by the same parameter within each of the separate channels, i.e. local coincidence [7].

The trip signal of SDS1 includes a seal-in logic circuit in order to prevent the trip decision from being reversed. The seal-in logic is the same as those of ladder logic circuits and is essentially a latch. For de-energize to trip, a trip input is connected to the normally closed trip signal. The trip input opens the final trip action contact as well as a corresponding normally closed seal-in trip contact that is installed in series with the trip signal. Upon de-energizing the trip signal, the normally closed seal-in trip contact opens and, no matter the value of the trip signal, the trip action remains de-energized and active. The three independent channels of SDS1, D, E and F, have completely independent power supplies, parameter sensors, and other instrumentation, trip computers, and annunciation devices [7]. Shutdown rods are divided into two banks. Each bank is supplied with redundant power supplies. The shut-off rods are suspended above the reactor core by energized direct

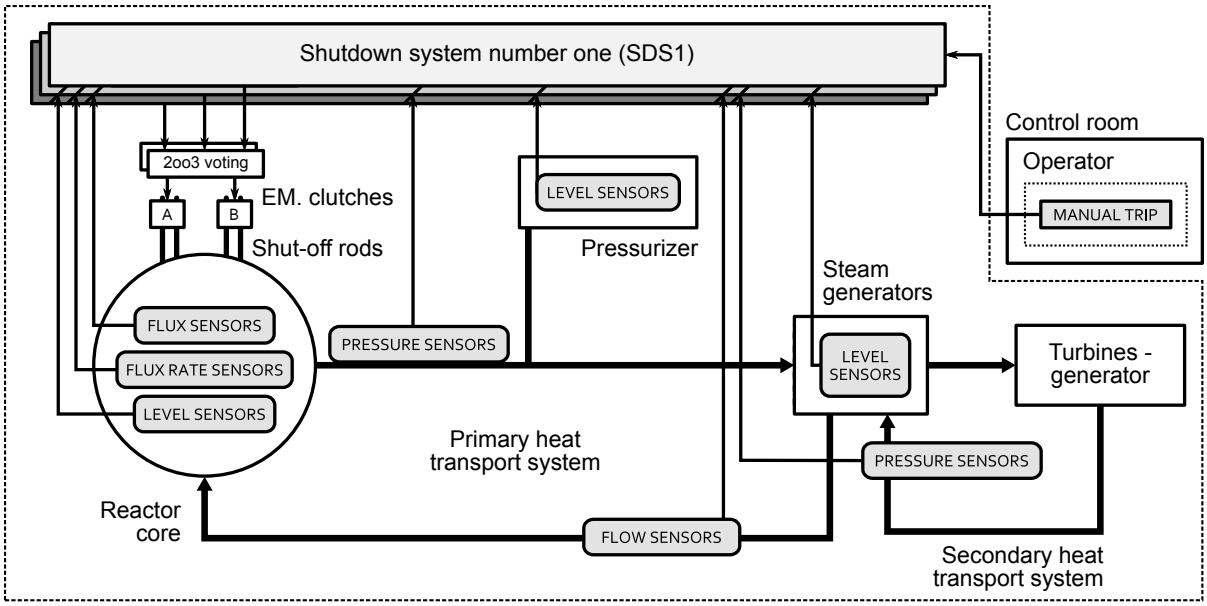

Figure 2.2: CANDU SDS1 safety parameters and related subsystems.

current clutches and coincident logic. Each clutch coil is held energized by the contacts of a separate relay. If a single relay fails, the remainder of the shut-off rods will drop into the reactor core [7].

The safety parameters that are monitored by SDS1 include neutron power, rate log neutron, heat transport system flow, heat transport system pressure, reactor building pressure, pressurizer level, steam generator level, steam generator feed-line pressure, and moderator level. These parameters and associated systems are illustrated in Figure 2.2. There are therefore nine measured variables which must remain within predetermined ranges or corresponding TSPs in order for the NPP to remain in a non-shutdown state. Moreover, some of these nine parameters include both high and low TSPs. The selection of these variables is performed to protect against all categories of process failures [7]. In addition, SDS1 may be activated manually by an operator from the main control room or secondary control area [123].

This research focuses primarily on the steam generator level safety parameter as well as the corresponding SGLL trip condition. The SGLL condition is specifically effective for protecting against secondary side failures including secondary side heat removal. Without secondary side heat removal, the energy transfer from the primary heat transport system to the steam generators, and subsequently the turbines, is disabled. Further, the mechanical structure of the steam generators may be compromised. This parameter is conditioned out at low neutron power level.

Within SDS1 and SDS2, one trip computer is utilized per channel. The trip computers are digital platforms that have replaced analog trip comparators and relay logic used in previous plants. Final 2oo3 voting, seal-in routines and shut-off mechanism actuation is performed using various relay circuits [124]. The relay circuits are controlled directly from the digital outputs of SDS1 and SDS2. The required insertion time of the shut-off rods following a trip detection is less than or equal to two seconds. Of this total time, the execution of the software within the logic solver of SDS1 is expected to be less than 100ms not exceeding 200ms. When SDS1 is in a tripped state, not more than two shut-off rods should be fully withdrawn. Reactor poison removal procedures and adjuster and mechanical control absorber withdrawal are disabled to ensure maximum shutdown capabilities. Also the deuterium moderator system is isolated from the reactor core to prevent the addition of pure moderator to the poisoned moderator. Conversely, when SDS2 is in a tripped state the same measures are taken and shut-off rods withdrawal is disabled.

2.2.3 Time-to-trip and shutdown system response time

Conventional NPP SDSs have relatively simple designs that rarely undergo functional enhancement. This is true even when the underlying technologies are being replaced or modernized. There are therefore limited number of events, reports, and studies related to reductions in time-to-trip or for achieving early shutdown. Although the timely activation of protection systems has always been considered during NPP design, the earliest known effort to reduce, or minimize, time-to-trip dates back only to the 1970s where reduced time-to-trip was stated as a benefit for modifying existing SDSs to include solid state devices [125]. Since then, with regards to regulations, a reduction in the technical specification for time-to-trip occurred as a result of response time testing at Peach Bottom NPP in 1980. This reduction resulted in excess critical power ratio without subsequent power uprating [126]. Another initiative to reduce time-to-trip was the removal of serially-connected redundant time-delay relays to meet existing technical specifications at Kewaunee NPP in 1992 [127].

During the 1980s, computerized trip computers were introduced within the NPP automatic protection systems. These computerized SDSs differ in operation from non-computerized systems in that they execute at predetermined regular intervals known as scan, or execution, intervals. For example, the computerized SDSs of CANDU SDS1 designs are required to produce a trip decision every 100ms [128, 129] in contrast to the decisions produced by non-computerized SDSs that include only a propagation delay. In either case, however, execution intervals and propagation delays demand only a small fraction, approximately $100 - 200$ms, of the entire amount of time required to insert sufficient

negative reactivity into the reactor core, between $1500 - 2000$ms for SDS1. The remainder of the time is largely required for the mechanical drop or injection of neutron absorbing materials.

Although computerized SDSs are designed to meet the same regulatory requirements governing existing SDSs [130], delays in response time became a concern in the 1990s due to the random nature of hardware failures within the trip computers, and the possibility of programming errors during development [131]. As a result, verification and validation (V&V) procedures were established to ensure clarity and traceability of SDS designs. At the same time, major efforts were undertaken to develop safety-critical fail-safe software that was of the highest possible quality. One such effort involved the development of SDS1 for the Darlington CANDU NPP [13]. Since then, many studies have investigated methods for the testing as well as V&V of SDS software and hardware [132].

Most recently, a team of researchers developed a status and risk monitoring system towards shortening protection system response time at Paks NPP in Hungary [133]. In addition, an unspecified change in shutdown instrumentation has been suggested to improve safety margins with respect to a specific accident and to ultimately ensure an earlier trip for an advanced CANDU reactor design [22]. Recent SDS research has also focused on reducing time-to-trip by replacing CPU/software implementations with faster, application specific FPGA/hardware implementations [18]. These replacements take advantage of the parallel processing capabilities of FPGAs over the sequential/limited-parallel processing capabilities of CPUs. Moreover, the use of FPGAs in NPPs has garnered commercial interest from the company Radiy in Ukraine [134]. The replacement of CPU-based systems with FPGA-based systems, however, is also generally performed without modification to

the existing trip decision-making algorithm or structure of the SDS logic [16, 135, 136].

Delays in time-to-trip or SDS response time

Although relatively small increases in time-to-trip can result in significant increases in heat production within the reactor core, no major accidents in the nuclear power industry are known to have resulted from delays in the shutdown decision-making process. That being said, the sequence of events for the Chernobyl NPP accident of 1986 did include two events that are related to time-to-trip. The events are: the intentional disregarding of trip signals by personnel; and a temporary increase in fission reactions upon insertion of the control and shut-off rods. Thus, the Chernobyl accident exemplifies the need for fast insertion of negative reactivity into the reactor core. In fact, the "severe shocks" reported during the accident occurred less than one minute after the manual trip button was pressed and the rods became stuck half-way into the reactor core [137].

One far less catastrophic event that was the direct result of an increased time-to-trip occurred at James A. FitzPatrick NPP in 1996 [138]. The root cause of the increase in time-to-trip, detected during periodic protection system timing tests, was a generic issue with the pilot solenoid valves for releasing neutron absorbing rods into the reactor core. The plant was allowed to return to operation following a five day shutdown for repairs. Another case of increased time-to-trip due to a generic issue was the slow response of reactor trip breakers at Calvert Cliffs NPP and Oconee NPP in 1985 [139]. The root causes of these increases in time-to-trip, which were also detected during response time testing, were the mechanical slipping of an armature toward a pole face, and the improper replacement of mounting hardware causing mechanical binding. The amounts of downtime for these cases,

however, are not known.

2.2.4 Optimal alarms

The combination of prediction and safety critical systems requires the use of highly accurate prediction algorithms. In a study by Martin, a KF-based predictor is combined with an optimal alarm for detecting level-crossing events, herein referred to as threshold-crossing events [41]. Optimal alarms are those which produce minimal false alarms for a fixed detection probability. To accomplish this, Martin finds the optimal area under the receiver operating characteristic (ROC) curve; ROC is a statistical tool that is used in hypothesis testing and decisions making theory that essentially relates TPR to FPR. The optimal alarm condition is a decision boundary based upon a likelihood ratio criterion. Optimal alarm regions must be approximated since they cannot be expressed in closed form when considering all of the time-steps within the prediction window. The optimal alarm condition provides an upper bound on the false alarm probability. It is expected that the prediction of an extreme value may be an alternative to using a single level based on a decision rule as with cumulative sum, sequential probability ratio test, generalized likelihood ratio, etc. The optimal threshold-crossing predictor has a null hypothesis which includes a predictable critical event whereas, with the three aforementioned tests, the null hypotheses are constructed to detect abrupt changes in model parameters [102].

This dissertation combines and expands on the two motivating works of Juricek *et al.* and Martin towards the development of a predictive automatic protection system that is able to make confident and reliable decisions. For this, the optimal alarm problem is

re-framed in a manner similar to that of Martin to consider the ROC space. An optimal sub-space is then selected as a function of the above-mentioned FPR and corresponding conditional probability. The TPR is calculated for each prediction within the prediction window, rather than for a combination of the predictions within the prediction window as in the case of Martin. This optimization relies on the validity that of the assumption that the prediction errors have a Gaussian probability distribution.

The foundations of optimal alarm theory for the optimal prediction of catastrophes with applications to Gaussian processes are formulated by de Mar in [140], although a KF is not used. The alarm system is said to be optimal if it detects the catastrophic event with high probability, and simultaneously gives a minimum number of false alarms. This statement corresponds directly with the current problem of predictive trip protection for an NPP. The work of de Mar considers the problem of forecasting sea level height. It is stated that the prediction of catastrophic sea levels alone is not a very interesting research problem. It is, however, interesting to consider the detection of these catastrophes without making too many false alarms. The predictive alarms are therefore determined to either be correct if the catastrophe does actually take place at the prediction horizon, and incorrect if the catastrophe does not take place. Thus, the predictive detections include a hypothesis regarding an impending catastrophe. Moreover, the result of this hypothesis can be measured once the system propagates forward in time to the prediction horizon, although, to be clear, de Mar does not investigate the relationship between his work and the theory of hypothesis testing.

Optimal alarms consider the proportion of detected or alarmed events as well as the proportion of correct alarms [140]. The optimal alarm then finds the predictor process

and alarm threshold that maximize the conditional probability of the event given the alarm under the constraint that the detection probability is equal to or greater than some predetermined value. Here, the detection probability is given as the conditional probability of the alarm given the event. In other words, with respect to hypothesis testing, the prediction horizon as well as the effective TSP can be selected as functions of the true and false positive and negative event occurrences.

Although Martin includes an example optimal alarm design, he does not specify the application for the design and instead cites similar optimal alarm research for auto-regressive moving average (with exogenous input) systems by Svensson [141]. Svensson, in turn, cites the work of de Mar, and also cites the detection of abrupt changes work of Basseville and Nikiforov [102]. Optimal alarm theory has more recently been applied or investigated for various other applications including earthquake prediction in [142], mining alarms in [143], and general industrial alarms in [144].

Chapter 3

Prediction under Uncertainty for Linear-Time-Varying Systems

The fundamental objective of this research is the development of an algorithm that predicts future values of safety parameter measurements. Safety parameters are the signals that are transmitted by safety sensors to be monitored by SDSs. The subsystems associated with the safety parameters are herein referred to individually as a system. In general, prediction algorithms may be composed of, but are not limited to, any one or a combination of the linear, nonlinear, adaptive, data-, or model-based algorithms as discussed in Section 2.1.1. Within this research, preference is given to model-based prediction algorithms that utilize existing knowledge regarding the mathematical models, operating conditions, and dynamic characteristics of the system and associated safety parameters. Preference is also given to prediction algorithms that consider stochastic descriptions of uncertainty, i.e. those uncertainties that are not defined precisely but are instead defined statistically through

the use of probability distributions. These descriptions of uncertainty, in turn, describe the uncertain behaviour of the system at current and future time-steps.

It is expected that the above objective will result in a prediction algorithm that is able to calculate the multi-step-ahead future values of safety parameter measurements for a system that may have time-varying parameters while taking into consideration various sources of uncertainties. Towards this objective, this chapter focuses specifically on prediction algorithms that are KF-based. The KF is selected since it conforms to the criteria discussed in the previous paragraph and is compatible with the state-space form of system modelling, a form that is common within predictive control literature [99]. In addition, the KF is well-established and is supported by vast bodies of related literature and applications, some of which are reviewed in Chapter 2.

This chapter introduces discrete-time stochastic state-space modelling as well as discrete-time KF-based estimation of system states and measurements for a system with LTV parameters. The KF-based state estimation procedure is then extended to both the multi-step-ahead state and measurement prediction problems. This extension results in two separate KF-based prediction algorithms. The first is a point-prediction algorithm that calculates the mean value of the expected future state and measurement. The second is an interval-prediction algorithm that calculates both the mean value as well as a confidence or prediction interval as an upper and lower bound of the expected future state and measurement. The selection of initial conditions for the estimation and prediction problem is also discussed.

This chapter identifies a number of considerations that are to be addressed when extending KF functionality to the multi-step-ahead prediction problem. The primary focus

of prediction is to obtain accurate descriptions of the uncertainty between the true and assumed model. This accuracy is improved through the use of the ALMF algorithm to estimate the state and measurement noise covariance. This chapter also investigates the effect that these descriptions of uncertainty have on the accuracy of the calculated mean estimates and predictions as well as the associated covariances, a consideration that is often overlooked within the KF-based state estimation literature. These considerations prompt further prediction algorithm development within subsequent chapters.

In summary, this chapter combines KF-based state and measurement prediction as well as ALMF-based noise covariance estimation to address the multi-step-ahead point- and interval- prediction problem. This combination of KF and ALMF algorithms allows for the KF to consider time-varying model parameters as well as time-varying descriptions of uncertainty. The ALMF noise covariance estimation algorithm also provides a mechanism for ensuring accurate interval-predictions since both the mean value of the estimates as well as the confidence intervals are functions of the estimated noise covariances. This is the first known study that applies the ALMF noise estimation procedure within the multi-step-ahead interval-prediction problem for time-varying systems.

In order to be somewhat succinct, this chapter does not cover the vast body of literature including extended methods, implementation considerations, and applications that are related to the KF. For a more complete treatment of KF-based estimation and prediction please refer to one of the following [44, 46, 47].

3.1 State-space Modelling, Prediction, and Uncertainty

This section investigates the relationship between uncertainty descriptions within the state-space form of modelling and the safety parameter prediction problem. This section begins by introducing state-space models for systems that have LTV parameters. The state-space model is then applied to the prediction problem. This section concludes with discussion regarding the effect of the uncertainties on the quality of prediction. These uncertainties include mismatch between the assumed and true system model parameters as well as discrepancies between the measured and true system signals. The former of these two uncertainties is often referred to as model mismatch.

Parameters differ from signals in that signals generally transfer variables between components of a system, e.g. inputs, outputs, states. In contrast, parameters describe the attributes of the various components within the system, e.g. amplitude, phase, or frequency of a sine wave. Signals therefore describe the manoeuvres that are provided to, and actions that are taken by, the components within a system. Signals are assigned values at all points in time, e.g. measurements. Meanwhile, parameters most often have constant values, or alternatively, have values that change as a function of some predetermined signal. Parameters are not necessarily assigned values at all time steps, e.g. parameters that are globally constant or have constant values that are assigned by operating point or region.

It is first assumed that the system can be modelled in the following discrete-time LTV

state-space form

$$x\left[k+1\right] = A\left[k\right]x\left[k\right] + B\left[k\right]u\left[k\right] \tag{3.1}$$

$$y\left[k\right] = C\left[k\right]x\left[k\right] + D\left[k\right]u\left[k\right] \tag{3.2}$$

where $k \in \mathbb{Z}^{n_k \times 1}$ is the discrete time-step or time-index with units s/T_s and T_s is the chosen sampling time. The state-space signals are as follows: $x \in \mathbb{R}^{n_x \times 1}$ is the system state vector, $u \in \mathbb{R}^{n_u \times 1}$ is the system input vector, and $y \in \mathbb{R}^{n_y \times 1}$ is the system measurement vector. Moreover, the state-space parameters are as follows: $A \in \mathbb{R}^{n_x \times n_x}$ is the state matrix, $B \in \mathbb{R}^{n_x \times n_u}$ is the input-to-state matrix, $C \in \mathbb{R}^{n_y \times n_x}$ is the state-to-measurement matrix, and $D \in \mathbb{R}^{n_y \times n_u}$ is the feed-through matrix. The two equations (3.1) and (3.2) are referred to respectively as the state and measurement equation. Here, the term measurement refers to the fact that signal y is generally the output that is transmitted by a physical sensor and is therefore measurable.

The state and measurement equations are combined in the block diagram of Figure 3.1 where q^{-1} is the backward time-shift operator. This diagram illustrates the predictive form of the state equation where the time dependence is between the future state, $x\left[k+1\right]$, and the current state, $x\left[k\right]$, rather than between the current, $x\left[k\right]$, and past, $x\left[k-1\right]$, states as is common within KF literature. One interpretation of the state and measurement equations assumes that the system matrices represent the following specific system components: A for the process dynamics, B for the actuator dynamics, C for the sensor dynamics, and D as a direct feed-through of the manipulating system input, u.

The LTV state-space form of (3.1) and (3.2) differs from the LTI state-space form

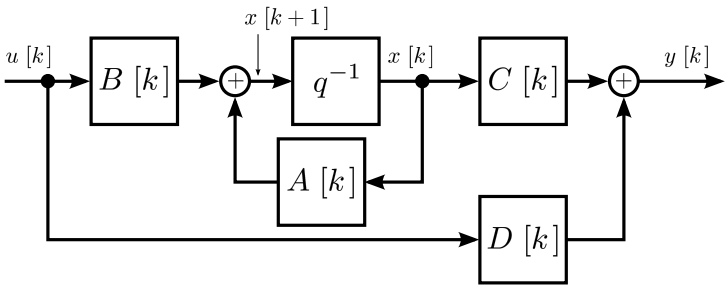

Figure 3.1: Combined state and measurement equations in (3.1) and (3.2) respectively.

that is usually assumed for the standard KF. More specifically, the parameters within the system matrices, A, B, C, and D, vary with time rather than being time-invariant. The LTV form is selected for study since it is a generalization of the linear parameter varying (LPV) system that is the main application studied within Chapter 6 and Chapter 7. In addition, the LTV form allows for a broader range of dynamic processes to be considered as a potential system when compared against either the LTI or LPV forms.

LTV systems are generally assumed to have parameters that are known functions of time whereas LPV systems have time-varying parameters that are dependent on some exogenous input, e.g. an element of the system input, u_θ. Both LTV and LPV systems do, however, have parameters that vary with time. An equivalence between the parameters of the LTV and LPV systems can therefore be established. First, the time-varying system matrices are defined in terms of a time-varying parameter vector. For example, the time-varying state matrix, A, is defined as a function of the time-varying parameter vector, θ, as follows.

$$A\,[k] \triangleq A\,(\theta\,[k]) \tag{3.3}$$

The values of the time-varying parameter vector, θ_u, are then defined as the values of an

LPV parameter vector, θ, as follows

$$\overbrace{\theta_u[k]}^{\text{LTV}} \triangleq \overbrace{\theta(u_\theta[k])}^{\text{LPV}} \tag{3.4}$$

where u_θ is the exogenous input that determines the values of parameter vector, θ. The relationship between the LTV state matrix, A, and the exogenous input, u_θ, is then established directly as follows

$$A[k] = A(\theta_u[k]) \tag{3.5}$$

where parameter vector, $\theta_u[k]$, is the time-dependent equivalent of the exogenous-input-based parameter vector, $\theta(u_\theta[k])$. These definitions and relationships hold for the remaining system matrices, B, C, and D.

In representing LPV systems as LTV it is not possible to calculate the parameters of LPV systems in advance if the future exogenous inputs, on which the parameters are dependent, are not known. This contrasts the parameters of the LTV model which are known functions of time and are therefore able to be calculated within the current time-step, k, for future time-steps, $k+i$ where $i = 1, \ldots, N_p$ and N_p is a positive integer representing a number of time-steps that is the length of the prediction window. It is assumed within this work, therefore, that the parameters of the LTV system are not explicit functions of time and cannot be calculated in advance.

Regarding the prediction problem, the state equation in (3.1) inherently provides a means for propagating the state vector to future time-steps, i.e. state predictions, as

follows

$$\begin{aligned} x[k+i] &= A[k+i-1]\,x[k+i-1] + B[k+i-1]\,u[k+i-1] \\ &= \prod_{j=0}^{i-1} A[k+i-1-j]\,x[k] \\ &\quad + \sum_{j_1=0}^{i-1} \prod_{j_2=0}^{k+i-2-j_1} A[k+i-1-j_2]\,B[k+j_1]\,u[k+j_1] \end{aligned} \tag{3.6}$$

where $\prod_{j=0}^{-1} = 1$ and $i = 1, \ldots, N_p$ is the time-step of prediction with N_p again representing the length of the moving prediction window. This final time-step, N_p, is also referred to as the prediction horizon. Given state predictions, it is possible to calculate measurement predictions by modifying the measurement equation in (3.2) as follows

$$y[k+i] = C[k+i]\,x[k+i] + D[k+i]\,u[k+i] \tag{3.7}$$

where i is as defined for (3.6).

The difficulty in calculating predictions using (3.6) and (3.7) is that the two equations are functions of an unknown and unmeasurable state vector, $x[k]$. In addition, the future model parameters, $A[k+i]$, $B[k+i]$, etc., are not known because the values of the parameters are dependent on unknown future system inputs, $u_\theta[k+i]$. It is therefore necessary to:

- approximate the unknown states of the system at the current time-step;
- make assumptions regarding the future model parameters and system inputs; and
- quantify or describe uncertainties within the state vector predictions that are a result

of the aforementioned assumptions.

First, given that state-space model of the underlying system can be constructed and the parameters of the model estimated, it is possible to approximate the unknown state vector, $x[k]$, through the use of a state observer. More precisely, state observers estimate the unknown state vector, $\hat{x}[k]$, as a function of system measurements and model parameters given that the LTV system model meets the following condition for uniform $N_{\mathcal{O}}$-step observability [145]

$$\operatorname{rank}(\mathcal{O}[k]) = \operatorname{rank}\left(\begin{bmatrix} C[k-N_{\mathcal{O}}] \\ C[k-N_{\mathcal{O}}+1]A[k-N_{\mathcal{O}}] \\ \vdots \\ C[k-1]\prod_{j=1}^{N_{\mathcal{O}}-1}A[k-j-1] \end{bmatrix}\right) = n_x \forall k \tag{3.8}$$

where $\mathcal{O}$ is the observability matrix and $N_{\mathcal{O}} \geq n_x$.

The KF is one form of state observer, or estimator, that calculates state estimates which are optimal in the minimal mean square sense of the state estimation error [27]. Thus, the KF is introduced within the prediction algorithm as a state observer rather than more directly as a state or measurement predictor. The function of the KF is then extended to the state or measurement prediction problem.

In the role of state observer, the KF assumes a system that is similar to the state-space form of (3.1) and (3.2) but also includes two additional additive noise terms. More specifically, it is assumed within the KF that the system can be modelled in the form of the following discrete-time LTV stochastic state-space model with additive state and

measurement noise sequences

$$x[k+1] = A[k]\,x[k] + B[k]\,u[k] + v_x[k] \tag{3.9}$$

$$y[k] = C[k]\,x[k] + D[k]\,u[k] + v_y[k] \tag{3.10}$$

where $v_x \in \mathbb{R}^{n_x \times 1}$ is the state noise vector, $v_y \in \mathbb{R}^{n_y \times 1}$ is the measurement noise vector, and all other parameters are as defined for the deterministic case in (3.1) and (3.2). Equations (3.9) and (3.10) are referred to as the stochastic state and stochastic measurement equations respectively. These equations are considered to be stochastic since the two noise terms are assigned probability distributions rather than being deterministic, or precise, values like those of the model parameter and the intended system input, u.

The stochastic state and measurement equations are combined in the block diagram of Figure 3.2. This diagram differs from the deterministic case of Figure 3.1 in that the two noise terms are added as inputs to the state and measurement signals. This diagram illustrates that the state noise has a direct influence on the state vector. Alternatively, the dimension of the state noise is sometimes assumed to differ from that of the state vector. For example, if the state noise affects the system in the same manner as the system input u, the state noise is multiplied by the input-to-state matrix B as $v_x = Bv_u$ where $v_u \in \mathbb{R}^{n_u \times 1}$. Thus, the input noise v_u may have different statistical properties than those of the state noise v_x.

The two additive noise terms, v_x and v_y, enable the KF-based state observer to consider the following uncertainties:

- a model that may not be an exact parametric or structural representation of the true

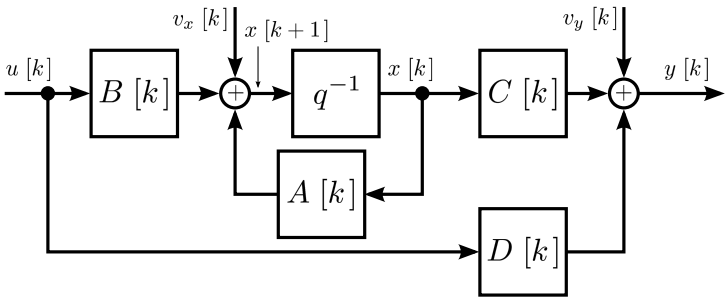

Figure 3.2: Combined stochastic state and measurement equations in (3.9) and (3.10).

system, i.e. model mismatch; and

- system input, state, and measurement signals that may include disturbances or noise with respect to the true signals of the system.

Within the standard KF, the two additive noise terms are assumed to belong to a white Gaussian probability distribution. More precisely, the KF is provided only the statistical properties or moments of the probability distribution for each of the additive noise terms and not the exact values of the noise samples. In addition, within certain elements of the state vector, it is not possible to measure the additive noise since the noise signals are internal to the system, i.e. unmeasurable. Thus, the KF-based state observer utilizes the structure of the model to estimate the state vector. The observer also uses the statistical descriptions of noise to filter the uncertainties within in the model parameters and measured signals with respect to the true system parameters and signals.

Returning to the prediction problem, the multi-step-ahead prediction equation of (3.6) is able to propagate, in a deterministic manner, an uncertain but optimal KF-based state estimate to a future time-step, i.e. an uncertain state prediction, $\hat{x}\,[k+i]$. This state prediction is not optimal, however, due to the predictions being calculated within the current time-step, k, when the assumed future model parameters and signals are not known

and may not represent exactly the true future system and signals. The result of these assumptions is an equation for propagating the state vector that is different than the true behaviour of the system, i.e. $\hat{x}\,[k+i]$ is not expected to be equal to $x\,[k+i]$. For example, state propagation may be performed by assuming that the future system matrices and inputs are equal to the values within the current time-step, k, as follows.

$$\hat{x}\,[k+i] = A\,[k]\,\hat{x}\,[k+i-1] + B\,[k]\,u\,[k] \tag{3.11}$$

Moreover, measurement predictions calculated using (3.7) are also not optimal, i.e. $\hat{y}\,[k+i]$ is not expected to be equal to $y\,[k+i]$, for the same reasons as for the state prediction and also since the measurement prediction is a function of the uncertain state prediction.

The assumptions that cause the predictions not to be optimal are similar to the modelling assumptions that are listed above for the KF-based state observer. In fact, during state estimation the state estimate $\hat{x}\,[k]$ is not expected to be equal to the true system state $x\,[k]$. It is possible, therefore, to extend the functionality and stochastic uncertainty descriptions of the KF-based state observer to the measurement prediction problem. This is accomplished in the same manner as for state estimation. In other words, by including various model and signal uncertainties within the statistical properties that are defined for the additive noise signals, v_x and v_y, for the stochastic state-space model of (3.9) and (3.10). In this manner, the KF is not only able to quantify a probabilistic description of uncertainty in the state estimates but can also quantify the uncertainties in the propagated state and measurement predictions. These concepts are formulated in the remaining sections of this chapter.

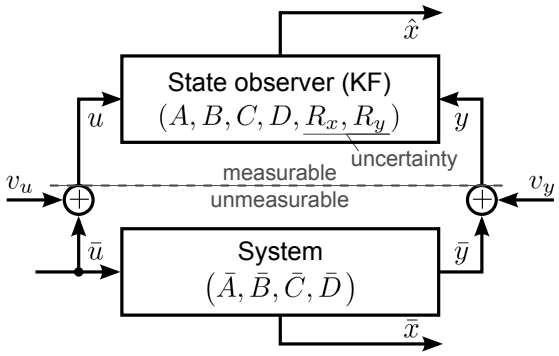

Figure 3.3: Connectivity between the system and a state observer, which may be KF-based, within the context of state estimation.

3.2 Kalman-Filter-Based State Estimation

The KF is able to perform state estimation by minimizing the mean squared error between the true values and the estimates of the system states. This minimization is a function of the system input and measurement as well as the model parameters as defined in (3.9) and (3.10). A simplified diagram of the state estimation problem is included in Figure 3.3. This diagram identifies the connections that are made between the state observer and the signals of the system. This diagram also indicates that the state observer is provided model parameters and receives system signals or variables that are not necessarily exact to the true system. More specifically, the true parameter and variable symbols are denoted by a bar accent, $\bar{\bullet}$, whereas the model parameter and measured signal symbols are included without accent marks.

KF state estimation accounts for uncertainties in the model parameters and input signals of the system through state noise covariance $R_x \in \mathbb{R}^{n_x \times n_x}$, and for uncertainties in the measurement signals through measurement noise covariance $R_y \in \mathbb{R}^{n_y \times n_y}$. These two parameters are the covariance matrices for the two additive noise terms v_x and v_y, from

(3.9) and (3.10) respectively. The effects of input noise v_u are assumed to be combined into v_x as a function of the input-to-state matrix, B, as stated in the discussion regarding Figure 3.2. The two noise vectors, v_x and v_y, are assumed to be white Gaussian noise sequences that satisfy the following statistical properties

$$E\{v_x[k]\} = E\{v_y[k]\} = 0$$

$$E\{v_x[k]\, v_x'[j]\} = \begin{cases} 0 & k \neq j \\ R_x[k] & k = j \end{cases}$$

$$E\{v_y[k]\, v_y'[j]\} = \begin{cases} 0 & k \neq j \\ R_y[k] & k = j \end{cases}$$

$$E\{v_x[k]\, v_y'[j]\} = 0 \quad \text{for all } k \text{ and } j \tag{3.12}$$

with expectation operator $E\{\bullet\}$, mean values $E\{v_x\}$ and $E\{v_y\}$, covariances $E\{v_x v_x'\}$ and $E\{v_y v_y'\}$, cross-covariance $E\{v_x v_y'\}$, and noise covariance matrices R_x and R_y respectively. In addition, $\bullet'$ indicates the transpose of a matrix or vector.

The noise sequences, v_x and v_y, are white in that the sequences are composed of serially uncorrelated samples and the sequence also has zero-mean and finite variance, i.e. a power spectral density that is constant for all frequencies [24]. Further, the noise sequences are Gaussian in that the samples within the sequence are statistically independent with a probability distribution that is completely specified using only the first and second statistical moments, i.e. mean and variance. The noise sequences are assumed to have Gaussian probability distributions due to the central limit theorem. In short, the central theorem

states that the sum of a sufficiently large number of independent random sequences has a Gaussian probability distribution with mean and variance equal to the sum of the means and variances of the sequences [146]. For the case where v_x and v_y are coloured noise, the structure of (3.9) and (3.10) may be achieved by extracting the coloured noise dynamics from the noise terms and augmenting the dynamics into the system state vector [46]. In addition, for non-linear dynamics or non-Gaussian error probability distributions the EKF and UKF may be utilized as discussed in Section 2.1.2.

KFs execute two stages within each time-step; update and predict [47]. Each stage has an associated state estimate $\hat{x} \in \mathbb{R}^{n_x \times 1}$; the updated, or *a posteriori*, state estimate $\hat{x}\left[k|k\right]$ and; the predicted, or *a priori*, state estimate $\hat{x}\left[k|k-1\right]$. The notation $[k|k-1]$ follows conditional probability where the *a priori* estimate is conditioned on information that is available prior to and including time-step $k-1$. The covariance of the state estimation error is then defined as follows

$$P_{\tilde{x}}\left[k|k\right] = E\left\{\tilde{x}\left[k|k\right]\tilde{x}'\left[k|k\right]\right\} \tag{3.13}$$

$$P_{\tilde{x}}\left[k|k-1\right] = E\left\{\tilde{x}\left[k|k-1\right]\tilde{x}'\left[k|k-1\right]\right\} \tag{3.14}$$

for the *a posteriori*, $\tilde{x}\left[k|k\right] = x\left[k\right] - \hat{x}\left[k|k\right]$, and *a priori*, $\tilde{x}\left[k|k-1\right] = x\left[k\right] - \hat{x}\left[k|k-1\right]$, state vectors respectively where $P_{\tilde{x}} \in \mathbb{R}^{n_x \times n_x}$. These state error covariances quantify the second statistical moment or variance of the state estimation error. In other words, the state estimate quantifies the mean expected value, whereas the state error covariance describes the probability distribution within the state-space over which the true system state is expected to belong.

3.2.1 The Kalman filter

The KF includes five equations in total. The first three equations update the state estimates as well as the state error covariances and the latter two equations propagate the state estimates and error covariances forward in time. Within the update stage, the KF gain, $K \in \mathbb{R}^{n_x \times n_y}$, is first calculated as follows.

$$K[k] = P_{\tilde{x}}[k|k-1] C'[k] \left(C[k] P_{\tilde{x}}[k|k-1] C'[k] + R_y[k]\right)^{-1} \tag{3.15}$$

This is the optimal gain that minimizes the mean squared estimation error as the trace of the *a posteriori* state error covariance, $P_{\tilde{x}}[k|k]$. The Kalman gain also maps the measurement space to the state-space. Next, the *a posteriori* state estimate is calculated as follows.

$$\hat{x}[k|k] = \hat{x}[k|k-1] + K[k] \left(y[k] - \left(C[k] \hat{x}[k|k-1] + D[k] u[k]\right)\right) \tag{3.16}$$

This equation calculates the optimal state estimate given the error between the newly acquired system measurements and the *a priori* KF-based measurement estimates. Finally, the *a posteriori* state error covariance matrix is calculated as follows

$$\begin{aligned} P_{\tilde{x}}[k|k] &= E\left\{\tilde{x}[k|k] \tilde{x}'[k|k]\right\} \\ &= E\left\{\left(x[k] - \hat{x}[k|k]\right)\left(x[k] - \hat{x}[k|k]\right)'\right\} \\ &= \left(\mathbb{I} - K[k] C[k]\right) P_{\tilde{x}}[k|k-1] \left(\mathbb{I} - K[k] C[k]\right)' + K[k] R_y[k] K'[k] \end{aligned} \tag{3.17}$$

where the covariance is updated as a function of the KF gain, and $\mathbb{I}$ is an identity matrix of appropriate dimension. Of these three equations, only the *a posteriori* state estimate is a function of system measurements, i.e. is updated according to the system measurements, whereas the two remaining equations are functions of model parameters and covariance matrices only. In other words, the state estimates are updated as a function of the KF-based state estimation accuracy whereas the elements of the Kalman gain vector and the state error covariance matrix are not.

The predict stage includes two equations. The *a priori* state estimate is calculated as follows.

$$\hat{x}\left[k+1|k\right] = A\left[k\right]\hat{x}\left[k|k\right] + B\left[k\right]u\left[k\right] \tag{3.18}$$

This is the model-based propagation of the *a posteriori* state estimate one time-step into the future. The *a priori* error covariance matrix is calculated in a similar manner as follows.

$$\begin{aligned} P_{\tilde{x}}\left[k+1|k\right] &= E\left\{\tilde{x}\left[k+1|k\right]\tilde{x}'\left[k+1|k\right]\right\} \\ &= E\left\{\left(x\left[k+1\right] - \hat{x}\left[k+1|k\right]\right)\left(\hat{x}\left[k+1|k\right] - \hat{x}\left[k+1|k\right]\right)'\right\} \\ &= A\left[k\right]P_{\tilde{x}}\left[k|k\right]A'\left[k\right] + R_x\left[k\right] \end{aligned} \tag{3.19}$$

This propagation is also model-based. Thus, the two predict stage equations are based solely on the parameters of the stochastic state-space system are not optimized or updated. For the full derivation of the KF-based state estimation equations, please refer to [44,46,47].

The *a posteriori* and *a priori* state estimation equations are combined in the block

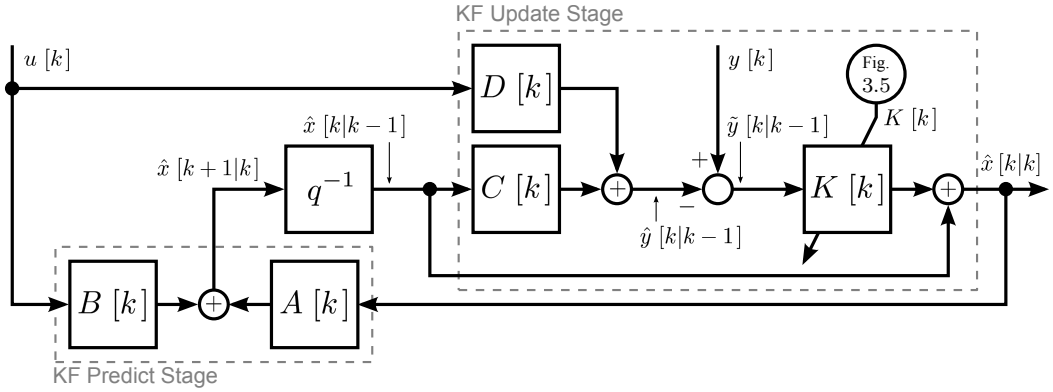

Figure 3.4: Combined *a posteriori* and *a priori* state estimation equations in (3.16) and (3.18) respectively; the angled arrow indicates an adaptive parameter, in this case $K\,[k]$.

diagram of Figure 3.4. In addition, the combined Kalman gain calculation as well as *a posteriori* and *a priori* state error covariance equations are included in Figure 3.5. The connectivity included in Figure 3.4 illustrates that the state estimates are a function of the error between the system measurements and the *a priori* estimate of the system measurement. Thus, the minimization performed by the KF, as illustrated in Figure 3.5, causes the state estimates to track, to some degree, the measurements that are received from the safety sensors installed within the system.

A summary of the KF-based state estimation procedure is provided in Algorithm 3.1 while an overview of the estimation procedure is illustrated in Figure 3.6. Algorithm 3.1 includes a count of the number of operations per loop (OPL) that are required to be calculated for a system with a single output or measurement. The measurement vector is assumed to be scalar for comparison of computational complexity against the algorithms that are developed in subsequent subsections. In addition, a non-scalar measurement would require calculation of the covariance matrix and cross covariances between measurements and also, more importantly, a computationally expensive matrix inverse in (3.15). This

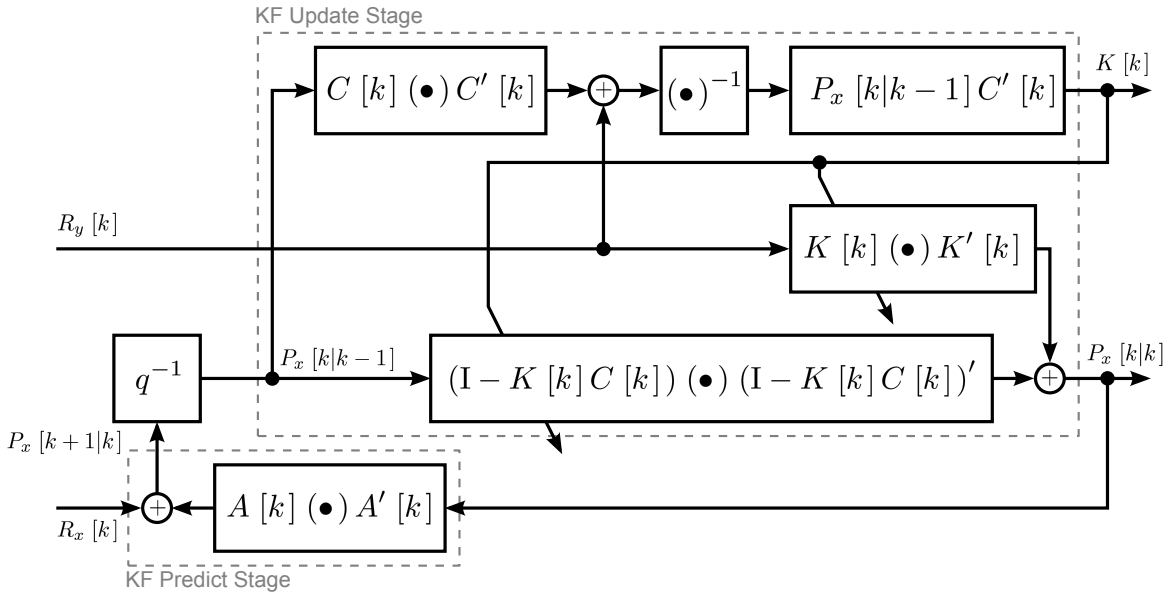

Figure 3.5: Combined Kalman gain equation in (3.15) as well as the *a posteriori* and *a priori* state estimation equations in (3.17) and (3.19) respectively; (•) indicates where the input variable is substituted within the equation of the corresponding block.

assumption allows for flexibility in selecting one of various methods for calculating the inverse within the Kalman gain equation e.g. processing the measurements separately [46]. The OPL tallies the number of multiplication and addition operations for all equation within the repeated loop of the algorithm. This loop includes only the equations that are executed within each time-step of the state estimation procedure. The OPL result may also be referred to as the arithmetic complexity of the algorithm.

A reduction in the number of total multiplication is utilized to improve algorithm performance when calculating symmetric matrices, e.g. $A\,[k]\,P_{\tilde{x}}\,[k|k]\,A'\,[k]$, where the $2n_x^3$ multiplications can be reduced to $\left(3n_x^3+n_x^2\right)/2$ operation and $2\left(n_x^3-n_x^2\right)$ additions can be reduced to $\left(3n_x^3-2n_x^2-n_x\right)/2$ operations. Moreover, scalar division is assumed to be performed by the Newton-Raphson method where for double-precision floating-point arithmetic, i.e. a mantissa of 52 digits plus the dropped leading one, eight multiplications

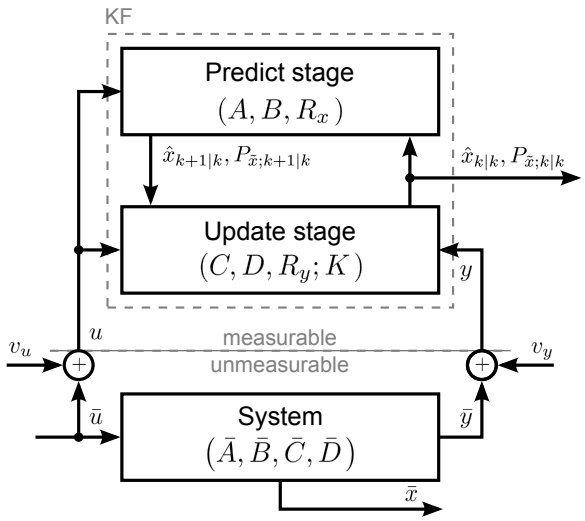

Figure 3.6: Connectivity between the system and the KF-based state estimation procedure of Algorithm 3.1.

Algorithm 3.1 Kalman-filter-based (KF) state estimation, KF_e.

Require: $A, B, C, D, u, y, R_x, R_y$
Initial conditions: $\hat{x}\left[0|0\right], P_{\tilde{x}}\left[0|0\right]$
Result: $\hat{x}\left[k|k\right], P_{\tilde{x}}\left[k|k\right]$

$k = 0$
[Initialization]
$\hat{x}\left[1|0\right] = A\left[0\right]\hat{x}\left[0|0\right] + B\left[0\right]u\left[0\right]$
$P_{\tilde{x}}\left[1|0\right] = A\left[0\right]P_{\tilde{x}}\left[0|0\right]A'\left[0\right] + R_x\left[0\right]$
{propagate $x\left[0\right]$ to $x\left[1\right]$}
loop
$k = k + 1$
{measure $y\left[k\right]$}
[State estimation (update)]
$K\left[k\right] = P_{\tilde{x}}\left[k|k-1\right]C'\left[k\right]\left(C\left[k\right]P_{\tilde{x}}\left[k|k-1\right]C'\left[k\right] + R_y\left[k\right]\right)^{-1}$
$\hat{x}\left[k|k\right] = \hat{x}\left[k|k-1\right] + K\left[k\right]\left(y\left[k\right] - \left(C\left[k\right]\hat{x}\left[k|k-1\right] + D\left[k\right]u\left[k\right]\right)\right)$
$P_{\tilde{x}}\left[k|k\right] = \left(\mathbb{I} - K\left[k\right]C\left[k\right]\right)P_{\tilde{x}}\left[k|k-1\right]\left(\mathbb{I} - K\left[k\right]C\left[k\right]\right)' + K\left[k\right]R_y\left[k\right]K'\left[k\right]$
[State propagation (predict)]
$\hat{x}\left[k+1|k\right] = A\left[k\right]\hat{x}\left[k|k\right] + B\left[k\right]u\left[k\right]$
$P_{\tilde{x}}\left[k+1|k\right] = A\left[k\right]P_{\tilde{x}}\left[k|k\right]A'\left[k\right] + R_x\left[k\right]$
{propagate $x\left[k\right]$ to $x\left[k+1\right]$}
end loop

OPL for scalar y: $6n_x^3 + 10.5n_x^2 + 5n_x + n_x n_u + 2n_u \in O\left(n_x^3\right)$

and seven additions are performed. The count included in Algorithm 3.1 reveals that the computational complexity of the KF-based state estimation routine is cubic with respect to the dimension of the state vector, or $\mathrm{KF}_e \in O\left(n_x^3\right)$ using big O notation.

For the LTI case, with jointly Gaussian distributed state and measurement, the KF is a minimum variance unbiased estimator and is therefore considered to be an efficient estimator [147]. Moreover, under the previously stated conditions, the KF is the best unbiased estimator. This may not, however, be the true in the case of KF-based state estimation for an LTV system. The ability of the KF to efficiently estimate the state of an LTV system must therefore be monitored. It is difficult to monitor directly the efficiency of the filter as efficiency is generally a relative metric. The ability of the filter to produce unbiased as well as consistent estimates can be monitored through the use of statistical testing as is presented in Chapter 5.

3.2.2 Related equations

Aside from the five standard equations, the KF enables the calculation of signals that provide additional information regarding the quality or accuracy of the state estimations. These signals also extend the usefulness of the KF to include measurement estimation and prediction. Three of the additional signals are extracted from the standard KF equations whereas two signals are alternative *a posteriori* interpretations of the standard *a priori* equations.

The first signal is the *a priori* measurement error that is embedded in (3.16). The *a priori* measurement error is equal to the difference between the current measurement and

the *a priori* measurement estimate as follows.

$$\begin{aligned}\tilde{y}\left[k|k-1\right] &= y\left[k\right] - \hat{y}\left[k|k-1\right] \\ &= y\left[k\right] - \left(C\left[k\right]\hat{x}\left[k|k-1\right] + D\left[k\right]u\left[k\right]\right)\end{aligned} \tag{3.20}$$

This measurement error is commonly used in statistical evaluations of KF performance. More precisely, in the case of optimal KF state estimates, the *a priori* measurement error is a white Gaussian sequence. This error is referred to as the innovation, a term that refers to the fact that new information regarding error statistics can be obtained from (3.20) at each time-step given independence between subsequent measurement errors.

The second signal is the *a priori* measurement estimate. This signal is embedded within the innovation calculation of (3.20) and, in turn, the state update equation of (3.16). The *a priori* measurement estimate applies the measurement equation of (3.10) to the *a priori* state estimate as follows.

$$\hat{y}\left[k|k-1\right] = C\left[k\right]\hat{x}\left[k|k-1\right] + D\left[k\right]u\left[k\right] \tag{3.21}$$

This estimate is also a one-step-ahead measurement prediction for time-step k where the state estimate is calculated using only information that is available prior to and including time-step $(k-1)$. Measurement prediction differs from state estimation in that the parameters $C\left[k\right]$ and $D\left[k\right]$ as well as signal $u\left[k\right]$ are assumed to be known. The one-step-ahead measurement prediction can also be calculated within the current time-step, k, for future time-step, $(k+1)$, as $\hat{y}\left[k+1|k\right]$ given again that the future parameters and signals are

assumed to be known.

The equivalent of the *a priori* measurement estimate within the update stage of the KF is the *a posteriori* measurement estimate. The *a posteriori* measurement estimate is the result of applying the measurement equation in (3.10) to the *a posteriori* state estimate as follows.

$$\hat{y}\left[k|k\right] = C\left[k\right]\hat{x}\left[k|k\right] + D\left[k\right]u\left[k\right] \tag{3.22}$$

The *a posteriori* measurement estimate is a filtered estimate of the system measurement that is optimal given that the model parameters and noise covariances provided to the KF accurately represent the true system and additive noise terms. In other words, the *a posteriori* measurement estimate provides an estimate of the measurement that is influenced to some degree by the assumed model on which the KF is based. These properties are also present within the *a priori* measurement estimate of (3.21).

The degree to which the estimates are influenced by either the model or the measurements is determined by the values of R_x and R_y. For example, assuming scalar state and measurement vectors and equal values of innovation, smaller values of R_y, i.e. $R_y \ll R_x$ will result in a larger magnitude of correction being applied to the state estimate. This increase in correction is due to the measurements being more uncertain with respect to the model as specified by the state noise covariance, R_x. This increase in correction may not necessarily, however, result in a reduction in error between the measurement estimate and the true system measurement, $\bar{y} - \hat{y}$, where $\overline{y}$ is the true system measurement.

The final two related equations are reinterpretations of the state error covariances in

the measurement domain rather than the state domain. The result is a measurement error covariance for each of the *a posteriori* and *a priori* measurement errors as follows

$$P_{\tilde{y}}[k|k] = C[k] P_{\tilde{x}}[k|k] C'[k] + R_y[k] \tag{3.23}$$

$$P_{\tilde{y}}[k+1|k] = C[k+1] P_{\tilde{x}}[k+1|k] C'[k+1] + R_y[k+1] \tag{3.24}$$

where $P_{\tilde{y}} \in \mathbb{R}^{n_y \times n_y}$. While measurement estimates quantify mean expected values, the measurement error covariance matrices describe the probability distribution over which within the measurement domain the true system measurements are expected to belong. The *a priori* measurement error covariance is included in the Kalman gain equation of (3.15).

3.2.3 Initial conditions, convergence, model selection, and bumpless transfer

The KF state estimation procedure includes two initial conditions; state, $\hat{x}[0|0]$, and state error covariance, $P_{\tilde{x}}[0|0]$ as provided in the calculation of $\hat{x}[1|0]$ and $P_{\tilde{x}}[1|0]$ in Algorithm 3.1. The initial state estimate is by definition an approximation of the true initial state within the system, whereas the initial state error covariance is an approximation of the error covariance that is consistent with the initial state estimate [148].

Due to the recursive form of the calculations within the KF, the initial conditions have a direct effect on the quality of the KF-based state estimates within the initial time-steps of estimation. This effect fades, however, with every iterative calculation of the Kalman gain

given that the estimations are convergent. The criteria for convergence of KF-based state estimates are discussed by Anderson and Moore [149] where it is stated that the uniform detectability of the following state and state-to-measurement matrix pair, $(A[k], C[k])$ is sufficient for there to exist a bounded sequence of Kalman gains, $K[k]$, such that the *a priori* state estimates are exponentially stable. In addition, the pair $(A[k], C[k])$ is uniformly detectable if there exists $N_{\mathcal{O}}, \underline{N}_{\mathcal{O}} \geq 0$ and constants d, b with $0 \leq d < 1, 0 < b < \infty$ such that whenever

$$\mathscr{D} = \left\| \prod_{i=1}^{N_{\mathcal{O}}} A[k - \underline{N}_{\mathcal{O}} - 1 + i]\, \zeta \right\| \geq d \|\zeta\| \tag{3.25}$$

for a given ζ and k, then

$$\zeta' \sum_{j_1=1}^{N_{\mathcal{O}}+1} \left(\left(\prod_{j_2=1}^{j_1-1} A[k - N_{\mathcal{O}} - 1 + j_2] \right)' C'[k - N_{\mathcal{O}} - 1 + j_1] \right)^{\underline{2}} \zeta \geq b\zeta'\zeta \tag{3.26}$$

where constant $b > 0$, $(\bullet)^{\underline{2}} = (\bullet)(\bullet)'$, $\prod_{j=0}^{-1} = 1$. Moreover, $N_{\mathcal{O}}$ is the length of the window over which uniform detectability is calculated which is the same definition as provided for observability in (3.8), and $\zeta \in \mathbb{R}^{n_x \times n_x}$ is an arbitrary matrix, e.g. $\xi = \mathbb{I}$ [149].

The detectability condition is weaker than the full rank criteria for uniform observability in (3.8). Thus, under the conditions of either detectability or observability, after the initial time-steps of convergence, the initial conditions will have little effect on estimation quality or accuracy. That being said, the computational complexity of calculating uniform detectability is quartic, i.e. $\bullet^4$, with respect to the dimension of the state vector, or $\mathscr{D} \in O(n_x^4)$, for the minimum possible window length that is equal to the dimension of the

state vector. It is more common, therefore, to monitor for divergence as a function of the state error covariance as discussed in Section 3.6 since the complexity of calculating detectability for an LTV system would add significant complexity to the KF-based state estimation algorithm [47].

The state estimates of a convergent KF are eventually independent of the initial conditions due to the asymptotic stability of the equations within the update stage as well as the Kalman gain [47]. That said, the following are recommended best practices for the selection of initial values for state and state error covariance. Given limited knowledge regarding the value of the initial state for the system, it is suitable to assign the initial estimate of the state as the zero-vector with appropriate dimensions as follows.

$$\hat{x}\left[0|0\right] = 0^{n_x \times 1} \tag{3.27}$$

The zero-vector is chosen so as not to excite the free-response of the system in a manner that contradicts the unknown system conditions. In addition, for a state domain with known extents or admissible range, $x_R \in \mathbb{R}^{n_x \times 1}$, it is possible to assume that the initial state at the center of state domain space. This case is covered more specifically in the following paragraphs as it is related to the initial condition for state error covariance.

For a system that is asymptotically stable with a system input that is known to have been constant for some time, the initial state vector can be approximated by solving the following set of linear equations associated with the steady state of the system.

$$\hat{x}\left[0|0\right] = \left(\mathbb{I} - A\left[0\right]\right)^{-1} B\left[0\right] u\left[0\right] \tag{3.28}$$

If the assumed conditions are accurate within the true system, the above initial state vector will result in a reduction in the number of time-steps within which the KF will converge to the true state.

In contrast, the initial value for the state error covariance must not be equal to zero, $P_{\tilde{x}}[0|0] \neq 0^{n_x \times n_x}$. The initial state error covariance represents prior knowledge regarding the initial state of the system [147]. This concept is supported in [148] where it is suggested that the initial state error estimate should be at most two times the expected standard deviation of error, $\sigma_{\tilde{x}} \in \mathbb{R}^{n_x \times 1}$, as follows

$$\tilde{x}[0|0] \leq 2\sigma_{\tilde{x}} \tag{3.29}$$

where for the initial conditions it can be assumed that $P_{\tilde{x}}[0|0] = \sigma_{\tilde{x}}[0|0]\,\sigma'_{\tilde{x}}[0|0]$. Although not included in equation form within [147] or [148], these suggestions result in the following condition regarding the initial state error covariance.

$$P_{\tilde{x}}[0|0] \geq 4E\left\{(x[0] - \hat{x}[0])(x[0] - \hat{x}[0])'\right\} \tag{3.30}$$

Alternatively, the initial state error covariance can consider a relative amount of error within the initial state estimate with respect to the admissible range of the state domain, $x_R \in \mathbb{R}^{n_x \times 1}$, as follows

$$P_{\tilde{x}}[0|0] = r_x^2 x_R x'_R \tag{3.31}$$

where r_x is a scaling parameter representing uncertainties in the initial condition as a

function of the expected admissible range for the state vector, e.g. $r_x = 0.001$ represents 0.1% full scale error in the assumed initial state.

By considering only the admissible range within the domain of the state vector, the following relationship can be established

$$P_{\tilde{x}}[0|0] = r_x^2 x_R x_R' \geq 2^2 \cdot E\left\{\left(x[0] - \hat{x}[0]\right)\left(x[0] - \hat{x}[0]\right)'\right\} \tag{3.32}$$

where for a maximum possible initial state error equal to the admissible range, the scaling parameter will be equal to two, $r_x = 2$. Alternatively, for known admissible range within the state domain, x_R, an initial state estimate of $\hat{x}[0|0] = 0.5x_R$ results in the initial state error covariance being one quarter of the case presented in (3.32), or $P[0|0] = x_R x_R'$. When compared to using the zero-vector of (3.27), these two sets of initial conditions improve the ability of the state error covariance to accurately describe the probability distribution of the true system state over the first few time-steps if there is little knowledge of the true initial state.

For KF-based state estimation of LTV systems, it is common for the system parameters to switch between operating points given some exogenous input to the system, e.g. the parameter-specifying exogenous input u_θ. This switching affects the accuracy of the KF-based estimates and predictions. For this reason, the developed KF estimation and prediction algorithms employ a quadratic transition between the previous and current model parameters that represent the system upon detecting a change, or switch, in the parameters as a function of the exogenous input. In other words, the KF undergoes a continuous, smooth, or bumpless transfer during conditions that are otherwise discontinuous,

potentially disruptive, or misleading.

The transfer is quadratic in that only a fraction of the state estimate for the current or newly selected parameters is combined with the state estimate for the previous model parameters. This fraction of the current state estimate increases as a quadratic function of time over the transfer window whereas the fraction of the previous state estimate decreases as a quadratic function of time where the sum of the two quadratic functions is equal to one within each time-step. The length of the window for this transition is a function of the change in the exogenous input. Thus, the transition window is longer for a parameter change that occurs during ramp manoeuvres whereas the transition is shorter for step changes in the exogenous input that is responsible for model selection. This is a simple form of bumpless transfer that is suitable for use in controllers that are limited in terms of computational power. For controllers that are more powerful, it may be advantageous to implement multiple KFs, one for each of the multi-model operating points or ranges.

3.3 Kalman-filter-based point-prediction

It is straightforward to extend the KF-based state observer to both the state and measurement point-prediction problems. In fact, the *a priori* state estimate equation of (3.18) is by definition the one-step-ahead prediction of the state estimate, hence the predict stage. A one-step-ahead point-prediction of the measurement can therefore be calculated directly from the *a priori* state estimate as follows

$$\hat{y}\left[k+1|k\right] = C\left[k+1\right]\hat{x}\left[k+1|k\right] + D\left[k+1\right]u\left[k+1\right] \tag{3.33}$$

where the future values of $C[k+1]$, $D[k+1]$, and $u[k+1]$ are assumed to be known, e.g. equal to values at the current time-step k, or $C[k]$, $D[k]$, and $u[k]$. Here, the term point-prediction refers to the fact that the predictions are quantified using only a single value rather than a range of values that have been assigned a probability distribution. In other words, point-predictions do not consider the error covariances associated with either the state or measurement estimates or predictions.

State estimates are propagated beyond one time-step, e.g. to a prediction horizon of N_p time-steps, by repeatedly iterating the *a priori* state estimate equation provided in (3.18). These repeated calculations result in an i-step-ahead state point-prediction for each time-step within the prediction window, $i = 1, \ldots, N_p$, as follows

$$\hat{x}[k+i|k] = A[k+i-1]\,\hat{x}[k+i-1|k] + B[k+i-1]\,u[k+i-1] \tag{3.34}$$

where the values of $A[k+i-1]$, $B[k+i-1]$, and $u[k+i-1]$ are assumed to be known for $i = 2, \ldots, N_p$. This equation is essentially the deterministic state equation of the state-space system model given in (3.1). Thus, the minimization of mean squared error that is performed within the *a posteriori* stage of the KF is not considered during the prediction process. Nor do the KF-based state estimates consider the state and measurement predictions that are propagated beyond one time-step into the future.

An i-step-ahead measurement point-prediction can be calculated directly using the i-step-ahead state predictions for each time-step within the prediction window as follows

$$\hat{y}[k+i|k] = C[k+i]\,\hat{x}[k+i|k] + D[k+i]\,u[k+i] \tag{3.35}$$

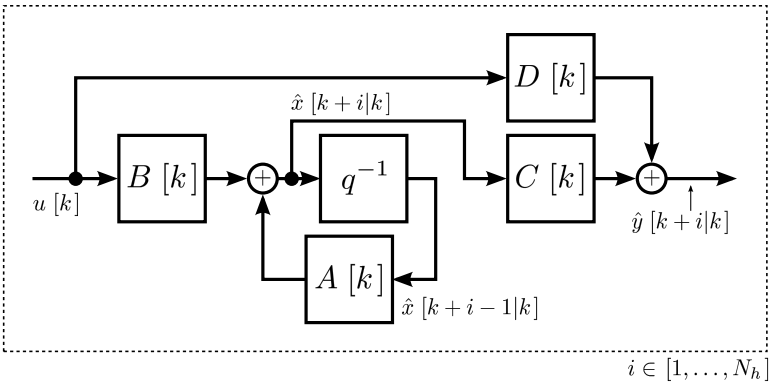

Figure 3.7: The *a priori* state estimate equation in (3.18) under the assumption that the future model parameters and system inputs have the same values as for current time-step, k.

where $C\,[k+i]$, $D\,[k+i]$, and $u\,[k+i]$ are assumed known. As for state propagation, this equation is essentially the deterministic measurement equation of the state-space system model given in (3.2).

The state and measurement point-prediction equations of (3.34) and (3.35) are combined in the block diagram of Figure 3.7 under the assumption that the future model parameters and system inputs have the same values as for current time-step, k. A block diagram of the more general case of (3.34) and (3.35) can be established through the replacement of $C\,[k]$ and $D\,[k]$ with values at time-step $(k+i)$, as well as $A\,[k]$, $B\,[k]$, and $R_x\,[k]$ with values at time-step $(k+i-1)$. It is not necessary to propagate the state error covariance in Figure 3.7 since the KF-based state and measurement point-predictions are independent of these future values.

A summary of the KF-based state and measurement point-prediction procedure is provided in Algorithm 3.2 under the same assumption of known future model parameters and system inputs as for Figure 3.7. Moreover, an overview of the point-prediction procedure is illustrated in Figure 3.8. An algorithm for the more general case of (3.34) and (3.35) can

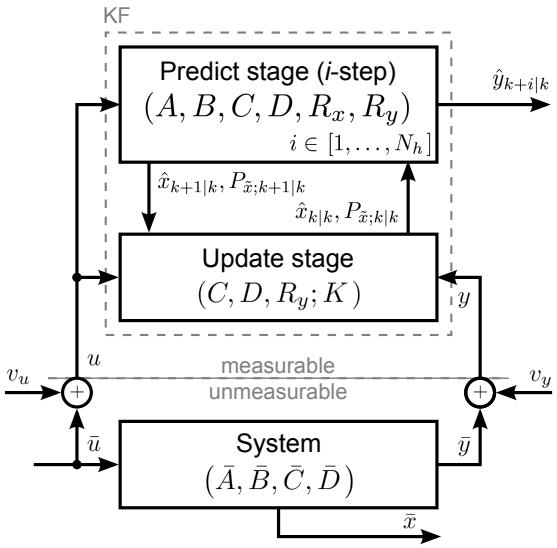

Figure 3.8: Connectivity between the system and the KF-based measurement prediction procedure of Algorithm 3.2.

be established by implementing the changes to time-indices as described for Figure 3.7. In addition, the state error covariance is not propagated beyond one time-step in to the future in the predict stage of Algorithm 3.2.

Algorithm 3.2 includes a count of the number of operations, or OPL, that are required to perform the point-prediction procedure for a scalar measurement. This count reveals that the computational complexity of the KF-based state and measurement point-prediction routine remains cubic with respect to the dimension of the state vector, or $\text{KF}_p \in O\left(n_x^3\right)$. The complexity of KF-based point-prediction is therefore of the same order as the KF-based state estimation presented in Algorithm 3.1. In other words, the added complexity that results from propagating the state vector and calculating the measurement prediction is relatively insignificant compared to the complexity of KF-based state estimation.

Although convergence is of concern within the KF state estimation portion of the KF-based prediction algorithm, the prediction equations provide no additional stability or

Algorithm 3.2 Kalman-filter-based (KF) state and measurement point-prediction, KF_p, under the assumption that the future model parameters and system inputs remain at the same values as for current time-step, k.

Require: $N_p, A, B, C, D, u, y, R_x, R_y$
Initial conditions: $\hat{x}\left[0|0\right], P_{\tilde{x}}\left[0|0\right]$
Result: $\hat{y}\left[k+i|k\right] \forall i = 1, \ldots, N_p$

```
k = 0
call [Initialization] from Algorithm 3.1
loop
  k = k + 1
  {measure y[k]}
  call [State estimation (update)] from Algorithm 3.1
  [N_p-step state propagation (predict)]
    for i = 1, ..., N_p do
    [i^th-step state propagation (predict)]
      x̂[k+i|k] = A[k] x̂[k+i-1|k] + B[k] u[k]
      ŷ[k+i|k] = C[k] x̂[k+i|k] + D[k] u[k]
    end for
  P_x̃[k+1|k] = A[k] P_x̃[k|k] A'[k] + R_x[k]
  {propagate x[k] to x[k+1]}
end loop
```

OPL for scalar y: $6n_x^3 + \frac{1}{2}\left(4N_p + 17\right)n_x^2 + \left(N_p + 6\right)n_x + N_p n_x n_u + \left(N_p + 2\right)n_u - N_p \in O\left(n_x^3\right)$

convergence concerns. This is due to the predict stage effectively being an open-loop propagation of the state vector to future time-steps. Convergence and stability only become a concern when prediction error is considered within the prediction algorithm since the current prediction error can have an destabilizing effect on the future prediction error. The potential for the modified forms of the KF-based prediction algorithm to become unstable is discussed further in Chapter 4.

Prediction error

It has been identified that KF-based point-predictions are not updated as a function of the prediction error for predictions that are propagated beyond one time-step. This lack of update remains true even after after the previous prediction horizons have passed and

the measurements corresponding to the predictions have been transmitted by the sensors and measured by the KF. In short, the KF-based point-prediction algorithm does not consider or even monitor whether or not the previously calculated predictions agree with the future system measurements. In contrast, the KF-based state estimates are updated as a function of the *a priori* measurement estimation error or innovation. There exists an opportunity, therefore, to compensate the calculated predictions for the error between the previous predictions and the future system measurements once measured, even if the cause of these prediction errors is unknown. Thus, a method for prediction error compensation is formulated in Section 4.1. In addition, Section 5.3 investigates various methods to statistically quantify the agreement between the calculated measurement predictions and the future system measurements.

Prediction with unknown future inputs

The KF-based point-prediction procedure presented in Figure 3.7 and Algorithm 3.2 is optimal in the mean squared sense with respect to estimation error for the LTI case with constant model parameter values and known future system inputs. For unknown future system inputs, however, the resulting point-predictions may no longer be optimal. These non-optimal conditions also apply when the model parameters are either explicit functions of time or functions of an exogenous system input, i.e. the LTV and LPV cases. Thus, the calculated point-predictions are only approximations of the future states or measurements. Given that the calculated predictions are eventually measured, it is possible to compensate the predictions for the known unknowns that are the assumed future model parameters and system inputs. This compensation is addressed along with the prediction

error compensation problem stated in the previous paragraph in Section 4.1.

Confidence in point-predictions

Finally, the measurement predictions returned by Algorithm 3.2 are single-valued mean estimates that correspond to each time-step within the prediction window. These single-valued estimates can then be used to make predictive decisions regarding the future behaviour of the system. In fact, each point-prediction represents, utilizing knowledge that is available up to the current time-step k, the value below which 50% of the future states and/or measurements are expected to occur and also above which 50% of the future states and/or measurements are expected to occur for each time-step within the prediction window. In other words, for a point-prediction that is equal to an arbitrary threshold, e.g. an alarm threshold or TSP, there is a 50% level of confidence at the current time-step, k, that the true future value will reach the threshold, i.e. that a threshold-crossing event will occur. There is also a 50% level of confidence at the current time-step, k, that the true future value will not reach the threshold and a threshold-crossing event does not occur. Thus, Section 3.4 and Section 3.5 extend the point-prediction problem to instead consider future state and measurement error covariances in order to make increasingly confident decisions regarding the future behaviour of the system and the probability of an impending threshold-crossing event.

3.4 Confidence and prediction intervals

State error covariances quantify uncertainties in the state estimates, $\hat{x}$, given that the state and measurement noise covariances accurately reflect the true uncertainties in the model and signals. Similarly, the measurement error covariances, $P_{\tilde{y}}$ in (3.23) and (3.24), quantify uncertainties for measurement estimates, $\hat{y}$. More specifically, state and measurement error covariance matrices include variances from which confidence and prediction intervals can be calculated for a predetermined and fixed one-tailed significance level, α, and corresponding percentage confidence level equal to $100\,(1-\alpha)\%$. The significance level is sometimes referred to as the confidence coefficient, [146].

Confidence intervals, as illustrated in Figure 3.9a), provide upper and lower limits or bounds for the estimates above and below which, given a population of estimation samples, it is expected that either $100\alpha\%$ or $100\,(1-\alpha)\%$ of the estimated values occur. Confidence intervals are therefore related to the probability density function (PDF) of a random variable.

The two confidence intervals that are included in Figure 3.9 have one-tailed significance levels of $\alpha \approx 2.3\%$ and $\alpha \approx 15.9\%$. The upper bound of Figure 3.9b) is the value at which $100\alpha\%$ of the estimates are expected to be greater than whereas $100\,(1-\alpha)\%$ are expected to be less than or equal to the bound as indicated by the shaded region. The shaded area is equal to the value of the cumulative distribution function (CDF) calculated for the interval between $-\infty$ and the upper bound for the specified significance level. The expected probability of the estimates occurring above the bound is referred to as the complementary

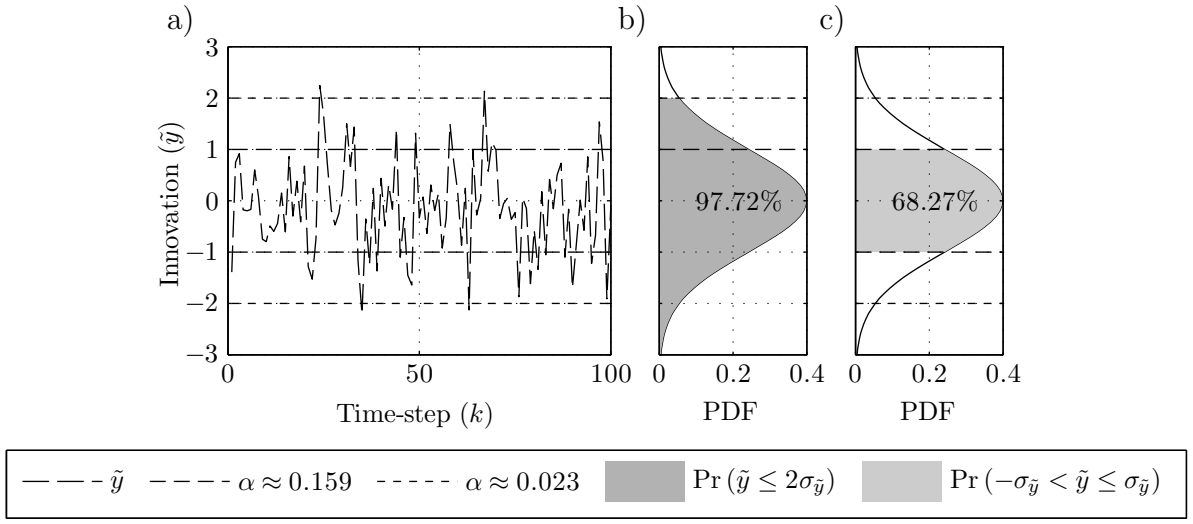

Figure 3.9: Confidence intervals of significance levels $\alpha \approx 0.023$ and $\alpha = 0.159$ for the a) respective outer and inner bounds of a sequence of measurement errors, $\tilde{y}$, and corresponding b) one-tailed bound as well as, c) two-tailed bound including probability density function (PDF).

CDF. These two probabilities are respectively calculated for the measurement error as follows

$$\Pr(\tilde{y} \leq z_\alpha \sigma_{\tilde{y}}) = 100\,(1-\alpha) \tag{3.36}$$

$$\Pr(\tilde{y} > z_\alpha \sigma_{\tilde{y}}) = 100\alpha = 1 - \Pr(\tilde{y} \leq z_\alpha \sigma_{\tilde{y}}) \tag{3.37}$$

where z_α is the score associated with the two-tailed significance level α, $\Pr(\bullet)$ is the probability for the occurrence of event $\bullet$, $\sigma_{\tilde{y}} \in \mathbb{R}^{n_y \times 1}$ is the estimated standard deviation of the measurement error and $\sigma_{\tilde{y}}\sigma'_{\tilde{y}} = P_{\tilde{y}}$. Alternatively, although a lower bound is not included in Figure 3.9, $100\,(1-\alpha)\%$ of the estimates are expected to be greater than the lower limit of the interval whereas $100\alpha\%$ are expected to be less than or equal to the limit. This lower

bound example has the following probabilities for the state error

$$\Pr\left(\tilde{x} > -z_{\alpha}\sigma_{\tilde{x}}\right) = 100\left(1-\alpha\right) \tag{3.38}$$

$$\Pr\left(\tilde{x} \leq -z_{\alpha}\sigma_{\tilde{x}}\right) = 100\alpha = 1 - \Pr\left(\tilde{x} \leq -z_{\alpha}\sigma_{\tilde{x}}\right) \tag{3.39}$$

with $\sigma_{\tilde{x}}$ as defined for (3.29).

The upper and lower limits are also the bounds within which, given a population of estimation samples, it is expected that $100\left(1-\underline{\alpha}\right)\%$ of the estimated values occur, where $\underline{\alpha}$ is the two-tailed significance level calculated as follows

$$\underline{\alpha} = 2\alpha. \tag{3.40}$$

The two-tailed confidence interval is illustrated in Figure 3.9c) with the probability of an estimate being within the bounds represented for measurement error as follows

$$\Pr\left(-z_{\underline{\alpha}}\sigma_{\tilde{y}} < \tilde{y} \leq z_{\underline{\alpha}}\sigma_{\tilde{y}}\right) = 100\left(1-\underline{\alpha}\right) \tag{3.41}$$

$$\Pr\left(\tilde{y} \leq -z_{\underline{\alpha}}\sigma_{\tilde{y}} \text{ or } \tilde{y} > z_{\underline{\alpha}}\sigma_{\tilde{y}}\right) = 100\alpha = 1 - \Pr\left(-z_{\underline{\alpha}}\sigma_{\tilde{y}} < \tilde{y} \leq z_{\underline{\alpha}}\sigma_{\tilde{y}}\right) \tag{3.42}$$

where $z_{\underline{\alpha}}$ is the score associated with the two-tailed significance level $\underline{\alpha}$. These concepts also apply to the limits of prediction intervals for predictions within a population of prediction samples. In general, the term confidence interval refers to both the confidence interval for estimates as well as the prediction interval for predictions. Within this work the term confidence interval is used in place of prediction interval. This allows for emphasis to be

placed on the level of confidence in the calculated predictions; this metric is considered valuable to the predictive decision-making process.

The two-tailed significance level, $\underline{\alpha}$, is a statistic that is symmetric about the mean of the estimate or estimation error. This is in contrast to the one-tailed significance level, α, that has different probabilities assigned for either the upper or the lower bounds. The majority of this section therefore refers the two-tailed significance level with the one-tailed statistic becoming of more importance within the one-tailed confidence calculations of Chapter 5. Moreover, the score, z, is also a symmetric statistical measure and is therefore often specified using the two-tailed significance level, $z_{\underline{\alpha}}$

For both the *a posteriori* and *a priori* state estimates, the upper and lower limits of the $100\,(1-\underline{\alpha})\%$ confidence interval are respectively calculated as follows [146]

$$\hat{x}^{u,\underline{\alpha}}\left[k|\bullet\right] = \hat{x}\left[k|\bullet\right] + z_{\underline{\alpha}}\left(P_{\tilde{x}}\left[k|\bullet\right]\right)^{\frac{1}{2}} \tag{3.43}$$

$$\hat{x}^{l,\underline{\alpha}}\left[k|\bullet\right] = \hat{x}\left[k|\bullet\right] - z_{\underline{\alpha}}\left(P_{\tilde{x}}\left[k|\bullet\right]\right)^{\frac{1}{2}} \tag{3.44}$$

where $z_{\underline{\alpha}}$ is as defined for (3.42), $\bullet$ is equal to $(k-1)$ for the *a priori* case and as k for the *a posteriori* case, and $\left(P_{\tilde{x}}\left[k|\bullet\right]\right)^{\frac{1}{2}}$ is the square root of the state error covariance that can be calculated using singular value decomposition (SVD) and/or various other eigendecomposition methods that utilize eigenvalues and eigenvectors to solve the multidimensional standard deviation problem [150] e.g. diagonalization or Cholesky decomposition. This square root is also the solution of $\sigma_{\tilde{x}}\left[k|\bullet\right]\sigma'_{\tilde{x}}\left[k|\bullet\right] = P_{\tilde{x}}\left[k|\bullet\right]$, if it exists. In other words, matrix $\sigma_{\tilde{x}}\left[k|\bullet\right]$ is said to be a square root of $P_{\tilde{x}}\left[k|\bullet\right]$ is $\sigma_{\tilde{x}}\left[k|\bullet\right]\sigma'_{\tilde{x}}\left[k|\bullet\right]$ is equal to $P_{\tilde{x}}\left[k|\bullet\right]$. For single-dimensional spaces the square root reduces to the standard arithmetic operation,

$\sqrt{\bullet}$.

Within (3.43) and (3.44), the score, $z_{\underline{\alpha}}$, represents the number of standard deviations between the mean state estimate and the upper and lower limits of the confidence interval within which it is expected that $100\,(1-\underline{\alpha})\%$ of the estimates occur. The score is therefore calculated as a function of two-tailed significance level, $\underline{\alpha}$, as follows

$$z_{\underline{\alpha}} = \sqrt{2}\mathrm{erf}^{-1}\,(1-\underline{\alpha}) = \Phi^{-1}\left(1-\frac{\underline{\alpha}}{2}\right), \tag{3.45}$$

where $\mathrm{erf}^{-1}\,(\bullet)$ is the inverse Gaussian error function and $\Phi^{-1}\,(\bullet)$ is the inverse cumulative Gaussian distribution function. The score is a fixed parameter that can be calculated in advance of executing KF-based algorithms as it is a function of only the fixed significance level, $\underline{\alpha}$.

Upper and lower limits of the $100\,(1-\underline{\alpha})\%$ confidence interval can also be calculated for either the *a priori* or *a posteriori* measurement estimates as follows [146]

$$\hat{y}^{u,\underline{\alpha}}\,[k|\bullet] = \hat{y}\,[k|\bullet] + z_{\underline{\alpha}}\,(P_{\tilde{y}}\,[k|\bullet])^{\frac{1}{2}} \tag{3.46}$$

$$\hat{y}^{l,\underline{\alpha}}\,[k|\bullet] = \hat{y}\,[k|\bullet] - z_{\underline{\alpha}}\,(P_{\tilde{y}}\,[k|\bullet])^{\frac{1}{2}} \tag{3.47}$$

where $z_{\underline{\alpha}}$ and $[k|\bullet]$ are as defined for (3.43) and (3.44). Here, the square root of the measurement error covariance can, in general, be calculated in the same manner as for the state interval-estimates as discussed for (3.43) and (3.44). More often, however, the square root is calculated as the arithmetic square root, $\sqrt{\bullet}$, for a single output system with scalar measurement, or as multiple individual square roots for a multiple output system

by considering individually each system measurement within the measurement along with the diagonal elements of the measurement error covariance matrix.

Extension of the confidence interval calculations to multi-step-ahead measurement prediction results in the following calculation for the upper and lower limits of the $100\,(1-\underline{\alpha})\%$ prediction interval for the measurements

$$\hat{y}^{u,\underline{\alpha}}\,[k+i|k] = \hat{y}\,[k+i|k] + z_{\underline{\alpha}}\,(P_{\tilde{y}}\,[k+i|k])^{\frac{1}{2}} \tag{3.48}$$

$$\hat{y}^{l,\underline{\alpha}}\,[k+i|k] = \hat{y}\,[k+i|k] - z_{\underline{\alpha}}\,(P_{\tilde{y}}\,[k+i|k])^{\frac{1}{2}} \tag{3.49}$$

with all variables as defined for 3.47. This extension can also be applied to (3.43) and (3.44) in order to calculate prediction intervals for the state vector. These i-step-ahead interval-predictions now require that the *a priori* state error covariance, $P_{\tilde{x}}$, is propagated to future time-steps. For the measurement interval-predictions, this propagation is due to the measurement error covariance, $P_{\tilde{y}}$, being a function of the state error covariance, $P_{\tilde{x}}$.

In Section 3.3, comparison of point-predictions against alarm thresholds resulted in only 50% confidence of a threshold-crossing actually occurring within the prediction horizon and an equal 50% confidence of a threshold-crossing not occurring. Using the confidence-based methods of this section, however, it is now possible to improve the confidence of predictive decision-making by considering the upper and lower bounds of the prediction interval as given in (3.48) and (3.47) respectively. In this manner, predictive decisions can be made with respect to specific levels of confidence as a function of the one-tailed significance level, α. More precisely, the use of one-tailed significance levels allows the prediction algorithm to consider, for impending threshold-crossings, levels of confidence that are greater than

50%. In addition, one-tailed significance levels of confidence that are less than 50% can be utilized to decide against a particular opposing decision regarding an impending threshold-crossing.

As in the case of point-predictions, interval-predictive decisions can be made within the domain of either the state or measurement. Within the state domain, the prediction intervals are functions of the square root of state error covariance as included in the *a priori* state predictions of (3.43) and (3.44). This square root, in turn, requires the calculation of the computationally complex SVD; SVD computations significantly affect the arithmetic complexity of the prediction algorithm. That being said, predictive decisions within the domain of the state are generally able to provide additional information regarding the impending conditions of the system and may be worth the added computational complexity. In contrast, under the assumption that the n_y signals of the measurement vector are independent, the matrix square roots included in the measurement predictions of (3.48) and (3.49) can be reduced to n_y individual square root operations, one for each element along the diagonal of the measurement error covariance matrix, $P_{\tilde{y}}$. The measurement domain is therefore the preferred domain for calculation of interval-predictions due to the prediction algorithm being less computationally complex than that of the state domain.

3.5 Kalman-filter-based measurement interval-prediction

To extend the KF-based point-prediction procedure to the measurement interval-prediction problem, it is required that the confidence intervals of the multi-step-ahead predictions be calculated. These intervals are, in turn, a function of the propagated *a priori* state error covariance. This propagation is straightforward since the *a priori* state error covariance of (3.19) is by definition the one-step-ahead prediction of the state error covariance, i.e. the predict stage within the KF-based state estimation procedure.

The state error covariance is propagated beyond one time-step, e.g. to a prediction horizon of N_p time-steps, by repeatedly calculating the *a priori* state error covariance provided in (3.19). This propagation is similar to that of the *a priori* state estimate in Section 3.3. These repeated calculations result in the following i-step-ahead state error covariance predictions for each time-step within the prediction window, $i = 1, \ldots, N_p$, as follows

$$P_{\tilde{x}}\left[k+i|k\right] = A\left[k+i-1\right] P_{\tilde{x}}\left[k+i-1|k\right] \left(A\left[k+i-1\right]\right)' + R_x\left[k+i-1\right] \tag{3.50}$$

where the future values of $A\left[k+i-1\right]$ and $R_x\left[k+i-1\right]$ are assumed to be known for $i = 2, \ldots, N_p$. This equation is a function of the state-space model parameters as defined in (3.9) as well as the state noise covariance that is provided to the KF-based state observer as defined in (3.12). Thus, in addition to the multi-step-ahead predictions, the minimization

of mean squared error that is performed within the *a posteriori* stage of the KF does not consider the state or measurement error covariances that are propagated beyond one time-step into the future.

The upper and lower bounds of the i-step ahead measurement interval-prediction can then be calculated as given in (3.48) and (3.49) respectively. These bounds are the summation of the mean KF-based measurement point-prediction, $\hat{y}\,[k+i|k]$, and the sign-specific half-width of the confidence interval; positive for the upper bound and negative for the lower bound. The half-width of the prediction interval is a function of a fixed significance level, $\underline{\alpha}$, where the upper and lower limits of the interval provide a bounds within which $100\,(1-\underline{\alpha})\%$ of the predicted values are expected to occur as illustrated in Figure 3.9c). The half-width is also a function of the measurement error covariance that is calculated for the i-step-ahead measurement prediction as follows

$$P_{\tilde{y}}\,[k+i|k] = C\,[k+i]\,P_{\tilde{x}}\,[k+i|k]\,C'\,[k+i] + R_y\,[k+i] \tag{3.51}$$

where $P_{\tilde{x}}\,[k+i|k]$ is defined in (3.50) and $C\,[k+i]$ and $R_y\,[k+i]$ are assumed known. Finally, the square root of the measurement error covariance is calculated using multiple individual square roots for a multiple output system where the system measurements are assumed to be independent and therefore have corresponding covariances that are the diagonal entries of the measurement error covariance matrix.

The i-step-ahead state and measurement error covariance equations of (3.50) and (3.51) are combined to calculate KF-based measurement interval-predictions in the block diagram of Figure 3.10 under the assumption that the future model parameters and system inputs re-

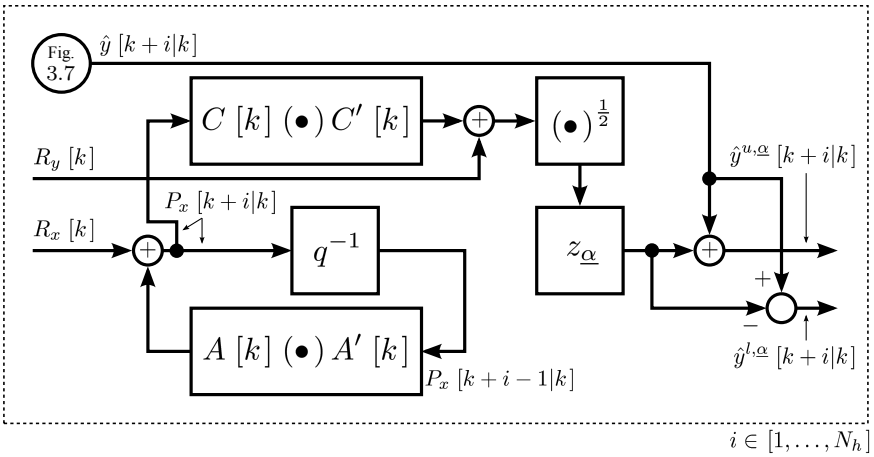

Figure 3.10: The *a priori* state error covariance equation in (3.19) under the assumption that the future model parameters and system inputs remain at the same values as for current time-step, k.

main at the same values as for the current time-step, k. In addition, the interval-predictions are a function of the i-step-ahead measurement point-prediction in Figure 3.7. A block diagram of the more general case formulated in (3.50) and (3.51) can be established through the replacement of $C\,[k]$, $D\,[k]$, and $R_y\,[k]$ with values at time-step $(k+i)$, as well as $A\,[k]$, $B\,[k]$, and $R_x\,[k]$ with values at time-step $(k+i-1)$.

A summary of the KF-based measurement interval-prediction procedure is provided in Algorithm 3.3 under the same assumption of known future model parameters and system inputs as for Figure 3.10. Moreover, an overview of the interval-prediction procedure is illustrated in Figure 3.11. An algorithm for the more general case that is formulated in (3.50) and (3.51) can be established by implementing the time index changes as described for Figure 3.10. In contrast to the point-predictive algorithm, the state error covariance is now propagated beyond one time-step into the future. In addition, the measurement error covariance, $P_{\tilde{y}}$, the half-width of the confidence interval, $h^{y,\underline{\alpha}}$, and the upper and lower bounds of the measurement interval-prediction, $\hat{y}^{u,\underline{\alpha}}$ and $\hat{y}^{l,\underline{\alpha}}$, are also calculated within

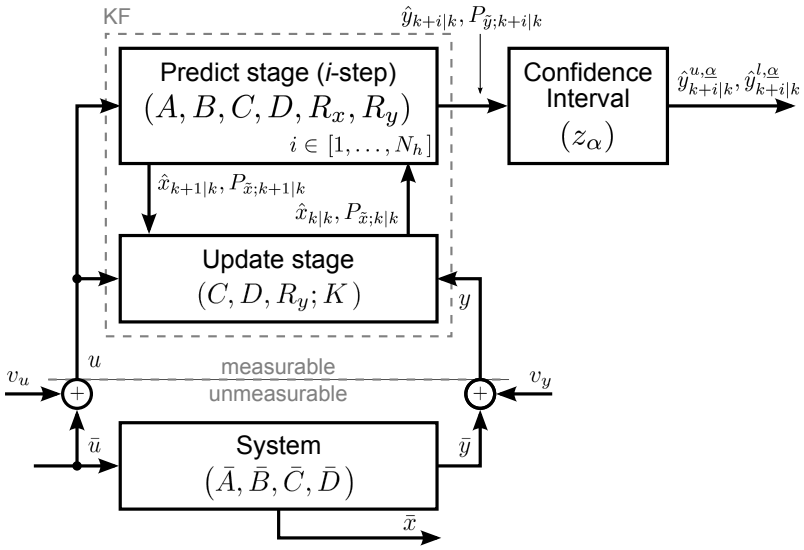

Figure 3.11: Connectivity between the KF-based measurement prediction as well as confidence interval calculation procedures of Algorithm 3.3.

each time-step of the prediction window.

Algorithm 3.3 includes a count of the number of operations, or OPL, that are required to perform the interval-prediction procedure for a scalar measurement. This count reveals that the computational complexity of KF-based measurement interval-prediction remains cubic with respect to the dimension of the state vector, or $\mathrm{KF}_{ip} \in O\left(n_x^3 N_p\right)$. The complexity does, however, increase in proportion to the length of the prediction window given as the prediction horizon N_p and is therefore greater than that of either the KF-based state estimation of Algorithm 3.1 or the KF-based point-prediction of Algorithm 3.2. This increase in complexity is due to the propagation of the state error covariance to the prediction horizon which alone is $O\left(n_x^3 N_p\right)$.

In order to calculate the complexity of the scalar square root operation, the square root is assumed to be performed using the reciprocal square root form of the Newton-Raphson method where double-precision floating-point accuracy is estimated to be achieved by

Algorithm 3.3 Kalman-filter-based (KF) measurement interval-prediction, KF_{ip}, under the assumption that the future model parameters and system inputs have the same values as for the current time-step, k.

Require: $N_p, A, B, C, D, u, y, R_x, R_y$
Initial conditions: $\hat{x}[0|0], P_{\tilde{x}}[0|0]$
Result: $\hat{y}[k+i|k], \hat{y}^{u,\underline{\alpha}}[k+i|k], \hat{y}^{l,\underline{\alpha}}[k+i|k] \; \forall i = 1, \ldots, N_p$

$k = 0$
call [Initialization] from Algorithm 3.1
loop
  $k = k + 1$
  {measure $y[k]$}
  call [State estimation (update)] from Algorithm 3.1
  [N_p-step state propagation (predict)]
    for $i = 1, \ldots, N_p$ **do**
    [i^{th}-step propagation (predict)]
      $\hat{x}[k+i|k] = A[k]\,\hat{x}[k+i-1|k] + B[k]\,u[k]$
      $\hat{y}[k+i|k] = C[k]\,\hat{x}[k+i|k] + D[k]\,u[k]$
      $P_{\tilde{x}}[k+i|k] = A[k]\,P_{\tilde{x}}[k+i-1|k]\,A'[k] + R_x[k]$
      $P_{\tilde{y}}[k+i|k] = C[k]\,P_{\tilde{x}}[k+i|k]\,C'[k] + R_y[k]$
    [i^{th}-step interval calculation]
      $h^{y,\underline{\alpha}} = z_{\underline{\alpha}}\left(P_{\tilde{y}}[k+i|k]\right)^{\frac{1}{2}}$
      $\hat{y}^{u,\underline{\alpha}}[k+i|k] = \hat{y}[k+i|k] + h^{y,\underline{\alpha}}$
      $\hat{y}^{l,\underline{\alpha}}[k+i|k] = \hat{y}[k+i|k] - h^{y,\underline{\alpha}}$
    end for
  {propagate $x[k]$ to $x[k+1]$}
end loop

OPL for scalar y: $3(N_p+1)n_x^3 + 5\left(N_p+\frac{3}{2}\right)n_x^2 + \frac{1}{2}(3N_p+13)n_x + N_p n_x n_u + (N_p+1)n_u + 28N_p \in O\left(n_x^3 N_p\right)$

performing fifteen multiplications and ten additions. The number of required square root computations is halved, however, by performing a single half-width calculation, denoted as $h^{y,\underline{\alpha}}$, rather than within each of the upper and lower interval equations.

Algorithm 3.3 returns, within each time-step of the prediction window, a range of measures on which to make decisions regarding the future behaviour of the system. This range of values is in contrast to the single-value that is produced within each time-step of the prediction window for the point-prediction algorithm of Algorithm 3.2. The upper and lower bounds of the interval-predictions are the two values within which $100\,(1-\underline{\alpha})\%$ of the measurements are expected to occur as illustrated in Figure 3.9c). This percentage is also the level of confidence that the future measurement will occur within the upper and lower limits. In contrast, there is $100\underline{\alpha}\%$ level of confidence that the measurement will occur outside the upper and lower bounds of the prediction interval. These are the confidence levels for a two-tailed symmetric predictive decision where a future measurement may either be greater than or less than alarm thresholds that are equal to the respective upper and lower bounds of the prediction interval, as in [41].

More specifically, a two-tailed predictive decision is illustrated in Figure 3.12 for a significance level of $\underline{\alpha} = 0.0004$ and corresponding confidence level of 99.96%. In this example, the innovations of Figure 3.12a) do not reach the upper or lower bounds. In fact, at a sample rate of one sample per day, the data confidence intervals plotted in Figure 3.12 correspond with a single sample reaching the confidence interval once every six years. The upper and lower bounds of the confidence interval provide measures by which to make decisions regarding an alarm-high as well as alarm-low thresholds. In Figure 3.12b), there is therefore a 0.04% probability that the innovation will reach either the alarm-high or

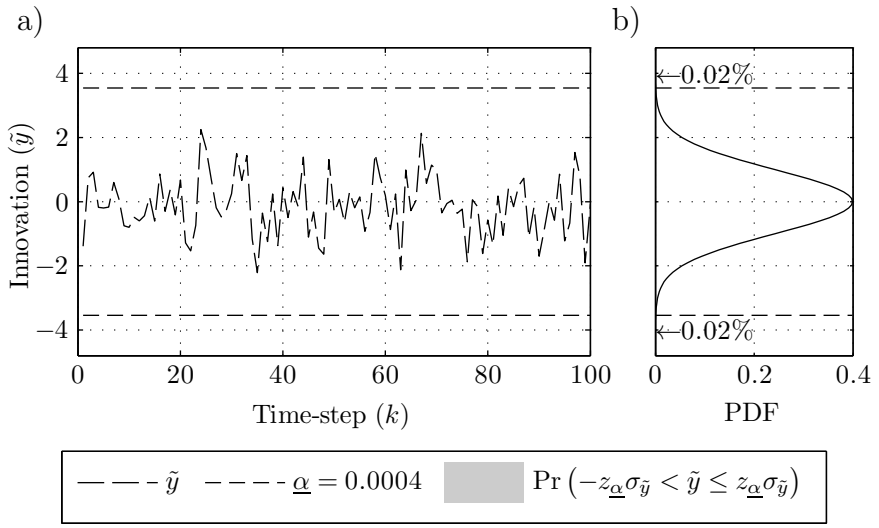

Figure 3.12: Confidence interval of significance level $\underline{\alpha} = 0.0004$ and level of confidence equal to 99.96% for the a) bounds of a sequence of measurement errors, $\tilde{y}$, and corresponding b) two-tailed predictive decision problem including probability density function (PDF) and the value of the cumulative probability outside of the bounds.

alarm-low thresholds.

For one-tailed predictive decisions, however, the upper and lower bounds are assigned confidence levels that correspond instead with the one-tailed significance level, α. In this case, the upper and lower bounds can each be assigned either $100\alpha\%$ or $100\,(1-\alpha)\%$ levels of confidence depending on one of two conditions for the decision being made. For example, there is $100\alpha\%$ level of confidence in a one-tailed decision regarding whether the future measurement will be less than an alarm threshold that is equal to the lower bound of the prediction interval. There is also $100\,(1-\alpha)\%$ level of confidence in deciding whether the future measurement will be greater than the same alarm-low threshold.

The lower bound illustrated in Figure 3.13 has a one-tailed confidence interval that corresponds to the case of Figure 3.12, i.e. one-tailed significance level $\alpha = 0.0002$ and a level of confidence of 99.98% that the innovation will be greater than a low-alarm threshold that is equal to the lower bound. If, however, the alarm threshold is instead equal to

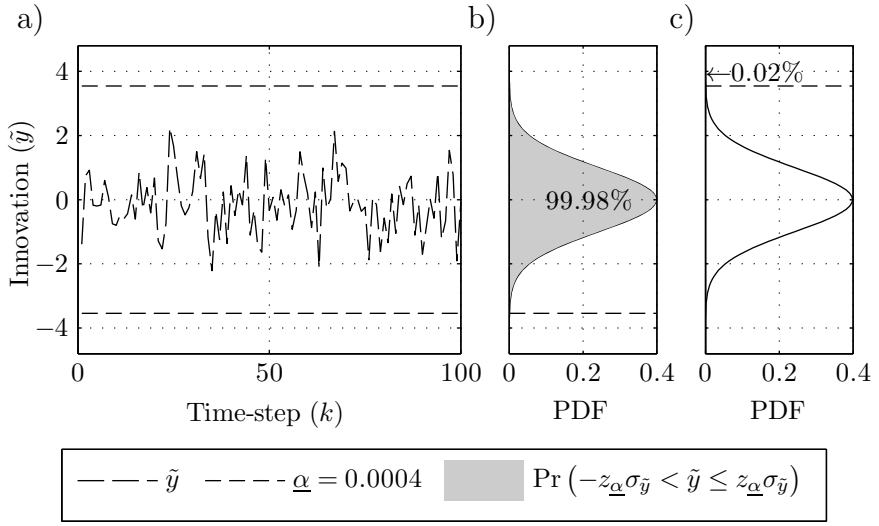

Figure 3.13: Confidence interval of one-tailed significance level $\underline{\alpha} = 0.0002$ and level of confidence equal to 99.98% for the a) bounds of a sequence of measurement errors, $\tilde{y}$, and corresponding b) one-tailed lower bound, as well as c) one-tailed upper bound including probability density function (PDF) and values of the cumulative probability within and outside of the bounds.

the upper bound, there are $100\,(1-\alpha)\%$ and $100\alpha\%$ levels of confidence that the future measurements will be less than and greater than the alarm-high threshold respectively. In this case, the upper bound of Figure 3.13, corresponds with a one-tailed significance level of $\alpha = 0.9998$ and a level of confidence of 0.02% that the innovation will be greater than an alarm-high threshold that is equal to the upper bound. Thus, as stated in Section 3.4, the one-tailed significance level requires that specific probabilities be assigned for the upper or the lower bounds with respect to alarm-high and alarm-low thresholds. In Figure 3.13b), it is very likely that the innovations will reach an alarm-high threshold that is equal to the lower bound. In contrast, in Figure 3.13c) it is very unlikely that the innovations will reach an alarm-high threshold that is equal to upper bound.

Accuracy of state noise covariance, R_x

The KF-based interval-prediction procedure, as presented within this subsection, requires that the assumed noise covariance values of R_x or R_y represent the true uncertainty within the states, inputs, and measurements to ensure the calculated error covariances provide valid probability distributions and confidence intervals. The purpose of these two noise covariance matrices is to quantify uncertainties within the state and measurement equations respectively. Moreover, the noise covariances also balance, within the KF, the uncertainty between the assumed model parameters, system inputs, and system measurements. In general, the diagonal elements of the measurement noise covariance matrix, R_y, can be calculated as the variances of the individual measurement signals at the output of the system at steady state or after detrending the measurement signal to remove any bias, drift, or other anticipated dynamics. In addition, the off-diagonal elements of this covariance matrix are equal to zero for independent measurements and are otherwise calculated as the covariances between each pair of elements within the measurement vector. In contrast, it is often difficult to calculate the state noise covariance matrix, R_x, due to the fact that the state noise covariance includes uncertainties for both the inputs as well as the state vector which is not necessarily entirely measurable [151]. These effects are therefore investigated in the following section, Section 3.6.

3.6 Noise covariances and uncertainty

KFs are able to perform state estimation through the use of a model that is a mathematical abstraction of the true system dynamic. The parameters of the model can be identified through system identification and parameter estimation procedures for an assumed system structure. Moreover, the parameters may also be assigned by first principles from a theory-based understanding of the individual components of the system or by black-box modelling and parameter estimation for which there is no assumption regarding system structure. No matter what method is used, the parameters are often uncertain and may not necessarily be an exact representation of the actual system parameters. This is especially true for systems that have LTV parameters where the parameters may be accurate for one operating condition but differ when the operating conditions change. Moreover, in the case of prediction, the conditions may differ from those that are anticipated. In addition to model uncertainties, there may also be uncertainties within the signals that are provided to, or measured by, the KF. This uncertainty may, for example, be the result of noise within the process or manipulating signals, poor placement or installation of sensors, signal processing and quantization, or interference within communication channels. Both modelling as well as signal uncertainties are annotated in the state observer of Figure 3.3.

As stated in Section 3.2, KF-based state observers account for uncertainties through the state and measurement noise covariances, R_x and R_y, as defined in (3.12) for the state and measurement noise vectors, v_x and v_y respectively. The resulting KF-based state estimates are optimal in the minimum mean squared sense, given that these noise

covariances accurately describe the true uncertainty of the identified model parameters and structure as well as the state and measurement signals. For LTI systems, the state and measurement noise are generally assumed to be time-invariant. For the LTV model of (3.9) and (3.10), however, it is more appropriate to consider noise covariances that are time-varying.

The state and measurement noise covariance matrices establish a respective balance between uncertainty in the model and inputs to the state equation against uncertainty in the system measurements and inputs to the measurement equation. This balance can be evaluated by determining the effect that changes in the magnitudes of the state and measurement noise covariances have on the resulting state estimates for scalar measurement vector, $y \in \mathbb{R}^{1\times 1}$. Regarding the system measurements, the state estimate is a function of the measurement noise covariance, $R_y[k] \in \mathbb{R}^{1\times 1}$, through the Kalman gain equation in (3.15). In contrast, the state estimate is effected by the state noise covariance, $R_x[k] \in \mathbb{R}^{n_x\times n_x}$, through the *a priori* state error covariance equation in (3.19).

Any changes to the elements of the Kalman gain vector, $\Delta K[k]$, that result from changes in the scalar measurement noise covariance, $R_y[k]$ to $(R_y[k] + \Delta R_y[k])$, can be defined in the following as a function of the *a priori* state error covariance (3.19)

$$\begin{aligned}\Delta K[k] &\triangleq K_\Delta[k] - K[k] \\ &= P_{\tilde{x}}[k|k-1]\,C'[k]\left(C[k]\,P_{\tilde{x}}[k|k-1]\,C'[k] + R_y[k] + \Delta R_y[k]\right)^{-1} \\ &\quad - P_{\tilde{x}}[k|k-1]\,C'[k]\left(C[k]\,P_{\tilde{x}}[k|k-1]\,C'[k] + R_y[k]\right)^{-1}\end{aligned} \tag{3.52}$$

where $K_\Delta[k]$ is the modified Kalman gain that results from the change in the noise covari-

ance. The change in Kalman gain can then be simplified by factoring the initial multiplicand $P_{\tilde{x}}[k|k-1]C'[k]$, finding a common denominator, and reorganizing the equation, although this is only possible for the scalar measurement case

$$\begin{aligned}\Delta K[k] &= P_{\tilde{x}}[k|k-1]C'[k]\left(\left(C[k]P_{\tilde{x}}[k|k-1]C'[k]+R_y[k]+\Delta R_y[k]\right)^{-1}\right.\\&\quad\left.-\left(C[k]P_{\tilde{x}}[k|k-1]C'[k]+R_y[k]\right)^{-1}\right)\\&= P_{\tilde{x}}[k|k-1]C'[k]\left(C[k]P_{\tilde{x}}[k|k-1]C'[k]+R_y[k]\right)^{-1}\\&\quad\cdot(-\Delta R_y[k])\left(C[k]P_{\tilde{x}}[k|k-1]C'[k]+R_y[k]+\Delta R_y[k]\right)^{-1}\end{aligned}\tag{3.53}$$

where the change in Kalman gain elements are inverse in sign with respect to the change in the magnitude of uncertainty in the system measurement, ΔR_y. The modified Kalman gain is then equal to the summation of the original Kalman gain, $K[k]$, and the change in Kalman gain of (3.53) as follows.

$$\begin{aligned}K_\Delta[k] &= P_{\tilde{x}}[k|k-1]C'[k]\left(C[k]P_{\tilde{x}}[k|k-1]C'[k]+R_y[k]\right)^{-1}\\&\quad\cdot\left(\mathbb{I}-\Delta R_y[k]\left(C[k]P_{\tilde{x}}[k|k-1]C'[k]+R_y[k]+\Delta R_y[k]\right)^{-1}\right)\\&= K[k]\left(\mathbb{I}-\Delta R_y[k]\left(C[k]P_{\tilde{x}}[k|k-1]C'[k]+R_y[k]+\Delta R_y[k]\right)^{-1}\right)\end{aligned}\tag{3.54}$$

The elements of the Kalman gain vector, $K[k]\in\mathbb{R}^{n_x\times 1}$ are therefore equal to the elements of the original gain minus the original gain elements multiplied by a function of the change in the measurement noise covariance, $R_y[k]$.

Thus, all else equal, an increase in uncertainty in a scalar measurement noise covariance, $R_y[k]$, results in the magnitude of the Kalman gain being reduced and the updated state

estimate tracking more closely the dynamic of the system model rather than the measurements. This relationship is restated in the following by calculating the limits of (3.54) with time-indices omitted for readability.

$$\lim_{\Delta R_y \to 0_+} K\left(\mathbb{I} - \frac{\Delta R_y}{C P_{\tilde{x}} C' + R_y + \Delta R_y}\right) = K \tag{3.55}$$

$$\lim_{\Delta R_y \to \infty} K\left(\mathbb{I} - \frac{\Delta R_y}{C P_{\tilde{x}} C' + R_y + \Delta R_y}\right) = 0^{n_x \times 1} \tag{3.56}$$

Alternatively, an increase in uncertainty in the state noise covariance, $R_x[k]$, results in the updated state estimate more closely tracking the measurement rather than the dynamic of the system model. To support this claim, the following equation defines the change in the Kalman gain, $\Delta K[k]$, for a change in the state noise covariance from $R_x[k]$ to $(R_x[k] + \Delta R_x[k])$ as a function of the *a priori* state error covariance (3.19) and scalar noise covariance, $R_y[k]$.

$$\begin{aligned}\Delta K[k] = &\left(P_{\tilde{x}}[k|k-1] + \Delta R_x[k-1]\right) C'[k] \\ &\cdot \left(C[k]\left(P_{\tilde{x}}[k|k-1] + \Delta R_x[k-1]\right) C'[k] + R_y[k]\right)^{-1} \\ &- P_{\tilde{x}}[k|k-1] C'[k] \left(C[k] P_{\tilde{x}}[k|k-1] C'[k] + R_y[k]\right)^{-1}\end{aligned} \tag{3.57}$$

Moreover, the original state noise covariance term, $R_x[k]$, is embedded within the *a priori* state error covariance $P_{\tilde{x}}[k|k-1]$ as follows

$$\begin{aligned}P_{\Delta,\tilde{x}}[k|k-1] &= A[k-1] P_{\tilde{x}}[k-1|k-1] A'[k-1] + R_x[k-1] + \Delta R_x[k-1] \\ &= P_{\tilde{x}}[k|k-1] + \Delta R_x[k-1]\end{aligned} \tag{3.58}$$

where $P_{\Delta,\tilde{x}}$ is the state error covariance that has been affected by the change in state noise covariance, ΔR_x. The change in Kalman gain can then be expanded to the following form

$$\begin{aligned}\Delta K\left[k\right] = {} & P_{\tilde{x}}\left[k|k-1\right]C'\left[k\right]\left(C\left[k\right]\left(P_{\tilde{x}}\left[k|k-1\right]+\Delta R_x\left[k-1\right]\right)C'\left[k\right]+R_y\left[k\right]\right)^{-1} \\ & - P_{\tilde{x}}\left[k|k-1\right]C'\left[k\right]\left(C\left[k\right]P_{\tilde{x}}\left[k|k-1\right]C'\left[k\right]+R_y\left[k\right]\right)^{-1} \\ & + \Delta R_x\left[k-1\right]C'\left[k\right]\left(C\left[k\right]\left(P_{\tilde{x}}\left[k|k-1\right]+\Delta R_x\left[k-1\right]\right)C'\left[k\right]+R_y\left[k\right]\right)^{-1}\end{aligned} \tag{3.59}$$

where for a positive-definite state noise covariance and a change in state noise covariance, ΔR_x, representing an increase in uncertainty within the state, the first two terms reduce the magnitude of the elements of the Kalman gain vector and the third term negates the aforementioned reduction. The effects of the three terms in (3.59) are combined in the following equation.

$$\begin{aligned}\Delta K\left[k\right] = {} & \Delta R_x\left[k-1\right]C'\left[k\right]R_y\left[k\right]\left(C\left[k\right]\left(P_{\tilde{x}}\left[k|k-1\right]+\Delta R_x\left[k-1\right]\right)C'\left[k\right]+R_y\left[k\right]\right)^{-1} \\ & \cdot\left(C\left[k\right]P_{\tilde{x}}\left[k|k-1\right]C'\left[k\right]+R_y\left[k\right]\right)^{-1}\end{aligned} \tag{3.60}$$

Thus, for a positive-definite $\Delta R_x\left[k\right]$, the magnitude of each element within the Kalman gain vector is increased with respect to the sign included in the state-to-measurement matrix, C.

In other words, all else equal, an increase in uncertainty in the state by ΔR_x results in the updated state estimate tracking more closely the measurement rather than the dynamic of the system model. As in (3.55) and (3.56), this relationship is restated in the following

by calculating the limits of (3.59) with time-indices again omitted for readability.

$$\begin{aligned}\lim_{\Delta R_x \to 0_+^{n_x \times n_x}} K_\Delta[k] &= K + \lim_{\Delta R_x \to 0_+^{n_x \times n_x}} \left(\frac{P_{\tilde{x}} C'}{C\left(P_{\tilde{x}} + \Delta R_x\right) C' + R_y} \right) \\ &\quad + \lim_{\Delta R_x \to 0_+^{n_x \times n_x}} \left(\frac{\Delta R_x C'}{C\left(P_{\tilde{x}} + \Delta R_x\right) C' + R_y} \right) - \frac{P_{\tilde{x}} C'}{C P_{\tilde{x}} C' + R_y} \\ &= K + \frac{0^{n_x \times 1}}{C P_{\tilde{x}} C' + R_y} = K \end{aligned} \tag{3.61}$$

$$\lim_{\Delta R_x \to \infty^{n_x \times n_x}} K_\Delta[k] = K + \frac{1}{R_y} - \frac{P_{\tilde{x}} C'}{C P_{\tilde{x}} C' + R_y} \tag{3.62}$$

Thus, as the magnitude of ΔR_x grows, so do the elements of the effected Kalman gain $K_\Delta[k]$.

ALMF-based noise covariance estimation

Noise covariances, R_x and R_y, affect the state estimation equation within the standard KF equations of Section 3.2.1. For the purpose of calculating state point-estimates, however, it is not essential that the assumed noise covariances reflect the model or signal uncertainties exactly. This is a result of the KF-based state observer updating the state estimates as a function of the system measurements [152]. In short, KFs have a structure that causes the state estimates to converge with the true system states even for gains that are not optimal. State noise covariances are often therefore assumed to be equal to the covariance of the input to the system [153], or calculated through trial and error or heuristic procedures [154].

In contrast, accurate noise covariances are essential when KF-based state estimation is being utilized to obtain an accurate description of the probability distribution for the state estimates as is required within the KF-based measurement interval-prediction procedure of

Section 3.5. Various techniques have been developed to address the estimation of state noise covariance. One technique uses an LS filter to estimate the covariance after calculating the time-lagged auto-covariance of the operational data [155, 156]. Another technique assumes that the inverse of a function of the state-to-measurement matrix, or $(C'C)^{-1}$, exists; an assumption that is very strong and is rarely satisfied in practice [151]. This research instead employs the ALMF presented by Myers and Tapley in [157] as it is more computationally efficient and makes fewer assumptions regarding model structure when compared to the aforementioned algorithms. Moreover, the ALMF is suitable for systems that have LTV parameters as well as time-varying noise covariances.

The ALMF includes four equations that estimate the state and measurement noise as well as the state and measurement noise covariance matrices. These four equations are supported by four additional equations that are calculated directly from the standard KF equations. Regarding measurement noise, the first of the two supporting equations is the *a priori* measurement estimation error of (3.20). The second supporting equation is the following modified *a priori* measurement error covariance that excludes the measurement noise covariance, $\hat{R}_y$, of the previous time-step, $(k-1)$.

$$\underline{P}_y\left[k|k-1\right] = P_{\tilde{y}}\left[k|k-1\right] - \hat{R}_y\left[k-1\right] = C\left[k\right] P_{\tilde{x}}\left[k|k-1\right] C'\left[k\right] \tag{3.63}$$

The next two equations form an ALMF for estimation of the measurement noise covariance. First, the mean measurement estimation error is calculated as an estimate of the

measurement noise, $\hat{v}_y \in \mathbb{R}^{n_y \times 1}$, as follows

$$\hat{v}_y[k] = \hat{v}_y[k-1] + \frac{1}{N_v}\left(\tilde{y}[k|k] - \tilde{y}[k-N_v|k-N_v]\right) \tag{3.64}$$

where N_v is the length of the window over which the covariance matrices are calculated, referred to hereafter as the covariance estimation window. The initial value of the measurement noise, $\hat{v}_y[0]$, is set equal to zero due to the assumption within the KF that measurement noise is serially uncorrelated or zero mean. This equation is a moving or rolling average of the *a posteriori* measurement estimation error over the covariance estimation window. Given the above estimate, the measurement noise covariance estimation can then be calculated as follows

$$\begin{aligned}\hat{R}_y[k] = \hat{R}_y[k-1] &+ \frac{1}{N_v - 1}\left(\left(\tilde{y}[k|k] - \hat{v}_y[k]\right)^{\underline{2}} - \left(\tilde{y}[k-N_v|k-N_v] - \hat{v}_y[k]\right)^{\underline{2}}\right) \\ &+ \frac{1}{N_v(N_v-1)}\left(\tilde{y}[k|k] - \tilde{y}[k-N_v|k-N_v]\right)^{\underline{2}} \\ &- \frac{1}{N_v}\left(\underline{P}_y[k|k-1] - \underline{P}_y[k-N_v|k-N_v-1]\right)\end{aligned} \tag{3.65}$$

where $(\bullet)^{\underline{2}}$ represents the square of the variable within the parentheses multiplied by the transpose of the same variable, or $(\bullet)(\bullet)'$.

The initial value of the measurement error covariance, $\hat{R}_y[0]$, is set equal to the measurement noise covariance that is calculated offline for the standard KF as described in Section 3.2.3. The following equation introduces the rolling or moving form of unbiased

estimation for the measurement noise covariance [157].

$$\hat{R}_y[N_v] = \frac{1}{N_v - 1}\sum_{j=1}^{N_v}\left((\tilde{y}[j|j] - \hat{v}_y[N_v])^{\underline{2}} - \frac{N_v - 1}{N_v}\underline{P}_y[j|j-1]\right)$$

$$= \hat{R}_y[N_v - 1] \tag{3.66}$$

$$+ \frac{1}{N_v - 1}\left((\tilde{y}[N_v|N_v] - \hat{v}_y[N_v])^{\underline{2}} - \frac{N_v - 1}{N_v}\underline{P}_y[N_v|N_v - 1]\right) \tag{3.67}$$

For the next time-step, the above equation is modified to be recursive by incorporating the moving estimate as follows

$$\begin{aligned}\hat{R}_y[N_v + 1] = \hat{R}_y[N_v] &\\ + \frac{1}{N_v - 1}&\left((\tilde{y}[N_v + 1|N_v + 1] - \hat{v}_y[N_v])^{\underline{2}} - \frac{N_v - 1}{N_v}\underline{P}_y[N_v + 1|N_v]\right)\\ - \frac{1}{N_v - 1}&\left((\tilde{y}[1|1] - \hat{v}_y[1])^{\underline{2}} - \frac{N_v - 1}{N_v}\underline{P}_y[1|0]\right)\\ = \hat{R}_y[N_v] + \frac{1}{N_v - 1}&\Bigg((\tilde{y}[N_v + 1|N_v + 1] - \hat{v}_y[N_v + 1])^{\underline{2}}\\ - (\tilde{y}[1|1] - \hat{v}_y[1])^{\underline{2}} &+ \frac{1}{N_v}(\tilde{y}[N_v + 1|N_v + 1] - \tilde{y}[1|1])\\ - \frac{N_v - 1}{N_v}&\left(\underline{P}_y[N_v + 1|N_v] + \underline{P}_y[1|0]\right)\Bigg)\end{aligned} \tag{3.68}$$

where the fourth term of $\frac{1}{N_v}(\tilde{y}[N_v + 1|N_v + 1] - \tilde{y}[1|1])$ compensates for the forgotten or lost mean measurement noise estimate, $\hat{v}_y[1]$, in the third term. The above equations are initialized within the first N_v time-steps as an accumulation of average values. This initialization procedure is deferred to the algorithms that are presented later on within this section.

The above ALMF procedure is also performed for the estimation of state noise covari-

ance. In this case, the first of the two supporting equations is the one-step-ahead state prediction error calculated as the following difference between the *a posteriori* and *a priori* state estimates

$$\tilde{\hat{x}}\left[k\right] = \hat{x}\left[k|k\right] - \hat{x}\left[k|k-1\right] \tag{3.69}$$

where $\tilde{\hat{x}}$ is the mean state estimation error. The second supporting equation is a function of the *a priori* and *a posteriori* state error covariances as well as the state noise covariance estimate, $\hat{R}_x$, from the previous time-step, $(k-1)$, and is calculated as follows.

$$\tilde{P}_x\left[k\right] = P_{\tilde{x}}\left[k|k-1\right] - \hat{R}_x\left[k-1\right] - P_{\tilde{x}}\left[k|k\right] \tag{3.70}$$

The remaining two equations form an ALMF for estimation of the state noise covariance. The mean state estimation error is calculated as an estimate of the state noise, $\hat{v}_x \in \mathbb{R}^{n_x \times 1}$, as follows

$$\hat{v}_x\left[k\right] = \hat{v}_x\left[k-1\right] + \frac{1}{N_v}\left(\tilde{\hat{x}}\left[k\right] - \tilde{\hat{x}}\left[k-N_v\right]\right) \tag{3.71}$$

where N_v is again the covariance estimation window. Although it is not necessary that the covariance estimation window for the state noise estimate be equal to the window for the measurement noise estimate, within the work the two windows are assumed to be equal. Given the above estimate, the state noise covariance estimation can then be calculated in

a second equation as follows

$$\hat{R}_x[k] = \hat{R}_x[k-1] + \frac{1}{N_v - 1}\left(\left(\tilde{\hat{x}}[k] - \hat{v}_x[k]\right)^{\underline{2}} - \left(\tilde{\hat{x}}[k-N_v] - \hat{v}_x[k]\right)^{\underline{2}}\right) + \frac{1}{N_v(N_v-1)}\left(\tilde{\hat{x}}[k] - \tilde{\hat{x}}[k-N_v]\right)^{\underline{2}} - \frac{1}{N_v}\left(\tilde{P}_x[k] - \tilde{P}_x[k-N_v]\right) \quad (3.72)$$

where $(\bullet)^{\underline{2}}$ is as defined for (3.65) with this form derived in the same manner as for the measurement noise in (3.67) and (3.68).

The initial value of $\hat{R}_x[0]$ may be calculated to include the known system input noise. This initial value may also be estimated by considering the *a priori* measurement error or innovation as discussed in Section 3.2.3. As with the measurement noise covariance, the above two equations are also moving averages and are therefore required initialized within the first N_v time-steps of calculation. This initialization is presented in addition to the ALMF noise covariance estimation algorithms in the following paragraphs. The diagonal elements of the estimated covariance matrices are reset to absolute values at every time-step. This reset is performed due to the potential for negative definite noise covariance matrices to occur as a result of numerical applications, especially when a small amount of data has been processed [157].

Summaries of the state and measurement covariance estimation procedures are provided as subroutines in Algorithm 3.4. The two subroutines are called from within any of the previously listed KF-based algorithms, e.g. state estimation or measurement prediction. Algorithm 3.4 includes a count of the number of operations, or OPL, that are required to perform state and measurement covariance estimation for a scalar measurement. These counts are assumed to be called from the KF-based measurement interval-prediction routine

of Algorithm 3.3. A reduction in the number of total multiplication is again utilized when calculating symmetric matrices, where n_x^2 multiplications can be reduced to $\left(n_x^2 + n_x\right)/2$ for the calculation of $(\bullet)^{\underline{2}}$.

Algorithm 3.4 Adaptive-limited-memory-filter-based (ALMF) measurement ALMF_y and state ALMF_x noise covariance estimation

[Measurement noise covariance estimation]

$$\tilde{y}\left[k|k-1\right] = y\left[k\right] - \left(C\left[k\right]\hat{x}\left[k|k-1\right] + D\left[k\right]u\left[k\right]\right)$$
$$\underline{P}_y\left[k|k-1\right] = P_{\tilde{y}}\left[k|k-1\right] - \hat{R}_y\left[k-1\right]$$
$$\hat{v}_y\left[k\right] = \hat{v}_y\left[k-1\right] + \tfrac{1}{N_v}\left(\tilde{y}\left[k|k\right] - \tilde{y}\left[k-N_v|k-N_v\right]\right)$$
$$\hat{R}_y\left[k\right] = \hat{R}_y\left[k-1\right] + \frac{1}{N_v-1}\left(\left(\tilde{y}\left[k|k\right] - \hat{v}_y\left[k\right]\right)^{\underline{2}} - \left(\tilde{y}\left[k-N_v|k-N_v\right] - \hat{v}_y\left[k\right]\right)^{\underline{2}}\right)$$
$$+ \frac{1}{N_v\left(N_v-1\right)}\left(\tilde{y}\left[k|k\right] - \tilde{y}\left[k-N_v|k-N_v\right]\right)^{\underline{2}}$$
$$- \frac{1}{N_v}\left(\underline{P}_y\left[k|k-1\right] - \underline{P}_y\left[k-N_v|k-N_v-1\right]\right)$$

OPL for scalar y: $17 \in O\left(1\right)$

[State noise covariance estimation]

$$\tilde{\tilde{x}}\left[k\right] = \hat{x}\left[k|k\right] - \hat{x}\left[k|k-1\right]$$
$$\tilde{P}_x\left[k\right] = P_{\tilde{x}}\left[k|k-1\right] - \hat{R}_x\left[k-1\right] - P_{\tilde{x}}\left[k|k\right]$$
$$\hat{v}_x\left[k\right] = \hat{v}_x\left[k-1\right] + \tfrac{1}{N_v}\left(\tilde{\tilde{x}}\left[k\right] - \tilde{\tilde{x}}\left[k-N_v\right]\right)$$
$$\hat{R}_x\left[k\right] = \hat{R}_x\left[k-1\right] + \frac{1}{N_v-1}\left(\left(\tilde{\tilde{x}}\left[k\right] - \hat{v}_x\left[k\right]\right)^{\underline{2}} - \left(\tilde{\tilde{x}}\left[k-N_v\right] - \hat{v}_x\left[k\right]\right)^{\underline{2}}\right)$$
$$+ \frac{1}{N_v\left(N_v-1\right)}\left(\tilde{\tilde{x}}\left[k\right] - \tilde{\tilde{x}}\left[k-N_v\right]\right)^{\underline{2}} - \frac{1}{N_v}\left(\tilde{P}_x\left[k\right] - \tilde{P}_x\left[k-N_v\right]\right)$$

OPL for scalar y: $6.5n_x^2 + 4.5n_x + 3 \in O\left(n_x^2\right)$

$(\bullet)^{\underline{2}} = (\bullet)(\bullet)'$

The first count reveals that the computational complexity for estimating the measurement covariance of a scalar measurement is less than the previously investigated algorithms, including KF-based state estimation. Moreover, the second count reveals that the computational complexity for estimating the state covariance is quadratic with respect to the dimension of the state vector, or $\text{ALMF}_x \in O\left(n_x^2\right)$. Again, this estimation is rather insignificant when compared against the standard KF equations. The subroutines of Algorithm 3.4 do, however, require the storage of $2N_v$ and $N_v n_x^2 + N_v n_x$ variables within the memory

of the controller for measurement and state covariance estimation respectively.

Initialization of the ALMF is performed within the subroutines of Algorithm 3.4 for both state and measurement covariance estimation. The two subroutines perform the calculations of Algorithm 3.4 but for a window of increasing length up to that of the noise estimation window, N_v. The initialization procedure begins after the KF gain and state estimates have somewhat converged from the assumed initial conditions, otherwise, the covariances will capture uncertainty due to the initial conditions. Thus, the subroutines are executed for N_v time-steps following the first N_v time-steps of executing the KF-based prediction algorithm. The number of operations that are required to execute each subroutine are not reported in Algorithm 3.5 since these subroutines are not regularly executed after the initialization procedure.

Algorithm 3.5 Initialization of the noise covariance estimation subroutines using adaptive limited memory filter (ALMF)

[Initialize measurement noise covariance estimation]

calculate $\tilde{y}\left[k|k-1\right]$ and $\underline{P}_y\left[k|k-1\right]$ as in Algorithm 3.4

$\hat{v}_y\left[k\right] = \frac{k-1}{k}\hat{v}_y\left[k-1\right] + \frac{1}{k}\tilde{y}\left[k|k\right]$

$\hat{R}_y\left[k\right] = \frac{k-2}{k-1}\hat{R}_y\left[k-1\right] + \frac{1}{k-1}\left(\tilde{y}\left[k|k\right] - \hat{v}_y\left[k\right]\right)^{\underline{2}} - \frac{1}{k}\underline{P}_y\left[k|k-1\right]$

[Initialize state noise covariance estimation]

calculate $\tilde{\hat{x}}\left[k\right]$ and $\tilde{P}_x\left[k\right]$ as in Algorithm 3.4

$\hat{v}_x\left[k\right] = \frac{k-1}{k}\hat{v}_x\left[k-1\right] + \frac{1}{k}\tilde{\hat{x}}\left[k\right]$

$\hat{R}_x\left[k\right] = \frac{k-2}{k-1}\hat{R}_x\left[k-1\right] + \frac{1}{k-1}\left(\tilde{\hat{x}}\left[k\right] - \hat{v}_x\left[k\right]\right)^{\underline{2}} - \frac{1}{k}\tilde{P}_x\left[k\right]$

$(\bullet)^{\underline{2}} = (\bullet)(\bullet)'$

Along with delaying initialization of the noise covariance estimation procedure for convergence of the KF state estimation, it is also important to select a covariance estimation window length that satisfies the assumed properties of the stochastic uncertainty between the model, signals, and system. The state noise window should be relatively long in comparison to the dynamic of the process modelled within the KF otherwise the state estimates

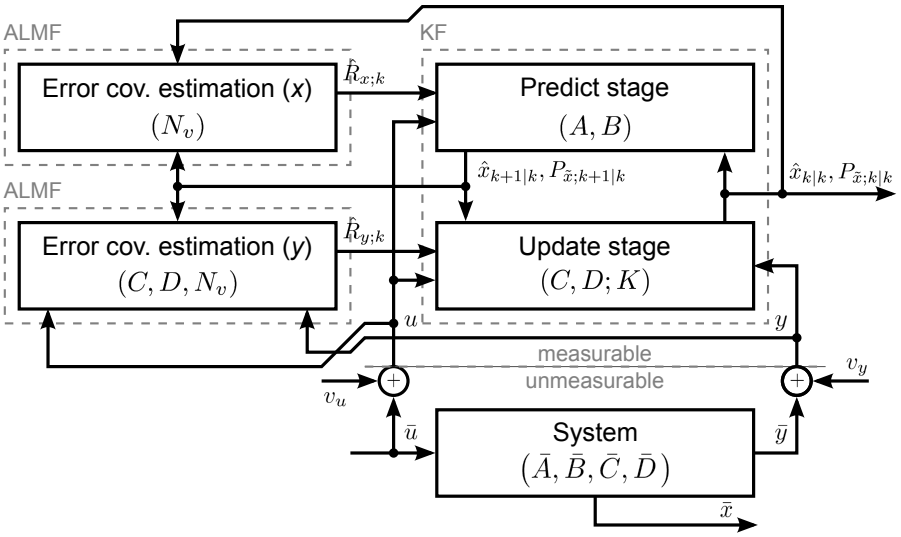

Figure 3.14: Connectivity between KF-based state estimation and the error covariance procedures of Algorithm 3.5.

will not be able to track the true dynamic response of the system and the estimates will not converge. In addition, the noise statistics should change relatively slowly in comparison to the system dynamic. Finally, as illustrated in Figure 3.14, the ALMF and KF work in a closed loop. Thus, the stability of the combined algorithm is dependent on the convergence of the KF while using the estimated noise covariances. This stability is a function of the covariance estimation window length.

A sample implementation of ALMF-based measurement and state noise covariance estimation within KF-based state estimation is provided in Algorithm 3.6. Moreover, an overview of the noise covariance estimation procedure is illustrated in Figure 3.14. This algorithm includes fewer assumptions regarding the noise covariance values in comparison to the standard KF-based state estimation routine of Algorithm 3.1, where the initial conditions for the covariance and the noise vector estimates are all that is now required to be specified. These initial conditions can be estimated by applying the ALMF noise covariance estimation algorithm to a set of training data. The training data may be obtained by

monitoring the dynamic response of the system under the different modes of operation for which estimates or predictions are to be calculated. Alternatively, the algorithm can be allowed to operate in a stand-alone mode at the onset of execution in order for the noise covariances to converge to values that are representative of the true uncertainties within the model parameters, system inputs, and system measurements.

Algorithm 3.6 ALMF/KF-based state estimation

Require: A, B, C, D, u, y, N_v
Initial conditions: $\hat{x}\left[0|0\right], P_{\tilde{x}}\left[0|0\right], \hat{R}_x\left[0\right], \hat{R}_y\left[0\right], \hat{v}_x\left[0\right], \hat{v}_y\left[0\right]$
Result: $\hat{x}\left[k|k\right], P_{\tilde{x}}\left[k|k\right], \hat{R}_x\left[k\right], \hat{R}_y\left[k\right]$

```
k = 0
call [Initialization] from Algorithm 3.1
  with R_x[0] replaced by R̂_x[0]
loop
  k = k + 1
  {measure y[k]}
  if k > N_v then
    call [Measurement noise covariance estimation] from Algorithm 3.4
  else
    call [Initialize measurement noise covariance estimation] from Algorithm 3.5
  end if
  call [State estimation (update)] from Algorithm 3.1
    with R_y[k] replaced by R̂_y[k]
  if k > N_v then
    call [State noise covariance estimation] from Algorithm 3.4
  else
    call [Initialize state noise covariance estimation] from Algorithm 3.5
  end if
  call [State propagation (predict)] from Algorithm 3.1
    with R_x[k] replaced by R̂_x[k]
  {propagate x[k] to x[k + 1]}
end loop
```

3.7 Monitoring for nonconvergence and divergence

The material of this section is largely based on the discussion regarding the detection and correction of anomalous behaviours that is included in [47]. These strategies provide an alternative to calculating observability at each time-step for LTI and potentially also LTV and LPV systems. Although, in the case of LPV systems, observability may be calculated offline for all known operating points prior to implementation of the model within the KF.

Convergence is first defined for a sequence of real vectors, denoted $\eta[k]$, with $k > k_\varepsilon$ for some k_ε and $|\eta[k] - \eta[\infty]| < \varepsilon$, by the following behaviour.

$$\lim_{k\to\infty} \eta[k] = \eta[\infty] \, \forall \varepsilon > 0 \tag{3.73}$$

In other words, the sequence of real vectors converges to a limit $\eta[\infty]$ if the norm of the difference between the limit and the current value of the vector is less than some finite positive value, ε. For finite length sequences this convergence can instead be represented by substituting $(k_\varepsilon + N)$ for ∞ in (3.73), where N is a positive integer representing a number of time-steps. Moreover, two vector sequences are said to converge if the difference between the sequences approaches the zero vector.

In contrast, divergence is defined for a sequence of real vectors, $\eta[k]$, and $|\eta[k]| > \varepsilon$ by the following behaviour

$$\lim_{k\to\infty} \eta[k] = \infty \forall \varepsilon > 0 \tag{3.74}$$

where $|\eta[k]|$ is said to grow without bound. It is more common, however, that the KF does not converge, rather than being strictly divergent. Nonconvergence is defined for a sequence of real vectors, $\eta[k]$, and $|\eta[k] - \eta[\infty]| < \varepsilon$ by the following behaviour

$$\lim_{k \to k_\varepsilon + N} \eta[k] = \underline{\eta}[k_\varepsilon + N] \, \forall \varepsilon > 0 \tag{3.75}$$

In other words, the sequence of real vectors converges to a limit, $\underline{\eta}[k_\epsilon + N]$, that is different than the true or desired limit of the sequence.

Within the KF, the following sequences may or may not converge or may even be divergent: the state vector, x, the mean-squared state, xx', the state estimate, $\hat{x}$, the estimation as well as prediction errors, $x - \hat{x}$, the error covariances, $P_{\tilde{x}}, P_{\tilde{y}}$, and in the case of the ALMF filter, the estimated noise covariances, $\hat{R}_x$ and $\hat{R}_y$.

For LTI systems, nonconvergence that is due to either the natural behaviour or unobservability of the system can be predicted by calculating steady state error covariances using the Riccati equation. The value of the error covariance can then either be determined to be bounded or to be growing without bound by evaluating the characteristic values of the covariance. For LTV systems, therefore, monitoring the magnitude of the error covariances provides a means by which to determine whether a system is diverging. More specifically, the characteristic values can be calculated by performing eigenvalue-eigenvector decomposition on the error covariances to test for negative values or large condition numbers.

In the case of nonconvergence, the error covariances will not grow without bounds. Moreover, in practice, it is not possible to measure state estimation error since the elements of the state vector cannot be measured. This unpredictable nonconvergence can be

caused by bad data, numerical problems, or mismodelling. For bad data, i.e. misleading measurements, it is not useful to monitor either the error covariance or Kalman gain since these values are not affected by the measurements. The innovations, however, can be inspected for discrepancies through statistical testing. Then the state noise covariance, R_x, may be artificially increased to improve recovery from erroneous measurement data if the erroneous data are not detected before having been processed by the KF.

Numerical problems within the algorithm can be detected by monitoring the behaviour of state error covariance. For example, larger *a posteriori* state error covariance than *a priori* error covariance is indicative of a numerical problem within the algorithm. These numerical problems can be remedied by improving the precision of the data within the KF implementation, e.g. double instead of single precision. There are also various other modifications to the standard KF equations that are considered to be more numerically robust, see [47].

The potential for mismatch between the model and the system may also result in non-convergence. Mismatch due to unmodelled state dynamics can be detected by Fourier analysis of the innovations and remedied by the addition of fictitious state noise covariance, as was the case for the numerical problems. Mismatch due to parametric modelling errors can also be detected within the innovation vector where, for time-varying parameters, either an EKF with unknown parameters as state variables, or the methods of Chapter 4 with the effects of the unknown parameters estimated as disturbance inputs can be utilized.

3.8 Summary

This chapter presents the state-space form of modelling a system as well as the recursive form of the KF state estimation equations, including the update and predict stages, for an LTV system. This chapter also considers the statistical descriptions of uncertainty that are provided as noise covariances to the KF and how these covariances relate to uncertainties regarding the operating conditions of the system.

The KF-based state estimation equations are extended to the multi-step ahead prediction problem with a focus on measurement rather than state prediction. The addition of uncertain future parameter values and signals is considered within the prediction algorithm through interval-prediction and adaptation of the noise covariances or uncertainty descriptions. Two strategies for KF-based prediction are therefore investigated. The first calculates only a single point-prediction for each time-step within the prediction window while the second instead calculates the bounds of the interval-prediction for each time-step. In utilizing the interval-based measurement prediction, decisions regarding the uncertain future measurements may be made by considering the bounds of the confidence interval for the predicted measurements rather than a single point-prediction. The result is a decision that corresponds with some level of confidence in the predicted measurement.

Adaptation of the noise covariances is achieved through the use of the ALMF noise covariance estimation algorithm. This adaptation of uncertainty descriptions allows the KF to consider time-varying uncertainty within the time-varying parameters as well as signals of the system. In addition, this chapter investigates the effect of state and measurement

noise and error covariances on the measurement predictions, confidence intervals, and Kalman gain. These aspects of the KF are often overlooked for the state estimation problem since the state estimates are, in general, point-estimates, the KF is in the Luenberger observer form, and the Kalman gain is updated according to the minimum mean squared error of the updated state error. For safety applications, however, it is essential that the interval-estimates are an accurate representation of prediction uncertainty as described by the selected level of confidence.

Chapter 4

Estimation of Disturbance Inputs for Prediction Error Compensation

Beyond the stochastic descriptions of system uncertainties that are considered in Chapter 3, it is also possible that the system dynamics are altered in a more deterministic manner. These deterministic discrepancies may be caused by the occurrence of an initiating event or unanticipated operations during transient to an abnormal condition. Initiating events are malfunctions, faults, or failures that result in a specific system dynamic operating beyond the boundaries of a predetermined region of normal operation. These initiating events and the resulting changes in the dynamic response of the system can also be considered abnormal conditions with respect to the model that is assumed within the KF. Moreover, the abnormal conditions or boundaries on the normal and safe operating regions are defined by the TSPs and safety-margins that are functions of predetermined physical limits for the system being protected as discussed in Section 1.1 and Section 2.2. In addition to the

above disturbances, the system may include time-varying parameters that are not known in advance and cannot be modelled in a stochastic or probabilistic form, e.g. using mean and covariance. It may be possible, however, to represent these changes in dynamics due to the time-varying parameters as deterministic disturbances to either the state or the measurement.

The objective of this chapter is to compensate the KF-based predictions of Chapter 3 for prediction errors that are the result of abnormal behaviour within the system or for safety parameter measurements that are otherwise diverging from predicted future values. This error compensations is made possible by estimating the disturbances that are affecting the state and measurement. In general, estimation algorithms may include, but are not limited to, the algorithms discussed in Section 2.1.3. Within this research, however, preference is given to estimation algorithms that consider deterministic models and signals. The consideration of deterministic disturbances complements the stochastic modelling of uncertainties that is considered by the KF-based prediction algorithm presented in Section 3. This concept is illustrated in Figure 4.1.

Although deterministic uncertainty may seem to be a contradiction of terms, these terms are often used together when referring to unknown or unanticipated changes in input and parameter values that are associated with systems that are defined precisely without the need for probabilistic descriptions [145]. In other words, stochastic and deterministic uncertainties are defined respectively as those values that are unknown but may be described using a probability distribution and those that are unknown but may be described by specific values [158]. To be clear, the terms stochastic and deterministic uncertainty are not known to be defined or stated explicitly as part of any standards or regulations and may

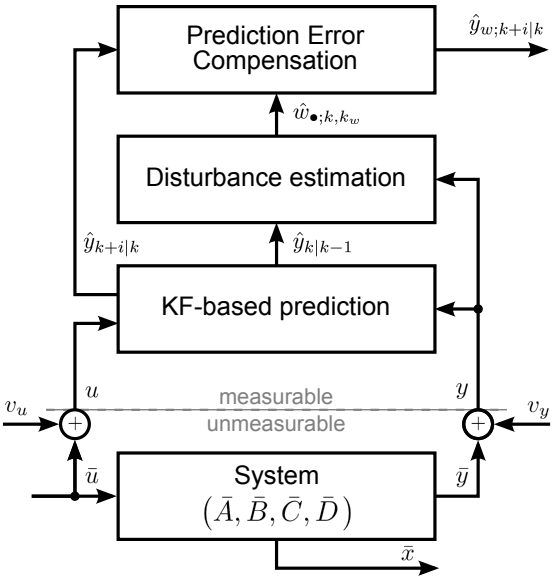

Figure 4.1: Disturbance estimation and prediction error compensation to complement the KF-based measurement prediction algorithms of Chapter 3.

therefore also be referred to by other names throughout literature.

The result of the above objective is a prediction algorithm that calculates the future values of safety parameter measurements for a system that may have time-varying parameters. This calculation takes into consideration various sources of uncertainties as well as the possible occurrence of abnormal conditions that may be uncertain with respect to the nominal system dynamic. In other words, the methods of this chapter allow for the prediction algorithm to consider that, during transient to an alarm threshold or TSP, the dynamic of the system may become a modified form of the model that is provided to the KF.

This chapter focuses specifically on disturbance estimation algorithms that are LS-based. The LS algorithm is chosen because it conforms to the criteria discussed in the previous two paragraphs and is compatible with the state-space form of modelling the system. In addition, LS estimation is a well-established method that is supported by vast

bodies of related literature and applications, some of which are reviewed in Chapter 2. The LS filter is combined with the KF in a KF/LS-based prediction algorithm where the LS disturbance estimates compensate for prediction error. This chapter therefore introduces a method of compensating for KF-based prediction error through LS-based estimation of disturbances in both the state and measurement signals of the system. This strategy is preferred over an augmented KF state or parameter estimation algorithm, as studied in [55], due to the augmented form requiring the specification of fictitious noise covariances or statistics, as $R_\bullet$ for the KF, for disturbances that are assumed to have deterministic dynamics.

Of the topics covered in this chapter, the formulation of LS-based disturbance input estimation is considered a major contribution since it is performed to compensate not only for possible disturbance inputs but also for the potentially unanticipated changes in the LTV parameters of the system. In addition, the LS-based estimation is performed from the perspective of compensating for prediction error as an unknown disturbance signal within the measurement equation. This is in addition to the state equation as performed by Juricek *et al.* [40]. This LS-based estimation is a simplification of the generalized likelihood ratio method performed by Basseville and Nikiforov [102].

More specifically, the method of this chapter allows for the originating time-step of occurrence for the initiating event to be reset rather than solving an optimization problem for a particular fault occurrence, as in the generalized likelihood ratio algorithm. This work also presents a solution to the LS estimation problem that considers disturbances that occur at an unknown time rather than at a known time as considered by Juricek *et al.* [40]. In addition, RLS solutions are formulated for the state and the measurement

disturbance input estimation problems. The two RLS solutions are then combined and the equations for prediction error as well as error covariance compensation are formulated. The KF, which is also a recursive algorithm, is considered throughout the development of the LS disturbance estimation procedures in order to achieve the combined KF/RLS-based prediction algorithm.

In summary, this chapter combines KF-based state and measurement prediction with ALMF-based noise covariance estimation and prediction error compensation through RLS-based disturbance input estimation. This chapter does not attempt, however, to cover the vast body of literature and applications that are related to the LS methods. For a more complete treatment of LS estimation of disturbance inputs refer to the text by Basseville and Nikiforov [102].

4.1 Least-Squares-based Estimation of Disturbance Inputs

It is expected that estimating and then compensating for prediction error will improve the accuracy of the predicted measurements and, in turn, the reliability of making predictive decisions. This section therefore introduces LS-based estimation of disturbances within the state and measurement equations of a system. More specifically, this section investigates the use of the LS filter to estimate a disturbance input with an assumed deterministic disturbance model or profile that is optimal with respect to the LS error between the current measurement and the *a priori* measurement estimate or prediction as defined in

(3.20). The estimated disturbances are then utilized to compensate for estimation error. These efforts are in support of extending the disturbance estimation problem to estimate and compensate for prediction error in Section 4.1.2 by propagating the disturbances to a predetermined prediction horizon. This work does not consider the robustness of the estimation and prediction error compensation routines to the selection of the disturbance model. The models are chosen to represent reasonable deviations in the system dynamic response over relatively short periods of time that may lead an abnormal condition.

Error between a predicted measurement and the true measurement may be caused by an additive disturbance within either the state or the measurement equation. It is therefore assumed that the system is modelled as a modified form of the discrete-time LTV stochastic state-space model in (3.9) and (3.10) that includes additive state and measurement disturbance sequences as follows

$$x\left[k+1\right] = A\left[k\right]x\left[k\right] + B\left[k\right]u\left[k\right] + v_x\left[k\right] + \Gamma_x\left[k, k_{w_x}\right]w_x\left[k, k_{w_x}\right] \tag{4.1}$$

$$y\left[k\right] = C\left[k\right]x\left[k\right] + D\left[k\right]u\left[k\right] + v_y\left[k\right] + \Gamma_y\left[k, k_{w_y}\right]w_y\left[k, k_{w_y}\right] \tag{4.2}$$

where $\Gamma_x \in \mathbb{R}^{n_x \times n_{w_x}}$ and $\Gamma_y \in \mathbb{R}^{n_y \times n_{w_y}}$ are the assumed deterministic dynamic profiles of the state and measurement disturbance respectively, $w_x \in \mathbb{R}^{n_{w_x} \times 1}$ and $w_y \in \mathbb{R}^{n_{w_y} \times 1}$ are the respective state and measurement disturbance inputs, and $k_{w_\bullet}$ is the time-step at which the disturbance is assumed to have initiated. In addition, system input, u as well as the disturbance profile, $\Gamma_\bullet$, are assumed to be deterministic. All other parameters and signals are as defined for the stochastic state-space model in (3.9) and (3.10). In this form, the disturbances provide a mechanism for estimating errors that are due to uncertain inputs

and system parameters, e.g. $\bar{A}[k] \neq A[k]$ and $\bar{u}[k] \neq u[k]$, that are not easily described by probability distributions.

The above disturbance profile and input pairs, $\Gamma_\bullet$ and $w_\bullet$, represent an accumulation of a set of $l \geq 1$ disturbances that can be modelled in the following state-space form for the state input disturbance

$$\begin{aligned}
\Gamma_\bullet[k, k_{w_\bullet}]\, w_\bullet[k, k_{w_\bullet}] &= \underline{\Gamma}_{\bullet,1}[k, k_{w_\bullet}]\, \gamma_{\bullet,1}[k, k_{w_\bullet}] + \cdots + \underline{\Gamma}_{\bullet,l}[k, k_{w_\bullet}]\, \gamma_{\bullet,l}[k, k_{w_\bullet}] \\
\gamma_{\bullet,1}[k, k_{w_\bullet}] &= \prod_{j=k_{w_\bullet}}^{k} \Gamma_{\bullet,1}[j, k_{w_\bullet}]\, \gamma_{\bullet,1}[k_{w_\bullet}, k_{w_\bullet}] \\
&\quad + \sum_{j_1=k_{w_\bullet}}^{k-1} \prod_{j_2=0}^{k-2-j_1} \Gamma_{\bullet,1}[k-1-j_2, k_{w_\bullet}]\, w_{\bullet,1}[k, k_{w_\bullet}] \\
&\vdots \\
\gamma_{\bullet,l}[k, k_{w_\bullet}] &= \sum_{j_1=k_{w_\bullet}}^{k-1} \prod_{j_2=0}^{k-2-j_1} \Gamma_{\bullet,l}[k-1-j_2, k_{w_\bullet}]\, w_{\bullet,l}[k, k_{w_\bullet}]
\end{aligned} \tag{4.3}$$

where $\prod_{j=0}^{-1} = \mathbb{I}$, $\gamma_{\bullet,\bullet} \in \mathbb{R}^{n_\bullet \times 1}$ are the individual disturbance profile components, e.g. bias, ramp, sinusoid, $\Gamma_{\bullet,\bullet} \in \mathbb{R}^{n_\bullet \times 1}$ and $\underline{\Gamma}_{\bullet,\bullet} \in \mathbb{R}^{n_\bullet \times 1}$ are the individual disturbance models that are representative of state and state-to-measurement matrices respectively, and $w_{\bullet,\bullet} \in \mathbb{R}^{n_\bullet \times 1}$ are the individual disturbance inputs.

The disturbance profile representation requires that the initial condition for each individual disturbance be equal to the zero vector $\gamma = 0^{n_\bullet \times 1}$, hence the first term series product reducing to zero in the latter component of (4.3). These dynamics are written as functions of free and forced response due to the disturbance profiles including the assumption of constant input, $w[k, k_{w_\bullet}]$, over the duration of the dynamic response, i.e. from $k_{w_\bullet}$ to k. The above disturbance models can also be represented in a more familiar state-space form

as follows

$$\text{state}\begin{cases} \gamma_{\bullet,1}\left[k,k_{w_x}\right] & = \Gamma_{\bullet,1}\left[k-1,k_{w_x}\right]\gamma_{\bullet,1}\left[k-1,k_{w_x}\right]+w_{\bullet,1}\left[k-1,k_{w_x}\right] \\ & \vdots \\ \gamma_{\bullet,l}\left[k,k_{w_x}\right] & = \Gamma_{\bullet,l}\left[k-1,k_{w_x}\right]\gamma_{\bullet,l}\left[k-1,k_{w_x}\right]+w_{\bullet,l}\left[k-1,k_{w_x}\right] \end{cases}$$

$$\text{meas.}\left\{\Gamma_{\bullet}\left[k,k_{w_y}\right]w_{\bullet}\left[k,k_{w_y}\right] = \underline{\Gamma}_{\bullet,1}\left[k,k_{w_y}\right]\gamma_{\bullet,1}\left[k,k_{w_y}\right]+\cdots+\underline{\Gamma}_{\bullet,l}\left[k,k_{w_y}\right]\gamma_{\bullet,l}\left[k,k_{w_y}\right]\right. \tag{4.4}$$

for the indicated set of state equations and the combined measurement equation.

The disturbance profiles, Γ_x and Γ_y, are usually in one of two forms; an offset that represents bias, or a ramp that represents drift, although any profile that can be modelled using (4.3) may also be included [40]. For example, the disturbance profile $\Gamma_x = \mathbb{I}$ injects an offset in state excitation with magnitude equal to the elements of the estimated state disturbance input. This profile is equivalent to a single component disturbance model of $\Gamma_{x,1} = 0^{n_x \times n_x}$ where the disturbance is equal to the individual disturbance input, $w_{\bullet,\bullet}$. In contrast, the disturbance profile $\Gamma_y = \begin{bmatrix} \mathbb{I} & T_s\left(k-k_{w_\bullet}\right)\mathbb{I} \end{bmatrix}$ injects a ramp in the measurement with both the offset and rate of change provided by the estimated disturbance input. This model is the combination of the previous component for bias disturbance, $\Gamma_{y,1} = 0^{n_y \times n_y}$, along with the ramp component of the disturbance model as $\Gamma_{y,2} = \mathbb{I}$.

For a system that is operating abnormally or with time-varying parameters the error between measurement, y, and the compensated measurement estimate, $\hat{y}_w$, can be decom-

posed into the following three terms

$$\tilde{y}_w\left[k|k-1\right] = \tilde{y}\left[k|k-1\right] - \rho_x\left[k, k_{w_x}\right] - \rho_y\left[k, k_{w_y}\right] \tag{4.5}$$

where $\rho_x \in \mathbb{R}^{n_y \times 1}$ and $\rho_y \in \mathbb{R}^{n_y \times 1}$ are the respective cumulative effects of the unknown state and measurement disturbances on the measurement estimation error, and $\tilde{y}$ is the *a priori* measurement innovation or residual that is not necessarily zero-mean due to the presence of the disturbance. In other words, it is assumed in the above equation that a non-zero mean measurement innovation, $\tilde{y}$, is caused by some deterministic modification to the input of the system. This error is to be compensated for by LS estimation of the disturbance input where the compensated error is denoted, $\tilde{y}_w$. The LS problem is then formulated to minimize the sum of the squared residuals with the following objective function

$$S = \sum_{j=k_{w_\bullet}}^{k} \left(\tilde{y}_w\left[j|j-1\right]\right)^2 = \sum_{j=k_{w_\bullet}}^{k} \left(\tilde{y}\left[j|j-1\right] - \rho_x\left[j, k_{w_x}\right] - \rho_y\left[j, k_{w_y}\right]\right)^2 \tag{4.6}$$

where each of the state and measurement disturbance can be processed individually with the latter of the disturbance estimations taking into consideration the compensation performed by the former disturbance estimation.

4.1.1 Estimation and estimation error compensation

The disturbance estimation procedures are developed separately for measurement and state disturbances within the first and second halves of this section respectively.

Disturbance to the measurement

In (4.2), the measurement, y, is affected by a known measurement disturbance profile, Γ_y, and an unknown measurement disturbance input, w_y. This measurement disturbance affects the *a priori* measurement estimate as a result of being propagated through the KF by the state update equation (3.16). The cumulative effect of the measurement disturbance on the *a priori* measurement estimate is therefore a function of known system parameters as well as the Kalman gain, or

$$\begin{aligned}
\rho_y\left[k, k_{w_y}\right] &= \left(y\left[k\right] - \hat{y}\left[k|k-1\right]\right) - \left(y\left[k\right] - \hat{y}_{w_y}\left[k|k-1\right]\right) \\
&= \hat{y}_{w_y}\left[k|k-1\right] - \hat{y}\left[k|k-1\right] \\
&= \Bigg(\Gamma_y\left[k, k_{w_y}\right] - C\left[k\right] A\left[k-1\right] \\
&\quad \cdot \sum_{j_1=1}^{k-k_{w_y}} \prod_{j_2=1}^{j_1-1} \underline{A}_y\left[k-j_2\right] K\left[k-j_1\right] \Gamma_y\left[k-j_1, k_{w_y}\right] \Bigg) w_y\left[k, k_{w_y}\right]
\end{aligned} \tag{4.7}$$

where $\sum_{j=1}^{0} = 0^{n_x \times n_{w_y}}$, and $\prod_{j=1}^{0} = \mathbb{I}$, with the partial cumulative effect of the propagation through the KF, denoted $\underline{A}_y\left[k\right]$, given in [102] as follows.

$$\underline{A}_y\left[k\right] = \left(I - K\left[k\right] C\left[k\right]\right) A\left[k-1\right] \tag{4.8}$$

The measurement disturbance is then simplified to be the product of a known time dependent matrix, $\underline{\rho}_y \in \mathbb{R}^{n_y \times n_{w_y}}$, that represents the cumulative effect of the measurement disturbance profile on the measurement and the unknown measurement disturbance input,

w_y, as follows.

$$\rho_y\left[k, k_{w_y}\right] = \underline{\rho}_y\left[k, k_{w_y}\right] w_y\left[k, k_{w_y}\right] \tag{4.9}$$

The objective function, S, for LS estimation of the measurement disturbance input is the following sum of the squared error between the *a priori* measurement error and the cumulative effect of the measurement disturbance.

$$S\left(w_y\right) = \sum_{j=k_{wy}}^{k} \left(\tilde{y}\left[j|j-1\right] - \underline{\rho}_y\left[j, k_{w_y}\right] w_y\left[j, k_{w_y}\right]\right)^2 \tag{4.10}$$

The solution to the LS disturbance input estimation problem is then defined by the following criteria or quadratic minimization

$$\hat{w}_y = \arg\min_{w_y} S\left(w_y\right) \tag{4.11}$$

where $\arg\min_{w_y}$ operates to find the value of w_y for which the objective function attains a minimum value. The solution to this minimization problem for the objective function in (4.10) is the estimated measurement disturbance input, $\hat{w}_y$, given in the weighted LS form or the weighted Markov estimator as follows

$$\begin{aligned}\hat{w}_y\left[k, k_{w_y}\right] = &\left(\sum_{j=k_{w_y}}^{k} \underline{\rho}'_y\left[j, k_{w_y}\right] \Lambda_y^{k-j} P_{\tilde{y}}^{-1}\left[j|j-1\right] \underline{\rho}_y\left[j, k_{w_y}\right]\right)^{-1} \\ &\cdot \left(\sum_{j=k_{w_y}}^{k} \underline{\rho}'_y\left[j, k_{w_y}\right] \Lambda_y^{k-j} P_{\tilde{y}}^{-1}\left[j|j-1\right] \tilde{y}\left[j|j-1\right]\right)\end{aligned} \tag{4.12}$$

where $P_{\tilde{y}}^{-1}$ scales the estimate with respect to the covariance of the measurement innovation, or *a priori* measurement residual, and Λ_y is a matrix with time-invariant forgetting factor, λ_y, and $\Lambda_y = \lambda_y \mathbb{I}$. These forgetting factors give exponentially diminishing weight to the measurement error samples, $\tilde{y}$, resulting in the most recent sample having the greatest effect on the LS estimation whereas the sample from time-step k_{w_y} has the least effect. More precisely, the filter defined in (4.12) is the Markov form of the weighted LS estimator as it utilizes the *a priori* covariance matrix, $P_{\tilde{y}}$, to maximize the probability that the *a priori* KF-based measurement residual is equal to zero. This minimal solution considers each of the *a priori* measurement estimation errors or innovations over the estimation window, $k_{w_y}, \ldots, k$.

Having estimated the measurement disturbance input, the KF-based *a priori* measurement prediction is then compensated as follows to include the cumulative effect of the LS-based measurement disturbance estimate that is assumed to have initiated at time-step, k_{w_y}.

$$\hat{y}_{w_y}[k|k-1] = \hat{y}[k|k-1] + \underline{\rho}_y\left[k, k_{w_y}\right] \hat{w}_y\left[k, k_{w_y}\right] \tag{4.13}$$

The combined KF/LS-based measurement estimate is therefore a modified form of (4.5) whereby only the measurement disturbance term is considered. In other words, the above compensation ignores for the time-being the cumulative effect of the state disturbance on the measurement estimation error, $\rho_x[k, k_{w_x}]$, as included in (4.5). Although the compensated measurement prediction is a more accurate prediction of the true future measurements, the prediction does not replace the *a priori* measurement estimate, $\hat{y}[k|k-1]$,

within the KF-based estimation and prediction procedure of Section 3.2. This separation of the compensated and original estimates is necessary for the LS objective function to capture the accuracy of the *a priori* KF-based estimates within each time-step of operation.

In addition to compensating the mean measurement estimate, the *a priori* measurement error covariance of (3.19) is compensated for the newly calculated measurement estimate, $\hat{y}_{w_y}$, as follows

$$\begin{aligned} P_{\tilde{y}_{w_y}}[k|k-1] &= E\left\{\tilde{y}_{w_y}[k|k-1]\,\tilde{y}'_{w_y}[k|k-1]\right\} \\ &= E\left\{\left(y[k]-\hat{y}_{w_y}[k|k-1]\right)\left(y[k]-\hat{y}_{w_y}[k|k-1]\right)'\right\} \\ &= E\left\{\left(y[k]-\hat{y}[k|k-1]-\underline{\rho}_y\left[k,k_{w_y}\right]\hat{w}_y\left[k,k_{w_y}\right]\right)^{\underline{2}}\right\} \\ &= P_{\tilde{y}}[k|k-1]+\underline{\rho}_y\left[k,k_{w_y}\right]P_{\hat{w}_y}\left[k,k_{w_y}\right]\underline{\rho}'_y\left[k,k_{w_y}\right] \\ &\quad -\underline{\rho}_y\left[k,k_{w_y}\right]P_{\hat{w}_y,\tilde{y}'}\left[k,k_{w_y}\right]-P'_{\hat{w}_y,\tilde{y}'}\left[k,k_{w_y}\right]\underline{\rho}'_y\left[k,k_{w_y}\right] \end{aligned} \tag{4.14}$$

where $P_{\hat{w}_y} \in \mathbb{R}^{n_{w_y}\times n_{w_y}}$ is the covariance of the estimated measurement disturbance input, $\hat{w}_y$, and $P_{\hat{w}_y,\tilde{y}'} \in \mathbb{R}^{n_{w_y}\times n_y}$ is the cross-covariance between the estimated disturbance input and the original *a priori* measurement innovation, $\tilde{y}[k|k-1]$. Here, the cumulative disturbance estimate is negative as a result of the disturbance being added to the measurement estimate and then subtracted from the measurement sample.

The calculation of these covariances is necessary to allow interval estimation and prediction problems to also consider the potential disturbances. The following covariances represent uncertainties in the estimated disturbance inputs. Thus, although the disturbance model or profile is deterministic and no noise statistics are assumed, the estimated

input has a defined covariance that results from noise within the $(k - k_{w_y})$ innovations that are considered over the LS estimation window.

The covariance of the measurement disturbance input, $\hat{w}_y$, is formulated for the weighted Markov estimator as a function of the cumulative measurement disturbance, $\underline{\rho}_y$, in the following equation.

$$\begin{aligned} P_{\hat{w}_y}\left[k, k_{w_y}\right] &= E\left\{\hat{w}_y\left[k, k_{w_y}\right] \hat{w}_y'\left[k, k_{w_y}\right]\right\} \\ &= E\left\{\left(\left(\sum_{j=k_{w_y}}^{k} \underline{\rho}_y'\left[j, k_{w_y}\right] \Lambda_y^{k-j} P_{\tilde{y}}^{-1}\left[j|j-1\right] \underline{\rho}_y\left[j, k_{w_y}\right]\right)^{-1}\right.\right. \\ &\quad \left.\left. \cdot \sum_{j=k_{w_y}}^{k} \underline{\rho}_y'\left[j, k_{w_y}\right] \Lambda_y^{k-j} P_{\tilde{y}}^{-1}\left[j|j-1\right] \tilde{y}\left[j|j-1\right]\right)^{\underline{2}}\right\} \\ &= \left(\sum_{j=k_{w_y}}^{k} \underline{\rho}_y'\left[j, k_{w_y}\right] \Lambda_y^{k-j} P_{\tilde{y}}^{-1}\left[j|j-1\right] \underline{\rho}_y\left[j, k_{w_y}\right]\right)^{-1} \end{aligned} \tag{4.15}$$

In addition, the cross-covariance between the measurement disturbance input, $\hat{w}_y$, and the *a priori* measurement estimation error, $\tilde{y}\left[k|k-1\right]$, is calculated as follows

$$\begin{aligned} P_{\hat{w}_y, \tilde{y}'}\left[k, k_{w_y}\right] &= E\left\{\hat{w}_y\left[k, k_{w_y}\right]\left(y\left[k\right] - \hat{y}\left[k|k-1\right]\right)'\right\} \\ &= E\left\{P_{\hat{w}_y}\left[k, k_{w_y}\right]\right. \\ &\quad \cdot \left(\sum_{j=k_{w_y}}^{k} \underline{\rho}_y'\left[j, k_{w_y}\right] \Lambda_y^{k-j} P_{\tilde{y}}^{-1}\left[j|j-1\right]\left(y\left[j\right] - \hat{y}\left[j|j-1\right]\right)\right) \\ &\quad \left. \cdot \left(C\left[k\right]\left(x\left[k\right] - \hat{x}\left[k|k-1\right]\right) + v_y\left[k\right]\right)'\right\} \end{aligned}$$

$$
\begin{aligned}
&= E\left\{ P_{\hat{w}_y}\left[k, k_{w_y}\right] \underline{\rho}'_y\left[k, k_{w_y}\right] \Lambda_y^0 P_{\tilde{y}}^{-1}\left[k|k-1\right] \right. \\
&\quad \cdot \left(C\left[k\right]\left(x\left[k\right] - \hat{x}\left[k|k-1\right]\right) + v_y\left[k\right]\right) \\
&\quad \left. \cdot \left(C\left[k\right]\left(x\left[k\right] - \hat{x}\left[k|k-1\right]\right) + v_y\left[k\right]\right)' \right\} \\
&= P_{\hat{w}_y}\left[k, k_{w_y}\right] \underline{\rho}'_y\left[k, k_{w_y}\right] P_{\tilde{y}}^{-1}\left[k|k-1\right] \left(C\left[k\right] P_{\tilde{x}}\left[k|k-1\right] C'\left[k\right] + R_y\left[k\right]\right) \\
&= P_{\hat{w}_y}\left[k, k_{w_y}\right] \underline{\rho}'_y\left[k, k_{w_y}\right] \qquad (4.16)
\end{aligned}
$$

where the summation over j is reduced to only the term associated with time-step, k, due to the measurement innovations at different time-steps being uncorrelated [159]. Moreover, the measurement innovation covariance cancels with the inverse measurement innovation covariance.

Disturbance to the state

In (4.1), state, $x\left[k+1\right]$, is affected by a known state disturbance profile, Γ_x, and an unknown state disturbance input, w_x. The state disturbance also indirectly affects the *a priori* measurement estimate as a result of being propagated through the KF by the state update equation (3.16). The cumulative effect of the state disturbance on the *a priori* measurement estimate is calculated as the following function of known system parameters and KF gain

$$
\begin{aligned}
\rho_x\left[k, k_{w_x}\right] &= \left(y\left[k\right] - \hat{y}\left[k|k-1\right]\right) - \left(y\left[k\right] - \hat{y}_{w_x}\left[k|k-1\right]\right) \\
&= C\left[k\right] \sum_{j_1=1}^{k-k_{wx}} \prod_{j_2=1}^{j_1-1} \underline{A}_x\left[k-j_2\right] \Gamma_x\left[k-j_1, k_{w_x}\right] w_x\left[k-1, k_{w_x}\right] \qquad (4.17)
\end{aligned}
$$

where again $\sum_{j=1}^{0} = 0^{n_x \times n_{w_x}}$, $\prod_{j=1}^{0} = \mathbb{I}^{n_x \times n_x}$, and $\underline{A}_x[k]$ is calculated as follows [102].

$$\underline{A}_x[k] = A[k](\mathbb{I} - K[k]C[k]) \tag{4.18}$$

This formulation of state disturbance is then simplified to be the product of a known time dependent matrix, $\underline{\rho}_x \in \mathbb{R}^{n_y \times n_{w_x}}$, and an unknown state disturbance input, w_x, as follows

$$\begin{aligned}\rho_x[k, k_{w_x}] &= C[k]\underline{\underline{\rho}}_x[k, k_{w_x}]\, w_x[k-1, k_{w_x}] \\ &= \underline{\rho}_x[k, k_{w_x}]\, w_x[k-1, k_{w_x}]\end{aligned} \tag{4.19}$$

where $\underline{\rho}_x$ is the cumulative effect of the state disturbance profile on the measurement, and $\underline{\underline{\rho}}_x \in \mathbb{R}^{n_x \times n_{w_x}}$ is the cumulative effect of the state disturbance profile on the state. The initial effect of the state disturbance profile on the measurement is as follows

$$\rho_x[k_{w_x}+1, k_{w_x}] = C[k_{w_x}+1]\,\Gamma_x[k_{w_x}, k_{w_x}]\, w_x[k_{w_x}, k_{w_x}] \tag{4.20}$$

where the cumulative effect of the disturbance profile at time-step $(k_{w_x}+1)$ is a function of the state-to-measurement matrix of the same time-step multiplied by the disturbance profile and input of the previous time-step as established in (4.1) and (4.5). In addition, the zero-step-ahead value of the cumulative value is $\rho_x[k_{w_x}, k_{w_x}] = 0^{n_y \times n_{w_x}}$, since the measurement is not affected by the disturbance which is assumed to have initiated at time-step k_{w_x}.

Although the disturbance input from the previous time-step, $w_x[k-1, k_{w_x}]$, affects

the measurement, $y[k]$, the estimate of the disturbance input is represented using the time-step of estimation as $\hat{w}_x[k, k_{w_x}]$. Thus, the current estimate of the state disturbance input is the expectation of the state disturbance input from the previous time-step, or $\hat{w}_x[k, k_{w_x}] = E\{w_x[k-1, k_{w_x}]\}$. The same representations are used for the cumulative effect of the state disturbances, as $\underline{\rho}_x$ and $\underline{\underline{\rho}}_x$. These relationships are established in the state equation definition of (4.1).

The weighted Markov estimate of the unknown disturbance input, $\hat{w}_x$, is calculated in the same manner as for the measurement disturbance in (4.12), with the following objective function

$$S_x(w) = \sum_{j=k_{w_x}}^{k} \underline{\lambda}_x[j] \left(\tilde{y}[j|j-1] - \underline{\rho}_x[j, k_{w_x}] w_x[j, k_{w_x}] \right)^2 \tag{4.21}$$

where $\underline{\lambda}_\bullet$ is the forgetting factor for each time-step within the estimation window. The quadratic minimization problem for LS estimation of state disturbance input is therefore as follows.

$$\hat{w}_x = \arg\min_{w_x} S(w_x) \tag{4.22}$$

The unique solution to this minimization problem is the estimated measurement distur-

bance input, $\hat{w}_x$, given in the weighted LS form as follows

$$\hat{w}_x\left[k, k_{w_x}\right] = \left(\sum_{j=k_{w_x}}^{k} \underline{\rho}_x'\left[j, k_{w_x}\right] \Lambda_x^{k-j} P_{\tilde{y}}^{-1}\left[j|j-1\right] \underline{\rho}_x\left[j, k_{w_x}\right]\right)^{-1} \cdot \left(\sum_{j=k_{w_x}}^{k} \underline{\rho}_x'\left[j, k_{w_x}\right] \Lambda_x^{k-j} P_{\tilde{y}}^{-1}\left[j|j-1\right] \tilde{y}\left[j|j-1\right]\right) \tag{4.23}$$

where $P_{\tilde{y}}^{-1}$ again scales the estimate with respect to the covariance of the measurement innovation and Λ_x is a matrix with time-invariant forgetting factor, λ_x, where $\Lambda_x = \lambda_x \mathbb{I}$. This state disturbance estimation procedure is a modified form of the disturbance estimation that is presented for the prediction of abnormal conditions in [40] which, in turn, cites methods for the detection of abrupt changes in [102].

Having estimated the state disturbance input, the KF-based *a priori* measurement prediction is then compensated in the following equation to include the cumulative effect of the LS-based state disturbance estimate that is assumed to have initiated at time-step, k_{w_x}.

$$\hat{y}_{w_x}\left[k|k-1\right] = \hat{y}\left[k|k-1\right] + \underline{\rho}_x\left[k, k_{w_x}\right] \hat{w}_x\left[k, k_{w_x}\right] \tag{4.24}$$

The above compensation ignores for the time-being the effect of the measurement disturbance to the measurement estimation error, $\rho_y\left[k, k_{w_y}\right]$, in (4.5). In addition to affecting the *a priori* measurement estimate, the state disturbance also affects the *a priori* state estimate, $\hat{x}\left[k|k-1\right]$. The updated *a priori* state estimate is therefore compensated as

follows.

$$\hat{x}_{w_x}[k|k-1] = \hat{x}[k|k-1] + \underline{\underline{\rho}}_x[k, k_{w_x}]\,\hat{w}_x[k, k_{w_x}] \tag{4.25}$$

As in the case of estimating the measurement disturbance, the compensated *a priori* measurement and state estimates remain separate from the standard KF procedure. This state compensation may be useful when considering the effect of disturbances within the state domain. It is not necessary, however, to compensate the state estimates while at the same time compensating the measurement predictions since in doing so the compensation would be doubled.

The *a priori* measurement error covariance in (3.19) is compensated for the newly calculated measurement estimate, $\hat{y}_{w_x}$, as follows

$$\begin{aligned} P_{\tilde{y}_{w_x}}[k|k-1] &= E\left\{\tilde{y}_{w_x}[k|k-1]\,\tilde{y}'_{w_x}[k|k-1]\right\} \\ &= E\left\{\left(y[k] - \hat{y}[k|k-1] - \underline{\rho}_x[k, k_{w_x}]\,\hat{w}_x[k, k_{w_x}]\right)^{\underline{2}}\right\} \\ &= C[k]\,P_{\tilde{x}}[k|k]\,C'[k] + R_y[k] + \underline{\rho}_x[k, k_{w_x}]\,P_{\hat{w}_x}[k]\,\underline{\rho}'_x[k, k_{w_x}] \\ &\quad - \underline{\rho}_x[k, k_{w_x}]\,P_{\hat{w}_x,\tilde{y}}[k] - P'_{\hat{w}_x,\tilde{y}}[k]\,\underline{\rho}'_x[k, k_{w_x}] \end{aligned} \tag{4.26}$$

where $P_{\hat{w}_x} \in \mathbb{R}^{n_{w_x} \times n_{w_x}}$ is the covariance of the estimated state disturbance input, $\hat{w}_x$, and $P_{\hat{w}_x,\tilde{y}} \in \mathbb{R}^{n_{w_x} \times n_y}$ is the cross-covariance between the estimated disturbance input and the original *a priori* measurement innovation, $\tilde{y}[k|k-1]$.

The covariance of the state disturbance input, $\hat{w}_x$, is calculated for the weighted Markov

estimator as the following function of the cumulative state disturbance, $\underline{\rho}_x$.

$$\begin{aligned} P_{\hat{w}_x}[k, k_{w_x}] &= E\left\{\left(\hat{w}_x[k, k_{w_x}]\right)\left(\hat{w}_x[k, k_{w_x}]\right)'\right\} \\ &= \left(\sum_{j=k_{w_x}}^{k} \underline{\rho}_x'[j, k_{w_x}]\, \Lambda_x^{k-j} P_{\tilde{y}}^{-1}[j|j-1]\, \underline{\rho}_x[j, k_{w_x}]\right)^{-1} \end{aligned} \tag{4.27}$$

In addition, the cross-covariance between the state disturbance input, $\hat{w}_x$, and the *a priori* measurement estimation error, $\tilde{y}[k|k-1]$, is calculated as follows

$$\begin{aligned} P_{\hat{w}_x,\tilde{y}}[k, k_{w_x}] &= E\left\{\left(\hat{w}_x[k, k_{w_x}]\right)\left(y[k] - \hat{y}[k|k-1]\right)'\right\} \\ &= P_{\hat{w}_x}[k, k_{w_x}]\, \underline{\rho}_x'[k, k_{w_x}] \end{aligned} \tag{4.28}$$

where, again, the summation over j is reduced to only the term associated with time-step k and the measurement innovations cancel [159].

4.1.2 Prediction error compensation

In this section, the LS-based disturbance input estimation procedure is extended to estimate and compensate for prediction errors over the prediction window. The development of disturbance prediction and prediction error compensation procedures are presented separately for prediction error that is due to a measurement and state disturbances within the first and second halves of this section respectively.

Disturbance to the measurement

The objective of prediction error compensation is to predict and compensate i-step-ahead measurement predictions for the error between the i-step-ahead KF-based measurement prediction and the corresponding eventual future measurement given an assumed measurement disturbance profile. Prediction error compensation is performed in the same manner as for the compensation of measurement estimation error in (4.13) or as follows.

$$\hat{y}_{w_y}\left[k+i|k\right] = \hat{y}\left[k+i|k\right] + \underline{\rho}_y\left[k+i, k_{w_y}\right]\hat{w}_y\left[k, k_{w_y}\right] \tag{4.29}$$

In addition, the propagated cumulative effect of the disturbance profile, $\underline{\rho}_y$, on the measurement prediction is calculated or propagated as follows

$$\begin{aligned}\underline{\rho}_y\left[k+i, k_{w_y}\right] = \Gamma_y\left[k+i, k_{w_y}\right] - C\left[k+i\right]A\left[k+i-1\right] \\ \cdot \sum_{j_1=1}^{k+i-k_{w_y}} \prod_{j_2=1}^{j_1-1} \underline{A}_y\left[k+i-j_2\right] K\left[k+i-j_1\right] \Gamma_y\left[k+i-j_1, k_{w_y}\right]\end{aligned} \tag{4.30}$$

where $\prod_{j=1}^{0} = \mathbb{I}^{n_y \times n_x}$.

For predictions that are beyond one time-step ahead, the Kalman gain is equal to zero, $K\left[k+i\right] \triangleq 0^{n_x \times n_y} \forall i > 1$. Thus, the cumulative effect of measurement disturbance profile

reduces to the following form

$$\begin{aligned}\underline{\rho}_y\left[k+i,k_{w_y}\right] &= \Gamma_y\left[k+i,k_{w_y}\right] - C\left[k+i\right]A\left[k+i-1\right] \\ &\quad\cdot\left(\sum_{j_1=1}^{i-1}\prod_{j_2=1}^{j_1-1}\underline{A}_y\left[k+i-j_2\right]K\left[k+i-j_1\right]\Gamma_y\left[k+i-j_1,k_{w_y}\right]\right. \\ &\quad\left.+\sum_{j_1=i}^{k+i-k_{w_y}}\prod_{j_2=1}^{j_1-1}\underline{A}_y\left[k+i-j_2\right]K\left[k+i-j_1\right]\Gamma_y\left[k+i-j_1,k_{w_y}\right]\right) \\ &= \Gamma_y\left[k+i,k_{w_y}\right] - C\left[k+i\right]A\left[k+i-1\right] \\ &\quad\cdot\sum_{j_1=i}^{k+i-k_{w_y}}\prod_{j_2=1}^{j_1-1}\underline{A}_y\left[k+i-j_2\right]K\left[k+i-j_1\right]\Gamma_y\left[k+i-j_1,k_{w_y}\right] \qquad (4.31)\end{aligned}$$

where substitution of a KF gain equal to zero has reduced the number of terms within the series summation by $(i-1)$. In addition, the remaining series product includes initial multiplicands, $\underline{A}_y\left[k\right]$, that are equal to $A\left[k-1\right]$, e.g. $\underline{A}_y\left[k+i-1\right]$ through $\underline{A}_y\left[k+1\right]$. This is also due to the Kalman gain in $\underline{A}_y\left[k+i\right]$, as defined in (4.8), being equal to zero. Thus, the simplified series product and resulting cumulative effect of the measurement disturbance profile are calculated as follows

$$\prod_{j=1}^{i-1}\underline{A}_y\left[k+i-j\right] = \prod_{j=1}^{i-1}A\left[k+i+j-1\right] \qquad (4.32)$$

$$\begin{aligned}\underline{\rho}_y\left[k+i,k_{w_y}\right] &= \Gamma_y\left[k+i,k_{w_y}\right] - C\left[k+i\right]A\left[k+i-1\right]\prod_{j=1}^{i-1}A\left[k+i-j-1\right] \\ &\quad\cdot\sum_{j_1=i}^{k+i-k_{w_y}}\prod_{j_2=i}^{j_1-1}\underline{A}_y\left[k+i-j_2\right]K\left[k+i-j_1\right]\Gamma_y\left[k+i-j_1,k_{w_y}\right]\end{aligned}$$

$$= \Gamma_y\left[k+i, k_{w_y}\right] - C\left[k+i\right] A\left[k+i-1\right] \prod_{j=1}^{i-1} A\left[k+i-j-1\right]$$
$$\cdot \sum_{j_1=1}^{k+1-k_{w_y}} \prod_{j_2=1}^{j_1-1} \underline{A}_y\left[k+1-j_2\right] K\left[k+1-j_1\right] \Gamma_y\left[k+1-j_1, k_{w_y}\right] \tag{4.33}$$

where the system matrices $A\left[k+i-1\right]$ and $C\left[k+i\right]$ are assumed to be equal to the values of the current time-step k. For example, the one time-step ahead cumulative effect of the measurement disturbance profile is calculated with assumed future system matrices as follows.

$$\underline{\rho}_y\left[k+1, k_{w_y}\right] = \Gamma_y\left[k+1, k_{w_y}\right] - C\left[k\right] A\left[k\right]$$
$$\cdot \sum_{j_1=1}^{k+1-k_{w_y}} \prod_{j_2=1}^{j_1-1} \underline{A}_y\left[k+1-j_2\right] K\left[k+1-j_1\right] \Gamma_y\left[k+1-j_1, k_{w_y}\right] \tag{4.34}$$

The i-step-ahead measurement error covariance of the compensated measurement is calculated by propagating the *a priori* measurement error covariance for measurement disturbance estimation in (4.14) as follows.

$$P_{\tilde{y}_{w_y}}\left[k+i|k\right] = E\left\{\left(y\left[k+i\right] - \hat{y}_{w_y}\left[k+i|k\right]\right)\left(y\left[k+i\right] - \hat{y}_{w_y}\left[k+i|k\right]\right)'\right\}$$
$$= P_{\tilde{y}}\left[k+i|k\right] + \underline{\rho}_y\left[k+i, k_{w_y}\right] P_{\hat{w}_y}\left[k, k_{w_y}\right] \underline{\rho}'_y\left[k+i, k_{w_y}\right]$$
$$- \underline{\rho}_y\left[k+i, k_{w_y}\right] P_{\hat{w}_y,\tilde{y}}\left[k+i, k_{w_y}\right]$$
$$- P'_{\hat{w}_y,\tilde{y}}\left[k+i, k_{w_y}\right] \underline{\rho}'_y\left[k+i, k_{w_y}\right] \tag{4.35}$$

The covariance of the measurement disturbance input, $P_{\hat{w}_y}\left[k, k_{w_y}\right]$, has the exact same value as is used for the weighted Markov estimator in (4.15) since the disturbance input estimate remains a function of the current time-step k. In contrast, the cross-covariance between the measurement disturbance input, $\hat{w}_y\left[k, k_{w_y}\right]$, and the i-step-ahead KF-based measurement prediction error, $\tilde{y}\left[k+i|k\right]$, is required to be propagated as follows

$$
\begin{aligned}
P_{\hat{w}_y,\tilde{y}}\left[k+i, k_{w_y}\right] &= E\left\{\hat{w}_y\left[k, k_{w_y}\right]\left(y\left[k+i\right]-\hat{y}\left[k+i|k\right]\right)'\right\} \\
&= E\Big\{P_{\hat{w}_y}\left[k, k_{w_y}\right]\underline{\rho}'_y\left[k, k_{w_y}\right]\Lambda_y^0 P_{\tilde{y}}^{-1}\left[k|k-1\right] \\
&\quad \cdot\left(C\left[k\right]\left(x\left[k\right]-\hat{x}\left[k|k-1\right]\right)+v_y\left[k\right]\right) \\
&\quad \cdot\left(C\left[k+i\right]\left(x\left[k+i\right]-\hat{x}\left[k+i|k\right]\right)+v_y\left[k+i\right]\right)'\Big\} \\
&= E\Bigg\{P_{\hat{w}_y}\left[k, k_{w_y}\right]\underline{\rho}'_y\left[k, k_{w_y}\right]\Lambda_y^0 P_{\tilde{y}}^{-1}\left[k|k-1\right]\left(C\left[k\right]\tilde{x}\left[k|k-1\right]+v_y\left[k\right]\right) \\
&\quad \cdot\Bigg(C\left[k+i\right]\prod_{j=0}^{i-1}A\left[k+j\right]\left(\left(\mathbb{I}-K\left[k\right]C\left[k\right]\right)\tilde{x}\left[k|k-1\right]-K\left[k\right]v_y\left[k\right]\right)' \\
&\quad +v_y\left[k+i\right]\Bigg)'\Bigg\} \\
&= P_{\hat{w}_y}\left[k, k_{w_y}\right]\underline{\rho}'_y\left[k, k_{w_y}\right]P_{\tilde{y}}^{-1}\left[k|k-1\right] \\
&\quad \cdot\left(C\left[k\right]P_x\left[k|k-1\right]\left(\mathbb{I}-K\left[k\right]C\left[k\right]\right)'+R_y\left[k\right]K'\left[k\right]\right) \\
&\quad \cdot\left(\prod_{j=0}^{i-1}A\left[k+j\right]\right)'C'\left[k+i\right] \qquad (4.36)
\end{aligned}
$$

where the i-step-ahead measurement innovation is rewritten as a function of the *a priori* state error, $\tilde{x}\left[k|k-1\right]$, and measurement noise covariance, v_x.

Disturbance to the state

Alternatively, the following extension of the state disturbance estimation procedure results in a method by which to predict the error between the i-step-ahead KF-based measurement prediction and the corresponding future measurement given an assumed state disturbance profile. The i-step ahead KF-based measurement prediction is then compensated to include the cumulative state disturbance. This extension to the prediction problem is, again, considered to be relatively straightforward with respect to the estimation procedure. The following methods are, however, necessary for the eventual development of a recursive solution to the LS problem as presented in Section 4.2.

Prediction error compensation is performed in the same manner as for the compensation of state estimation error in (4.24) and as follows.

$$\hat{y}_{w_x}[k+i|k] = \hat{y}[k+i|k] + \underline{\rho}_x[k+i, k_{w_x}]\,\hat{w}_x[k, k_{w_x}] \tag{4.37}$$

where the cumulative effect of the disturbance profile, $\underline{\rho}_x$, on the measurement prediction is calculated as the propagated form of (4.17), or

$$\underline{\rho}_x[k+i, k_{w_x}] = C[k+i] \sum_{j_1=1}^{k+i-k_{w_x}} \prod_{j_2=1}^{j_1-1} \underline{A}_x[k+i-j_2]\,\Gamma_x[k+i-j_1, k_{w_x}] \tag{4.38}$$

with $\prod_{j=1}^{0} = \mathbb{I}$.

To simplify the estimation of prediction error for predictions that are beyond one time-

step ahead, the cumulative effect of state disturbance profile is expanded as follows.

$$\underline{\rho}_x\left[k+i, k_{w_x}\right] = C\left[k+i\right] \cdot \left(\sum_{j_1=2}^{k+i-k_{w_x}} \prod_{j_2=1}^{j_1-1} \underline{A}_x\left[k+i-j_2\right] \Gamma_x\left[k+i-j_1, k_{w_x}\right] + \Gamma_x\left[k+i-1, k_{w_x}\right] \right) \tag{4.39}$$

Moreover, as is the case during propagation of the measurement disturbance in (4.31), the series product includes initial multiplicands, $\underline{A}_x\left[k\right]$, that are equal to $A\left[k\right]$ due to the Kalman gain in $\underline{A}_x\left[k+i\right]$ as in (4.18) being equal to zero. Thus, the cumulative effect for a state disturbance profile is simplified as follows

$$\underline{\rho}_x\left[k+i, k_{w_x}\right] = C\left[k+i\right] \left(\prod_{j=1}^{i-1} A\left[k+i-j\right] \cdot \sum_{j_1=2}^{k+i-k_{w_x}} \prod_{j_2=i}^{j_1-1} \underline{A}_x\left[k+i-j_2\right] \Gamma_x\left[k+i-j_1, k_{w_x}\right] + \Gamma_x\left[k+i-1, k_{w_x}\right] \right) \tag{4.40}$$

using the equivalent series product of (4.32) where the state-to-measurement matrix, $C\left[k+i\right]$, is assumed to be equal to the value of the current time-step k. For example, the one time-step ahead cumulative effect of the measurement disturbance profile is calculated as follows.

$$\underline{\rho}_x\left[k+1, k_{w_x}\right] = C\left[k\right] \sum_{j_1=2}^{k+1-k_{w_x}} \prod_{j_2=i}^{j_1-1} \underline{A}_x\left[k+1-j_2\right] \Gamma_x\left[k+1-j_1, k_{w_x}\right] + \Gamma_x\left[k, k_{w_x}\right] \tag{4.41}$$

The i-step-ahead measurement error covariance of the compensated measurement is

calculated by propagating the *a priori* measurement error covariance for state disturbance estimation in (4.26) as follows.

$$\begin{aligned} P_{\tilde{y}_{w_x}}[k+i|k] &= E\left\{\left(y[k+i]-\hat{y}_{w_x}[k+i|k]\right)\left(y[k+i]-\hat{y}_{w_x}[k+i|k]\right)'\right\} \\ &= P_{\tilde{y}}[k+i|k]+\underline{\rho}_x[k+i,k_{w_x}]\,P_{\hat{w}_x}[k,k_{w_x}]\,\underline{\rho}'_x[k+i,k_{w_x}] \\ &\quad -\underline{\rho}_x[k+i,k_{w_x}]\,P_{\hat{w}_x,\tilde{y}}[k+i,k_{w_x}] \\ &\quad -P'_{\hat{w}_x,\tilde{y}}[k+i,k_{w_x}]\,\underline{\rho}'_x[k+i,k_{w_x}] \end{aligned} \tag{4.42}$$

The covariance of the state disturbance input, $P_{\hat{w}_x}[k,k_{w_x}]$, is a function of time-step k and therefore retains the exact same value as for the weighted Markov estimator in (4.27). In contrast, the cross-covariance between the state disturbance input, $\hat{w}_x$, and the i-step-ahead KF-based measurement prediction error, $\tilde{y}[k+i|k]$, is propagated in the same manner as for the measurement disturbance in (4.36) as follows.

$$\begin{aligned} P_{\hat{w}_x,\tilde{y}}[k+i,k_{w_x}] &= E\left\{\hat{w}_x[k,k_{w_x}]\left(y[k+i]-\hat{y}[k+i|k]\right)'\right\} \\ &= P_{\hat{w}_x}[k,k_{w_x}]\,\underline{\rho}'_x[k,k_{w_x}]\,P_{\tilde{y}}^{-1}[k|k-1] \\ &\quad \cdot\left(C[k]\,P_x[k|k-1]\left(\mathbb{I}-K[k]\,C[k]\right)'+R_y[k]\,K'[k]\right) \\ &\quad \cdot\left(\prod_{j=0}^{i-1}A[k+j]\right)'C'[k+i] \end{aligned} \tag{4.43}$$

4.2 Recursive Least Squares Formulation of Disturbance Estimation and Prediction Error Compensation

This section formulates recursive algorithms for the LS or Markov disturbance estimators and predictors that are presented in Section 4.1. The recursive form of the LS algorithm provides the benefit of requiring less computational power and a smaller amount of data storage; these two resources are limited within the chosen safety-PLC in comparison to high performance CPUs with near limitless amounts of data storage. The RLS algorithm achieves reduction in computational requirements by processing the measurement sample of the current time-step rather than the entire block of $(k - k_{w_\bullet})$ measurement samples as performed by the standard LS filter. The RLS algorithm also avoids the calculation of matrix inverses through the use of the matrix inversion lemma. As a recursive algorithm, the RLS estimates do, however, suffer from error due to initial conditions as the LS estimate converges to the optimal solution over the initial estimates.

Although the RLS algorithm is stated in the following, the derivation of the RLS algorithm from the standard LS filter is left to the cited literature [24]. The following sections instead focus on the extension of the RLS algorithm to the state and measurement disturbance estimation problem. This formulation differs from conventional RLS in that the given cumulative effect of the disturbance does not inherently support recursion and is therefore modified. Moreover, the time-step of initiation for the disturbance input is pe-

riodically reset. This resetting function allows for the disturbance estimation algorithm to accurately reflect the potential for a disturbance to occur at any time-step. Moreover, disturbance input resetting is made to coincide with the covariance reset procedure that is performed within the standard RLS algorithm. An alternating RLS filter configuration is then developed to eliminate inaccuracies in compensation due to erroneous initial estimates during filter convergence.

The solution to the LS disturbance estimation problem of Section 4.1.1 is restated in the following general form for disturbances within either the measurement or state equation, i.e. $\bullet$ represents either x or y,

$$\hat{w}_{\bullet}\left[k, k_{w_{\bullet}}\right] = P_{\hat{w}_{\bullet}}\left[k, k_{w_{\bullet}}\right] \left(\sum_{j=k_{w_{\bullet}}}^{k} \underline{\rho}'_{\bullet}\left[j, k_{w_{\bullet}}\right] \Lambda_{\bullet}^{k-j} P_{\tilde{y}}^{-1}\left[j|j-1\right] \tilde{y}\left[j|j-1\right] \right) \tag{4.44}$$

where $P_{\hat{w}_{\bullet}}$ is the covariance of the respective disturbance inputs as defined in (4.15) and (4.27). Given an initial estimate of the disturbance input, $\hat{w}_{\bullet}\left[k_{w_{\bullet}}, k_{w_{\bullet}}\right]$, the Markov estimation problem has the following well-known recursive solution

$$\begin{aligned} \hat{w}_{\bullet}\left[k, k_{w_{\bullet}}\right] &= \hat{w}_{\bullet}\left[k-1, k_{w_{\bullet}}\right] \\ &\quad + \mathcal{K}_{\bullet}\left[k\right] \left(P_{\tilde{y}}^{-\frac{1}{2}}\left[k|k-1\right] \tilde{y}\left[k|k-1\right] - \varrho_{\bullet}\left[k, k_{w_{\bullet}}\right] \hat{w}_{\bullet}\left[k-1, k_{w_{\bullet}}\right] \right) \end{aligned} \tag{4.45}$$

where $\varrho_{\bullet}$ is the normalized cumulative effect $\varrho_{\bullet}\left[k, k_{w_{\bullet}}\right] = P_{\tilde{y}}^{-\frac{1}{2}}\left[k|k-1\right] \underline{\rho}_{\bullet}$, and $\mathcal{K}_{\bullet}$ is the

RLS gain matrix [24]. The RLS gain matrix is, in turn, calculated as follows

$$\mathcal{K}_{\bullet}\left[k\right]=\lambda_{\bullet}^{-1}\mathcal{P}_{\bullet}\left[k-1,k_{w_{\bullet}}\right]\varrho_{\bullet}^{\prime}\left[k,k_{w_{\bullet}}\right]\left(\mathbb{I}+\lambda_{\bullet}^{-1}\varrho_{\bullet}\left[k,k_{w_{\bullet}}\right]\mathcal{P}_{\bullet}\left[k-1,k_{w_{\bullet}}\right]\varrho_{\bullet}^{\prime}\left[k,k_{w_{\bullet}}\right]\right)^{-1} \tag{4.46}$$

where $\mathcal{P}_{\bullet}$ is the covariance of the disturbance estimate. Given an initial estimate of the disturbance estimate covariance, $\mathcal{P}_{\bullet}\left[k_{w_{\bullet}},k_{w_{\bullet}}\right]$, the covariance is calculated as follows.

$$\mathcal{P}_{\bullet}\left[k,k_{w_{\bullet}}\right]=\left(\mathbb{I}-\mathcal{K}_{\bullet}\left[k\right]\varrho_{\bullet}\left[k,k_{w_{\bullet}}\right]\right)\Lambda_{\bullet}^{-1}\mathcal{P}_{\bullet}\left[k-1,k_{w_{\bullet}}\right] \tag{4.47}$$

Within the above equations, $P_{\hat{w}_{\bullet}}$ and $\mathcal{P}_{\bullet}$ are both the covariance of the disturbance estimate, $\hat{w}_{\bullet}$. The disturbance estimate covariance is conveniently calculated within the standard recursive form of the LS filter as follows

$$P_{\hat{w}_{\bullet}}\left[k,k_{w_{\bullet}}\right]=\mathcal{P}_{\bullet}\left[k,k_{w_{\bullet}}\right] \tag{4.48}$$

and the two variables, $P_{\hat{w}_{\bullet}}$ and $\mathcal{P}_{\bullet}$, are therefore interchangeable throughout the remainder of this work.

4.2.1 Disturbance to the measurement

The recursive nature of the RLS solution to the measurement disturbance estimation problem is only of value if the various parameters within the RLS solution can also be calculated in a recursive manner. The cumulative effect of the measurement disturbance profile, as

established in (4.7) and (4.9), is therefore modified to the following recursive form

$$\underline{\rho}_y\left[k, k_{w_y}\right] = \Gamma_y\left[k, k_{w_y}\right] - C\left[k\right] A\left[k-1\right] \psi_y\left[k, k_{w_y}\right] \tag{4.49}$$

where ψ_y is referred to as the pseudo cumulative effect of the measurement disturbance profile. More precisely, ψ_y is the cumulative effect of the measurement disturbance on the *a posteriori* state of time-step, $(k-1)$. The recursive calculation of the pseudo cumulative effect is then performed as follows

$$\begin{aligned}
\psi_y\left[k, k_{w_y}\right] &= \sum_{j_1=1}^{k-k_{w_y}} \prod_{j_2=1}^{j_1-1} \underline{A}_y\left[k-j_2\right] K\left[k-j_1\right] \Gamma_y\left[k-j_1, k_{w_y}\right] \\
&= K\left[k-1\right] \Gamma_y\left[k-1, k_{w_y}\right] \\
&\quad + \underline{A}_y\left[k-1\right] \sum_{j_1=1}^{k-1-k_{w_y}} \prod_{j_2=1}^{j_1-1} \underline{A}_y\left[k-j_2-1\right] \\
&\quad \cdot K\left[k-j_1-1\right] \Gamma_y\left[k-j_1-1, k_{w_y}\right] \\
&= K\left[k-1\right] \Gamma_y\left[k-1, k_{w_y}\right] + \underline{A}_y\left[k-1\right] \psi_y\left[k-1, k_{w_y}\right] \qquad (4.50) \\
\psi_y\left[k-1, k_{w_y}\right] &= \sum_{j_1=1}^{k-1-k_{w_y}} \prod_{j_2=1}^{j_1-1} \underline{A}_y\left[k-1-j_2\right] K\left[k-1-j_1\right] \Gamma_y\left[k-1-j_1, k_{w_y}\right] \qquad (4.51)
\end{aligned}$$

where $\psi_y\left[k_{w_y}-1, k_{w_y}\right] = 0^{n_x \times n_{w_y}}$, $\Gamma_y\left[k_{w_y}-1, k_{w_y}\right] = 0^{n_y \times n_{w_y}}$ and the cumulative effect, $\underline{\rho}_y$, is now a function of values that are dependent only on the current time-step, k, as well as the previous time-step, $(k-1)$. The RLS estimate of the measurement disturbance input

is then calculated using the general RLS solution of (4.45) as follows

$$\hat{w}_y\left[k, k_{w_y}\right] = \hat{w}_y\left[k-1, k_{w_y}\right] + \mathcal{K}_y[k]\left(P_{\tilde{y}}^{-\frac{1}{2}}[k|k-1]\,\tilde{y}[k|k-1] - \varrho_y\left[k, k_{w_y}\right]\hat{w}_y\left[k-1, k_{w_y}\right]\right) \quad (4.52)$$

where $\hat{w}_y\left[k_{w_y}-1, k_{w_y}\right] = 0^{n_{w_y}\times 1}$.

The recursive calculation of the *a priori* measurement error covariance, $P_{\tilde{y}_{w_y}}$, is straightforward since covariance, $P_{\hat{w}_y}\left[k, k_{w_y}\right]$, as well as cross-covariance, $P_{\hat{w}_y,\tilde{y}}\left[k, k_{w_y}\right]$, do not require any modifications to be calculated in a recursive manner. More specifically, from (4.48), the covariance of the measurement disturbance estimate, $P_{\hat{w}_y}$, is given directly within the RLS filter as $\mathscr{P}_y$, (4.47). In addition, the cross-covariance between the measurement disturbance input, $\hat{w}_y$, and the *a priori* measurement estimation error, $\tilde{y}[k|k-1]$, is the product of the disturbance estimate covariance and the cumulative effect of the disturbance profile as established in (4.14) and is not reliant on any parameters prior to the current time-step k. Thus, this covariance is calculated in the same manner as for the LS filter using (4.16).

For prediction, the combined KF/LS measurement prediction of (4.29) is a function of the i-step-ahead cumulative effect of the measurement disturbance profile, $\underline{\rho}_y\left[k+i, k_{w_y}\right]$. For the one-step-ahead prediction, the cumulative effect is calculated as the following propagated form of (4.49) under the assumption that the state-to-measurement matrix $C[k+1]$ is equal to that of the current time-step

$$\underline{\rho}_y\left[k+1, k_{w_y}\right] = \Gamma_y\left[k+1, k_{w_y}\right] - C[k]\,A[k]\,\psi_y\left[k+1, k_{w_y}\right] \quad (4.53)$$

where the disturbance profile is assumed known and the one-step-ahead pseudo cumulative effect is calculated as follows

$$\psi_y \left[k+1, k_{w_y}\right] = K\left[k\right] \Gamma_y \left[k, k_{w_y}\right] + \underline{A}_y \left[k\right] \psi_y \left[k, k_{w_y}\right] \tag{4.54}$$

with initial value $\psi_y \left[k_{w_y}, k_{w_y}\right] = 0^{n_x \times n_w}$.

For propagation beyond one time-step, the Kalman gain, $K\left[k+i-1\right]$, is equal to zero within $\underline{A}_y \left[k+i-1\right]$ as defined in (4.8). The pseudo cumulative effect reduces, as in (4.33), to the following form

$$\psi_y \left[k+i+1, k_{w_y}\right] = A\left[k\right] \psi_y \left[k+i, k_{w_y}\right] \tag{4.55}$$

with the future state matrices, $A\left[k+i\right]$, replaced by the state matrix of the current time-step, $A\left[k\right]$. The cumulative effect of the measurement disturbance profile is then calculated using the i-step-ahead propagated form of (4.49) as follows

$$\underline{\rho}_y \left[k+i, k_{w_y}\right] = \Gamma_y \left[k+i, k_{w_y}\right] - C\left[k\right] A\left[k\right] \psi_y \left[k+i, k_{w_y}\right] \tag{4.56}$$

where the values of the system matrices are assumed to be equal to those of the current time-step k.

In the above formulation the current and future values of the disturbance profile are assumed known. Although not a requirement for propagating the RLS disturbance estimates, it may also be assumed that the disturbance profile, Γ_y, can be calculated in a recursive manner. For example, the disturbance profile corresponding with a ramp input

can be recursively calculated as follows.

$$\Gamma_y\left[k+i,k_{w_y}\right]=\Gamma_y\left[k+i-1,k_{w_y}\right]+\left[\begin{array}{cc} 0^{n_y\times\frac{n_w}{2}} & \mathbb{I} \end{array}\right] \tag{4.57}$$

The i-step-ahead measurement error covariance, $P_{\tilde{y}_{w_y}}$, as given in (4.35), is a function of the current covariance of the measurement disturbance input estimate, $P_{\hat{w}_y}\left[k,k_{w_y}\right]$, as well as the i-step-ahead cross-covariance between the disturbance input estimate and the *a priori* measurement error, $P_{\hat{w}_y,\tilde{y}}\left[k+i,k_{w_y}\right]$. In Section 4.1.2 it was determined that, for prediction, it is only necessary to propagate the cross-covariance since the measurement disturbance input covariance is equal to the value of the current time-step. Propagation of the cross-covariance is made possible by simplifying the series product within (4.36) as follows

$$\begin{aligned} P_{\hat{w}_y,\tilde{y}}\left[k+i,k_{w_y}\right]=&P_{\hat{w}_y}\left[k,k_{w_y}\right]\underline{\rho}'_y\left[k,k_{w_y}\right]P_{\tilde{y}}^{-1}\left[k|k-1\right]\\ &\cdot\left(C\left[k\right]P_x\left[k|k-1\right]\left(\mathbb{I}-K\left[k\right]C\left[k\right]\right)'+R_y\left[k\right]K'\left[k\right]\right)\\ &\cdot\mathcal{A}'\left[k+i\right]C'\left[k+i\right] \end{aligned} \tag{4.58}$$

where the product is replaced by the cumulative effect of the state matrix, $\mathcal{A}\left[k+i\right]$. This cumulative effect of state matrix is essentially the state transition matrix over the prediction window and is calculated recursively using an initial value of $\mathcal{A}\left[k\right]=\mathbb{I}$ as follows.

$$\mathcal{A}\left[k+i\right]=\prod_{j=0}^{i-1}A\left[k+j\right]$$

$$= A\left[k+i-1\right]\prod_{j=0}^{i-2} A\left[k+j\right]$$

$$= A\left[k+i-1\right]\mathcal{A}\left[k+i-1\right] \tag{4.59}$$

Algorithm 4.1 reorganizes the RLS-based measurement disturbance input estimation and prediction procedures into two stages, update and predict. This structure mimics that of the KF introduced in Section 3.2 and eliminates redundant calculations whereby $\psi_y\left[k,k_{w_y}\right]$, $\Gamma_y\left[k,k_{w_y}\right]$, and $\underline{\rho}_y\left[k,k_{w_y}\right]$ are calculated within the predict stage and then returned to the update stage. The calculation of pseudo cumulative effect is then modified from (4.50) in an effort to reduce the computational complexity of extending RLS disturbance input estimation to the recursive prediction error compensation problem as follows.

$$\begin{aligned}\psi_y\left[k+i,k_{w_y}\right] &= K\left[k+i-1\right]\Gamma_y\left[k+i-1,k_{w_y}\right] \\ &\quad + \underline{A}_y\left[k+i-1\right]\psi_y\left[k+i-1,k_{w_y}\right]\end{aligned} \tag{4.60}$$

With this modification, the initial value of the pseudo cumulative effect, ψ_y, remains as for the unmodified form since the initial value of the disturbance profile, Γ_y, is also equal to zero. The initial value for the cumulative effect of the measurement disturbance profile is, however, modified to be equal to the initial measurement disturbance profile, or $\underline{\rho}_y\left[k_{w_y},k_{w_y}\right] = \Gamma_y\left[k_{w_y},k_{w_y}\right]$.

Algorithm 4.1 includes a count of the number of OPL that are required to execute the algorithm for a system with a single output, or scalar measurement. This assumption

Algorithm 4.1 Update and predict stages of the recursive least squares (RLS) measurement disturbance input estimation and prediction error compensation procedure, $RLS_{y,ip}$.

[Measurement disturbance estimation (update)]

$$\underline{\rho}_y\left[k,k_{w_y}\right]=\Gamma_y\left[k+i,k_{w_y}\right]-C\left[k\right]A\left[k-1\right]\psi_y\left[k,k_{w_y}\right]$$

$$\underline{P}_{\tilde{y},}\left[k|k-1\right]=P_{\tilde{y}}^{-1}\left[k|k-1\right]$$

$$\underline{\underline{P}}_{\tilde{y}}\left[k|k-1\right]=\underline{P}_{\tilde{y},}^{\frac{1}{2}}\left[k|k-1\right]$$

$$\varrho_y\left[k,k_{w_y}\right]=\underline{\underline{P}}_{\tilde{y}}\left[k|k-1\right]\underline{\rho}_y\left[k,k_{w_y}\right]$$

$$\mathcal{K}_y\left[k\right]=\lambda_y^{-1}\mathcal{P}_y\left[k-1,k_{w_y}\right]\underline{\varrho}_y'\left[k,k_{w_y}\right]\cdot\left(1+\lambda_y^{-1}\varrho_y\left[k,k_{w_y}\right]\mathcal{P}_y\left[k-1,k_{w_y}\right]\underline{\varrho}_y'\left[k,k_{w_y}\right]\right)^{-1}$$

$$\hat{w}_y\left[k,k_{w_y}\right]=\hat{w}_y\left[k-1,k_{w_y}\right]+\mathcal{K}_y\left[k\right]\left(\underline{\underline{P}}_{\tilde{y}}\left[k|k-1\right]\tilde{y}\left[k|k-1\right]-\varrho_y\left[k,k_{w_y}\right]\hat{w}_y\left[k-1,k_{w_y}\right]\right)$$

$$\mathcal{P}_y\left[k,k_{w_y}\right]=\left(\mathbb{I}-\mathcal{K}_y\left[k\right]\varrho_y\left[k,k_{w_y}\right]\right)\Lambda_y^{-1}\mathcal{P}_y\left[k-1,k_{w_y}\right]$$

OPL for scalar y: $2n_{w_y}^3+6n_{w_y}^2+2n_{w_y}n_x+6n_{w_y}+2n_x^2+56\in O\left(n_{w_y}^3\right)$

[Measurement disturbance estimation (predict)]

$$\psi_y\left[k+i,k_{w_y}\right]=K\left[k+i-1\right]\Gamma_y\left[k+i-1,k_{w_y}\right]+\left(\mathbb{I}-K\left[k+i-1\right]C\left[k+i-1\right]\right)A\left[k+i-2\right]\psi_y\left[k+i-1,k_{w_y}\right]$$

update $\Gamma_y\left[k+i,k_{w_y}\right]$

$$\underline{\rho}_y\left[k+i,k_{w_y}\right]=\Gamma_y\left[k+i,k_{w_y}\right]-C\left[k\right]A\left[k\right]\psi_y\left[k+i,k_{w_y}\right]$$

$$\mathcal{A}\left[k+i\right]=A\left[k+i-1\right]\mathcal{A}\left[k+i-1\right]$$

$$P_{\hat{w}_y,\tilde{y}'}\left[k+i,k_{w_y}\right]=\mathcal{P}_y\left[k,k_{w_y}\right]\underline{\rho}_{-y}'\left[k,k_{w_y}\right]\underline{P}_{\tilde{y}}\left[k|k-1\right]\cdot\left(C\left[k\right]P_x\left[k|k-1\right]\left(\mathbb{I}-K\left[k\right]C\left[k\right]\right)'+R_y\left[k\right]K'\left[k\right]\right)\cdot\mathcal{A}'\left[k+i\right]C'\left[k+i\right]$$

$$\hat{y}_{w_y}\left[k+i|k\right]=\hat{y}\left[k+i|k\right]+\underline{\rho}_y\left[k+i,k_{w_y}\right]\hat{w}_y\left[k,k_{w_y}\right]$$

$$P_{\tilde{y}_{w_y}}\left[k+i|k\right]=P_{\tilde{y}}\left[k+i|k\right]+\underline{\rho}_y\left[k+i,k_{w_y}\right]\mathcal{P}_y\left[k,k_{w_y}\right]\underline{\rho}_y'\left[k+i,k_{w_y}\right]-\underline{\rho}_y\left[k,k_{w_y}\right]P_{\hat{w}_y,\tilde{y}'}\left[k+i,k_{w_y}\right]-P_{\hat{w}_y,\tilde{y}'}'\left[k+i,k_{w_y}\right]\underline{\rho}_y'\left[k+i,k_{w_y}\right]$$

OPL for scalar y: $4N_pn_{w_y}^2+4N_pn_{w_y}n_x^2+5N_pn_{w_y}n_x+6N_pn_{w_y}+4N_pn_x^3+8N_pn_x^2-N_pn_x\in O\left(N_pn_x^3\right)$

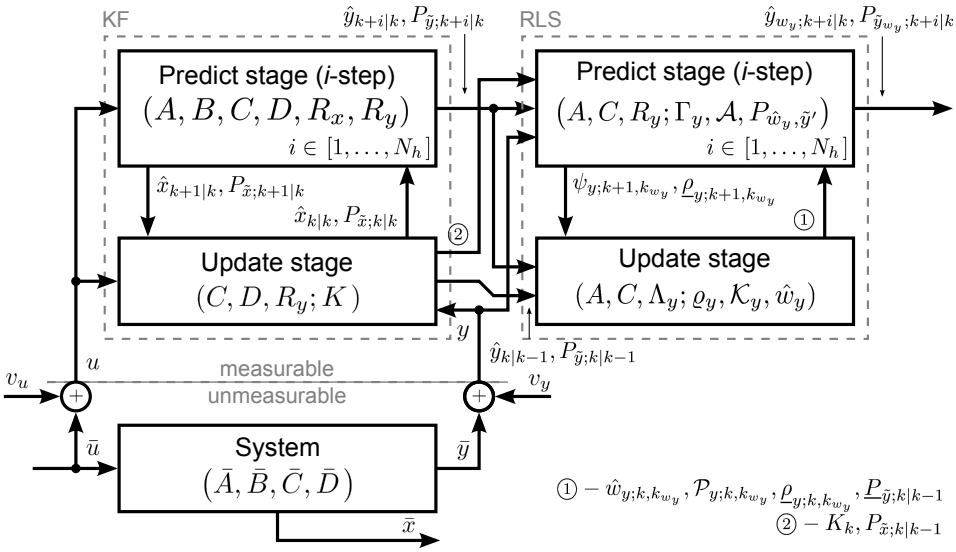

Figure 4.2: Connectivity between KF-based measurement prediction and the measurement disturbance estimation and prediction error compensation procedure of Algorithm 4.1.

follows those that were made for the KF in the algorithms of Section 3.2. The count does not include the operations required for updating the disturbance profile as this value varies with the profile of the assumed disturbance. The computational complexity of the RLS-based measurement disturbance interval-supporting estimation, prediction, and compensation procedure is cubic with respect to the dimension of the state vector multiplied by the prediction horizon, or $RLS_{y,ip} \in O\left(n_x^3 N_p\right)$. Finally, an overview of the measurement disturbance estimation and prediction error compensation procedure is illustrated in Figure 4.2.

4.2.2 Disturbance to the state

The formulation of a recursive solution to the LS problem for a disturbance within the state equation shares many similarities with that of the RLS solution for a disturbance within the measurement equation presented in the previous section. That said, the equations

are modified to consider effects of the state disturbance rather than the measurement disturbance. For example, as in the case of the measurement disturbance, the cumulative effect of the state disturbance profile established in (4.17) is also modified to be in the following recursive form

$$\underline{\rho}_x [k, k_{w_x}] = C [k] \psi_x [k, k_{w_x}] \tag{4.61}$$

where ψ_x is referred to as the pseudo cumulative effect of the state disturbance profile on the measurement estimate. More precisely, ψ_x is the cumulative effect of the state disturbance on the *a priori* state of the current time-step, k. The pseudo cumulative effect can then be calculated in a recursive manner that is similar to that of (4.50) as follows

$$\begin{aligned}
\psi_x [k, k_{w_x}] &= \sum_{j_1=1}^{k-k_{w_x}} \prod_{j_2=1}^{j_1-1} \underline{A}_x [k - j_2] \Gamma_x [k - j_1, k_{w_x}] \\
&= \Gamma_x [k-1, k_{w_x}] \\
&\quad + \underline{A}_x [k-1] \sum_{j_1=1}^{k-1-k_{w_x}} \prod_{j_2=1}^{j_1-1} \underline{A}_x [k - j_2 - 1] \Gamma_x [k - j_1 - 1, k_{w_x}] \\
&= \Gamma_x [k-1, k_{w_x}] + \underline{A}_x [k-1] \psi_x [k-1, k_{w_x}] \qquad (4.62) \\
\psi_x [k-1, k_{w_x}] &= \sum_{j_1=1}^{k-1-k_{w_x}} \prod_{j_2=1}^{j_1-1} \underline{A}_x [k - 1 - j_2] \Gamma_x [k - 1 - j_1, k_{w_x}] \qquad (4.63)
\end{aligned}$$

where $\psi_x [0, k_{w_x}] = 0^{n_x \times n_w}$ and the cumulative effect, $\underline{\rho}_x$, is now a function of values that are dependent only on the current time-step, k, as well as the previous time-step, $(k-1)$. The RLS estimate of the state disturbance input is then calculated using the general RLS

solution of (4.45) as follows

$$\hat{w}_x\left[k, k_{w_x}\right] = \hat{w}_x\left[k-1, k_{w_x}\right] + \mathcal{K}_x\left[k\right]\left(P_{\tilde{y}}^{-\frac{1}{2}}\left[k|k-1\right]\tilde{y}\left[k|k-1\right] - \varrho_x\left[k, k_{w_x}\right]\hat{w}_x\left[k-1, k_{w_x}\right]\right) \tag{4.64}$$

where $\hat{w}_x\left[k_{w_x}-1, k_{w_x}\right] = 0^{n_{w_x}\times 1}$.

The recursive calculation of the *a priori* measurement error covariance, $P_{\tilde{y}_{w_x}}$, has the same formulation as for the measurement disturbance case. Basically, covariance $P_{\hat{w}_x}\left[k, k_{w_x}\right]$ as well as cross-covariance $P_{\hat{w}_x,\tilde{y}}\left[k, k_{w_x}\right]$ do not require any modification to be calculated recursively: the covariance of the disturbance estimate, $P_{\hat{w}_x}\left[k, k_{w_x}\right]$ is given as $\mathcal{P}\left[k, k_{w_x}\right]$; and the cross-covariance between the measurement disturbance input, $\hat{w}_x$, and the *a priori* measurement estimation error, $\tilde{y}\left[k|k-1\right]$, is calculated in the same manner as for the LS filter using (4.28).

For prediction, the combined KF/LS measurement prediction of (4.37) is again a function of the i-step-ahead cumulative effect of the state disturbance profile, $\underline{\rho}_x\left[k+i, k_{w_x}\right]$. For the one-step-ahead prediction, the cumulative effect is calculated as the following propagated form of (4.61) under the assumption that the state-to-measurement matrix $C\left[k+1\right]$ is equal to that of the current time-step, or as follows

$$\underline{\rho}_x\left[k+1, k_{w_x}\right] = C\left[k\right]\psi_x\left[k+1, k_{w_x}\right] \tag{4.65}$$

where the one-step-ahead pseudo cumulative effect is calculated as follows

$$\psi_x\left[k+1, k_{w_x}\right] = \Gamma_x\left[k, k_{w_x}\right] + \underline{A}_x\left[k\right]\psi_x\left[k, k_{w_x}\right] \tag{4.66}$$

with initial value $\psi_x\left[k_{w_x}, k_{w_x}\right] = 0^{n_x \times n_w}$.

For propagation beyond one time-step, the Kalman gain, $K\left[k+i-1\right]$, is equal to zero within $\underline{A}_x\left[k+i-1\right]$ as defined in (4.18) and the pseudo cumulative effect is instead in the reduced form of (4.33) as follows

$$\psi_x\left[k+i+1, k_{w_x}\right] = \Gamma_x\left[k+i, k_{w_x}\right] + A\left[k\right]\psi_x\left[k+i, k_{w_x}\right] \tag{4.67}$$

where it is assumed that the future state matrices, $A\left[k+i\right]$, are equal to that of the current time-step, $A\left[k\right]$. The cumulative effect of the measurement disturbance profile is then calculated using the i-step-ahead propagated form of (4.61) as follows

$$\underline{\rho}_x\left[k+i, k_{w_x}\right] = C\left[k\right]\psi_x\left[k+i, k_{w_x}\right] \tag{4.68}$$

where the values of the system matrices are also assumed to be equal to those of the current time-step k.

The i-step-ahead measurement error covariance, $P_{\tilde{y}_{w_x}}$, as given in (4.42), is a function of the current covariance of the state disturbance input estimate, $P_{\hat{w}_x}\left[k, k_{w_x}\right]$, as well as the i-step-ahead cross-covariance between the disturbance input estimate and the *a priori* measurement error, $P_{\hat{w}_x,\tilde{y}}\left[k+i, k_{w_x}\right]$. As in the case of the measurement disturbance, it is again only necessary to propagate the cross-covariance to future time-steps since the state

disturbance input covariance is equal to the value of the current time-step. The propagation of the cross-covariance is made possible by simplifying (4.43) in the same manner as for the measurement disturbance as follows

$$\begin{aligned} P_{\hat{w}_x,\tilde{y}}\left[k+i,k_{w_x}\right] = {} & P_{\hat{w}_x}\left[k,k_{w_x}\right]\underline{\rho}'_x\left[k,k_{w_x}\right]P_{\tilde{y}}^{-1}\left[k|k-1\right] \\ & \cdot\left(C\left[k\right]P_x\left[k|k-1\right]\left(\mathbb{I}-K\left[k\right]C\left[k\right]\right)'+R_y\left[k\right]K'\left[k\right]\right) \\ & \cdot\mathcal{A}'\left[k+i\right]C'\left[k+i\right] \end{aligned} \tag{4.69}$$

where the cumulative effect of the state matrix, $\mathcal{A}\left[k+i\right]$, is defined in (4.59).

Algorithm 4.2 reorganizes the RLS-based state disturbance input estimation and prediction procedures into a two stage structure, update and predict. As with the measurement disturbance input estimation procedure, the structure of Algorithm 4.2 mimics that of the standard KF equations introduced in Section 3.2. The calculation of pseudo cumulative effect is again a modified form of (4.62) to reduce the computational complexity of extending RLS disturbance input estimation to the recursive disturbance input prediction problem. Thus, the initial value of the pseudo cumulative effect, $\psi_x\left[k,k_{w_x}\right]$, is also modified to include the initial value of the measurement disturbance profile, or $\psi_y\left[k,k_{w_x}\right]=0^{n_x\times n_w}$.

Algorithm 4.2 includes a count of the number of OPL that are required to execute the algorithm for a system with a single measurement as is the case for the algorithms of Section 3.2. The count does not include the operations required for updating the disturbance profile as this value varies with the profile of the assumed disturbance. The computational

Algorithm 4.2 Update and predict stages of the recursive least squares (RLS) state disturbance input estimation and prediction error compensation procedure $RLS_{x,ip}$.

[State disturbance estimation (update)]

$$\underline{\rho}_x [k, k_{w_x}] = C [k] \psi_x [k, k_{w_x}]$$
$$\underline{P}_{\tilde{y},} [k|k-1] = P_{\tilde{y}}^{-1} [k|k-1]$$
$$\underline{\underline{P}}_{\tilde{y}} [k|k-1] = \underline{P}_{\tilde{y},}^{\frac{1}{2}} [k|k-1]$$
$$\varrho_x [k, k_{w_x}] = \underline{\underline{P}}_{\tilde{y}} [k|k-1] \underline{\rho}_x [k, k_{w_x}]$$
$$\mathcal{K}_x [k, k_{w_x}] = \lambda_x^{-1} \mathcal{P}_x [k-1, k_{w_x}] \underline{\varrho}'_x [k, k_{w_x}]$$
$$\left(1 + \lambda_x^{-1} \varrho_x [k, k_{w_x}] \mathcal{P}_x [k-1, k_{w_x}] \underline{\varrho}'_x [k, k_{w_x}]\right)^{-1}$$
$$\hat{w}_x [k, k_{w_x}] = \hat{w}_x [k-1, k_{w_x}]$$
$$+ \mathcal{K}_x [k, k_{w_x}] \left(\underline{\underline{P}}_{\tilde{y}} [k|k-1] \tilde{y} [k|k-1] - \varrho_x [k, k_{w_x}] \hat{w}_x [k-1, k_{w_x}]\right)$$
$$\mathcal{P}_x [k, k_{w_x}] = (\mathbb{I} - \mathcal{K}_x [k, k_{w_x}] \varrho_x [k, k_{w_x}]) \Lambda_x^{-1} \mathcal{P}_x [k-1, k_{w_x}]$$

OPL for scalar y: $2n_{w_x}^3 + 6n_{w_x}^2 + 2n_{w_x} n_x + 6n_{w_x} + n_x + 56 \in O\left(n_{w_x}^3\right)$

[State disturbance estimation (predict)]

$$\psi_x [k+i, k_{w_x}] = \Gamma_x [k+i-1, k_{w_x}]$$
$$+ A [k+i-1] (\mathbb{I} - K [k+i-1] C [k+i-1]) \psi_x [k+i-1, k_{w_x}]$$
update $\Gamma_x [k+i, k_{w_x}]$
$$\underline{\rho}_x [k+i, k_{w_x}] = C [k] \psi_x [k+i, k_{w_x}]$$
$$\bar{\mathcal{A}} [k+i] = A [k+i-1] \mathcal{A} [k+i-1]$$
$$P_{\hat{w}_x, \tilde{y}} [k+i, k_{w_x}] = \mathcal{P}_x [k, k_{w_x}] \underline{\rho}'_x [k, k_{w_x}] \underline{\underline{P}}_{\tilde{y}} [k|k-1]$$
$$\cdot \left(C [k] P_x [k|k-1] (\mathbb{I} - K [k] C [k])' + R_y [k] K' [k]\right)$$
$$\cdot \mathcal{A}' [k+i] C' [k+i]$$
$$\hat{y}_{w_x} [k+i|k] = \hat{y} [k+i|k] + \underline{\rho}_x [k+i, k_{w_x}] \hat{w}_x [k, k_{w_x}]$$
$$P_{\tilde{y}_{w_x}} [k+i|k] = P_{\tilde{y}} [k+i|k] + \underline{\rho}_x [k+i, k_{w_x}] \mathcal{P}_x [k, k_{w_x}] \underline{\rho}'_x [k+i, k_{w_x}]$$
$$- \underline{\rho}_x [k, k_{w_x}] P_{\hat{w}_x, \tilde{y}'} [k+i, k_{w_x}] - P'_{\hat{w}_x, \tilde{y}'} [k+i, k_{w_x}] \underline{\rho}'_x [k+i, k_{w_x}]$$

OPL for scalar y: $4N_p n_{w_x}^2 + 4N_p n_{w_x} n_x^2 + 4N_p n_{w_x} n_x + 6N_p n_{w_x} + 4N_p n_x^3 + 6N_p n_x^2 - N_p n_{w_x} \in O\left(N_p n_x^3\right)$

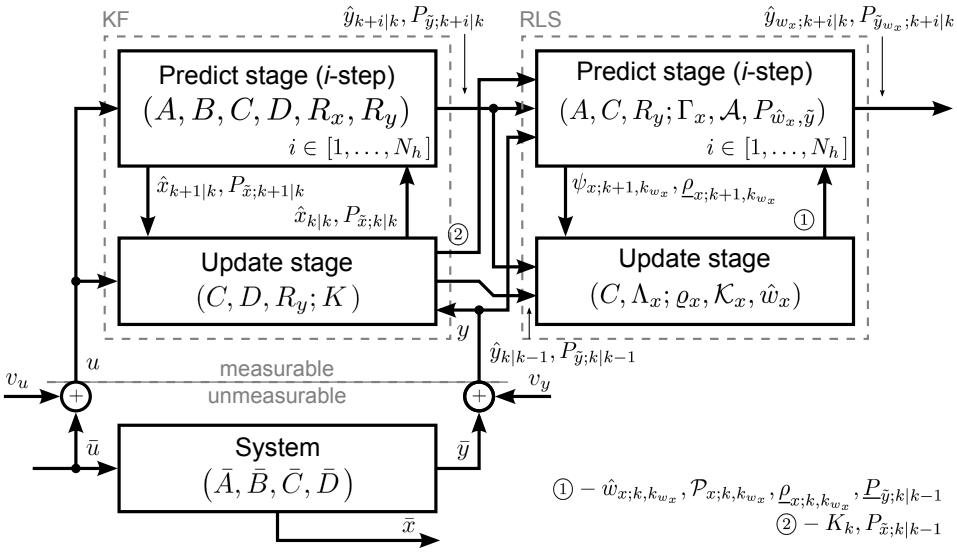

Figure 4.3: Connectivity between KF-based measurement prediction and the measurement disturbance estimation and prediction error compensation procedure of Algorithm 4.1.

complexity of the RLS-based measurement disturbance interval-supporting estimation, prediction, and compensation procedure is cubic with respect to the dimension of the state vector multiplied by the prediction horizon, or $RLS_{x,ip} \in O\left(n_x^3 N_p\right)$. For a scalar state vector, the measurement disturbance prediction algorithm requires $3N_p + 1$ more arithmetic operations than for the state disturbance algorithm. An overview of the state disturbance estimation and prediction error compensation procedure is illustrated in Figure 4.3.

Common oversights Within both the measurement and state disturbance estimation procedures, it is imperative that the measurement innovation, $\tilde{y}$, is calculated using the unmodified or uncompensated KF-based state estimation procedure. In addition, the future values of the Kalman gain, $K\left[k+i\right]$, must be assigned values of zero as the KF-based update stage is not executed within the measurement prediction procedures of Chapter 3.

Compensating for estimation error Although compensation of estimation error rather than prediction error is beyond the scope of this work, the following provides a brief outline for compensation. These compensation techniques may be useful within other non-predictive decision making processes. For the purpose of estimation error compensation, the estimated measurement disturbance input and measurement error covariance are combined with the *a priori* measurement prediction and error covariance in the same manner as for the LS filter using (4.13) and (4.14) respectively. Moreover, it is possible to compensate the *a posteriori* measurement estimate and error covariance by reformulating (4.14). In addition, the recursively estimated state disturbance input and measurement error covariance may be combined with the *a priori* measurement prediction and error covariance in the same manner as for the LS filter using (4.24) and (4.26) respectively. Please refer to the following section for more information regarding the implementation of both state and measurement disturbance estimation. Moreover, as with the prediction compensation procedure, it is imperative that the compensated estimates remain separate from the closed-loop of the KF procedure.

4.2.3 Disturbances to both the measurement and state

It is possible to estimate state disturbance inputs while also estimating measurement disturbance inputs. These combined estimations require, however, that one of the two disturbances be selected as the primary disturbance, i.e. the disturbance that is to be estimated first. Within the combined estimation procedure it is also necessary to consider the cross-covariance between the estimated state and measurement disturbance inputs.

In the following, the measurement disturbance is considered to be primary and the state disturbance secondary.

First, the measurement innovation, $\tilde{y}\left[k|k-1\right]$, that is considered by the secondary or last calculated estimation is modified to include the estimated compensation of prediction error that is calculated in the primary estimation problem. For the case where the measurement disturbance is primary, the measurement disturbance is first calculated by considering the measurement innovation that is equal to the actual measurement minus the *a priori* KF-based measurement estimate, or one-step-ahead measurement prediction. In contrast, the measurement innovation for the secondary state disturbance input estimation routine is offset by the most recently calculated cumulative effect of the measurement disturbance profile multiplied by the most recently estimated measurement disturbance input as follows

$$\tilde{y}_{w_y}\left[k|k-1,k_{w_y}\right]=\tilde{y}\left[k|k-1\right]-\underline{\rho}_{y}\left[k,k_{w_y}\right]\hat{w}_{y}\left[k,k_{w_y}\right] \tag{4.70}$$

where the subscript $\bullet_{w_y}$ indicates the inclusion of measurement disturbance input within the *a priori* measurement estimation error. This estimation error is equivalent to the error associated with the compensated *a priori* measurement estimate of (4.13).

Next, the normalizing covariance of the measurement innovation, $P_{\tilde{y}}\left[k|k-1\right]$, for the secondary state disturbance estimation algorithm is compensated to consider the covariance of the estimated disturbance input as well as the cross-covariance between the estimated disturbance input and the measurement innovation. The measurement innovation that is considered by the secondary state disturbance input estimation procedure is there-

fore equal to the updated covariance, $P_{\tilde{y}_{w_y}}\left[k|k-1,k_{w_y}\right]$, that is calculated within the primary measurement disturbance input estimation procedure, or (4.14).

Estimation of the state disturbance is then performed as formulated in Section 4.2.2. Moreover, the state disturbance propagation also follows the methods of Section 4.2.2. The prediction error is then compensated as follows.

$$\hat{y}_w\left[k+i|k\right]=\hat{y}\left[k+i|k\right]+\underline{\rho}_y\left[k+i,k_{w_y}\right]\hat{w}_y\left[k,k_{w_y}\right]+\underline{\rho}_x\left[k+i,k_{w_x}\right]\hat{w}_x\left[k,k_{w_x}\right] \quad (4.71)$$

The above three modifications to Algorithm 4.2 allow the state and measurement disturbance estimation routines to be combined.

In addition, the i-step ahead combined measurement error covariance, $P_{\tilde{y}_{w_x}}\left[k+i|k\right]$, of Algorithm 4.2 is modified to consider the cumulative effects of both the state and measurement disturbance estimations for disturbances that are assumed to initiate at time-steps $k_w=\left\{k_{w_x},k_{w_y}\right\}$ as follows

$$\begin{aligned}
P_{\tilde{y}_w}\left[k+i|k,k_w\right] &= E\left\{\left(\tilde{y}\left[k+i\right]-\hat{y}_{w_y}\left[k+i|k,k_{w_y}\right]-\hat{y}_{w_c}\left[k+i|k,k_{w_x}\right]\right)^{\underline{2}}\right\} \\
&= E\left\{\left(\tilde{y}\left[k+i\right]-\underline{\rho}_y\left[k+i,k_{w_y}\right]\hat{w}_y\left[k,k_{w_y}\right]\right.\right. \\
&\quad \left.\left.-\ \underline{\rho}_x\left[k+i,k_{w_x}\right]\hat{w}_c\left[k,k_{w_x}\right]\right)^{\underline{2}}\right\} \\
&= P_{\tilde{y}_{w_y}}\left[k+i|k,k_{w_y}\right]+\underline{\rho}_x\left[k+i,k_{w_x}\right]P_{\hat{w}_c}\left[k,k_{w_x}\right]\underline{\rho}'_x\left[k+i,k_{w_x}\right] \\
&\quad -\underline{\rho}_x\left[k+i,k_{w_x}\right]P_{\hat{w}_c,\tilde{y}}\left[k+i,k_{w_x}\right]-P'_{\hat{w}_c,\tilde{y}}\left[k+i,k_{w_x}\right]\underline{\rho}'_x\left[k+i,k_{w_x}\right] \\
&\quad +\underline{\rho}_y\left[k+i,k_{w_y}\right]P_{\hat{w}_y,\hat{w}_c}\left[k,k_w\right]\underline{\rho}'_x\left[k+i,k_{w_x}\right] \qquad (4.72)
\end{aligned}$$

where cross-covariance $P_{\hat{w}_y,\hat{w}_c}$ introduces an additional term beyond those of the state and

measurement disturbance input estimation procedures, cross-covariance $P_{\hat{w}_c,\tilde{y}}$ is a modified form of the cross-covariance established within (4.69), and covariance $P_{\hat{w}_c}$ is calculated in the same manner as $\mathscr{P}_x$ within the general RLS equation (4.47).

The cross-covariance between the state disturbance input estimate, $\hat{w}_c$, and the measurement innovation, $\tilde{y}$, is calculated as follows

$$\begin{aligned}
P_{\hat{w}_c,\tilde{y}}\left[k+i,k_{w_x}\right] &= E\left\{\hat{w}_c\left[k,k_{w_x}\right]\left(y\left[k+i\right]-\hat{y}\left[k+i|k\right]\right)'\right\} \\
&= E\left\{\left(P_{\hat{w}_c}\left[k,k_{w_x}\right]\left(\sum_{j=k_{w_x}}^{k}\underline{\rho}'_x\left[j,k_{w_x}\right]\Lambda_x^{k-j}P_{\tilde{y}_c}^{-1}\left[j|j-1\right]\right.\right.\right. \\
&\quad \left.\left.\left.\cdot\left(\tilde{y}\left[j|j-1\right]-\underline{\rho}_y\left[j,k_{w_y}\right]\hat{w}_y\left[j,k_{w_y}\right]\right)\right)\right)\tilde{y}'\left[k+i|k\right]\right\} \\
&= P_{\hat{w}_c}\left[k,k_{w_x}\right]\underline{\rho}'_x\left[k,k_{w_x}\right]P_{\tilde{y}_c}^{-1}\left[k|k-1\right] \\
&\quad \cdot\left(\left(C\left[k\right]P_x\left[k|k-1\right]\left(\mathbb{I}-K\left[k\right]C\left[k\right]\right)'+R_y\left[k\right]K'\left[k\right]\right)\right. \\
&\quad \left.\cdot\mathscr{A}'\left[k+i\right]C'\left[k+i\right]-\underline{\rho}_y\left[k,k_{w_y}\right]P_{\hat{w}_y,\tilde{y}}\left[k+i,k_{w_y}\right]\right) \\
&= P_{\hat{w}_x,\tilde{y}}\left[k+i,k_{w_x}\right] \\
&\quad -P_{\hat{w}_c}\left[k,k_{w_x}\right]\underline{\rho}'_x\left[k,k_{w_x}\right]P_{\tilde{y}_c}^{-1}\left[k|k-1\right]\underline{\rho}_y\left[k,k_{w_y}\right]P_{\hat{w}_y,\tilde{y}}\left[k+i,k_{w_y}\right]
\end{aligned} \tag{4.73}$$

where the cross-covariance between the estimated measurement disturbance input and the measurement innovation is zero for time-steps k_{w_x} through $(k-1)$, and $P_{\hat{w}_y,\tilde{y}}$ is given in (4.36).

The i-step ahead combined measurement error covariance is then modified to include the cross-covariance between the estimated state and measurement disturbance inputs.

The cross-covariance is calculated in the following non-recursive form

$$
\begin{aligned}
P_{\hat{w}_y,\hat{w}_c}\left[k,k_w\right] &= E\left\{\hat{w}_y\left[k,k_{w_y}\right]\hat{w}_c'\left[k,k_{w_x}\right]\right\} \\
&= E\left\{\left(P_{\hat{w}_y}\left[k,k_{w_y}\right]\left(\sum_{j=k_{w_y}}^{k}\underline{\rho}_y'\left[j,k_{w_y}\right]\Lambda_y^{k-j}P_{\tilde{y}}^{-1}\left[j|j-1\right]\tilde{y}\left[j|j-1\right]\right)\right)\right. \\
&\quad\cdot\left(P_{\hat{w}_c}\left[k,k_{w_x}\right]\left(\sum_{j=k_{w_x}}^{k}\underline{\rho}_x'\left[j,k_{w_x}\right]\Lambda_x^{k-j}P_{\tilde{y}_c}^{-1}\left[j|j-1\right]\tilde{y}\left[j|j-1\right]\right.\right.\right. \\
&\quad\left.\left.\left.-\sum_{j=k_{w_x}}^{k}\underline{\rho}_x'\left[j,k_{w_x}\right]\Lambda_x^{k-j}P_{\tilde{y}_c}^{-1}\left[j|j-1\right]\underline{\rho}_y\left[j,k_{w_y}\right]\hat{w}_y\left[j,k_{w_y}\right]\right)\right)'\right\} \\
&= P_{\hat{w}_y}\left[k,k_{w_y}\right]\left(\sum_{j=k_{w_y}}^{k}\underline{\rho}_y'\left[j,k_{w_y}\right]\Lambda_y^{k-j}\right. \\
&\quad\cdot\left(\mathbb{I}-P_{\tilde{y}}^{-1}\left[j|j-1\right]P_{\hat{w}_y,\tilde{y}}'\left[j,k_{w_y}\right]\underline{\rho}_y'\left[j,k_{w_y}\right]\right) \\
&\quad\left.\cdot\left(P_{\tilde{y}_c}^{-1}\left[j|j-1\right]\right)'\left(\Lambda_x^{k-j}\right)'\underline{\rho}_x\left[j,k_{w_x}\right]\right)P_{\hat{w}_c}'\left[k,k_{w_x}\right] \qquad (4.74)
\end{aligned}
$$

where the cross-covariance of the measurement innovation cancels with the inverse covariance and the cross-covariance between the measurement innovation and the estimated measurement disturbance input is given as the transpose of (4.16). It is possible to calculate the above cross-covariance in a recursive manner within the update stage of the secondary RLS disturbance estimation algorithm by separating the series summation from the covariance matrices of the current time-step as follows.

$$
P_{\hat{w}_y,\hat{w}_c}\left[k,k_w\right] = P_{\hat{w}_y}\left[k,k_{w_y}\right]\Omega\left[k,k_{w_x}\right]P_{\hat{w}_c}'\left[k,k_{w_x}\right] \qquad (4.75)
$$

The cumulative effect of the state and measurement disturbance profiles on the cross-

covariance of the estimated disturbance inputs is also calculated recursively as follows

$$\begin{aligned}\Omega\left[k, k_{w_x}\right] = \Lambda_x \Omega\left[k-1, k_{w_x}\right] \Lambda_x' + \underline{\rho}_y'\left[k, k_{w_y}\right] \\ \cdot \left(\mathbb{I} - P_{\tilde{y}}^{-1}\left[k|k-1\right] P_{\hat{w}_y,\tilde{y}}'\left[k, k_{w_y}\right] \underline{\rho}_y'\left[k, k_{w_y}\right]\right) \\ \cdot \left(P_{\tilde{y}_c}^{-1}\left[k|k-1\right]\right)' \underline{\rho}_x\left[k, k_{w_x}\right] \end{aligned} \tag{4.76}$$

where $\Omega\left[k_{w_x}-1, k_{w_x}\right] = 0^{n_{w_y} \times n_{w_x}}$.

Algorithm 4.3 combines the RLS-based measurement and state disturbance input estimation and prediction procedures into a two stage structure, update and predict. The updated algorithm also includes the calculation of the necessary cross-covariances. The number of OPL are not calculated for this algorithm, since the number of operations have already been tallied for the two estimation in previous presented algorithms.

4.2.4 Resetting the disturbance and RLS covariance

The recursive ability of the RLS filter brings about many advantages to the disturbance estimation problem, e.g. a reduction in computational complexity and data storage requirements. Through the use of the forgetting factor, $\Lambda_\bullet$, it is possible for the RLS filter to operate indefinitely as the algorithm places a higher weight on the most recent data. The forgetting factor can allow for better adjustment with the compromise of reduced stability. That said, it is only possible to make the disturbance estimation procedure entirely recursive with respect to the disturbance profile for a subset of the profiles that may support recursion. Moreover, for those profiles that due support recursion, the computational complexity of the recursions may become limiting. For this reason, this work propagates the

Algorithm 4.3 RLS/KF-based measurement interval-prediction with combined measurement and state disturbance input estimation and prediction error compensation where the measurement disturbance is considered primary.

Require: $N_p, A, B, C, D, u, y, R_x, R_y, \Lambda_y$
Initial conditions: $\hat{x}\left[0|0\right], P_{\tilde{x}}\left[0|0\right]$
Result: $\hat{y}_w\left[k+i|k\right], \hat{y}_w^{u,\underline{\alpha}}\left[k+i|k\right], \hat{y}_w^{l,\underline{\alpha}}\left[k+i|k\right] \forall i = 1, \ldots, N_p$

```
k = 0
call [Initialization] from Algorithm 3.1
loop
  k = k + 1
  {measure y[k]}
  call [Measurement disturbance estimation (update)] from Algorithm 4.1
  call [State disturbance estimation (update)] from Algorithm 4.2
    with ỹ and P_ỹ replaced by the compensated ỹ_{w_y} and P_{ỹ_{w_y}}
  call [State estimation (update)] from Algorithm 3.1
  for i = 1, ..., N_p do
    call [i^th-step propagation (predict)] from Algorithm 3.3
    call [Measurement disturbance estimation (predict)] from Algorithm 4.1
    call [State disturbance estimation (predict)] from Algorithm 4.2
    call [i^th-step interval calculation] from Algorithm 3.3
      with ŷ and P_ỹ replaced by the compensated ŷ_w and P_{ỹ_w}
  end for
  {propagate x[k] to x[k+1]}
end loop
```

disturbance profile forward in time from an initiating time-step, k_w. It is therefore necessary to update this initiating time-step in order to continuously monitor for the occurrence of a disturbance.

The reset procedure is performed periodically after a given number of time-steps. The values which are reset include, if necessary, the disturbance profile, $\Gamma_\bullet$, as well as the initial value of the disturbance estimate covariance, $\mathscr{P}_\bullet$ and all of the cumulative variables, $\psi_\bullet$, $\underline{\rho}_\bullet$, and Ω. The estimated disturbance input is not reset, as the most previously calculated estimate is considered to be a good initial guess for the reset estimation problem.

The choice of forgetting factor affects the tracking, convergence, and stability of the RLS filter. This is even more important given the time-varying KF/RLS dual state and input estimation problem. This work does not establish the criteria for selection of a sufficiently stable forgetting factor. It is important that the forgetting factor be set at a value that is relatively near to and less than unity. As the value of the forgetting factor approaches unity, the RLS filter takes into account more historical data within the estimation problem. Thus, larger values of forgetting factor generally improve the stability of the RLS filter. More specifically, the effect of the forgetting factor on the measurement error at time-step $(k - k_w)$ can be calculated as λ^{k-k_w} . For example, a forgetting factor of 0.99 applies a weight of 0.366 or 36.6% to the measurement error that was observed at 100 time-steps into the past.

Alternating dual RLS filter configuration The reset procedure of this section occasionally results in erroneous disturbance estimations due to the initial conditions within the RLS filter. An alternate strategy to alleviate these errors is to duplicate the distur-

bance estimation and prediction algorithms and to switch between the dual RLS filters, e.g. from one RLS filter for measurement disturbance to another RLS filter for measurement disturbance, and the same for state disturbance. This alternating dual configuration can be performed for either of, or both of, the state and measurement disturbance estimation algorithms. A simplified example of this alternating configuration is given in Algorithm 4.4.

The simplest mechanism for switching between the active and inactive RLS filters is to do so at regular intervals. This switching function is denoted Θ in Figure 4.4 as well as Algorithm 4.4. In this work, however, a convergence detection algorithm has been implemented to determine a suitable time-step at which to switch between the filters. The measurement and state disturbance algorithms are therefore switched at different time-steps, i.e. not in unison. Upon switching, the RLS covariance of the inactive filter as well as the initiating time-step of the disturbance are reset. Once the RLS solution has converged, the algorithm switches back to the original RLS filter. This convergence detection procedure is repeated indefinitely. Convergence is detected by monitoring the magnitude of a moving average for the mean squared error in the measurement prediction that would be achieved through the use of the inactive filter. The remaining details of this mechanism are not significant to the contribution of this thesis and are therefore not documented.

4.2.5 Adaptive-limited-memory-filter-based noise covariance estimation

This section considers the combination of the ALMF noise covariance estimation algorithm within the alternating dual configuration of RLS-based disturbance estimation. This final configuration combines, in an elegant manner, all the algorithms that have been formulated within this work. The ALMF-based noise covariance estimation algorithm determines the statistical uncertainty in the state and measurement error. These errors are affected by the RLS-based disturbance estimation. Thus, when used in conjunction with the RLS filters, the ALMF algorithm is modified to consider the compensated prediction error. The following modifications are included in Algorithm 4.4.

For the estimation of measurement noise covariance, the ALMF algorithm is modified to consider the compensated *a priori* measurement error and error covariance, $\tilde{y}_w$ and $P_{\tilde{y}_w}$, rather than those that are produced by the KF-based prediction algorithm alone, i.e $\tilde{y}$ and $P_{\tilde{y}}$. Thus, the measurement noise covariance considers the compensation that is performed as a result of estimating the state and measurement disturbances. The result is that the measurement error covariance more accurately represents the uncertainty in the compensated errors.

For the estimation of state noise covariance, the modifications to the ALMF are more involved. The state noise covariance is a function of the error between the *a posteriori* and *a priori* state estimates, $\hat{x}\left[k|k\right] - \hat{x}\left[k|k-1\right]$. Although the disturbance is applied to the true state, as defined in (4.1), the state disturbance affects the state estimates through the same equation as for the measurement disturbance. In other words, the only means by

Algorithm 4.4 RLS/KF-based measurement interval-prediction with ALMF noise covariance estimation, dual combined measurement and state disturbance input estimation and prediction error compensation where the measurement disturbance is considered primary

Require: $N_p, A, B, C, D, u, y, R_x, R_y, \Lambda_y$
Initial conditions: $\hat{x}[0|0], P_{\tilde{x}}[0|0]$
Result: $\hat{y}_w[k+i|k], \hat{y}_w^{u,\underline{\alpha}}[k+i|k], \hat{y}_w^{l,\underline{\alpha}}[k+i|k] \, \forall i = 1, \ldots, N_p$

```
k = 0
call [Initialization] from Algorithm 3.1
loop
  k = k + 1
  {measure y[k]}
  call [Measurement disturbance estimation (update)] from Algorithm 4.1
  call [Alternate-measurement disturbance estimation (update)] from Algorithm 4.1

  call [State disturbance estimation (update)] from Algorithm 4.2
    with ỹ and P_ỹ replaced by the compensated ỹ_{w_y} and P_{ỹ_{w_y}}
  call [Alternate-state disturbance estimation (update)] from Algorithm 4.2
    with ỹ and P_ỹ replaced by the compensated ỹ_{w_y} and P_{ỹ_{w_y}}
  evaluate switching function, Θ, and select active disturbance estimates
  call [Measurement noise covariance estimation] from Algorithm 3.4
    with ŷ and P_ỹ replaced by the compensated ŷ_w and P_{ỹ_w}
  call [State estimation (update)] from Algorithm 3.1
  call [State noise covariance estimation] from Algorithm 3.4
    with x̂[k|k] and P_x̃[k|k] replaced by x̲[k|k] and P̲_x̃[k|k]
  for i = 1, ..., N_p do
    call [i^th-step propagation (predict)] from Algorithm 3.3
    call [Measurement disturbance estimation (predict)] from Algorithm 4.1
      with R_y replaced by R̂_y
    call [Alternate-measurement disturbance estimation (predict)] from Algorithm 4.1
      with R_y replaced by R̂_y
    call [State disturbance estimation (predict)] from Algorithm 4.2
      with R_y replaced by R̂_y
    call [Alternate-state disturbance estimation (predict)] from Algorithm 4.2
      with R_y replaced by R̂_y
    evaluate switching function, Θ, and select active prediction errors
    call [i^th-step interval calculation] from Algorithm 3.3
      with ŷ and P_ỹ replaced by the compensated ŷ_w and P_{ỹ_w}
  end for
  {propagate x[k] to x[k+1]}
end loop
```

which to measure a disturbance in the state is through the measurement, y. Moreover, the measurement affects the state estimates through the update equation in (3.16). Thus, the *a posteriori* state estimate is updated as follows for the purpose of state noise covariance estimation.

$$\underline{\hat{x}}\left[k|k\right] = \hat{x}\left[k|k\right] + K\left[k\right]\left(-\underline{\rho}_{y}\left[k, k_{w_y}\right]\hat{w}_{y}\left[k, k_{w_y}\right] - \underline{\rho}_{x}\left[k, k_{w_x}\right]\hat{w}_{x}\left[k, k_{w_x}\right]\right) \tag{4.77}$$

This update eliminates the impact of the disturbances on the state estimate without embedding the error compensation routine within the standard KF equations.

When both the state and measurement disturbance estimation routines are active, the ALMF algorithm is modified to consider the cross-covariance between the two disturbance input estimates in the same manner as in (4.72) for prediction error compensation. These covariances are calculated within the update stage of the secondary RLS disturbance estimation algorithm, however, rather than the prediction stage as included in the combined state and measurement disturbance Algorithm 4.3. The chosen forgetting factor, $\lambda_{\bullet}$, should allow the RLS-based disturbance estimates to be more responsive to error than the ALMF-based noise covariance estimates given covariance estimation window, N_v. Moreover, for LTV systems where the model parameters may be assigned from a multi-model lookup table, it is imperative that bumpless transfer is included within all of the KF and LS or RLS equations.

The KF-based measurement interval-prediction, RLS-based disturbance estimation and prediction error compensation, as well as ALMF-based noise covariance estimation are combined in Figure 4.4. This overview also includes the dual combined measurement

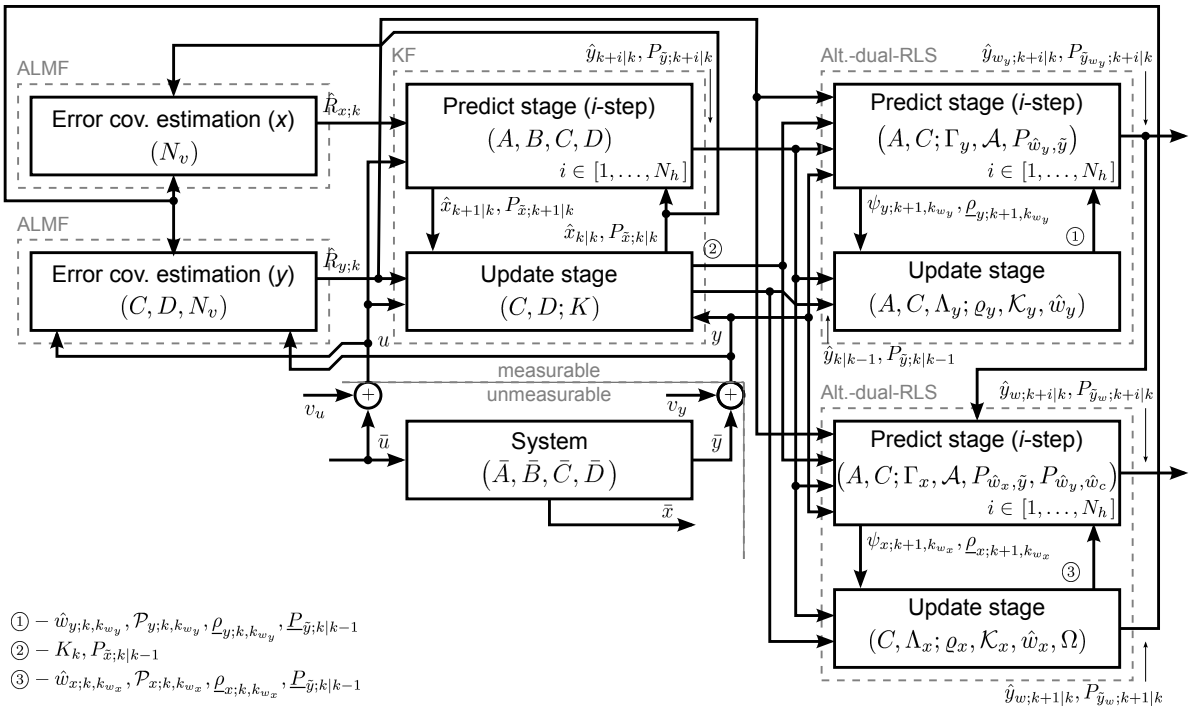

Figure 4.4: Connectivity between KF-based measurement prediction and the measurement disturbance estimation procedure of Algorithm 4.1.

and state disturbance input estimation where the measurement disturbance is considered primary.

4.3 Summary

This chapter presents the LS solution to the disturbance estimation problem. This estimation procedure is performed in addition to the KF-based state estimation of Chapter 3 in order to consider deterministic changes in the operating conditions or signals of the system. The LS problem is formulated for additive input disturbances to both state and measurement of the system. The disturbance model is included within the estimation routine as a profile as opposed to the alternate method of augmenting the state matrix. This form of estimation circumvents the selection of fictitious noise covariance for disturbances

that are considered to be deterministic.

A recursive solution to the LS disturbance estimation problem is also formulated. This recursive procedure includes the related covariances between the estimated disturbance input and the measurement residual or innovation. The recursive solution does not, however, include the ability to recursively update the initial time-step for the assumed disturbance. For this reason, an alternating dual-RLS filter configuration is developed whereby the two RLS filters switch upon detection of the compensated prediction error converging to within some margin of accuracy with respect to the measurement signal. The RLS disturbance input estimation procedure is then combined with the ALMF noise covariance estimation routine of Chapter 3. The result is a prediction algorithm that incorporates three forms of estimation and two forms of uncertainty for LTV systems.

Chapter 5

Predictive Shutdown and Assessment of Prediction Quality

Chapter 3 and Chapter 4 address many of the prediction-related objectives that make up this dissertation work. The remaining methodology-related objectives can be separated into two main tasks. The first is the development of PSDSs using the algorithms formulated in Chapter 3 and Chapter 4. The second is the enhancement of the developed PSDS to consider or assess prediction quality as well as the probability of a true or false impending trip condition.

Regarding the development of a PSDS, this chapter introduces a benchmark conventional SDS design that is a simplified portion of CANDU SDS1 as introduced in Section 2.2. The conventional SDS is modified to include the KF-based prediction algorithm of Section 3.2. A block diagram of the basic structure for conventional SDS as well as the modular addition of the prediction algorithm is illustrated within the context of SISs in

Figure 5.1a) and Figure 5.1c) respectively. By including KF-based prediction, the PSDS is able to consider stochastic uncertainty within the system, model, parameters, and signals. The PSDS is then further modified within this chapter to include the noise covariance estimation algorithm of Section 3.6 as well as the prediction error compensation algorithm of Section 4.1. These modifications are illustrated respectively in Figure 5.1d) and Figure 5.1e). The addition of RLS-based disturbance estimation enables the PSDS to consider deterministic uncertainty, e.g. errors within the model parameter as well as disturbances within the system inputs. Moreover, the addition of an ALMF-based noise covariance estimation algorithm enables the PSDS to consider changes in the statistical descriptions of the uncertainties that are provided to the KF. Each of the KF-based as well as the KF/RLS-based PSDS designs is derived using both the point- and the interval-prediction methods of Chapter 3. This chapter therefore introduces two point-PSDS designs and two interval-PSDS designs.

In utilizing a KF as the foundation of the prediction algorithm as well as an RLS filter to compensate for prediction error, the point- and interval-PSDS designs are able to calculate accurate predictions even though the system may be operating under uncertain conditions, e.g. those conditions that are compatible with the assumed model of disturbance input. That said, multi-step-ahead KF-based predictions are calculated in an "open-loop" manner since the prediction algorithm does not take into consideration the value of past multi-step-ahead predictions. In other words, the KF-based measurement predictions and error covariances are not functions of the error in predictions that are propagated beyond one time-step. This is in contrast to the one-step ahead KF-based predictions that affect KF-based estimates in a "closed-loop" manner through the update of the mean *a posteriori*

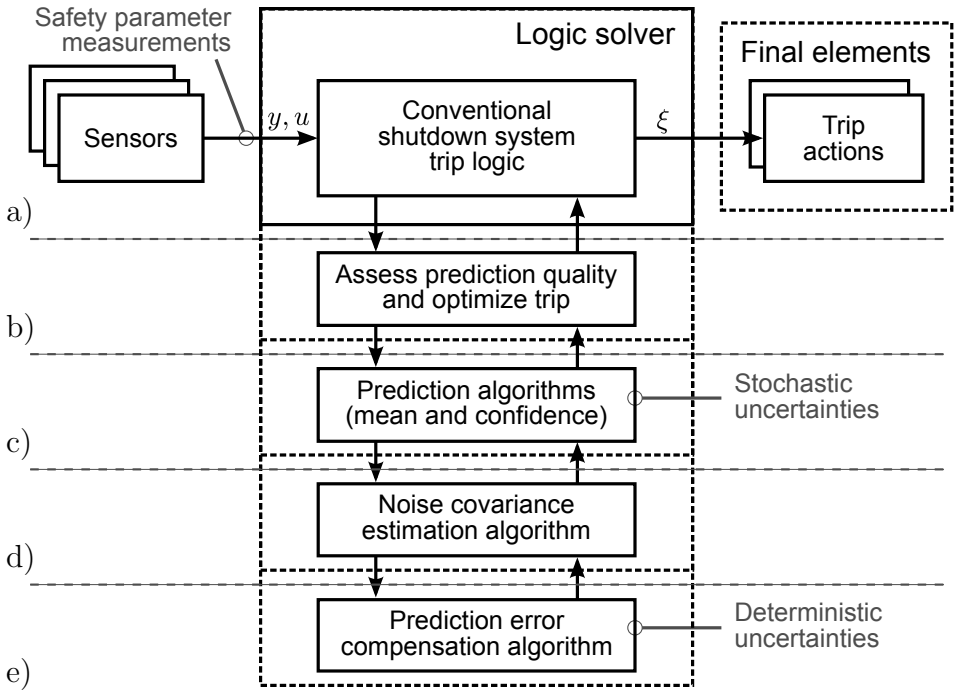

Figure 5.1: Modular modification of a) conventional SDS logic to include the following capabilities b) prediction quality assessment and alarm/trip optimization, c) safety parameter prediction, d) uncertainty or noise covariance estimation, and c) prediction error compensation, all within the context of safety instrumented systems (SISs).

state estimate as a function of the *a priori* measurement error within the state update equation (3.16). Thus, a secondary objective of this chapter is to monitor and asses the quality of past predictions in an effort to improve the capability of the PSDS designs to make accurate predictive decisions. This objective differs from that of Chapter 3 in that the predictions and the prediction algorithm are being tested for quality rather than the predictions only being compensated for errors.

The algorithms of Chapter 3 do not monitor for bias or drift in the predicted measurements or discrepancies in the measurement prediction error covariances. Given the assumption of a Gaussian probability distribution for prediction errors within the KF, however, various statistical tests can be performed on the errors to determine whether the assumed system model, signal, and noise characteristics match those of the true sys-

tem [147, 148]. These tests provide a means for assessing prediction quality within each time-step of the prediction window, as performed in [40]. Those predictions that are considered to be of sufficient quality given the statistical test criteria are then selected for comparison against the TSP. The result is an effective prediction horizon that is adapted as a function of prediction quality. Statistical testing, hypothesis testing, and optimal alarm theory are then combined in an effort to adapt and optimize trip initiation in a manner similar to the work of Martin [41]. More specifically, by including optimal alarm theory, it is possible to not only adapt the effective prediction horizon but also to adapt a metric that represents expected mean prediction error by maximizing the probability of an impending trip condition given an alarm or trip. These two features are included in the prediction quality assessment and trip optimization block of Figure 5.1b).

The above objectives result in a PSDS that is not only able to calculate future values of safety parameter measurements under uncertain conditions, but is also aware of the quality of the predictions that are being made. Moreover, the PSDS is able to adapt the effective prediction horizon and predicted measurement metric so that the shutdown procedure is activated at a time that is considered to be optimal. In this manner, the probability of spurious and missed trip occurrences can be minimized. In general, this chapter presents PSDS designs that emphasize simplicity and modularity. All of the proposed PSDS designs include the conventional trip detection mechanism in order to guarantee the occurrence of a trip decision that cannot, under any circumstances, be made at a time which is later than that of the conventional SDS. This research considers the well-established IB , NIS , and IW tests for assessing the statistical properties of the predictions that are calculated by the KF and RLS algorithms [147]. The hypothesis testing methods t investigated within

this research include the calculation of TPR and FPR . These two rates are closely related to the ROC that is utilized within some optimal alarm research [41] as well as the false positive, Type I, and false negative, Type II, errors that correspond to spurious or missed trip activations within SDS. The PSDS designs also incorporate a prediction selection function that is responsible for adapting the prediction horizon or metric that is to be compared against the TSP.

Of the topics covered in this chapter, the formulation of the point- and interval-PSDS designs is considered a major contribution since these designs are the first known predictive methods within the application of NPP shutdown. In addition, this chapter presents the first known investigation into the relationship between the ROC space of optimal alarm theory and the NPP shutdown decision-making procedures. Finally, the PSDS designs of this chapter achieve the main aim set out within the motivation of this dissertation work.

In summary, the first two sections of this chapter introduce a conventional SDS design and then combine the algorithms of Chapter 3 and Chapter 4 to achieve PSDS designs of varying capabilities and functionalities. The third section of this chapter enhances the PSDS design to assess the quality of the predictive decisions. The third section also presents the adaptation of prediction horizon as well as the metric that is to be compared against the TSP. This adaptation is optimized with respect to the quality of the predicted measurements. This chapter does not attempt to cover all aspects of SDS design or the vast body of literature related to applied probability, and statistical and hypothesis testing. For a more complete treatment of NPP safety and SDS methods please refer to one of the many safety-related IAEA technical documents [1] or international standards including those of the IEC [117, 118]. Alternatively, for a review of applied probability, as well as statistical

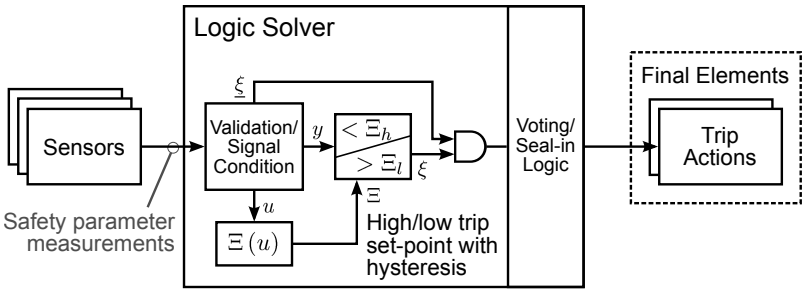

Figure 5.2: Conventional shutdown system (SDS) in the context of safety instrumented systems (SISs).

and hypothesis testing refer to the text by Papoulis [146, 148] or Bar-Shalom [148], and the course notes of Reid [147].

5.1 A Conventional Shutdown System Design

The structure of a conventional SDS logic solver is included in the context of SISs in Figure 5.2. A conventional trip occurs upon detecting a threshold-crossing event that involves a safety parameter reaching a corresponding TSP. Conventional SDS logic solvers generally include signal conditioning and validation logic as well as a comparator and corresponding hysteresis threshold. The conditional logic of the comparator most often considers a TSP that is constant, but TSPs may also be varied linearly with respect to some major system parameter, e.g. another signal received by the SDS that is related to the system being protected. The logic solver also incorporates, or is supported by, coincidence voting and seal-in logic components, as reviewed in Section 2.2.2 [129]. The voting/seal-in block is located at the edge of the logic solver since these functions may either be included within the trip logic, or implemented using relay logic or other technologies that are external to the trip computer.

The SDS illustrated in Figure 5.2 includes an isolated logic solver that makes trip decisions for a single safety parameter measurement, y, according to either a high or low alarm-threshold or TSP, Ξ. In contrast, conventional SDSs generally include multiple instances of this trip logic for safety parameter measurements that represent many NPP subsystems. These logic solvers are connected between the same sensors and final elements, and therefore have access to a number of safety-related signals or safety parameter measurements. For example, although included in Figure 5.2, safety parameter measurement, u, is not directly considered within the trip logic of the current safety parameter, y.

The sensors included in Figure 5.2 are the safety-related devices that provide the safety parameters measurements, y and u, from the NPP subsystems. In contrast, the final elements or trip actions are the physical means by which, upon shutdown, negative reactivity is introduced to the reactor core to stop the fission chain reactions, e.g. shut-off rods or neutron poison. In addition, the trip actions are usually divided into two or more groups. For example, each shut-off rod may be assigned to one of two banks where all rods of the same bank are release using a single electrical signal that controls the electro-mechanical clutch that keeps the rods suspended above the reactor core.

The function of the comparator block within the trip logic is to compare the safety parameter measurement, y, of the current time-step against a corresponding TSP, $\Xi \triangleq \{\Xi_h, \Xi_l\}$. For software-based SDSs, the logic is executed on a time-interval known as an execution interval or scan time, e.g. 100ms. If the safety parameter is found to be equal to or beyond either a high or a low TSP, Ξ_h or Ξ_l, the trip signal, $\xi \triangleq \{\xi_h, \xi_l\}$, is de-energized. The SDS therefore detects a threshold-crossing event. The conditional logic for

conventional trip is defined as follows

$$\xi_h[k] = \begin{cases} 1 & y[k] < \Xi_h \\ 0 & \text{otherwise} \end{cases}, \xi_l[k] = \begin{cases} 1 & y[k] > \Xi_l \\ 0 & \text{otherwise} \end{cases} \tag{5.1}$$

where ξ_h and ξ_l are the resulting high and low trip signals respectively. Here, a trip signal equal to 1 indicates continued operation without trip whereas a signal equal to 0 indicates a trip occurrence, i.e. de-energize to trip. In Figure 5.2, the notations Ξ and ξ indicate either a high or low TSP and corresponding trip signal for high and low trip logic respectively. In practice, the TSP can vary as a function, $\Xi(u)$, of some major system parameter, e.g. u. Although this feature is included in Figure 5.2, the TSPs of this study have constant values.

The comparator block of Figure 5.2 includes a hysteresis offset that is combined with the TSP. The hysteresis offset prevents jitter within the trip signal that may be caused by fluctuations in the safety parameter measurement. For example, measurement fluctuations may result in a down-crossing and subsequent up-crossing of a low TSP. Under these conditions, the SDS will not de-energize and then re-energize without a significant reversal in the dynamics of the system that provides the measurement. The measurements that are input to the SDS may be acquired from multiple redundant sensors for the same physical variable. In some cases, these input signals undergo filtering, compensation, and/or averaging prior to being compared against the TSP. These features are include in Figure 5.2 as the validate/signal condition block. All safety parameter measurements are monitored to be within the valid range of the electrical signal characteristics for the safety transmitter,

e.g. a $4-20$mA sensor that is transmitting 3.0mA. Safety parameters that are detected to be invalid result in the parameter being de-energized within the voting logic. This validity or error check is performed through the use of the validation trip signal, $\underline{\xi}$. A fault in the sensor of a safety parameter therefore results in an increased probability of spurious trip for the multi-channel SDS.

5.2 Predictive Shutdown System Designs

KF-based point-predictions, as formulated in Section 3.3, are a function of prior information that specifies a model and uncertainty for a given system and corresponding signals. This information provides a KF predictor the ability to anticipate the mean trajectory of a given system over a prediction window to some prediction horizon. When KF-based point-predictions are calculated for safety parameter measurements within a system being protected, this ability provides a means for making trip decisions at a time which is earlier than for the case of conventional decision-making systems since the conventional systems wait for the occurrence of the impending event. These mean anticipated trajectories or point-predictions are therefore the foundation of the point-PSDS design.

The KF also has the ability, as a stochastic filter, to describe the anticipated trajectory in terms of a probability distribution. This probability distribution can be interpreted as a measure of confidence in the calculated predictions within each time-step of the prediction window. KF-based interval-predictions, as formulated in Section 3.5, include the same prior information as the KF-based point-predictions but also assign specific levels of confidence to the bounds of an interval of the anticipated trajectories. KF-based interval-predictions

result in trip decisions that occur earlier than for conventional decision-making but also have a certain level of confidence in the occurrence of an impending abnormal condition. In comparison, trip decisions that are made using the mean prediction values of the point-PSDS have a level of confidence in the impending trip condition of 50%. Interval-predictions are therefore utilized to calculate the upper and lower bounds of a confidence-interval, one of which corresponds to a level of confidence that is greater than 50%. The greater of the two bounds is the inner bound with respect to the domain of safe operating conditions. Confidence-interval-based decisions are expected to counteract spurious trips that may be encountered when using the point-PSDS design.

RLS disturbance estimation and prediction error compensation provide an additional means of enhancing the point- and interval-PSDS designs. The main aim of either the point- or interval-PSDS designs is to predict abnormal conditions that would eventually be detected by the conventional SDS. It is therefore important that the predictions accurately represent the future dynamic response of the model and the potential occurrence of uncertain conditions that may arise during the transient to an abnormal condition. In compensating the predictions for the estimate of the prediction error, the predictions are forced to follow the safety parameter measurements more closely than the response of the model that is provided to the KF or even the optimal KF-based predictions. Error compensation therefore benefits the PSDS by allowing the prediction algorithm to be more accurate with respect to impending abnormal conditions. This is especially true for uncertain conditions that are deterministic in nature and can be modelled as some form of additive disturbance input.

Within the nuclear industry, strict regulations regarding sensor quality as well as sensor

redundancies help to ensure that the sensor measurements are reliable. This has a direct impact on the uncertainties assumed within the KF since it is less likely for the measurements to be uncertain. For example, an averaging function or voting mechanism applied to four high quality redundant steam generator level sensors results in a very reliable measurement that has low uncertainty. For industries that have less sensor reliability and increased uncertainty measurement, the above configuration can be modified to compare both the compensated as well as the uncompensated measurement predictions against the corresponding TSP. This modified design is subject, however, to a potential increase in spurious trip occurrences due to the addition of a parameter being compared against the TSP. That said, the potential for model-based trip is not included within the trip coverage of the conventional SDS. Although the KF-based predictions are assessed within the results of this work, a PSDS design that compares both the KF and KF/RLS-based predictions against a TSP is considered to be beyond the scope of this study.

It is also possible to perform KF-based prediction for multiple safety parameters within the SDS. It is recommended, however, that each of the safety parameters be considered independent of the remaining parameters in order to reduce computational complexity as well as the interconnection between the safety parameter calculations. This strategy should not have any impact on the independence of the SDS since the predicted safety parameters are those that were already monitored by the SDS. Moreover, the KF algorithm does not rely on any single common variable between the parameters.

5.2.1 Point-PSDS: point-predictive shutdown system

The structure of the point-PSDS is included in the block diagram of Figure 5.3. A point-predictive trip occurs upon predicting a threshold-crossing event that involves the mean-value of a predicted measurement reaching a corresponding TSP, Ξ. This TSP is the same value as is used for conventional trip. In this configuration, the logic solver is modified to include a KF-based prediction algorithm that considers a system model as well as various constraints and uncertainties. Point-predictive decisions are made by comparing safety parameter measurement predictions against the conventional TSPs. The structure of the point-PSDS is a modular evolution of conventional SDS that does not require additional sensors or hardware modifications. This requirement does, however, assume that the system input to the KF, u, is available as a safety parameter measurement or can be calculated as a function of others parameters. The conventional trip logic remains active within all of the proposed PSDS designs as a backup to the predictive trip mechanism, i.e. measurements are also compared directly to the TSPs. The conventional trip logic is implemented within the point-PSDS design in the same manner as described for the conventional SDS in Section 5.1. The upper limit of time-to-trip is therefore guaranteed to be equal to that of the conventional SDS given that the PSDS has an equivalent scan time. In other words, the addition of the point-prediction algorithm is only able to improve upon the response time of the conventional SDS.

Safety parameter measurements are predicted using the KF prediction block of Figure 5.3 and the KF-based measurement point-prediction equations of Algorithm 3.2. Although the measurement predictions are propagated to prediction horizon, N_p, the a predictive

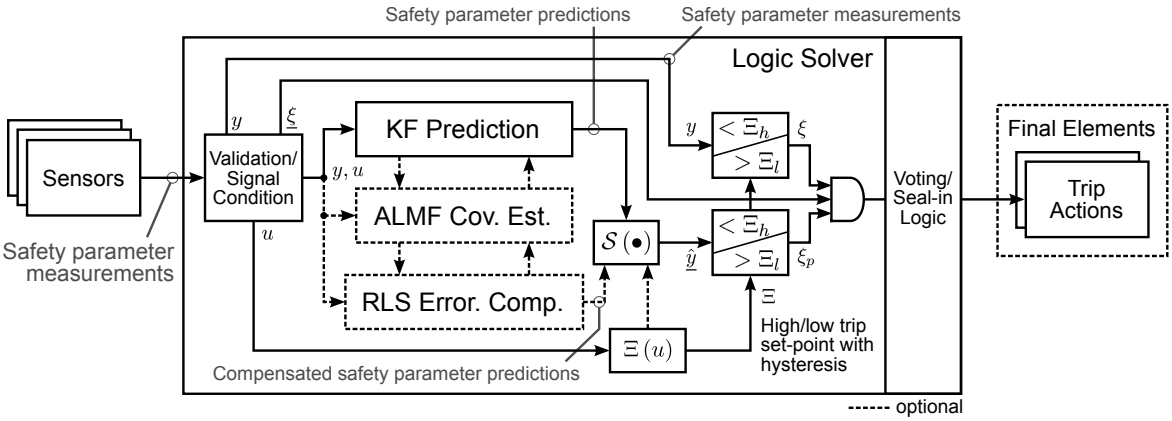

Figure 5.3: KF/RLS-based point-predictive shutdown system (point-PSDS) in the context of safety instrumented systems (SISs) with the option for activating RLS or ALMF algorithms.

trip occurs if any of the measurement predictions within the prediction window reach either a high or low TSP, Ξ_h or Ξ_l. Thus, a maximum or minimum of the predictions within the prediction window is selected to be compared against either a high or a low TSP respectively. The selected prediction is the output of the selection function block, and function $\mathcal{S}$, as follow

$$\underline{\hat{y}}\,[k] = \mathcal{S}\left(\hat{y}\,[k+i|k]\right) = \begin{cases} \max\left(\hat{y}\,[k+i|k]\right) & \text{for } \Xi_h \\ \min\left(\hat{y}\,[k+i|k]\right) & \text{for } \Xi_l \end{cases}, \forall i = 1, \ldots, N_p \tag{5.2}$$

where max and min return the maximum and minimum of the point-predictions that are calculated within the prediction window. If the selected safety parameter point-prediction, $\underline{\hat{y}}$, is equal to or beyond either a high, Ξ_h, or a low TSP, Ξ_l, then the trip signal, $\xi_p \triangleq \{\xi_{p,h}, \xi_{p,l}\}$, is de-energized. The conditional logic for this point-predictive trip is defined as

follows.

$$\xi_{p,h}[k] = \begin{cases} 1 & \underline{\hat{y}}[k] < \Xi_h \\ 0 & \text{otherwise} \end{cases}, \xi_{p,l}[k] = \begin{cases} 1 & \underline{\hat{y}}[k] > \Xi_l \\ 0 & \text{otherwise} \end{cases} \tag{5.3}$$

In addition, the conditional logic for the backup conventional trip that remains active within the point-PSDS are defined in (5.1).

The presence of system-model mismatch or input disturbances can cause the KF-based measurement predictions to deviate from the future measurements. This is the case for many practical dynamical systems where the model parameters may be time-varying or when disturbances are present. Error compensation is made possible by performing RLS-based estimation of disturbance inputs for an assumed disturbance profile as included in Algorithm 4.1 and Algorithm 4.2. These algorithms are included in Figure 5.3 as the optional RLS error compensation block. Functionally, the algorithms propagate the estimated disturbance models over the prediction window in order to compensate error within the safety parameter predictions. The compensated predictions are denoted $\hat{y}_{w_{xy}}$, $\hat{y}_{w_y}$, or $\hat{y}_{w_x}$ for the respective state and measurement, measurement, and state disturbance input cases. As in the case of the KF-based point-PSDS, the maximum or minimum compensated prediction value is then selected within function $\mathcal{S}$ of (5.2) where $\hat{y}$ is replaced by the corresponding compensated safety parameter predictions $\hat{y}_{w_{xy}}$, $\hat{y}_{w_y}$, or $\hat{y}_{w_x}$.

The ALMF covariance estimation block of Figure 5.3 allows for the KF to consider state and measurement noise covariances, R_x and R_y, that are unknown or time-varying. This is often the case for the state noise covariance since this covariance is not easily measured. Many studies therefore approximate covariance values through trial-and-error, or utilize

other methods that are referred to as being ad-hoc. In contrast, the ALMF-based noise covariance estimation routine, as included in Algorithm 3.6, estimates the noise covariance as a function of state and measurement errors that are calculated within the KF. The ALMF algorithm also provides a mechanism for detecting divergence within the KF whereby specific values within the two noise covariances may be growing without bounds. It is recommended that these conditions be monitored and the covariance estimation routine either reset or constrained if the covariance values approach the limits given the model of the system.

When both the RLS and the ALMF algorithms are included, the ALMF-based measurement noise covariance estimation algorithm is modified to consider the compensated *a priori* measurement prediction and measurement error covariance whereby $\tilde{y}[k|k-1]$ is replaced by $(y[k|k-1] - \hat{y}_{w_\bullet}[k|k-1])$ and $\underline{P}_y[k|k-1]$ by $P_{\tilde{y}_{w_\bullet}}$ with $w_\bullet$ indicating either the state or measurement disturbance. Moreover, the ALMF-based state noise covariance estimation algorithm is similarly modified whereby $\tilde{\hat{x}}[k]$ is replaced by $\tilde{\hat{x}}[k] + K[k](\hat{y}_{w_\bullet}[k|k-1] - y[k|k-1])$ while the state error covariance equation remains unmodified.

5.2.2 Interval-PSDS: interval-predictive shutdown system

The interval-PSDS uses KF-based stochastic descriptions of prediction uncertainty to make confidence based decisions regarding impending abnormal conditions. An interval-predictive trip occurs upon predicting a threshold-crossing event that involves the bounds of a predicted confidence-interval reaching a corresponding TSP, Ξ. This TSP is the same

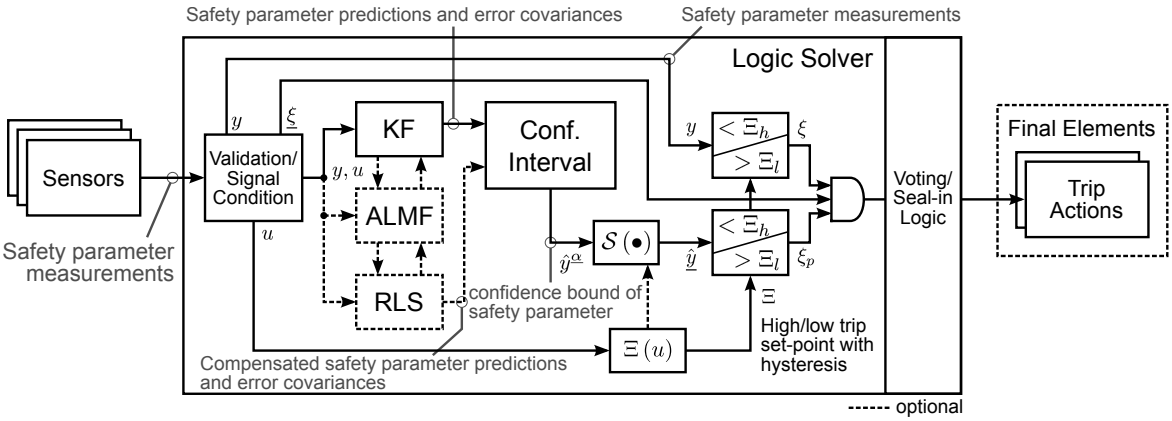

Figure 5.4: KF/RLS-based interval-predictive shutdown system (interval-PSDS) in the context of safety instrumented systems (SISs) with the option for activating RLS or ALMF algorithms.

value as is used for point-predictive and conventional trip. The structure of the interval-PSDS is included in the block diagram of Figure 5.4. Interval-predictive decisions are made by comparing the upper or lower bounds of a confidence interval for the safety parameter measurement predictions against the conventional TSPs. As is the case for the point-PSDS design, the structure of the interval-PSDS is a modular evolution of the conventional SDS which does not require additional sensors or hardware modifications. Moreover, the conventional trip logic is implemented within the interval-PSDS design in the same manner as described for the point-PSDS and conventional SDS in Section 5.1. The addition of the interval-prediction algorithm is, again, only able to improve upon the response time of the conventional SDS.

That said, the interval-PSDS does result in a delayed trip when compared against the point-PSDS design. This is a result of the interval-PSDS waiting for a specific level of confidence in an impending abnormal condition to be achieved. The point- and interval-PSDS designs have the potential, therefore, to result in increased false and missed trip occurrences respectively. These occurrences should be considered prior to implementation,

in order to reduce conflict with existing standards and regulations.

Safety parameter measurements and measurement error covariances are predicted using the KF prediction block of Figure 5.4 as well as the KF-based measurement interval prediction equations of Algorithm 3.3. The interval-PSDS design differs from the point-PSDS designs in that the state error covariance is propagated to the prediction horizon, N_p, and the measurement error covariance, $P_{\tilde{y}}$, is calculated at each time-step within the prediction window. These measurement predictions and error covariances are then combined within the confidence interval block of Figure 5.4 for a specific one-tailed significance level, α, and corresponding two-tailed significance level, $\underline{\alpha}$, as introduced in Section 3.5. The result is a set of confidence-based prediction values, $\hat{y}^{\underline{\alpha}} \triangleq \{\hat{y}^{l,\underline{\alpha}}, \hat{y}^{u,\underline{\alpha}}\}$, that bound the measurement predictions within each time-step of the prediction window.

For a high TSP, Ξ_h, the lower bounds represent a level of confidence that is greater than 50%. In contrast, for a low TSP, Ξ_l, the upper bounds correspond to a level of confidence that greater than 50%. For example, a low level trip with a two sided significance level of $\underline{\alpha} = 5\%$ results in an upper bound being compared against the TSP. This upper bound is expected to be higher in value than 97.5% of the expected future safety parameter measurements within the corresponding time-step of the prediction window. Thus, when the upper bound reaches the low TSP, the interval-PSDS has a level of confidence greater than or equal to 97.5% that the measurements will also reach the low TSP within that specific time-step of the prediction window.

The interval-predictive trip logic is designed to trip if any of the either lower or upper bound values within the prediction window reach either a high or low TSP respectively. This functionality is equivalent to the $\mathcal{S}$ function within the point-PSDS design, but for

different prediction values. Thus, a maximum or minimum of the specific bound within the prediction window is selected within $\mathcal{S}$ function block as follows, and is to be compared against either a high or a low TSP respectively.

$$\underline{\hat{y}}\,[k] = \mathcal{S}\left(\hat{y}^{\underline{\alpha}}\,[k+i|k]\right) = \begin{cases} \max\left(\hat{y}^{l,\underline{\alpha}}\,[k+i|k]\right) & \text{for } \Xi_h \\ \min\left(\hat{y}^{u,\underline{\alpha}}\,[k+i|k]\right) & \text{for } \Xi_l \end{cases}, \forall i = 1, \ldots, N_p \tag{5.4}$$

If the selected bound of the safety parameter interval-prediction, $\underline{\hat{y}}$, is equal to or beyond either a high, Ξ_h, or a low TSP, Ξ_l, then the trip signal, ξ_p, is de-energized. The conditional logic for an interval-predictive trip is therefore defined as it was for the point-PSDS in (5.3). In addition, the conditional logic for the backup conventional trip is as defined in (5.1).

Compensation of prediction error can also be included within the interval-PSDS design by including the RLS-based disturbance input estimation as formulated for both state and measurement disturbance inputs in Algorithm 4.3. Otherwise, the state or measurement disturbance input estimation routines can be performed separately by individually implementing Algorithm 4.2 or Algorithm 4.1 respectively. These algorithms are included in the RLS block of Figure 5.4. Functionally, the algorithms propagate the estimated disturbance model and the calculated cross-covariances over the prediction window in order to compensate error within the safety parameter predictions as well as the error covariance that provides a probability distribution for the safety parameter predictions. The compensated predictions are denoted $\hat{y}_{w_{xy}}$, $\hat{y}_{w_y}$, or $\hat{y}_{w_x}$ for the respective state and measurement, measurement, and state disturbance input cases.

For interval-prediction, the disturbance estimation algorithm calculates the auto-covariance

of the estimated disturbance input as well as the cross-covariance between the estimated input and the *a priori* measurement estimation error. These two covariances are then combined with the measurement error covariance of the KF within the confidence interval block so that the distribution of the compensated predictions is accurate given the secondary estimation problem. The confidence interval block then calculates the upper and lower bounds and the maximum or minimum compensated prediction bound is selected using the $\mathcal{S}$ function of (5.2) where $\hat{y}^{\underline{\alpha}}$ is replaced by the corresponding compensated bound of the safety parameter prediction.

Covariance noise estimation has a more significant role in improving the quality of the interval-predictions than it does for the point-predictions. The reason for this increased role is that KF-based point-predictions are minimum variance estimates of the state or measurement under a variety of model-mismatch and disturbance conditions. Moreover, the point-predictions are optimal when the model matches the system and the noise within the state and measurement equations is white and Gaussian. In contrast, the performance of the error covariances is not so well defined and may even be erroneous. These errors are often overlook in the literature since the KF is most often utilized for point-estimation purposes. In other words, although the point-estimates are optimal given that the information provided to the KF is accurate, this is not the case for the state and measurement error covariances. These covariances may not reflect the true uncertainty within the state or measurement estimates or predictions. The erroneous covariances occur as a result of insufficient or misleading state or measurement noise covariances being provided to the KF. More precisely, small variations in the assumed noise covariances have minimal impact on the quality of the KF-based prediction, but profound impact within the descriptions of un-

certainty regarding these predictions. Thus, when implementing the interval-PSDS design it is recommended that some form of covariance noise estimation be performed or, in the least, that a formal method for calculating the state error covariance be employed.

The primary benefit of the interval-PSDS is the ability of the consider uncertainty regarding the calculated predictions. Where the point-PSDS produces a trip upon the point-prediction reaching the TSP, the interval-PSDS instead waits until the TSP has been reached with a predetermined level of confidence. The interval-PSDS therefore benefits safety-critical decisions that have high productivity losses associated with alarm or shutdown. That said, measures of confidence in decision-making, whether calculated within the interval-PSDS or otherwise, quantify the belief that is held by a decision-making mechanism given a specific set of prior information or knowledge, that an impending condition is going to occur. Both the point- and interval- PSDS, however, remain unaware of the performance or accuracy of past predictions. Thus, the remainder of this chapter aims to assess the quality of previously calculated predictions in order to establish a PSDS design that is aware of the prediction algorithm performance.

5.3 Prediction Quality Assessment

The point- and interval-PSDS designs, as formulated in Section 5.2, consider prior knowledge and prediction uncertainty but do not consider prediction quality. This section aims to determine the quality of the predictions that are calculated using the prediction, error compensation, and noise estimation algorithms of Chapter 3. The quality of the calculated predictions is assessed according to a predetermined significance level, α or $\underline{\alpha}$, through the

use of statistical tests and hypothesis testing methods. The significance level in turn specifies the false positive or Type I error rate, FPR. The statistical tests assess whether or not the prediction errors are zero mean, or unbiased, and white with an accurately estimated measurement prediction error covariance [147, 148]. The results of the tests are utilized to optimize the performance of the predictive decision-making mechanism with respect to the probability of an impending abnormal condition. These methods allow for enhancement of both the point- and interval-PSDS designs by adapting the effective prediction horizon as well as prediction bias within the optimal-PSDS design of Section 5.3.3.

Within the point- and interval-PSDS designs, the prediction algorithms are provided models of the system as well as the disturbances that may be affecting the state or measurement signals. The accuracy of the calculated predictions relies on the validity of these assumed models as well as the assumed, or calculated in the case of the ALMF, statistical properties regarding uncertainty in the signals and the model parameters. More precisely, these uncertainties are the state and measurement noise covariances, R_x and R_y respectively. Section 5.3.1 investigates three statistical tests that can be utilized to assess the validity of these assumptions as a function of measurement prediction error and error covariance for each time-step within the prediction horizon. If these assumptions are erroneous, the prediction error may either be biased or time correlated, or have a covariance descriptions that are either too wide or too narrow. In being able to identify these erroneous properties of the predictions, the predictive decision-making mechanism of the PSDS design can then be enhanced to consider prediction quality at each time-step within the prediction window.

In general, predictions are unbiased if the mean of the error distribution is equal to zero.

Those predictions that are either unbiased or biased slightly toward the TSP provide the benefit of reducing the probability of a missed detection with the drawback of increasing the probability of false detection. Those predictions that are unbiased or lead the measurements toward the TSP therefore improve safety. In contrast, predictions that are biased away from the TSP and toward the center of the normal operating region may decrease safety since these biases result in a delay to the predictive trip decision, a reduction in the probability of false detection, and an increase in the probability of a missed detection. Biases affect point- and interval-based predictive decisions equally since both the point-prediction as well as the bound of the confidence-interval are affected by the offset that is the bias. It is beneficial, therefore, to either reduce or detect bias within each of the PSDS designs in order to prevent the occurrence of a false or missed trip events.

Regarding covariance quality, the measurement prediction error covariance is considered exact if the variance of the measured prediction errors is equal to the predicted error covariance. For interval-PSDS designs that utilize levels of confidence greater than 50%, an estimated covariance that is wider than the measured covariance results in an increased probability of missed detection with the benefit of decreasing the probability of false trip. This is due to the confidence intervals of the prediction being wider than the confidence associated with the actual covariance of the error and not representing the true uncertainty in the eventual measurements. In contrast, for interval-PSDS designs that utilize levels of confidence that are less than 50%, the wider estimated covariance causes increased probability of false detections and decreased missed detections. The quality of the predictive decisions within the interval-PSDS design are therefore a function of level of confidence in the predictions. This level of confidence is, in turn, a function of the error covariance.

Thus, it is important, when using the interval-PSDS, that the observed variance of prediction error is approximately equal to the expected variance.

In addition to prediction quality, Section 5.3.3 investigates the extension of hypothesis testing to optimal alarm theory. In general, hypothesis testing aims to determine the outcomes of statistical tests that lead to a rejection of the null hypothesis according to a pre-specified level of significance, α, e.g. the probability that the predicted measurement will occur outside a confidence interval of some significance level. Within this work, the hypothesis tests consider the null hypothesis of an impending abnormal condition and the alternate hypothesis of continued operation under normal conditions, see Figure 1.1. In this manner, it is then possible to quantify the ability of the statistical test outcomes to either "not reject" or to "reject" the null hypothesis of the impending abnormal condition. This ability is measured through the calculation of true and false positive rates, TPR and FPR [41].

By quantifying the performance optimizing rates within each time-step of the prediction window and for a set of hypothetical mean predictions errors, the PSDS designs are able to not only adapt the effect prediction window but also the score associated with the bounds of the confidence interval. These adaptations are discussed with respect to the ROC space that is constructed with TPR and FPR metrics as axes. The PSDS design is then enhanced by means of optimal alarm theory to consider an upper bound on the probability of false trip within each time-step of the prediction window.

5.3.1 Hypothesis testing

This section introduces three statistical tests that are each able to determine, for a given level of significance, α, whether a sequence of random variables, or measurement prediction errors, correspond with a given covariance, e.g. the measurement error covariance. It is expected that performing these tests prior to initiating shutdown will result in an increase in the accuracy of the predictive trip decisions. This increase in accuracy is achieved by adapting the effective prediction window to consider only those predictions that are within time-steps of the prediction window that are assessed not to be beyond a sufficient level of quality. Moreover, hypothesis testing relates significance level, α, to Type I or false positive errors. The performance of the prediction algorithm is therefore made to have an upper bound on the probability of a false positive event. Within the nuclear industry, this event corresponds to a missed trip occurrence; false positive is a false detection of the normal condition.

Hypothesis testing involves a sequence of tests with respect to a null hypothesis, H_0, that is considered the default condition and an alternate hypothesis, H_1, that is the condition to be proven. The null hypothesis either fails to be rejected, reject$'$, or is rejected, reject, by means of some statistical test. The results of a series of hypothesis tests can be organized using an error matrix or contingency table as included in Table 5.1 [160]. Error matrices provide a means for quantifying the results of a hypothesis test within one of four of the following outcomes: TP are those conditions that are hypothesized to be alternate and are actually alternate, FP are those conditions that are hypothesized to be alternate and are actually null, FN are those conditions that are hypothesized to be null and are actually

Table 5.1: Error matrix.

Hypothesized condition/ predicted hypothesis	True condition: H_0	True condition: H_1
reject$'$ (H_0)	True Negative (TN) $(1-\alpha)$	False Negative (FN) Type II error
reject (H_0)	False Positive (FP) Type I error (α)	True Positive (TP)

alternate, and TN are those conditions that are hypothesized to be null and are actually null. Of these values, TP and TN correspond with correct decisions whereas FP and FN are incorrect. These values may either be percentages or rates, as is common in hypothesis testing, or a tally of a number of outcomes, as is more often used for binary classification. This table is referred to as the error matrix due to the FP and TN outcomes representing errors in the hypothesis testing procedure [160].

As stated previously, FP outcomes correspond with Type I errors or those events where the null hypothesis is true, H_0, but is rejected, reject (H_0). This type of error corresponds with a false alarm since the test statistic indicates that the null condition is false when it is actually true. For NPP SDSs, an FP is referred to as a missed trip, i.e. the presence of an abnormal condition without any trip action being activated. In contrast, the FN outcome corresponds with a Type II error or those outcomes where the null hypothesis is true, H_1,

but is rejected, reject$'$ (H_0). This type of error corresponds with a missed alarm since the test statistic indicates that the null condition is true when it is actually false. For NPP SDSs, an FN is referred to as false trip, i.e. a trip action being activated while operating under normal conditions.

The error matrix introduces various metrics that are functions of TP, FP, FN, and TN rates from within the error matrix [160]. Of these metrics, optimal alarm theory focuses on the TPR, FPR that make up the domain of the ROC [41], with the latter rate the metric over which optimal alarms are optimized. Optimal alarm theory also considers a third metric known as the negative preditive value (NPV). First, the TPR and FPR metrics are conditional probabilities and corresponding ratios: for TPR as follows

$$P_{\text{TPR}} = P\left(\text{reject}\left(H_0\right)|H_1\right) = \frac{P\left(\text{reject}\left(H_0\right) \cap H_1\right)}{P\left(H_1\right)} = \frac{TP}{TP + FN} \tag{5.5}$$

and for FPR as follows.

$$P_{\text{FPR}} = P\left(\text{reject}\left(H_0\right)|H_0\right) = \frac{P\left(\text{reject}\left(H_0\right) \cap H_0\right)}{P\left(H_0\right)} = \frac{FP}{FP + TN} \tag{5.6}$$

The TPR is therefore the probability of rejecting the null hypothesis given that the true condition is the alternate hypothesis. The TPR is also the ratio of TP outcomes to the total number of occurrences for which the alternate hypothesis is determined to be true. In contrast, FPR is the probability of rejecting the null hypothesis given that true condition is the null hypothesis. The FPR is the ratio of FP occurrences to the total number of occurrences that are the null hypothesis. In addition, the NPV metric is the following

conditional probability and corresponding ratio.

$$P_{\text{NPV}} = P\left(H_0|\text{reject}'\left(H_0\right)\right) = \frac{P\left(H_0 \cap \text{reject}'\left(H_0\right)\right)}{P\left(\text{reject}'\left(H_0\right)\right)} = \frac{TN}{TN + FN} \tag{5.7}$$

The NPV is therefore the probability of a null hypothesis given that the null hypothesis was predicted or, more formally, not rejected. The NPV is the ratio of TN outcomes to the total number of null hypotheses that were not rejected.

The above hypothesis tests are made possible through the statistical tests of the following sections. These tests are commonly used for Gaussian probability distributions. The tests are the result of likelihood ratio tests that identify the distribution or score against which the calculated tests statistics are to be compared. The tests of the following sections are performed for a predetermined test window of length, N_t, and either the one-tailed significance level, α, or two-tailed significance level $\underline{\alpha}$. The tests are implemented in either a moving average or a cumulative sum form. The moving average forms are straightforward for the IB and IW tests with the cumulative form of the NIS test being transformed to a moving average by dividing the test result by the length of the test window. The moving average implementation of these algorithms is realized in the same manner as for the basic strategy of estimating noise in Algorithm 3.4 with initialization given in Algorithm 3.5. Alternatively, each of the IB and IW tests can be transformed into a cumulative form whereby the averaging operations are removed from the recursive equations of Algorithm 3.4 and the cumulative sum is divided by the length of the test window.

In addition to verifying prediction quality, the following statistical tests can be interpreted as predictive hypotheses regarding the eventual safety parameter measurement error

with respect to the probability distribution of the safety parameter prediction. These hypotheses correspond to events within the above error matrix that quantify the ability of the prediction algorithm to predict the statistical conditions of an impending safety parameter measurement. The hypothesis testing methods essentially determine whether the value of the eventual measurement satisfies, with some predetermined probability, the predicted condition. This determination is performed for each time-step within the prediction window. This hypothesis testing procedure is then re-framed within the context of optimal alarms for predictive shutdown in Section 5.3.2.

The length of the statistical test window, N_t, is selected as a function of the significance level, $\underline{\alpha}$, within the statistical test while also considering the maximum rate of change of the dynamic response. The length of the window maintains a balance between detection precision and the potential for delay or lag within the test results. For example, a statistical test with a significance level of 5% and test window of length, $N_t = 10000$ requires the calculated test metric of 9374 samples to be within specific bounds in order for prediction quality to be validated. After determining that prediction is not of sufficient quality, the test may return an insufficient result for the remainder of the 10000 time-steps. On the other hand, in the case of a test window of length, $N_t = 100$, only 94 of the 100 samples are required to be within the bounds. In comparing the two configurations, the first example has lower sensitivity in deciding that the predictions may be inaccurate whereas the second example has a higher rate of rejecting potentially anomalous deviations from the assumed probability distribution of the predictions. The test window must be sufficiently long in order to allow for a reasonable estimate of the full precision for the selected significance level, e.g. with $N_t = 100$, the estimate of 94 samples is similar to the full precision value of

93.74 samples. Longer test windows are therefore required for higher significance levels.

Within this study, the test window is assumed to be of sufficient length that the number of degrees of freedom within the samples do not have an impact on the distribution of the errors. For smaller sample sizes the Student's t-distribution and t-test as well as the F-distribution and Hotelling's T^2-test are recommended in place of the Z- and χ^2-tests [40, 161].

5.3.1.1 Innovation bound or Z test

The first of the three statistical tests is referred to as the IB test but is also known as either the one- or two-tailed Z test. The two-tailed IB is also a form of the innovation magnitude bound test [147]. The IB test determines within each time-step of the prediction window whether there is any bias in the calculated predictions. The test is performed over a sequence of length N_t by calculating the Z statistic that is equal to the mean prediction error divided by the mean standard error of the predictions. The Z statistic is then compared against critical values that are the scores associated with a predetermined one- or two-tailed significance level, α or $\underline{\alpha}$. These scores have the same underlying principle as the $z_\bullet$ scores calculated for the confidence intervals in Section 3.4.

The test metric, $\mathcal{T}_\mathcal{Z}$, captures the boolean result of a two-tailed IB test performed over a range of N_t time-steps prior to the current time-step k as follows

$$\underline{\mathcal{T}}_\mathcal{Z}[k,i] = \frac{1}{N_t}\sum_{j=k-N_t+1}^{k}\frac{\tilde{y}[j|j-i]}{\sqrt{P_{\tilde{y}}[k|k-1]}/\sqrt{N_t}} = \frac{1}{\sqrt{N_t}}\sum_{j=k-N_t+1}^{k}\frac{\tilde{y}[j|j-i]}{\sqrt{P_{\tilde{y}}[k|k-1]}} \tag{5.8}$$

$$\mathcal{T}_{\mathcal{Z}}[k,i] = \begin{cases} 1 & \text{otherwise} \\ 0 & \begin{cases} \text{if } \underline{\mathcal{T}}_{\mathrm{Z}}[k,i] \leq -\mathcal{Z}(\alpha) \\ \quad \text{or } \underline{\mathcal{T}}_{\mathrm{Z}}[k,i] \geq \mathcal{Z}(\alpha) \text{ for a two-tailed test} \end{cases} \end{cases} \tag{5.9}$$

with the one-tailed IB test as follows

$$\mathcal{T}_{\mathcal{Z}}[k,i] = \begin{cases} 1 & \text{otherwise} \\ 0 & \begin{cases} \text{if } \underline{\mathcal{T}}_{\mathrm{Z}}[k,i] \leq -\mathcal{Z}(\alpha) \text{ for a lower one-tailed test} \\ \text{if } \underline{\mathcal{T}}_{\mathrm{Z}}[k,i] \geq \mathcal{Z}(\alpha) \text{ for an upper one-tailed test} \end{cases} \end{cases} \tag{5.10}$$

where $\mathcal{Z}(\bullet)$ are the critical values against which the test metric is compared for a predetermined significance level, and i is the time-step within the prediction window. In addition, $\tilde{y}[j|j-i]$ is the prediction innovation, or the prediction error made i time-steps into the past, as defined in (3.20) or for the disturbance input estimation problem in (4.5), and $P_{\tilde{y}}[j|j-i]$ is the innovation covariance for a single measurement signal, also made i time-steps into the past, as defined in (3.24) and modified for the disturbance estimation problem in Section 4.2. The $\underline{\mathcal{T}}_{\mathcal{Z}}$ metric is the z-score of the observed measurement prediction error and error covariance pairs averaged over the test window. The square root of the measurement error covariance in (5.8) is calculated for each measurement of a non-scalar measurement vector separately using the diagonal values of the covariance matrix.

The two-tailed IB test returns a true value if the mean prediction error for a specific time-step of the prediction window is within the bounds of the confidence interval at a rate of $100(1-\underline{\alpha})\%$. Alternatively, the one-tailed IB test returns a true value if the

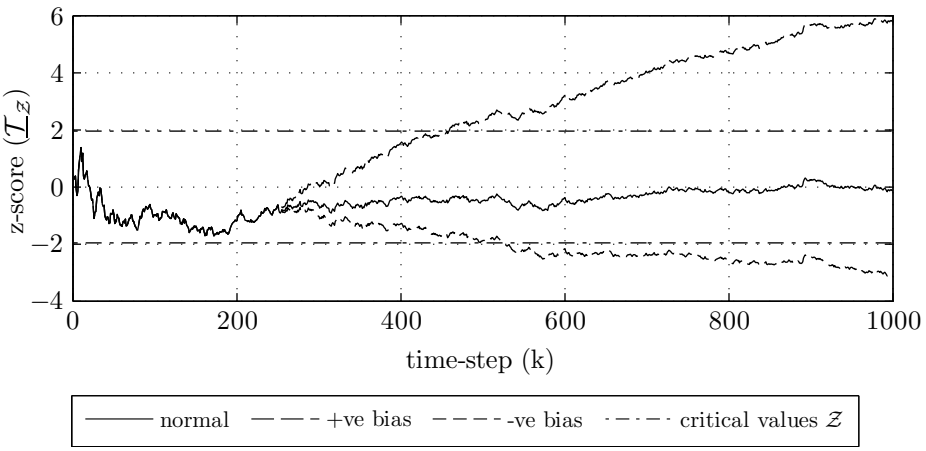

Figure 5.5: IB or Z test statistics and critical values for unbiased prediction error as well as positive and negative biases that are introduced at time-step 250.

mean prediction error is either less than or greater than the upper and lower bounds of the confidence interval at a rate of $100\,(1-\alpha)\%$. For both one- and two-tailed tests, an average z-score that is greater than the upper critical value indicates, with probability greater than or equal to $100\,(1-\alpha)\%$, that the predictions have a positive bias. In contrast, if the average z-score is less than the lower critical, there is greater than or equal to $100\,(1-\alpha)\%$ probability that the predictions errors have a negative bias. These concepts are included in the scores and critical values that are illustrated in Figure 5.5.

5.3.1.2 Normalized innovations squared or chi-squared χ^2 test

The second statistical test is known as the NIS test but is also known as either the one- or two-tailed chi-squared, χ^2, test [147]. The NIS test determines whether the calculated predictions are unbiased and have an accurately described variance within a predetermined probability or significance level, α for the one-tailed test and $\underline{\alpha}$ for the two-tailed test. The NIS test is performed by calculating, for each time-step of the prediction window, the time-average of the normalized innovation or predicted measurement error squared over a given

sequence of prediction errors that are assumed to be time-independent. The average is then compared against critical values that are the confidence interval of the χ^2 distribution with a number of degrees of freedom, N_χ, equal to the dimension of the measurement vector multiplied by the length of the given innovation sequence. In the case of RLS-based disturbance input estimation, the number of degrees of freedom is reduced by the number of estimated disturbance input parameters, $\left(n_{w_x} + n_{w_y}\right)$. The NIS test uses the χ^2 probability distribution rather than the Gaussian distribution of the Z-test due to the fact that the normalized square of Gaussian distributed random variables are distributed according to the chi-squared distribution.

Test metric $\mathcal{T}_{\chi^2}$ captures the boolean result of a NIS test performed over a range of N_t time-steps prior to the current time-step k for time-step i within the prediction window as follows

$$\underline{\mathcal{T}}_{\chi^2}[k,i] = \sum_{j=k-N_t+1}^{k} \tilde{y}'[j|j-i]\, P_{\tilde{y}}^{-1}[j|j-i]\, \tilde{y}[j|j-i] \tag{5.11}$$

$$\mathcal{T}_{\chi^2}[k,i] = \begin{cases} 1 & \text{otherwise} \\ 0 & \begin{cases} \text{if } \underline{\mathcal{T}}_{\chi^2}[k,i] < \chi^2\left(\frac{\alpha}{\overline{\overline{2}}}, N_\chi\right) \\ \quad \text{or } \underline{\mathcal{T}}_{\chi^2}[k,i] > \chi^2\left(1-\frac{\alpha}{\overline{\overline{2}}}, N_\chi\right) \text{ for a two-tailed test} \end{cases} \end{cases} \tag{5.12}$$

or for the one-tailed test as follows

$$\mathcal{T}_{\chi^2}[k,i] = \begin{cases} 1 & \text{otherwise} \\ 0 & \begin{cases} \underline{\mathcal{T}}_{\chi^2}[k,i] < \chi^2(\alpha, N_\chi) \text{ for a lower one-tailed test} \\ \underline{\mathcal{T}}_{\chi^2}[k,i] > \chi^2(1-\alpha, N_\chi) \text{ for an upper one-tailed test} \end{cases} \end{cases} \tag{5.13}$$

where $\tilde{y}$, i and $P_{\tilde{y}}$ are as defined for the IB test in (5.9). Further, $\left[\chi^2\left(\frac{\alpha}{2}, N_t\right), \chi^2\left(1-\frac{\alpha}{2}, N_t\right)\right]$ are the critical values of the test statistic or the confidence interval for the χ^2 distribution with N_χ degrees of freedom, two-tailed significance level, $\underline{\alpha}$, and one-tailed significance level, α. The $\underline{\mathcal{I}}_{\chi^2}$ metric is the cumulative normalized innovation squared. This cumulative value is distributed according to the χ^2 probability distribution and can therefore be directly compared against χ^2 distribution for N_χ degrees of freedom. Alternatively, the time-averaged metric, $\underline{\mathcal{I}}_{\chi^2}/N_t$, can be compared against critical values that are divided by the number of time-steps, χ^2/N_t.

The NIS test returns a true value for a specific time-step within the prediction window if the mean normalized innovations squared are within the specified confidence interval of the χ^2 distribution. More specifically, for the two-tailed test, if the calculated average of the test statistic is within the confidence interval of the χ^2 distribution, the predictions are determined with a probability equal to the value $(1-\underline{\alpha})$ to be unbiased and to have accurate prediction error covariance. Otherwise, the predictions are determined either be biased or to have an erroneous covariance. If the calculated average of the test statistic is less than the upper critical value of the χ^2 distribution, the predictions are determined, with a probability equal to the $(1-\alpha)$, to be unbiased and to have a prediction error covariance that is sufficiently large with respect to the observed measurement errors. For test statistics that are greater than the lower critical value, the predictions are determined to have a prediction error covariance that is sufficiently small according to the observed prediction errors, again with a probability equal to the $(1-\alpha)$. In other words, the lower critical value determines whether the prediction error covariance is too large and not whether any prediction bias is present. The NIS test does not therefore distinguish between covariance

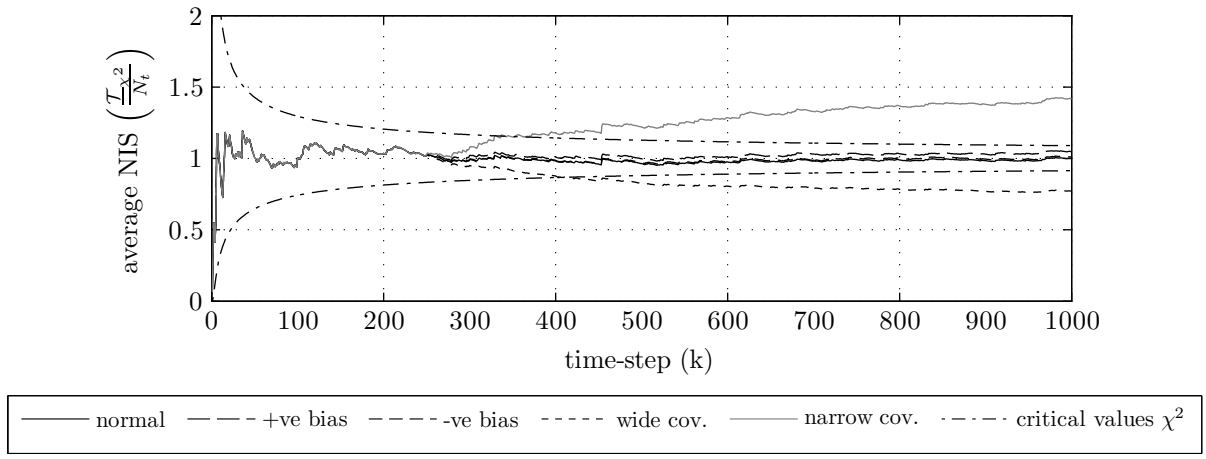

Figure 5.6: NIS or χ^2 test statistics and critical values for unbiased prediction error as well as positive and negative biases, and over and underestimated error covariances that are introduced at time-step 250.

conditions and the presence of bias within the predictions. These concepts are included in the NIS and critical values that are illustrated in Figure 5.6. In Figure 5.6, the biases do not cause the test statistic to reach the critical values of the χ^2 distribution. The NIS test is therefore not as sensitive to bias as the Z test.

Combining the IB and NIS tests results in the ability to determine whether predictions are either biased or include a wide or narrow estimated error covariance. The combined test results and corresponding conditions are summarized in Table 5.2. The NIS is, in general, more capable at detecting changes in covariance as is observed in Figure 5.6 where the biases of Figure 5.5 are not detected by the NIS test but are by the IB test.

5.3.1.3 Innovation whiteness or autocovariance test

The final statistical test is referred to as the IW or autocorrelation test [147]. This test is computationally demanding since it calculates auto-covariance through self-convolution of the prediction error signal for each time-step of the prediction horizon. The IW test

Table 5.2: Condition table for combination IB and NIS tests.

Condition	**IB**	**NIS**
Wide error covariance	n/a	one-tailed (lower)
Narrow error covariance	n/a	one-tailed (upper)
Positive bias	one-tailed (upper)	one-tailed (upper)
Negative bias	one-tailed (lower)	one-tailed (upper)

determines whether or not the prediction errors are serially correlated. The test is performed by calculating the autocorrelation vector of a given sequence of prediction errors for each time-step within the prediction window. The autocorrelation vector is then normalized using the zero-lag autocorrelation. The IW test involves calculating the ratio of the number of entries in the autocorrelation vector that are within the bounds of a specific confidence interval to the total number of total number of entries in the autocorrelation vector, excluding the zero-lag autocorrelation result. The bounds of the interval are, once more, a function of the two-tailed significance level, $\underline{\alpha}$, and corresponding value, $(1 - \underline{\alpha})$, i.e. the level of confidence of the autocorrelation vector entries being within the interval. The computed ratio is then compared against the expected value, $(1 - \underline{\alpha})$. If the two values are similar, the prediction errors are determined to be serially uncorrelated, or white.

The following test variable $\mathcal{T}_{\text{IW}}$ captures the boolean result of an IW test performed

over a range of N_t time-steps prior to the current time-step k as follows,

$$\mathcal{T}_{\mathrm{IW}}[k,i] = \begin{cases} 1 & \text{otherwise} \\ 0 & \text{if } \frac{1}{N_t}\sum_{\tau=0}^{N_t-1}\left(\left|\frac{r(k,\tau,i)}{r(k,0,i)}\right| \leq \frac{z_{\underline{\alpha}}}{\sqrt{N_t}}\right) < (1-\underline{\alpha})^2 \end{cases} \tag{5.14}$$

where

$$r(k,\tau,i) = \frac{1}{N_t}\sum_{j=k-N_t+1}^{k-\tau}\left(\tilde{y}'[j|j-i]\,\tilde{y}[j+\tau|j+\tau-i]\right), \tag{5.15}$$

with the other parameters as defined for both the IB and NIS tests in (5.9) and (5.12) respectively. The IW test is equal to one unless, given a predetermined number of time-steps and maximum lag over which to calculate the autocorrelation, the autocorrelation vector entries either do not peak at a lag equal to zero, i.e. $\tau = 0$, or the remaining entries occur outside the predetermined confidence interval at a rate that is greater than $100\,(1-\underline{\alpha})\%$. The IW test is not investigated any further within the PSDS designs as the convolution of the prediction error sequences is expected to increase the scan time within the predictive logic solver of the PLC implementation. In other words, the computational complexity of the IW test will force the PSDS designs to exceed current industry requirements for time-interval between subsequent trip decisions.

5.3.2 Optimal alarms

Optimal alarms optimize the effective alarm-threshold for a potential threshold-crossing event. Within the context of NPP SDSs, an alarm instance may be considered a TSP

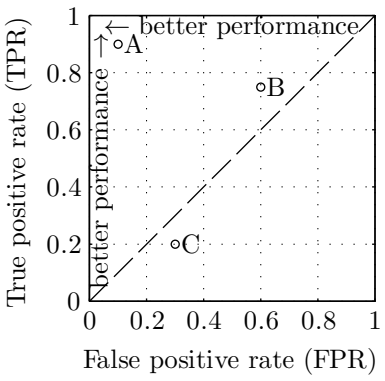

Figure 5.7: Receiver operating characteristic (ROC) space.

and the threshold-crossing event a trip occurrence. The alarms may also be considered as various other messages, indications, and warnings that are presented to NPP operators. The application of optimal alarm theory within NPP SDSs may then be considered as optimal trip. More generally, the use of the term alarm within optimal alarm theory is independent of the severity of the corresponding threshold-crossing event.

Within optimal alarm theory, the TPR and FPR metrics provide a measure by which to compare the performance of competing prediction algorithms. For this, the ROC graph of Figure 5.7 depicts relative trade-offs between benefits or TP outcomes and costs or FP outcomes that correspond to the performance of statistical tests in predicting an impending condition. The ROC space is defined between 0 and 1 on both the horizontal axis of FPR and the vertical axis of TPR. The dashed line that divides the ROC space in upper left and lower right triangular halves represents a fair coin-flip or a random guess between one of two events.

The upper left half of the ROC space, e.g. "A" in Figure 5.7, represents favourable performance as the high values of TPR correspond with high probability of correctly detecting an alternate hypothesis while the low values of FPR correspond with low probability of

incorrectly detecting an alternate hypothesis. In other words, for high values of TPR there is high probability in predicting the alternate hypothesis given a true alternate hypothesis condition. Alternatively, for low values of FPR there is low probability in predicting the alternate hypothesis given the null hypothesis condition.

In contrast to high TPR with low FPR, the upper right corner of the ROC space, e.g. "B" in Figure 5.7, represents high TPR along with high FPR. This combination of rates indicates a rather high probability in predicting the alternate hypothesis given that the null hypothesis condition is present, i.e. high probability of false alarm or missed trip. Moreover, the lower left corner of the ROC space, e.g. "C" in Figure 5.7, represents low TPR along with low FPR, or low probability in predicting the alternate hypothesis given a true alternate hypothesis condition. It is straightforward to refer to false and missed alarms as Type I and Type II errors respectively, since the connotation of false or missed alarm events is counter-intuitive with respect to the SDS application. Moreover, by specifying error type rather than false and missed alarm, the definitions of the mistaken conditions are directly related to the hypotheses.

Hypothesis testing metrics like TPR, FPR, and FNR make it possible to determine, through the use of statistical tests, whether a prediction algorithm is accurate. These hypothesis tests can then be utilized to determine whether those predictions that have reached the TSP are: correct and an abnormal condition occurs, a true trip; are erroneous and an abnormal condition does not occur, a false trip or Type II error, or are; erroneous and an abnormal condition does occur, a missed trip or Type I error. The hypothesis tests are reformulated within optimal alarm theory whereby the hypothesis is referred to as an alarm and the eventual event is referred to as a catastrophe. Within the nuclear industry,

these events correspond respectively to trip and abnormal conditions as follows

$$P_{\text{TPR}} = P\left(\mathbb{T}'|\mathbb{A}_b'\right) \tag{5.16}$$

$$P_{\text{FPR}} = P\left(\mathbb{T}'|\mathbb{A}_b\right) \tag{5.17}$$

$$= P\left(\text{reject}\left(H_0\right)|H_0\right) \tag{5.18}$$

$$P_{\text{FNR}} = P\left(\mathbb{T}|\mathbb{A}_b'\right) \tag{5.19}$$

$$= P\left(\text{reject}'\left(H_0\right)|H_1\right) \tag{5.20}$$

$$P_{\text{TNR}} = P\left(\mathbb{T}|\mathbb{A}_b\right) \tag{5.21}$$

where $\mathbb{T}$ is the trip event, $\mathbb{A}_b$ is the abnormal event with subscript "b" included to distinguish this symbol from the alarm symbol "A" that is common within optimal alarm theory, also $\bullet'$ indicates the logical complement of the boolean variable substituted in place of $\bullet$. A false negative e predictive event is therefore the correct rejection of an abnormal condition whereas the false positive predictive event is the incorrect predictive acceptance of a normal condition.

Optimal alarm theory is utilized in [41] to optimize and alarm region or decision boundary that results in the fewest possible false alarms for a fixed detection probability [141]. This optimization process places a constraint on the FPR while maximizing the NPV. Within [41], optimal alarm theory is then applied to the case of a symmetric two-sided threshold-crossing event. In other words, a parameter that is monitored and alarms on high and low alarms that are symmetric about a mean value. In addition, Martin assumes a steady state solution to the KF. An optimal alarm region is then calculated considering

the probability that a threshold-crossing event will occur within a prediction window. This probability is calculated as the complement of the intersection for the individual probabilities that the threshold-crossing events do not occur within each time-step of the prediction window. The optimal alarm region is then defined as the region within which an impending threshold-crossing event has a probability of occurrence that is greater than some critical value. This optimization considers the intersection of the Gaussian distributions of prediction error within each time-step of the prediction window for which an approximate solution is found. The performance of optimal alarm conditions is then compared against red-line and predictive alarm systems in terms of TPR and FPR as well as the area under the curve within the ROC space. It is determined that the optimal alarm system performs better than either of the other two alarm systems.

The shutdown problem considered within this work is a one-sided threshold-crossing problem. Rather than calculating an optimal alarm region, this work aims to identify optimal predictions and corresponding time-steps within the prediction window as a function of the TPR and FPR. This work differs from that of [41] in that the complexity of the optimal alarm algorithm must adhere to certain constraints regarding computational power. This work also considers the online solution of the KF for time-varying systems rather than the simplified steady state solution of the KF. This work does not calculate the intersection of multivariate Gaussian distributions within an online KF-based prediction algorithm, as the computational complexity of these operations are considered beyond the capabilities of the intended industrial computer platform or safety-PLC.

Alarm systems are accurate if the rate of correctly detected normal conditions against all normal conditions is near to one. In other words, the TPR is approximately equal to

one. If at the same time, the rate of correct abnormal conditions against all hypothesized trips is at a maximum, the alarm system is said to be optimal. This rate is the NPV metric. This work therefore identifies the optimal or most effective of the time-steps within the prediction window. Thus, the optimal alarm adapts the effective prediction horizon at which predictive decisions are made.

In designing the optimal alarm, the FPR is first specified by the significance level, α, of the statistical test where $P_{\text{FPR}} = \alpha$ for a one-tailed test. This optimal range constrains the maximum upper bound regarding the probability of Type I error or missed trip. This constrained range is included in the ROC space of Figure 5.8. The NPV is then calculated for each combination of time-step within the prediction window and hypothesized mean of the prediction error. The optimal value of NPV is identified as a function of the prediction error and error covariance. This optimization is performed as follows

$$P_{\underline{\text{NPV}}}[k] = \max_{i} \left(P_{\text{NPV}}[k+i|k] \right) \tag{5.22}$$

where $P_{\underline{\text{NPV}}}$ is the optimal TPR within the current prediction window. The relationship between NPV and TPR is then established by solving for FN in (5.7) as follows

$$FN = \frac{TN\left(1 - P_{\text{NPV}}\right)}{P_{\text{NPV}}} \tag{5.23}$$

with the result substituted into (5.5) in the following equation.

$$P_{\text{TPR}} = \frac{TP}{TP + FN} = \frac{TP}{TP + \frac{TN(1-P_{\text{NPV}})}{P_{\text{NPV}}}} \tag{5.24}$$

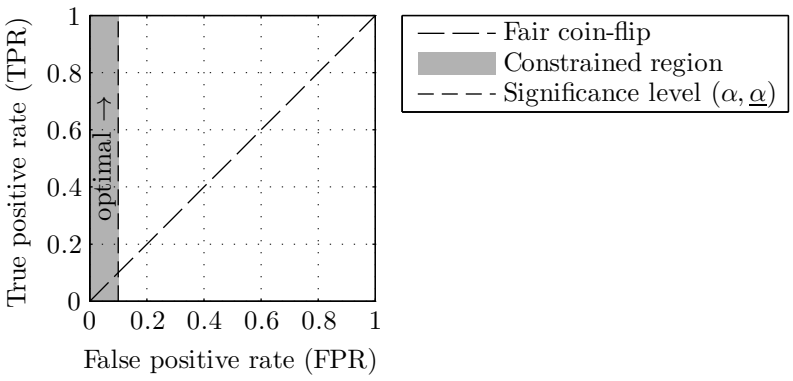

Figure 5.8: Constrained region and optimal behaviour of the optimal alarm within the receiver operating characteristic (ROC) space.

Since the aim of the optimal alarm is to maximize P_{NPV}, the following limit demonstrates the effect of optimization on P_{TPR}.

$$\lim_{P_{\text{NPV}} \to 1} P_{\text{TPR}} = \frac{TP}{TP + 0} = 1 \tag{5.25}$$

Thus, the optimal alarm not only maximizes P_{NPV} but also P_{TPR}. By maximizing the probability of an abnormal condition given a trip decision, the predictive decision-making algorithm is forced to the upper left corner of the ROC space as is illustrated in Figure 5.8.

In contrast to FPR or missed trip rate, the design of NPP SDSs also considers the false trip rate. False trip occurrences are Type II errors that are captured by the FNR metric within hypothesis testing. Optimal alarm theory specifies a maximum FPR for Type I errors. There is no such maximum imposed on the FNR. The relationship between NPV and FNR can be established, however, by substituting FN of (5.23) into the following

equation.

$$P_{\text{FNR}} = \frac{FN}{FN+TP} = \frac{\frac{TN(1-P_{\text{NPV}})}{P_{\text{NPV}}}}{\frac{TN(1-P_{\text{NPV}})}{P_{\text{NPV}}}+TP} = \frac{TN\,(1-P_{\text{NPV}})}{TN\,(1-P_{\text{NPV}})+P_{\text{NPV}}TP} \tag{5.26}$$

As for the P_{TPR}, the optimal or maximal P_{NPV} effects P_{FNR} by the following limit.

$$\lim_{P_{\text{NPV}}\to 1} P_{\text{FNR}} = \frac{0}{0+P_{\text{NPV}}TP} = 0 \tag{5.27}$$

Thus, the optimal alarm not only maximizes P_{NPV} and P_{TPR}, but also minimizes Type II errors and the FNR, P_{FNR}. The remaining tasks as well as details regarding optimal prediction shutdown are left to the optimal-PSDS design of Section 5.3.3.

5.3.3 Optimal-PSDS: optimal predictive shutdown system

Hypothesis testing provides a means to consider the quality of a specific prediction algorithm and to optimally adapt the predictive decision-making mechanism within an advanced combined point- and interval-PSDS design. The structure of one such optimal-PSDS design is included in Figure 5.9. This design includes the capability to make decisions using either point- or interval-predictions, and to select an effective prediction horizon and prediction bias in an optimal manner. In this optimal design, the logic of the KF and CI block are as described for the interval-PSDS design of Section 5.2.2. The statistical and hypothesis testing block and optimal alarm functions are added to the design. The structure of the optimal-PSDS design is again a modular evolution of conventional SDS which does not require additional sensors or hardware modifications. Moreover, the conventional

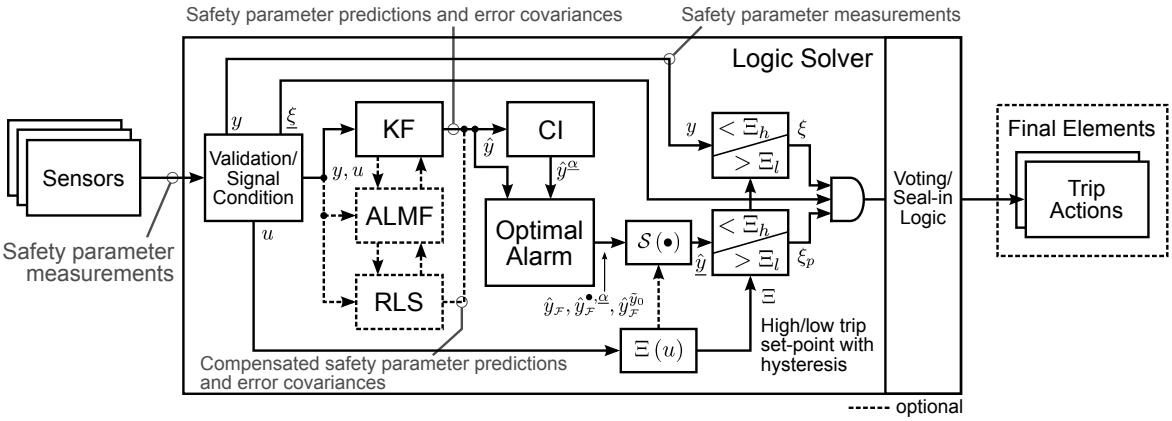

Figure 5.9: KF/RLS-based optimal-predictive shutdown system (optimal-PSDS) in the context of safety instrumented systems (SISs) with the option for activating RLS or ALMF algorithms.

trip logic remains active within the optimal-PSDS design and is implemented as described in Section 5.1. The addition of the optimal-prediction algorithm is, again, only able to improve the response time of the conventional SDS.

For interval prediction with statistical testing, the measurement predictions and error covariances are combined within the CI block of Figure 5.9 for a specific one-tailed significance level α and corresponding two-tailed significance level $\underline{\alpha}$. This results in a set of confidence-based prediction values, $\hat{y}^{\underline{\alpha}} \triangleq \left\{\hat{y}^{l,\underline{\alpha}}, \hat{y}^{u,\underline{\alpha}}\right\}$, that bound the measurement predictions within each time-step of the prediction window. The predictions are then processed by one or more of the statistical tests described in Section 5.3.1. When more than one statistical test is performed, a logical function, $\mathcal{F}$, for combining the multiple tests is defined as is described in the experimental setup of Section 6.6. The statistical tests are performed using the same significance level, α or $\underline{\alpha}$, that corresponds with the bounds of the confidence interval in Section 3.4. The result of the statistical testing procedure is a subset, $\hat{y}_{\mathcal{T}}^{\underline{\alpha}}$, of the confidence interval bounds including only the values from those time-steps within the prediction window that are within the constrained region of the ROC space. The subset of

verified bounds is defined as follows for interval-predictions

$$\hat{y}_{\mathcal{F}}^{\bullet,\underline{\alpha}}[k+i] = \begin{cases} \hat{y}^{\bullet,\underline{\alpha}}[k+i|k] & \text{if } \mathcal{F}(\mathcal{T}_\bullet) \\ y[k] & \text{otherwise} \end{cases}, \forall i = 1, \ldots, N_p \tag{5.28}$$

where $\hat{y}_{\mathcal{T}}^{\bullet,\underline{\alpha}}$ is a subset over the prediction window of either point-predictions or upper or lower bounds depending on the configuration of the optimal-PSDS. The $\bullet, \underline{\alpha}$ notation is included for the upper and lower bound to be indicated whereas $\mathcal{T}_\bullet$ indicates the chosen test or set of tests. For point-predictions, the above equation is simplified to the following form.

$$\hat{y}_{\mathcal{F}}[k+i] = \begin{cases} \hat{y}[k+i|k] & \text{if } \mathcal{F}(\mathcal{T}_\bullet) \\ y[k] & \text{otherwise} \end{cases}, \forall i = 1, \ldots, N_p \tag{5.29}$$

The optimal alarm then considers the identified subset of prediction values. The supremum of the entire set of prediction values is the prediction within the constrained subset that has the minimum value inside bound of confidence interval. Here, inside refers to the bound being on the side of the normal operation with respect to the point-prediction, e.g. the upper value for a low TSP. This is essentially the same functionality as the $\mathcal{S}$ function provides within the interval-PSDS design. Thus, a maximum or minimum of the subset of bound values is selected to be compared against either a high or a low TSP respectively using the output of the $\mathcal{S}$ function block as in (5.4).

It is not only possible to use the optimal alarm to adapt the effective prediction horizon but also to adapt a bias in the prediction that is to be compared against the alarm-threshold

or TSP. For example, the statistical tests of Section 5.3.1 can be modified to consider a mean prediction error, $\tilde{y}_b$, that is equal to some value other than zero. For example, a mean prediction error equal to one standard deviation in the positive and negative directions of the measurement domain. The statistical tests are then able to provide boolean decisions that select a subset of the time-steps within the prediction window that are satisfied for a specific mean prediction error. The subset of the prediction window for which the prediction time-steps and assumed mean prediction errors or biases are found to be valid is then calculated as $\hat{y}_{\mathcal{T}}^{\tilde{y}_b}[k+i]$ in the form of (5.29). Moreover, the maximum NPV and therefore TPR can be calculated for each time-step of the prediction window as well as the assumed mean prediction biases. These concepts can even be extended to consider multiple covariances and distributions other than the Gaussian distribution although these extensions are beyond the scope of this work.

The optimal-PSDS design is the final of the PSDS designs proposed within this dissertation. It is the successful culmination of the methodology-related objectives outlined in Section 1.2. By incorporating hypothesis testing within the PSDS design, the predictive decision-making mechanism gains an awareness as to the quality of the predictions that are being made. The decision-making mechanism is also able to monitor the occurrence of false positive and false negative decisions, i.e. Type I and Type II errors in the predictions. Finally, hypothesis testing provides the ability to quantify the probability that the prediction algorithm is able to either correctly or incorrectly predict an impending condition whether the shutdown procedure is activated, or otherwise.

5.4 Summary

Three enhanced PSDS designs are developed within this chapter. In addition, a conventional SDS design is also presented. Each of the PSDS design includes a conventional SDS mechanism as a backup to the predictive decision-making algorithm. The following is a summary of each individual PSDS design.

The first design, or point-PSDS, calculates KF-based point-predictions with the option of utilizing the RLS disturbance estimation algorithm of Chapter 4 and the ALMF noise covariance estimation algorithm of Chapter 3. The point-PSDS design compares each point-prediction within the prediction window against the alarm-threshold or TSP in order to make a predictive decision regarding an impending condition.

The second design is the interval-PSDS which calculates KF-based interval-predictions. Within this design, the inner bound of the confidence interval for a specific significance level is compared against the TSP for each time-step of the prediction window. The inner bound is the bound that is on the normal operating side of a point-prediction, e.g. an upper bound for a low level TSP. These inner bounds correspond to confidence levels that are greater than 50% in the future measurement. The interval-PSDS may also make use of the RLS and ALMF algorithms, as is the case for the point-PSDS. In fact, it is recommended that the ALMF algorithm be implemented for the state noise covariance and levels of confidence to have improved accuracy. This recommendation is due to the confidence interval of the predictions being a direct function of the measurement error covariance.

The third design is the optimal-PSDS that utilizes either the point- and interval-

predictions. The optimal alarm constrains the probability of a Type I error or missed trip occurrence to the rate of significance level α. The prediction window is therefore adapted to include only those time-steps or values that adhere to the aforementioned constraint. The optimal alarm then selects the prediction that has the maximum probability for correctly identifying normal operating conditions. The point- or interval-prediction of the selected time-step within the prediction horizon is compared against the TSP. The optimal alarm process, including hypothesis testing, are developed within this chapter. These functionalities enable the predictive algorithm to consider the quality of previously calculated predictions.

Chapter 6

Experimental Setup

This chapter describes and distinguishes between the simulation and experimental platforms that have been constructed for evaluation of the PSDS designs proposed in Chapter 5. For each of the two platforms, the conventional and predictive SDSs monitor and predict the dynamic response of the water level within the steam generator subsystem of an NPP. The SDSs also make trip decisions regarding abnormal conditions that are related to the steam generator system being protected. This subsystem is one of a collection of subsystems that transmit safety parameter measurements to the NPP SDSs as reviewed in Section 2.2.

The purpose of a steam generator within an NPP is to transfer thermal energy from the reactor core to the turbines of an electrical generator. The steam generator also accommodates the conversion of thermal energy into kinetic energy while maintaining physical separation between the coolants of the primary and secondary heat transport loops, i.e. the reactor and steam generator coolants. In order to accomplish these two tasks in a safe

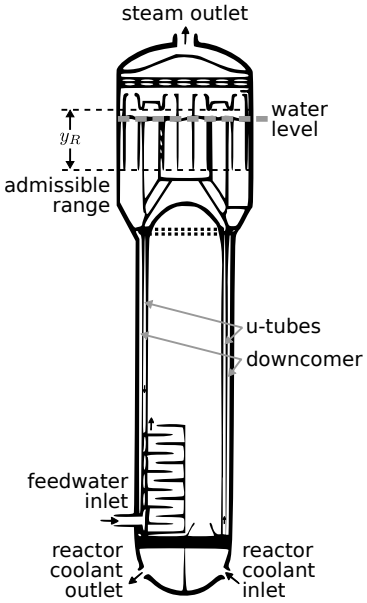

Figure 6.1: U-tube steam generator with admissible range, y_R.

manner, the steam generator water level is regulated within a narrow range of the steam generator tank height between low and high TSPs. This narrow range of operation that is considered to be valid is known as the admissible range, y_R. The admissible range is therefore the range of operation within which the steam generator water level is expected to remain under normal operating conditions. The structure of a generic u-tube steam generator is provided in Figure 6.1 including primary and secondary side inlets and outlets. This steam generator form is referred to as a u-tube generator due to the heat exchanger tubes being formed in an inverted "U" shape, as labelled in Figure 6.1.

Of the two TSPs, the high steam general level TSP prevents excess steam moisture as this may cause damage to the turbine blades. Thus, water level measurements that meet or exceed the high TSP cause the SDS to trigger a turbine trip. In contrast, water level measurements that are equal to or lower than the low TSP cause the SDS to trigger a reactor trip. This low TSP prevents the NPP from operating with reduced capability

for removing heat from the reactor core. This low TSP also prevents the heat exchanger u-tubes from becoming uncovered as this hazardous condition is likely to cause damage to the heat exchanging tubes. In order to prevent these potentially hazardous conditions, the steam generator level high (SGLH) and low (SGLL) safety parameters are included in the SDSs of various NPP designs including SGLL within SDS1 of the CANDU reactor design [162].

Although the SGLL trip parameter is of interest within this study, it is more often the case that the neutronic safety parameters are used to determine SDS response time specifications [163]. That said, there are three primary justifications for applying the proposed predictive shutdown methods to the SGLL condition rather than those that correspond with the neutronic parameters. The first justification is the complex inverse response characteristic that is exhibited by the steam generator water level dynamic. In other words, the steam generator water level has a dynamic response that is non-intuitive and potentially difficult to forecast without the use of a mathematical model for reference. The second justification is the vast body of literature regarding control and modelling of steam generator water level dynamics. This body of literature includes the application of predictive algorithms to perform model-based prediction and the construction of simulation and experimental test facilities or platforms. The final justification is the ability to implement the PSDS designs for the SGLL parameter within an actual safety PLC and physical experimental platform. The result of this implementation is the evaluation of a modern yet computationally constrained PLC-based PSDS that monitors a real-world physical system being protected. Thus, by considering the SGLL safety parameter, both the simulated as well as physical or real-world performance of the PSDS algorithms are analyzed.

Another reason for not studying the neutronic parameters is that those parameters would require the construction of a much more elaborate experimental setup and physical experimentation would not have been possible. In addition, the nonlinear dynamics of the neutronic reactions within the reactor core are expected to be beyond the capabilities of the standard KF, and may require the use of the EKF or UKF as well as a more powerful computational platform. It is expected that these computational requirements may be satisfied through the use of an FPGA or a graphical processing unit. These more powerful platforms are, however, beyond the scope of this study.

The simulation and experimental platforms are illustrated in Figure 6.2a) and Figure 6.2b) respectively. The simulation platform includes discrete-time MATLAB implementations of: a magnitude and frequency scaled model of the steam generator water level dynamic known as the Irving model; a three element proportional integral (PI) controller for steam generator water level regulation; and conventional SDS as well as the proposed PSDS designs. In contrast, the experimental platform replaces the simulated components with a physical system as well as industry-standard process and safety controllers. The physical system is known as the plate level system (PLS) with level dynamics compensated to match a scaled form of the Irving steam generator model. For experimentation, the three element PI closed-loop water level controller is implemented within a Siemens PCS-7 DCS and the conventional SDS and PSDS designs are implemented within a Tricon v9 triple modular redundant safety PLC. Pictures of each of the PLS, the PLC, and the DCS are included in Figure 6.2b). Each of these components is described in more detail in the subsequent sections of this chapter.

The PLS, the water level controller, and the safety PLC communicate through hard-

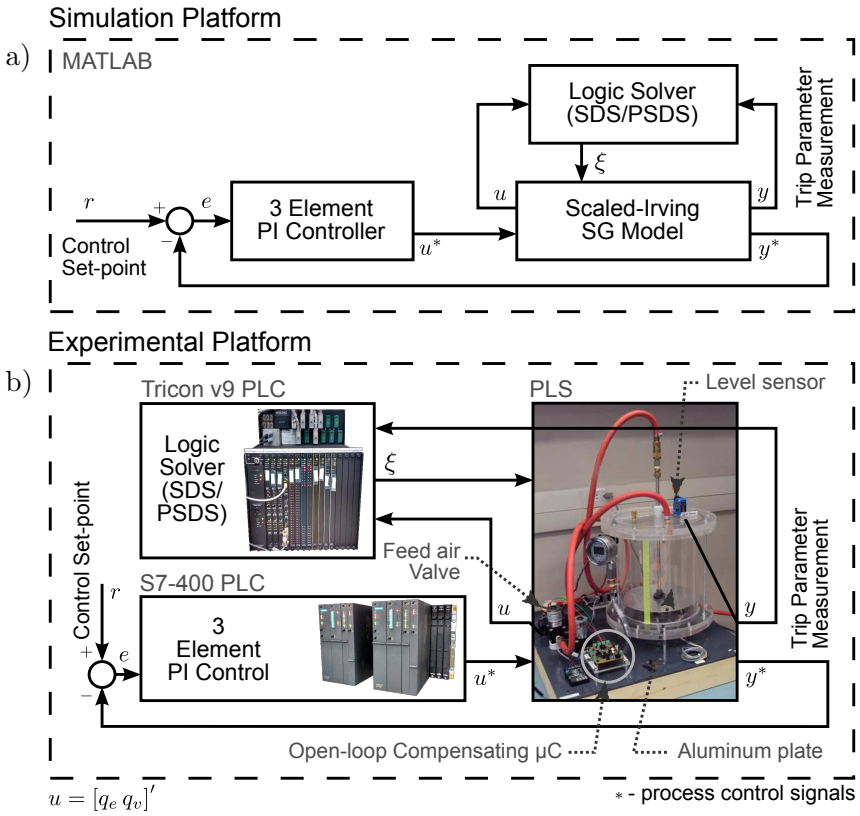

Figure 6.2: The a) simulation and b) experimental platforms.

wired individually shielded twisted pair cables using industry standard $4-20$mA signals. These signals are annotated as u and y in the experimental platform of Figure 6.2. Within the nuclear power generating industry, safety parameter sensors and signals are physically independent of those of the process control systems. This is especially true for the signals that provide the safety parameters to any of the SDSs. Thus, the two sets of feedwater flow-rate and level sensors are assumed to be wired separately. This separation is included in Figure 6.2 with the process control set of signals indicated by an asterisk, e.g. system input u^* and system output or measurement, y^*. In reality, the PLS of the experimental platform has only a single laser level sensor that measures the distance from the top of the tank to the floating plate. It is therefore assumed within this work that the safety and

process measurements, y and y^*, are transmitted by the same level sensor. To alleviate this assumption, this study does consider experimental cases where the safety system input u deviates from the process control input u^*. These case are referred to as having an unmeasured initiating event in Chapter 7.

Upon shutdown, the trip signal, ξ, that is output by the SDS or PSDS has no effect on steam generator water level, whether simulated or experimental. This assumption does not hinder the ultimate objective of the trip procedure which is to activate, in a timely manner, the insertion or injection of negative reactivity via the shutdown mechanisms, e.g. shut-off rods or neutron poison, into the reactor core. In other words, all events that occur after the actuation of the shutdown procedure are irrelevant to the timing analysis performed within this study. This work does not, therefore, study of the impact that reductions in time-to-trip have on specific safety margins. The time response for activating trip, or the shutdown procedure, is the primary characteristic of interest within this study. Although the steam generator water level does undergo shutdown-related manoeuvres, these manoeuvres do not effect the insertion or injection of negative reactivity into the reactor core.

Within the simulation platform, the trip signal is captured as a boolean variable for time-to-trip analysis. The experimental platform, however, includes two indicator lamps, one for conventional shutdown, and one for predictive shutdown. These lamps are individually de-energized by the Tricon v9 safety PLC when a trip condition has been detected within the either the conventional or predictive SDS. The trip signals generated by the PLC are also acquired as a 10-bit integer with values that represent which of the four types of trip are active: conventional, point-predictive, interval-predictive, or optimal-predictive.

The remainder of this chapter presents details regarding the design and implementation

of each component within the simulation and experimental platforms. The chapter begins with a description of the physical experimental plant or PLS in Section 6.1. Section 6.2 then introduces the steam generator subsystem that is the system being protected studied throughout the remainder of this dissertation work. Section 6.2 also introduces the open-loop dynamic response of the steam generator water level. Section 6.3 discusses closed-loop control of the steam generator water level while the scenarios or operating modes under which the shutdown systems are tested are discussed in Section 6.4. The initiating events that cause abnormal conditions or the water level to drop to the SGLL TSP within the steam generator of the simulation and experimental platforms are then discussed in Section 6.5 respectively. The chapter then concludes by presenting the considerations for implementing the SDS and PSDS designs. This final section also discusses expectations regarding the performance of the SDS and proposed PSDSs within the simulations and experiments of Chapter 7.

6.1 Physical System

The original purpose for constructing the PLS was to allow for the testing of various control system algorithms and industrial communication protocols using modern DCS and PLC platforms. Mechanically, the PLS consists of a cylindrical tank containing an aluminum plate that is manoeuvred vertically along a central rod by changes in pressure within the volume of air below the plate. Operationally, the plate level is controlled by manipulating a solenoid valve which affects the feed air flow-rate into the bottom of the tank. Further, a laser displacement sensor measures the level of the plate for feedback into a level control

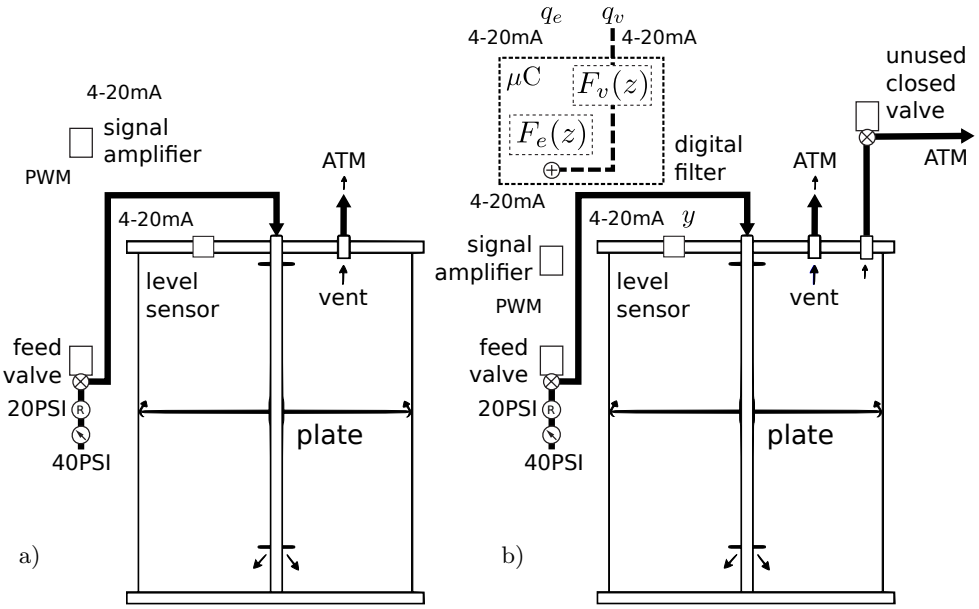

Figure 6.3: Functional diagram of the physical plate level system (PLS) in the a) nominal and b) compensated, or modified, form.

system.

A picture of the PLS is included in the experimental setup of Figure 6.2. In addition, a more detailed functional diagram of the original or nominal PLS provided in Figure 6.3a). The PLS of Figure 6.3a) includes a solenoid valve driver or signal amplifier that converts the $4-20$mA signals to pulse width modulated (PWM) signals that are appropriate for manipulating the solenoid valve. Figure 6.3a) also includes the pressures in pounds per square inch (PSI) units at the supply and the regulator as well as the atmospheric pressure (ATM) at the outer side of the vent orifice.

The dynamic response of the nominal PLS is that of a single integrator requiring an offset input for steady state operation. In other words, the plate will steadily rise or fall given the feed air flow-rate input deviates from a particular value at which the plate floats. The PLS can therefore be thought of as a water tank with a leak of constant flow-rate. For the purpose of this research, the single integrator dynamic response of the plate level is

modified, or compensated, to mimic an industry-standard model of steam generator water level response known as the Irving steam generator model. This matching of dynamic water level response is achieved through the design and implementation of an open-loop compensator within a Microchip PIC micro-controller (μC). The μC is installed in-line with the control signal to the solenoid valve driver of the feed air valve.

The open-loop compensator introduces a second manipulated variable and imposes a more complex non-minimum phase, or inverse response, characteristic within the level dynamics of the PLS. The feedwater and steam flow-rate signals are combined within the compensating μC after being output from the two digital filters, F_e and F_v respectively. These filters produce a feed air flow-rate that forces the plate-level to match the level dynamics of a scaled form of Irving steam generator model by manipulating the single feed air flow-rate valve. Aside from compensating for the steam generator level dynamics, the μC is also utilized to linearize the response of the nominal physical system. More precisely, the dynamic response of the plate level has a maximum rate of falling, or decrease, that is equivalent within the Irving model to a loss in water level of 443mm/s. Thus, the rate of rise, or increase, is constrained not to exceed the falling rate by restricting the operating range of feed-air valve.

Although the compensator is open-loop, it is installed within a closed-loop control system and is therefore able to be calibrated. The calibration sequence is performed during closed-loop control of the nominal PLS at steady state for a level set-point of 50%. During calibration a "float" offset variable is set equal to an average of over 200 samples of the feedwater flow-rate control signal. This calibration allows for a more accurate dynamic response with respect to the target steam generator model. These calibrations are per-

formed periodically to mitigate changes in the dynamic response of the nominal plant that are caused by variations in the mechanics or temperature of the solenoid valve.

A picture of the modified PLS is included within the experimental platform of Figure 6.2. In addition, a detailed functional diagram of the modified PLS including the two digital filters of the open-loop compensating μC is provided in Figure 6.3b). In Figure 6.2, input variable u includes both the feedwater flow-rate, q_e, and steam flow-rate, q_v, manipulated variables. The feedwater flow-rate is the output of the closed-loop water level control system whereas the steam flow-rate is a function of the current operating power level within the NPP. Figure 6.3b) illustrates these two signals separately. The feedwater flow-rate, steam flow-rate, and plate-level signals form the basic requirement for steam generator water level control. These signals also enable KF-based prediction of the open-loop steam generator system. The additional valve that exits the top of the tank remains closed within this work.

6.2 The Scaled-Irving Model

The dynamic response of the steam generator water level can be characterized by the Irving steam generator model as introduced in [164]. The Irving model is a fourth-order LPV model which exhibits a complex inverse response characteristic known as swell and shrink [28, 165]. The dynamic response of the plate level within the PLS is compensated to match a scaled form of the Irving model. This scaling is performed in order to accommodate the size and dynamic response of the nominal PLS. The scaled-Irving model is defined in the following frequency domain LPV transfer function that includes the standard Irving

Table 6.1: Irving model parameters, steam flow-rates as well as control intervals, and controller gains at specific power levels.

Θ (%)	**5**	**15**	**30**	**50**	**100**
q_v(kg/s)	57.4	180.8	381.7	660	1435
G_1	0.058				
G_2	9.63	4.46	1.83	1.05	0.47
G_3	0.181	0.226	0.310	0.215	0.105
τ_1	41.9	26.3	43.4	34.8	28.6
τ_2	48.4	21.5	4.5	3.6	3.4
Υ	119.6	60.5	17.7	14.2	11.7

model modified by two scaling gains

$$Y(s) = K_m \left(\frac{G_1}{s} - \frac{G_2(\Theta)}{\tau_2(\Theta)\, s + K_f} \right) (Q_e(s) - Q_v(s)) + \frac{K_m G_3(\Theta)\, s}{s^2 + 2K_f \tau_1^{-1}(\Theta)\, s + K_f^2 \left(\tau_1^{-2}(\Theta) + 4\pi^2 \Upsilon^{-2}(\Theta) \right)} \underline{Q}_e(s) \tag{6.1}$$

where s is the complex Laplace variable and frequency parameter, $Y(s)$ is the water level with units mm, $\underline{Q}_e(s)$ is the feedwater flow-rate with units kg/s, $Q_v(s)$ is the steam flow-rate with units kg/s, K_f is a frequency scaling gain, K_m is a magnitude scaling gain, and the remaining parameters are given in Table 6.1.

The Irving model is frequency scaled by a factor of $K_f = 10$ to better match the steady state rate of change of the water level to dynamics of the plate level. This factor of frequency scaling results in the ability to investigate the performance of the prediction algorithms for a system with faster dynamics than those of the relatively slow steam generator water level response. In addition to frequency scaling, the magnitude of the Irving model is scaled by

a factor of $K_m = \frac{y_{R,\mathrm{PLS}}}{y_R} = 0.0525K_f$ as a function of the admissible range of the water level within the steam generator, $y_R = 4000$mm, and that of the PLS, $y_{R,\mathrm{PLS}} = 210$mm, as well as the frequency scaling gain of the target steam generator, $K_f = 10$. The frequency scaling gain is included in the calculation of the magnitude gain due to the frequency scaling gain causing the magnitude of the output to be modified by a multiplicative factor of $1/K_f$. The admissible range of the steam generator water level is therefore assumed to be equivalent to the range of plate level range within the PLS. Thus, the maximum 210mm of water level height within the PLS is assigned the maximum range of operation within the steam generator, i.e. 4000mm while 0mm is chosen the bottom of the admissible range for both.

The original Irving model parameters are provided in Table 6.1 as given in [164]. These parameters are scale independent due to the inclusion of the magnitude and frequency scaling gains, K_f and K_m, in (6.1). The model parameters are linearly interpolated between reactor power levels, Θ, and steam flow-rates, q_v, in real-time within both the simulation and experimental platforms. For experimentation, interpolation is performed within the compensating μC with the two open-loop compensator filters of Figure 6.3 calculated as $F_e(s) = Y(s) H_{\mathrm{PLS}}(s) / \underline{Q}_e(s)$ and $F_v(s) = Y(s) H_{\mathrm{PLS}}(s) / Q_v(s)$, discretized with a sampling time of 10ms, inverted, and subtracted from the forcing feedwater or steam flow-rate input to ensure the stability of the modified PLS. Here, H_{PLS} is the continuous-time transfer function form of the nominal PLS. It is also possible to discretize the continuous-time Irving steam generator and nominal PLS models and then perform the above calculations for the digital filter directly. For more on the analytical compensation technique that was performed to design the open-loop compensating digital filter, refer to [166].

The open-loop step response of the Irving model is included in Figure 6.4a) for a 10kg/s

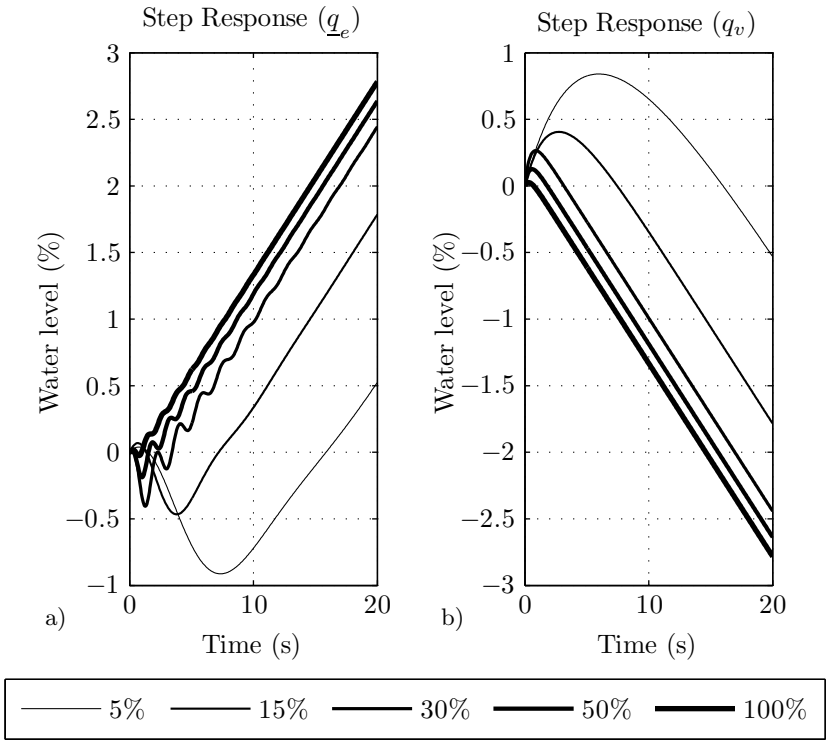

Figure 6.4: Open-loop response of the scaled-Irving model to a 10kg/s step increase in a) feedwater flow-rate, $\underline{q}_e$, and b) steam flow-rate, q_v.

or 0.5% step increase in feedwater flow-rate and also in Figure 6.4b) for a 10kg/s or roughly 0.7% step increase in steam flow-rate at each of the five operating points, power levels, or steam flow-rates, q_v, that are included in Table 6.1.

The inverse response characteristic occurs for both an increase and a decrease in either feedwater or steam flow. For changes in feedwater flow, the characteristic is the result of the difference in temperature between the feedwater and the inventory water. For changes in steam flow, the characteristic is the result of the difference in pressure between the steam and the bubbles within the inventory water. A change in either flow-rate causes bubbles to expand and contract, hence swell and shrink. In addition, as in Figure 6.4a), the step response due to a change in feedwater flow includes an oscillatory term. This oscillation is the result of feedwater and condensing water mixing in the downcomer. The non-intuitive

inverse response characteristic is the dynamic that complicates the prediction problem and is one of the justifications for studying the SGLL safety parameter within the SDS.

Although the PLS is made to mimic the above scaled-Irving model through open-loop compensation, the simulation platforms utilizes a discrete-time state-space form of the scaled-Irving model. The scaled-Irving steam generator model of (6.1) is therefore converted, as in [167], to the following continuous-time state-space representation

$$\dot{x}(t) = K_m A(\Theta) x(t) + B(\Theta) \begin{bmatrix} q_v(t) \\ q_e(t) \end{bmatrix} \tag{6.2}$$

$$y(t) = \begin{bmatrix} 1 & 1 & 1 & 0 & 0 \end{bmatrix} x(t) \tag{6.3}$$

where

$$A(\Theta) = \begin{bmatrix} 0 & 0 & 0 & 0 & K_m G_1 \\ 0 & \frac{-K_f}{\tau_2}(\Theta) & 0 & 0 & \frac{-K_m G_2(\Theta)}{\tau_2(\Theta)} \\ 0 & 0 & \frac{-2K_f}{\tau_1}(\Theta) & K_f & K_m G_3(\Theta) \\ 0 & 0 & -\underline{\Upsilon}(\Theta) & 0 & 0 \\ 0 & 0 & 0 & 0 & -K_m \end{bmatrix}, B(\Theta) = \begin{bmatrix} -K_m G_1 & 0 \\ \frac{K_m G_2(\Theta)}{\tau_2(\Theta)} & 0 \\ 0 & 0 \\ 0 & 0 \\ 0 & K_m \end{bmatrix} \tag{6.4}$$

and $\underline{\Upsilon}(\Theta) = \left(\tau_1^{-2} + 4\pi^2 \Upsilon^{-2}(\Theta)\right) K_f$, $x_5(t) = \underline{q}_e(t)$, $\underline{Q}_e(s) = \frac{Q_e(s)}{s+1}$ is a filter acting on the feedwater valve, $y(t)$ is the steam generator water level, $q_v(t)$ is the steam flow-rate, and $q_e(t)$ is the feedwater flow-rate control signal.

The continuous-time model is then discretized by bi-linear transformation to the discrete-time KF-compatible state-space form of (3.9) and (3.10) where the system matrices A, B, C

and D are functions of Θ rather than continuous-time t, or discrete-time k, i.e. an LPV system. The initial condition for the state vector is assigned as $x\left[0\right] = \left[0, 0, 0, 0, 0\right]'$. The effects of these initial conditions on the simulation results are eliminated, however, by allowing the system to settle to an initial steady state operating point prior to experimentation. Thus, any initial transient behaviour within the response of the scaled-Irving model occurs in the time-steps prior to the plotted simulation and experimental data sets.

6.3 Closed-loop Control

This section provides a design overview for a gain scheduled three-element PI controller to control steam generator water level [28, 165, 167, 168]. The controller is implemented within both MATLAB as well as a DCS. The controller has three inputs: water level, y, feedwater flow-rate, q_e, and steam flow-rate, q_v. The relationship between these variables is represented in the frequency domain by following transfer function

$$\begin{aligned} Q_e\left(s\right) = & \frac{K_C\left(\Theta\right)\left(K_I\left(\Theta\right)s+1\right)}{2K_I\left(\Theta\right)s+1} \\ & \cdot\left(Q_v\left(s\right)+\frac{K_{CO}\left(\Theta\right)\left(K_{IO}\left(\Theta\right)s+1\right)}{2K_{IO}\left(\Theta\right)s+1}\left(\mathcal{R}\left(s\right)-Y\left(s\right)\right)\right) \end{aligned} \tag{6.5}$$

where $\mathcal{R}\left(s\right)$ is the control set-point, and the remaining parameters are given in Table 6.2.

The continuous-time controller in (6.5) is discretized with a sampling time of $T_s =$ 100ms to satisfy the two control intervals listed as T_{CI} in Table 6.2. The controller is then tuned to be asymptotically stable using the gains listed in Table 6.1. In addition, the feedwater flow-rate is limited in magnitude from 0 to 2000 kg/s and the steam flow-rate

Table 6.2: Control intervals, and controller gains for the discretized controller within power level operating ranges.

Θ (%)	**5**	**15**	**30**	**50**	**100**
q_v(kg/s)	57.4	180.8	381.7	660	1435
q_v^*(kg/s)	119.1	281.25	520.85	1047.5	1435
T_{CI} (s)	0.5		0.2		
K_I	$3.5\tau_2$	τ_2			
K_C	5.0	1.0			
K_{CO}	0.100	0.315	0.266	0.460	1.000
K_{IO}	$0.2K_I$	$5.0K_I$			

from 0 to 1435kg/s within both the simulation and experimental platform. Inputs q_e and q_v are both included in the deterministic input u^* of Figure 6.2. The discretized control logic is programmed using structured text within a function block of the Siemens PCS-7 DCS. The controller design also includes an additional integral gain at the level error input in order to reduce steady state error at low power levels due to the plate level system having a relatively large dead band surrounding the floating point. For consistency, this integral gain is also implemented within the simulation platform.

During normal operation, the control intervals and the controller gains are selected as a function of mid-point steam flow-rate q_v^*. For example, a gain of $K_{CO} = 0.1$ is active in the steam flow-rate range 0 to 119kg/s. It is assumed that measurement and process noise level are constant over all power levels, e.g. R_x and R_y do not change with q_v^*. If this assumption does not hold, the various prediction algorithms of Chapter 3 can be extended to consider different noise levels for power level, q_v^*, by substituting the assumed values into the covariance matrix calculations.

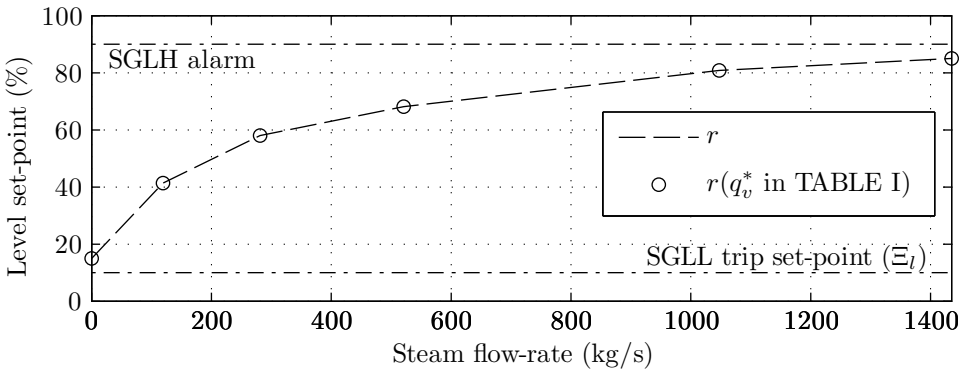

Figure 6.5: Swell-based set-point function, steam generator level low (SGLL) trip set-point and level high (SGLH) alarm threshold.

The reference level of the steam generator, denoted r, is a function of the mid-point steam flow-rates given as q_v^* in Table 6.2. This set-point function is known as the swell-based set-point function and is plotted in Figure 6.5 [165]. The use of a function rather than a constant benefits heat transfer from the primary to secondary side of the NPP and reduces the potential for reaching alarm levels and TSPs that are also included in Figure 6.5, e.g. the SGLL TSP denoted as Ξ_l.

6.4 Operating Modes

The steam generator operates within one of two manoeuvres, known as power transients, at the time of injecting an initiating event for an eventual shutdown. The two manoeuvres provide a realistic operating scenario for the study of SDS performance. The following power transients are based on those studied in [28]:

a) step-wise power increase (SWPI) (5 to 40%): a series of step-increases in power demand from 5% to 40% at steps of 5% power incrementing every 150s once above 15% and 250s otherwise; and

b) power ramp-down (PRD) (30 to 5%): a ramp-down in power from 30% to 5% at an approximate rate of 5% per minute.

The above percentages are with respect to full power where full power refers to both the operating point of the nuclear reactor core and the operating point for steam flow to the high pressure turbine otherwise referred to as the steam flow-rate. For the experimental platform, the operating modes are programmed within a reference function block in the Siemens controller using structured text. The scenarios are activated manually after the PLS settles to steady state given the initial power level and water level set-point, e.g. 5% for SWPI and 30% for PRD.

The closed-loop step responses of the two power transients are included in Figure 6.6 where y_{sim} is the simulated steam generator water level, y_{exp} is the experimental steam generator water level, r is the reference water level, and Ξ_l is the SGLL TSP. The power transients are initiated 10s into each scenario. Moreover, time-step zero is the time-step at which the system has been determined to have achieved a stable steady state condition at the initial power level. All data previous to time-step zero is omitted from the plotted results and analyses. The closed-loop responses of Figure 6.6 demonstrate good control performance and relatively tight control when compared with the MPC results of [28].

In addition to the above two power transients, this work also investigates the performance of the predictive shutdown routines under the conditions of an unanticipated change in the water level set-point. This transient is referred to as the set-point disturbance (SPD) and is made to occur at an initial power level of 30%. The set-point steps to one of two values. The nontrip-SPD scenario causes the steam generator water level to nearly reach

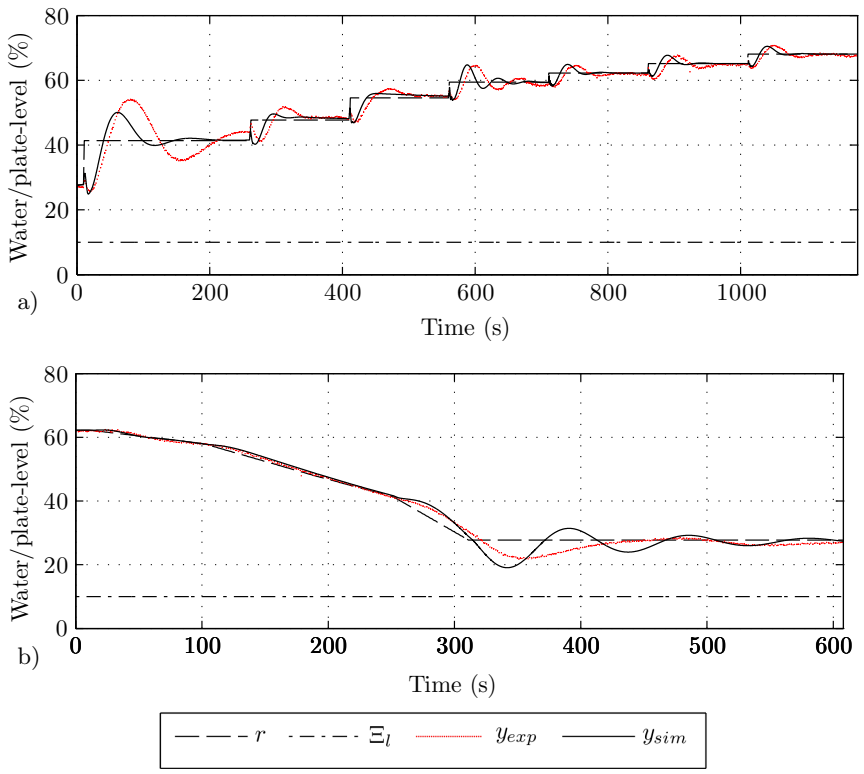

Figure 6.6: Steam generator water level responses to power transients a) step-wise power increase (SWPI) from 5% to 40%, and b) power ramp down (PRD) from 30% to 5% initiated at 10s.

the SGLL TSP whereas the trip-SPD scenario causes the water level to only barely reach the SGLL TSP. This operating mode differs from the power transients in that the steam generator water level is not being forced to an abnormal condition of operation, but instead either nearly or just reaches the TSP.

The closed-loop step response for the nontrip-SPD is included in Figure 6.7. For nontrip-SPD, the value of the water level set-point is offset from the calculated swell and shrink set-point of 62.24% to the near-trip value of 29.1%. In contrast, although not included in Figure 6.7, a modified set-point of 29% is used in the alternative case that does result in a trip condition, i.e. trip-SPD. To emphasize that the set-point offset is a disturbance, the water level set-point of Figure 6.7 is plotted at the unmodified level of 62.24% over the

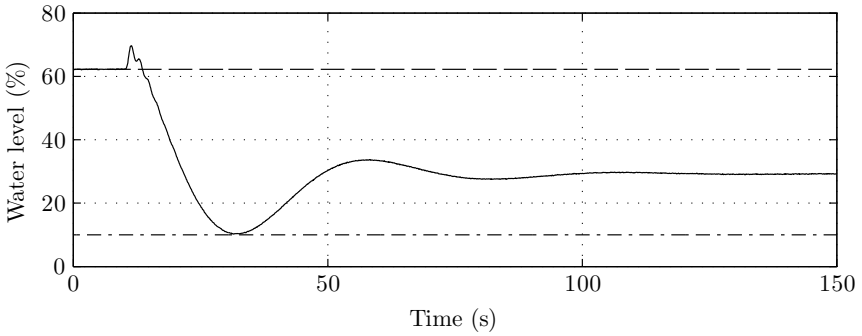

Figure 6.7: Steam generator water level response to an unanticipated step change in water level set-point at a power level of 30% with set-point made equal to 29.1% at 10s. This is the nontrip-SPD transient.

entire duration of the simulation. The two SPD scenarios are not investigated within the experiments of this study. Although it is possible to implement the SPD scenarios within the experimental platform, the impact of the SPD scenarios is best observed through simulation. The SPD scenarios are, however, recommended for future experimental study in order to better understand the capabilities of the PSDS design with regards to false- or spurious- and missed-trip occurrences.

6.5 Postulated Initiating Event

The power transients and set-point function of the previous sections are designed to prevent the steam generator water level from reaching the level high and low TSPs, SGLH and SGLL. It is therefore necessary to force the water level to the boundary between normal and abnormal conditions. This is achieved by activating an initiating event that causes the steam generator level to transient to the boundaries of the admissible range, beyond the TSPs. Postulated initiating events are those which are hypothesized during or known from the NPP design process to cause a specific trip occurrence. A postulated initiating event

for the SGLL trip condition is the loss of feedwater flow into the steam generator. Although this is not the only PIE for the SGLL trip condition, the loss of feedwater flow-rate has a direct effect on the steam generator water level. This specific PIE is able to be implemented within the physical PLS of the experimental platform as included in Figure 6.2.

The loss of feedwater PIE is also referred to as a loss of secondary side cooling. This is due to the feedwater on the secondary side of the steam generator being at a lower temperature than that of the inventory within the steam generator. The feedwater therefore provides cooling to the steam generator water inventory. Without secondary side cooling, the inventory continues to be heated by the high temperature primary side heavy water that flows through the heat exchanger tubes at the base of the steam generator. After some time, the temperature within the steam generator rises and more steam is produced. The inventory within the steam generator is then reduced and the heat exchanging tubes may become uncovered. This uncovering, in turn, results in more significant temperature increases and the potential for damage to the steam generator tubes. It is assumed within the Irving model, and therefore within the simulation and experimental platforms, that the water exits the steam generator as steam only. Within an NPP, this steam is directed to the high power turbine, discharged to the atmosphere, or re-routed to the condenser having bypassed the turbine. In other words, within this investigation, there is no mechanism to reduce the water level by allowing water to flow out of the steam generator tank.

For both simulation and experiment, the loss of feedwater PIE is injected by activating a flow malfunction within the feedwater valve of the secondary side heat transport loop. The malfunction is realized through a linear scaling back, or reduction, of feedwater flow-rate by 1.0%/s at the manipulated variable of the closed-loop level controller. The PIE malfunction

is activated exactly 200s after the first power transient manoeuvre that is a step in the case of SWPI and the first manoeuvre within the ramp of PRD. This PIE is not utilized for the SPD transients since the SPD transient investigates predictive shutdown for a system that is not being forced to an abnormal condition. In other words, the unanticipated step causes the system to approach the SGLL TSP. For the experimental platform, the PIE functionality is programmed within a PIE function block using structured text. The PIE function block is then triggered by the aforementioned reference function block that specifies the power transient manoeuvres.

6.6 Shutdown Systems

The PSDS designs that are proposed in Chapter 5 are compared against a benchmark conventional SDS within the simulations and experiments of Chapter 7. This section outlines the design criteria that are shared by each of the conventional and predictive SDSs, e.g. TSP Ξ_l, or are specific to each of the predictive SDSs, e.g. prediction horizon, N_p, and significance level, α.

Most significantly, the conventional and predictive SDSs utilize a SGLL TSP, Ξ_l, that is equal to 10% of the admissible range as included in Figure 6.5. This use of a constant TSP differs from practice where the SGLL TSP is a function of the reactor power level, Θ. Here, the TSP is held constant to reduce the complexity of analyzing the performance of the PSDS designs. The use of a variable TSP requires that the prediction algorithms are modified to compare predictions against an expected future TSP. Although relatively simple to implement, the expectation of the TSP introduces additional uncertainty within the

predictive shutdown problem and is therefore beyond the scope of the current investigation.

Both the conventional and predictive shutdown algorithms are implemented without the use of redundant shutdown channels or trip computers. For example, simulated as well as experimental conventional shutdowns occur when the level measurement reaches 10% of the admissible range within a single SDS logic solver; the SGLL TSPs are therefore 400mm and 21mm for the Irving steam generator and the PLS respectively. In practice, the relay logic of the trip chain has a k-out-of-n configuration of either local or general coincidence as discussed in Section 2.2. This investigation instead focuses on the time response for a single safety parameter within a single SDS channel that does not include coincidence logic. This simplification does not impact the relevance of the results since each of the channels within a specific SDS generally make trip decision using equivalent SDS functions or logic.

The shutdown logic that is implemented within the experimental function block for the conventional SDS is a port of the FORTRAN code that provides the shutdown mechanism within the Darlington NPP training simulator that is maintained by Ontario Power Generation (OPG). Upon shutdown, the trip signal at the output of the SDS is de-energized. The comparator and TSP of the SDS function block operate with a hysteresis equal to 1% of the admissible range of water level. The hysteresis prevents jitter within the trip signal that is output by the comparator block as discussed in Section 5.1. The conventional SDS comparator block is also implemented within the PSDS designs where the prediction values are input to the comparator. In this manner, each of the prediction components is added to the PSDS as a modular extension of the conventional SDS logic. It is recommend that the PSDS designs of Chapter 5 include conventional SDS logic so that the safety parameter measurements can be compared directly against the TSP. This backup conventional SDS

function is, however, removed within the simulation and experimental results of Chapter 7 so that the performance of the prediction algorithms can be assessed independent of conventional SDS functionality.

The PSDS designs are expected to provide trip decisions at a time which is earlier than that of the conventional SDS. Moreover, the PSDSs are designed as modular extensions of the conventional solution to the SDS problem. Thus, the experimental SDS and PSDS implementations are limited to scan times or execution intervals of 100ms. This particular scan time is chosen as it is within the design requirement for SDS1 of the CANDU NPP. The scan times are reported within the experimental platform by the Tricon v9 safety PLC. These time are documented for each of the conventional and predictive SDS algorithms in Section 7.2. The simulation platform includes full implementations of each prediction and shutdown algorithm from Chapter 3 and Chapter 5 respectively with no restrictions on the amount of time taken to complete the required calculations. Within the experimental platform, however, the above scan times result in the RLS estimation algorithm being implemented in a less complex form. These and other SDS and PSDS specific design criteria are described in the following sections.

6.6.1 Predictive shutdown, the Kalman filter, and point-prediction

In general, each of the PSDS designs consists of a combination of the following three components:

a) calculation of the safety parameter measurement predictions or confidence intervals

by some form of KF-based prediction;

b) compensation of prediction error or error covariance by RLS-based estimation of disturbances to the state and measurement equations of the prediction model; and

c) assessment of prediction quality by statistical and hypothesis testing and selection of an optimal safety parameter prediction.

The point- or interval-predictions are then input to a comparator in the same manner as for the conventional SDS logic and a trip decision is made. The functionality of the PSDS therefore responds as though the prediction were a sample of the safety parameter measurement signal.

Within all PSDS designs, the KF includes the following reduced-order state-space form of the scaled-Irving steam generator water level model introduced in (6.2) and (6.3)

$$\dot{x}(t) = \begin{bmatrix} 0 & 0 & K_m G_1 \\ 0 & \frac{-K_f}{\tau_2}(\Theta) & \frac{-K_m G_2(\Theta)}{\tau_2(\Theta)} \\ 0 & 0 & -K_m \end{bmatrix} x(t) + \begin{bmatrix} -K_m G_1 & 0 \\ \frac{K_m G_2(\Theta)}{\tau_2(\Theta)} & 0 \\ 0 & K_m \end{bmatrix} \begin{bmatrix} q_v(t) \\ \tilde{q_e}(t) \end{bmatrix} \tag{6.6}$$

$$y(t) = \begin{bmatrix} 1 & 1 & 0 \end{bmatrix} x(t) \tag{6.7}$$

where $x_3(t) = q_e(t)$, all other signals are defined as in (6.2) and (6.3), and all parameters are defined in Table 6.1. This continuous-time model is then discretized by bi-linear transformation to the discrete-time KF-compatible state-space form of (3.9) and (3.10) where the system matrices A, B, C and D are functions of Θ as opposed to being functions of time. The parameters of the state-space model are active within the KF over the range leading up to the mid-point steam flow-rates, q_v^*. Moreover, these parameters, as well as

the deterministic input to the system, u, are assumed constant with values of time-step, k, over the prediction window, time-steps $(k+1)$ to $(k+N_h)$.

The reduced-order model of (6.6) and (6.7) is implemented in favour of the full-order Irving model to conserve computational power within the Tricon v9 safety PLC. The Tricon v9 does not inherently support matrix operations. Thus, discrete-time implementations of the KF equations are first realized within MATLAB. The equations are then converted to structured text by iterating through and outputting structured text compatible equations for each of the KF and other required matrix calculations. Use of the third rather than fifth order model, therefore, saves a significant number of addition and multiplication operations and allows the scan time of the safety-PLC to be reduced.

The initial conditions of the KF state estimate and state-error covariance for the reduced-order state-space representation are respectively chosen as $\hat{x}\,[0|0] = [0,0,0]'$, and $P_{\tilde{x}}\,[0|0] = 100\mathbb{I}^{3\times 3}$. The initial state value matches that of the state-space Irving model in (6.2) and (6.3). To keep the initial conditions from affecting the simulation and experimental results, the water level response as well as the KF are allowed to settle to steady state prior to beginning the power transient sequence. In other words, within all simulation and experimental results, the dynamic water level response of the steam generator system as well as KF gain are at steady state at time-step zero, $k = 0$. Thus, any initial transient behaviour of the system or the KF estimates and predictions occurs in the time-steps prior to the plotted data sets.

Output y of the scaled-Irving model is the steam generator water level. The steam generator level signal is a standard safety parameter within SDSs, including CANDU SDS1. This signal is the safety parameter measurement prediction that is output by the KF

prediction block in Figure 5.3. Input u and q_v of the scaled-Irving model are the steam generator feedwater and steam flow-rate and are the two inputs from the sensors illustrated in Figure 5.3. In this work, it is assumed that the steam generator feedwater and steam flow-rates are available to the SDS although this may not always be the case in practice, and is not the case for CANDU SDS1. It is therefore assumed that the feedwater and steam flow-rate variables are available to the SDS, or can be calculated as a function of other safety parameters. In addition, the PLS of the experimental platform does not include a feedwater flow-rate sensor device. The feedwater flow-rate is therefore calculated as a function of the manipulated variable transmitted by the process controller. This assumption has little impact on the timing study as it is likely that the process and safety instrumentation in a NPP would have similar values for a given set of signals.

Within all PSDS designs, the KF propagates the state and state error covariance predictions to a prediction horizon of up to twenty time-steps into the future, or $N_h = 20$. This horizon is equal to that 2.0s that is the expected total amount of time between the time of trip detection and insertion of sufficient negative reactivity into the reactor core for SDS1 of the CANDU NPP design. This study also investigates the use of various other, shorter, prediction horizons down to three time-steps, or $N_h = 3$. This lower limit is one time-step longer than the required maximum time interval between subsequent trip decisions. In other words, a predictive trip detection at a prediction horizon of three time-steps results in the shutdown procedure being activated prior to the time of detection within the conventional SDS. In addition, within the optimal-PSDS design, the prediction window is adapted to have an effective prediction horizon as a function prediction quality and probability of an impending abnormal condition. In the end, the ultimate objective of this work

is to make accurate predictions using short horizons rather than speculative and potentially erroneous predictions using long horizons.

6.6.2 Noise covariances, stochastic uncertainty, and the adaptive limited memory filter

It is assumed within the KF that the system being protected includes additive noise terms within both the state and measurement equations as v_x and v_y respectively, i.e. the stochastic state-space form of (3.9) and (3.9). These additive noise terms represent uncertainty in the estimation and prediction procedure with respect to the real-world measurement and input signals, as well as system-model mismatch, e.g. parameter error. The additive measurement noise terms represent the variations that are present within the $4 - 20$mA signal transmitted by the laser level sensor. This noise is not, however, present within the simulated measurements. An additive measurement noise term, v_y, with covariance $R_y = 6.24\text{mm}^2$ is therefore added to the measurement equation (6.3) of the simulated steam generator system in MATLAB. This value of R_y is estimated off-line from steady state PLS level measurements. The measurement noise of the simulation platform therefore matches that of the experimental platform and the above value of R_y is assumed within the KF of both platforms.

The value of the state noise covariance for the PLS is not as easy to estimate as the measurement noise covariance, given PLS measurements. This is due to the fact that the true system states cannot be measured. What is known is that there exists system-model mismatch between the dynamic response of the PLS and that of the scaled-Irving model

and the state noise covariance is not equal to zero. Thus, the state noise covariance is approximated by bounding the *a priori* measurement estimate within the first standard deviation confidence interval of the *a priori* measurement error covariance. In other words, the state noise covariance is approximated to satisfy the probability distribution of the *a priori* measurement prediction error or measurement innovations. This approximation is possible due to the *a priori* measurement prediction, $y\left[k|k-1\right]$, being a function of the state noise covariance, $R_x\left[k-1\right]$, with known measurement noise covariance, $R_y\left[k\right]$, as defined in (3.19), (3.46), (3.47), and (3.24).

The simulation state noise covariance matrices are calculated to have the values listed in Table 6.3 for each of the five operating ranges. These values are calculated by analyzing the covariance of the *a priori* prediction error while utilizing the RLS-based measurement disturbance estimation algorithm. More specifically, the covariance values correspond to a 10% expansion of the measurement error covariance, $P_{\tilde{y}}$, during normal operation prior to and after a 5% step change in steam flow-rate that crosses the nominal power levels of the five different operating points. These relatively large magnitudes in comparison to the measurement noise variance, R_y indicate that the KF considers the provided model to be more uncertain than the measurements.

For the simulation platform, state noise is not added to the state equation of the steam generator system as was the case for the measurement noise. This is due to the simulation platform already including system-model mismatch. That being said, the model mismatch within the system is known and as a result the state noise covariances for simulation have values that are less than those of the experimental platform. The state noise covariances for simulation are listed in Table 6.3. These values are calculated in the same manner as for

Table 6.3: State noise covariance estimates for use without ALMF.

Θ (%)	**5**	**15**	**30**	**50**	**100**
Simulation $\hat{R}_x$	diag(95.2)	diag(96.7)	diag(109.2)	diag(113.9)	diag(115.4)

the experimental platform but without the use of the RLS-based disturbance estimation algorithm.

The state noise covariance also accounts for uncertainty in the effect of the future system input, $u[k+1]$ on the measurement equation, as in (3.10). As for the measurement noise, there is no noise present within the simulated system inputs. An additive input noise term, v_u, with covariance $R_u = 0.624\text{kg}^2/\text{s}^2$ is therefore added to the system input, $u[k]$, of the simulated steam generator system. For experimentation, the ALMF noise covariance estimation algorithm is utilized without estimation of the state noise covariance matrices.

The above procedures are considered to be superior to the trial-and-error approach that is utilized in many studies for the offline estimation of state noise covariance. The state noise covariances are still, however, offline estimates of time-varying parameters. These parameters are therefore erroneous during operating conditions that are different than those that were present when the covariances were estimated. To counteract this problem, the ALMF procedure of Section 3.6 is utilized. The ALMF algorithm utilizes initial conditions for the state and measurement covariances that are equal to the low power estimations of Table 6.3. The noise covariance estimates for both the measurement and state are calculated over an estimation window of length $N_v = 100$. The window length for noise covariance estimation is chosen as a function of the dynamic response and expected trajectories of the steam generator system. In other words, the noise covariances, which change with the

dynamics of the system, are not expected to vary significantly over a period of 10s. Noise covariance estimation is not performed until after the KF has converged within the initial time-steps of simulation or experiment. This delay in calculation prevents the covariances from becoming artificially large and potentially triggering an unnecessary trip.

6.6.3 Disturbance inputs, deterministic uncertainty, and the recursive least squared filter

In addition to the use of the KF for prediction, prediction error is compensated by RLS estimation using (4.9). For simulation and experimentation, the disturbance is assumed to be a ramp function with a disturbance profile defined as $\Gamma\left[k+i, k_w\right] = \begin{bmatrix} 1 & iT_s \end{bmatrix}$ for $i = [1, \ldots, N_p]$. Unlike for the KF, the RLS estimation in (4.9) does not support a fully recursive implementation. For this reason, the RLS algorithm considers a specific instance of a disturbance that initiated at time-step k_w. In other words, the initialization of the disturbance does not move forward in time at each time-step. The time-step of the disturbance initialization may therefore be 100 time-steps into the past, i.e. $k_w = (k - 100)$. At the next time-step the disturbance will have initiated $(k - 101)$ time-steps into the past.

In order to reset the disturbance initialization time-step, a dual RLS algorithm is proposed in Section 4.2.4. In this configuration, a duplicate RLS algorithm performs the same disturbance estimation as the original RLS algorithm. The disturbance estimation algorithm then switches between the two RLS algorithms at the time-step in which the duplicate RLS estimation and corresponding measurement prediction error estimate have been determined to have converged to a steady state solution of a predetermined accuracy.

This switching mechanism is described in the following equation

$$\hat{w} = \begin{cases} \hat{w}_2 & \text{if } \hat{w}_1 \text{ and } \mathcal{F}_c\left(\underline{\rho}_y\left[k+i, k_{w_{y,1}}\right]\hat{w}_y\left[k, k_{w_{y,1}}\right]\right) \\ \hat{w}_1 & \text{if } \hat{w}_2 \text{ and } \mathcal{F}_c\left(\underline{\rho}_y\left[k+i, k_{w_{y,2}}\right]\hat{w}_y\left[k, k_{w_{y,2}}\right]\right) \end{cases}, \forall i = 1, \ldots, N_p \tag{6.8}$$

where $\hat{w}_1$ and $\hat{w}_2$ are the duplicate disturbance estimates, and $k_{w_{y,1}}$, $k_{w_{y,2}}$ are the time-steps of the disturbance initialization considered by the original and duplicate RLS algorithms respectively. Moreover, $\mathcal{F}_c$ is the function that determines whether or not the estimated prediction error has converged within either the original or duplicate algorithm.

The RLS disturbance estimation algorithm is of the exponentially weighted LS form. These weights help the algorithm to better respond to changes in the deterministic uncertainty and also the changes that are due to the LTV parameters of the system. Thus, the RLS estimation considers recently measured prediction errors more heavily. The RLS algorithm uses a forgetting factor for the measurement disturbance estimate that of $\lambda_y = 0.99$ where $\Lambda_y\left[k, k_{w_y}\right] = \text{diag}\left(\lambda_y^{k-k_{w_y}}, \ldots, \lambda_y\right)$. In contrast, the state disturbance estimation algorithm utilizes a forgetting factor of $\lambda_x = 0.995$ where $\Lambda_x\left[k, k_{w_x}\right] = \text{diag}\left(\lambda_x^{k-k_{w_x}}, \ldots, \lambda_x\right)$. These forgetting factor values are chosen to be very near to unity in order to reduce the possibility of instability within the disturbance estimation procedure. Moreover, the forgetting factor for the state disturbance responds more slowly to changes in the disturbance than the measurement disturbance, again, to reduce the possibility for instability within the algorithm. When combining the KF, the ALMF, and RLS filter it is essential to consider the possibility for the three estimates to become unstable. Within this work, the stability of the combined filter is verified first through the use of the MATLAB

based simulation while taking into account the precision of the PLC operations. More specifically, the functional blocks of the PLC pass single-precision floating-point values with double-precision values utilized within the structure text of any given function block.

For experimentation, only the measurement disturbance estimation, RLS_y, is implemented. This reduction in functionality is due to the increased computational complexity that would be required by the state disturbance estimation procedure. Although it is possible to implement the state disturbance estimation procedure, RLS_x, within the Tricon v9 PLC, the scan time of the controller exceeded the regulatory limit of 100ms. That said, a more directed effort that aims to optimize the arithmetic within the RLS algorithm may result in the possibility of implementing the complete algorithm. This effort is, however, beyond the scope of this study. The RLS-based state disturbance estimation procedure is instead implemented and investigated alongside the measurement disturbance estimation algorithm through simulation only.

6.6.4 Point-, interval- and optimal-predictive shutdown system designs

The point-PSDS design calculates predictions up to a prediction horizon of N_p time-steps into the future. Two different values of N_p are investigated in Chapter 7 in order to analyze the reduction in time-to-trip that is possible via point-predictions within the predictive decision-making process. A point-predictive trip does not necessarily, however, occur at the prediction horizon. This is due to the fact that any point-predicted threshold-crossing event over the entire prediction window will result in a predictive trip, e.g. $\hat{y}\left[k+3|k\right] \leq \Xi_l$

with $N_p = 10$. For simulation, the point-PSDS is studied while including the ALMF-based noise covariance estimation algorithm. The point-PSDS is also studied in combination with the RLS-based state and measurement disturbance estimation algorithm. For experiment, the point-PSDS is always investigated in conjunction with the RLS-based disturbance estimation for the measurement error as well as ALMF-based estimation of the noise covariances. This combination of KF and RLS algorithms is necessary during experiment in order to accommodate for deterministic uncertainty and system-model mismatch.

The interval-PSDS design shares many of the same criteria that have been established for the point-PSDS above. For example, the interval-PSDS design calculates predictions up to a prediction horizon of N_p time-steps into the future. Moreover, a number of prediction horizons are investigated. In addition, the confidence interval of the interval-PSDS design has a two-sided significance level of $\underline{\alpha} = 0.05$ or 5%. This is equivalent to a one-tailed significance level of $\alpha = 0.025$ or 2.5%. Thus, an interval-predictive trip occurs when there is a level of confidence equal to 97.5% in impending abnormal condition. For simulation, the interval-PSDS is studied without modification and is also modified to include the ALMF-based noise covariance estimation algorithm and the RLS-based state and measurement disturbance estimation algorithm. More specifically, interval-PSDS simulation results investigate the additional functionality of ALMF-based noise covariance estimation since the noise covariances have a direct effect on the calculated intervals. During experiment, the interval-PSDS is again always investigated in conjunction with the RLS-based disturbance estimation. The experimental interval-PSDS results also provide insight into the accuracy of the predicted intervals when utilizing the ALMF noise covariance estimation algorithm.

The optimal-PSDS design operates under different criteria than those of the point- and

interval-PSDS designs. The optimal-PSDS design makes use of statistical tests to assess the quality of the previously calculated predictions. The simulations and experiments of Chapter 7 use the one-tailed IB or Z test as well as the one-tailed NIS or χ^2 test. The experimental results, however, implement only the Z test. The IB test is the lower one-tailed test since the error is defined as the measurement minus the prediction and the decision is being made for a low-valued TSP, Ξ_l. These tests are described in Section 5.3.1. In assessing prediction quality, the optimal-PSDS is able to adapt the effective prediction horizon. Predictions are calculated to a prediction horizon of N_p time-steps into the future and the results of the statistical tests are then utilized form a subset of the predictions that are assessed to be of sufficient quality with respect to a given Type I error rate also known as the FPR. The Type I error rate of this study is also the two-tailed significance level of $\underline{\alpha} = 5\%$. An optimal-prediction is then selected from the subset of quality predictions as a function of the mean measurement prediction and the measurement error covariance.

The adaptive and optimized abilities of optimal alarm theory are extended to consider, through statistical testing, whether the mean measurement predictions have non-zero error or are biased. More specifically, the optimal-PSDS design not only considers each time-step within the prediction window, but also multiple possible mean prediction biases for each of the prediction time-steps. The biases are calculated as a function of the measurement error covariance. For simulation and experiment, the following set of standard deviations for possible bias are investigated, $\tilde{y}_b = -2, -1, 0, 1, 2$, where $\tilde{y}_b$ is the set of assumed prediction biases. The optimal-PSDS is also studied with only the zero-valued assumption for mean prediction error.

6.7 Summary

This chapter presents the assumed system, operating conditions, events, and shutdown configurations for the simulations and experiments performed in Chapter 7. The physical system being protected is the steam generator or boiler within the NPP. A model of the steam generator water level is given as the Irving steam generator model. This model is scaled in frequency and magnitude to better support an existing physical experimental platform known as the plate level systems. The physical platform involves a plate level being vertically manipulated along a rod within an acrylic tank. A closed-loop controller is developed for the control of the non-minimum phase Irving steam generator model as well as the scaled-Irving physical plate level system.

The steam generator is assumed to be operating within one of three modes. The first two modes are common power transients for increases and decreases in the power level of the reactor core and steam flow rate into the turbines of the electrical generator within the NPP. More specifically, the two power transients are step-wise power increase or SWPI and power ramp down or PRD. The third mode is an unanticipated change in the steam generator water level set-point. This mode of operation is referred to as a disturbance in the set-point, or SPD. An abnormal condition is forced within the steam generator as the results of a PIE known as the loss of secondary side coolant or feedwater flow, and also the set-point disturbance. The timing of this initiating event, and the rate of decrease in feedwater flow are consistent over all simulations and experiments.

All SDSs, including the PSDS designs, utilize the same TSP equal to 10% of the admissi-

ble range of operation for the steam generator. The prediction algorithms within the PSDS design consider a reduced-order scaled-Irving model. Moreover, the various assumptions and initial conditions regarding the KF, the ALMF, and the RLS filter are discussed in Section 6.6. This chapter closes by describing each of the point-, interval-, and optimal-PSDS configurations that are to be investigated in Chapter 7.

Chapter 7

Results and Analysis

This chapter investigates the use of the PSDS designs that are developed in Chapter 5 within the simulation and experimental platforms of Chapter 6. More specifically, the following results and analyses investigate the ability of the PSDS designs to detect abnormal conditions within a system being protected at a time which is earlier than that of a benchmark conventional SDS design. This investigation therefore aims to determine whether the predictions and detections are accurate under a variety of uncertain conditions. This investigation also aims to determine whether the enhanced PSDS designs can minimize the occurrence of erroneous predictive decisions, i.e. spurious and false or missed trip detections. The following results are an extension of the KF/LS point-PSDS results presented in [169].

The results of this work demonstrate that, given a short-term prediction horizon and low uncertainty in future values of the model parameters and deterministic inputs, the proposed predictive SDS achieves a reduced time-to-trip. Further, this work demonstrates

that it is possible to implement the proposed PSDS design within an industry standard safety PLC while meeting current scan time requirements, although an FPGA might be beneficial for a multiple parameter PSDS design. Finally, although the proposed predictive SDS takes into consideration the possibility of a spurious trip occurring, the ability of the shutdown algorithm to compensate for an anticipated spurious trip is considered to be beyond the scope of this dissertation. This functionality would also go against the regulatory requirements of initiating shutdown procedures upon detecting a safety parameter reaching a TSP.

7.1 Simulation Results

The following simulations compare the proposed PSDS algorithms against a benchmark conventional SDS design. The simulations are organized into separate sections where each section investigates a specific case of uncertainty in terms of either: the model mismatch between the true system and the predictive model provided to the KF within the PSDS; or anomalous signals that are available within the PSDS. More precisely, the first case includes normal conditions for the system, model, and related signals with relatively little uncertainty. The second case, however, includes an uncertain condition regarding the system and assumed model. The KFs of all the PSDS designs are provided the reduced-order model introduced in Section 6.6. The additional uncertainties for each case are specified as follows.

- Case 1: multi-model selection with ideal signal availability
- Case 2: parameter error multi-model selection with ideal signal availability

Multi-model matching refers to the model parameters within the prediction algorithm being equal to those of the nearest operating point. This nearest operating point is a function of the exogenous steam flow-rate input that is assumed to be available as a safety parameter within the SDS. The parameters within the KF therefore differ from the systems parameters that vary linearly between the operating points. Ideal signal availability specifies that both the feedwater and steam flow-rate inputs are available to the PSDS.

Table 7.1 provides a summary of the PSDS designs that are investigated within each of the above cases. PIEs and subsequent SGLL trip occurrences are simulated for each of the proposed PSDS and conventional SDS methods during two normal operating modes: once while operating within the SWPI power transient, and again while operating within the PRD power transient. The performance of each PSDS is also studied during an unanticipated control manoeuvre referred to as the SPD transient. The * symbol indicates that the ALMF covariance estimation algorithm is active within all PSDS methods with the effect of the algorithm specifically investigated for the KF-based interval-PSDS of Case 1.

The following simulation results provide insight into the performance of the proposed PSDS designs within a controlled environment and under conditions that are not possible within the experimental platform. Moreover, the selected operating modes and uncertain conditions include a realistic yet broad set of conditions for evaluating the performance of the proposed PSDS designs. Within all simulations, the time-to-trip values do not include signal processing, relay activation, or the physical displacement of the neutron absorbing materials, e.g. dropping of the shut-off rods or injection of neutron poison. In other words, the processing time within the logic solver of all simulated SDSs, both conventional and predictive, is assumed to be instantaneous.

Table 7.1: Summary of the PSDS methods that are investigated within each simulation case. * indicates both with and without the ALMF

Case 1: reduced-order multi-model
a) KF point-PSDS
b) ,c) KF interval-PSDS*
d) KF optimal-PSDS
Case 2: reduced-order multi-model with parameter error
a) KF point-PSDS
b) KF/RLS point-PSDS
c) KF/RLS interval-PSDS
d) KF/RLS optimal-PSDS

The dynamic response of steam generator water level is first illustrated for a loss of feedwater flow PIE during SWPI and PRD power transients in Figure 7.1a) and Figure 7.1b) respectively. Within these figures, y is the water level, r is the control set-point, $\Xi_l = 10\%$ is the SGLL TSP, k_e is the initial time-step of the PIE, k_d is the time of trip detection by the conventional SDS, and $\Delta k_c = k_d - k_e$ is the conventional time-to-trip, or the difference in time between the time of detection and the time at which the initiating event was initiated.

In Figure 7.1, the SWPI and PRD power transients both begin at 10s with the PIE injected 200s later at $k_e = 210$s. The occurrence of the PIE results in inverse response characteristics in addition to those that are due to only the power transient manoeuvres as illustrated in Figure 6.6. These inverse response characteristics have a significant and non-intuitive effect on the amount of time required for the water level to transient to the TSP. For example, although the decreasing water level observed during the PRD suggests

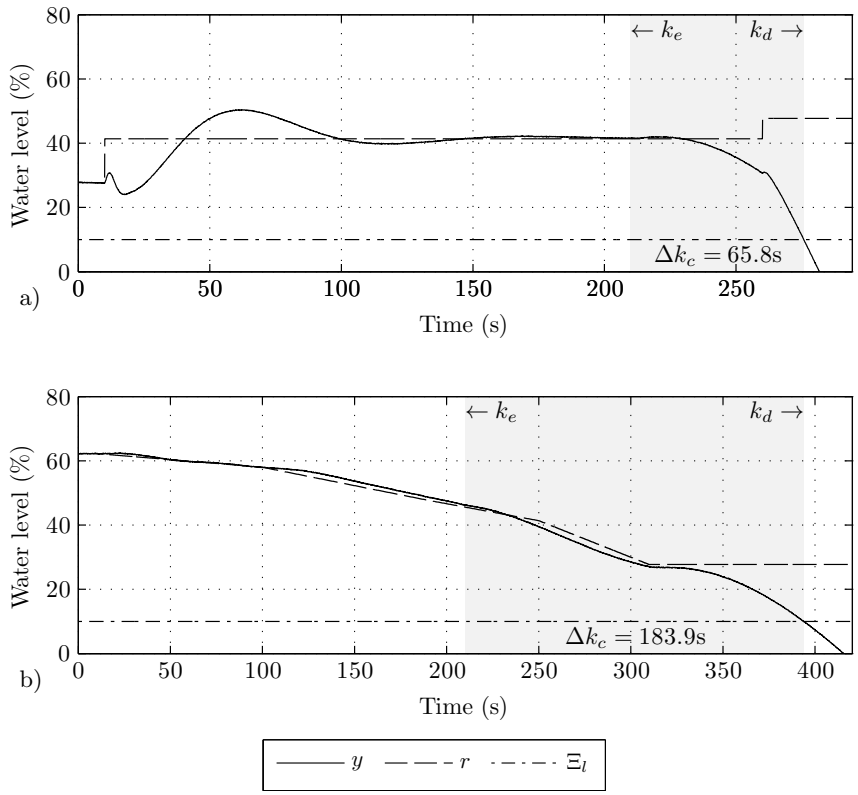

Figure 7.1: Benchmark: simulated conventional SGLL trip occurrences due to loss of feedwater flow PIE during a) SWPI and b) PRD power transients.

that the level will reach the TSP in less time than for the SWPI power transient, the inverse response characteristic causes the opposite to occur. In the following results, the PSDS designs are expected to accurately anticipate these complex dynamic responses so as to avoid false and missed trip occurrences.

The dynamic response of steam generator water level is also illustrated for the trip-SPD transient in Figure 7.2. This is the response to an unanticipated step change in water level set-point from a nominal value of 62.24% to an anomalous value of 29.0%. The trip-SPD transient results in a response similar to that of the nontrip-SPD case as previously illustrated in Figure 6.7 except that in this case the safety parameter reaches the SGLL TSP. In the following results, the various PSDS designs are expected to discern the subtle

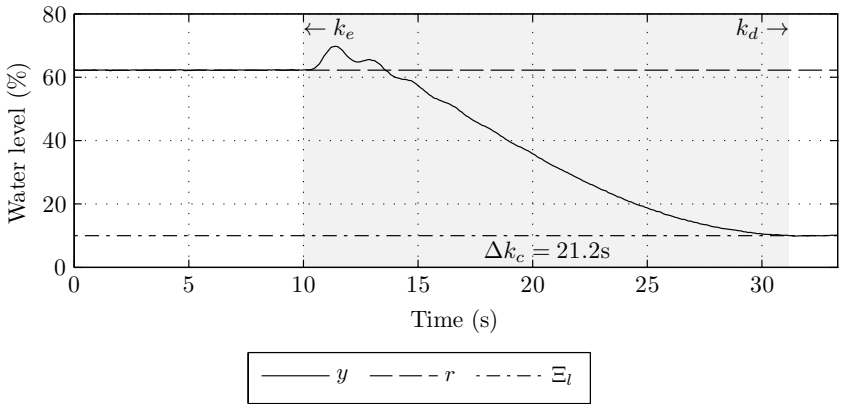

Figure 7.2: Benchmark: simulated conventional SGLL trip occurrences due to a disturbance in the water level set-point from a normal value of 62.24% to an anomalous value of 29.0%.

difference in the minimum measurement value for the trip-SPD and nontrip-SPD cases.

7.1.1 Benchmark: Conventional shutdown

Conventional SDSs trip when a safety parameter measurement, $y\,[k]$, reaches the corresponding TSP, Ξ_l. This event is also referred to as a down-crossing of the steam generator water level with the low trip threshold or TSP Ξ_l. Conventional time-to-trip is measured from the time-step of injecting the PIE to the time-step when the safety parameter measurement reaches the TSP.

The time-to-trip results of the simulated conventional trip occurrences are 65.7s for SWPI and 183.9s for PRD as observed in Figure 7.1 and also 21.2s for trip-SPD as observed in Figure 7.2. These results are the benchmarks against which the simulated PSDS time-to-trip results are compared. For ease of reference, the benchmarks are restated along with all other simulation results in Table 7.3 at the end of this section.

The time-steps immediately surrounding the conventional trip detections of Figure 7.1

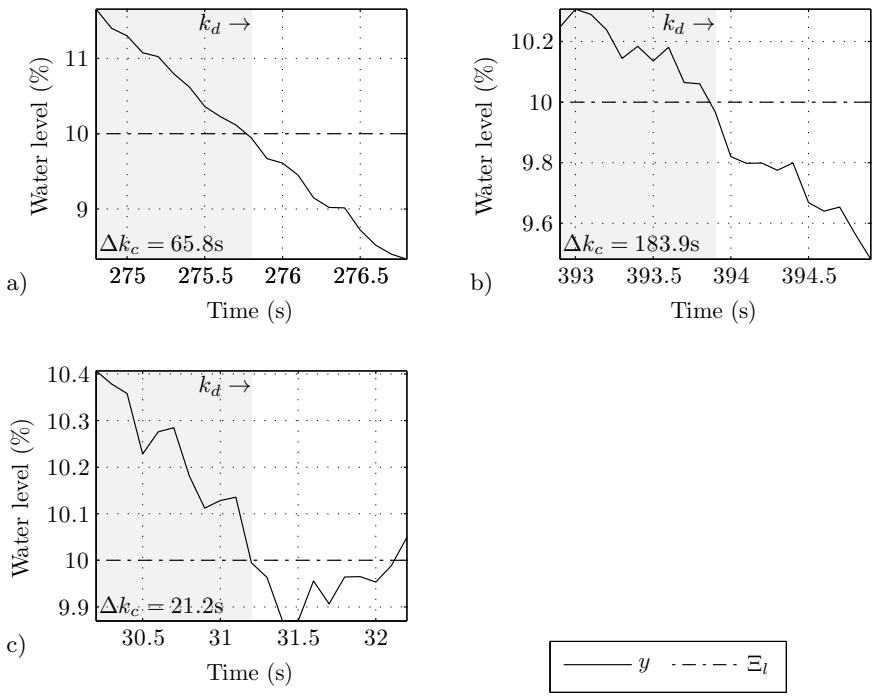

Figure 7.3: Benchmark: time-steps surrounding conventional SGLL trip occurrences plotted for a) SWPI as in Figure 7.1a), b) PRD as in Figure 7.1b), and c) trip-SPD as in Figure 7.2.

and Figure 7.2 are highlighted in Figure 7.3a), Figure 7.3b) and Figure 7.3c) respectively. These plots provide visual verification of the time-step of conventional trip detections, k_d. This is the time-step of the down-crossing event of the steam generator water level for the alarm-threshold that is the TSP. As expected, the conventional trip detections occur at the same time-step in which the water level measurement reaches the SGLL TSP.

Shutdown decisions are maintained through the use of a hysteresis threshold. This trip is prevented from deactivating as long as the variations in safety parameter measurement remain beyond the hysteresis threshold. For example, the trip decision in Figure 7.3c) is not reversed upon the later up-crossing event of the TSP.

The time of trip for the conventional shutdown decision and the time-to-trip are both

affected by the variation or noise within the measurement signal. In other words, the time of trip decision could vary by a number of time-steps depending on the magnitude of the variance for the measurement noise. This variation in time-to-trip is not directly analyzed within this work, but does have an effect on the benchmark analysis. This work instead focuses on comparing single instances of conventional and predictive trip to observe the fundamental capabilities of the predictive trip mechanisms. In addition, KF-based prediction removes this variability by filtering the measurement signal. Depending on the magnitude of the state and measurement noise covariances, the KF effectively reduces the variance of the predicted signal. Thus, it is not essential to evaluate the variation in time-to-trip to observe the relative benefits of the point-, interval-, and optimal-PSDS designs. It is, however, recommended that a study of the variation in time-to-trip be performed prior to implementation.

7.1.2 PSDS Case 1: Reduced-order multi-model

This first predictive shutdown case considers reduced-order multi-model matching between the simulated scaled-Irving model and the predictive models within the KFs of the various PSDS designs. More specifically, the model parameters of the simulated system are interpolated between the operating points of Table 6.1. In contrast, the model within the KF of the PSDS uses the nearest operating point in terms of power level or steam flow-rate, $q_v\,[k]$, to select the corresponding set of model parameters from Table 6.1. The nearest power level operating points, Θ, are documented for all possible steam flow-rates in Table 7.2. The modelling conditions for this case have the least uncertainty of all the simulation

Table 7.2: Power level selection by steam flow-rate to determine the active scaled-Irving parameters within the KF of the PSDS.

q_v(kg/s)	0-119.1	119.1-281.25	281.25-520.85	520.85-1047.5	1047.5-1435
Θ (%)	5	15	30	50	100

cases in terms of model mismatch. Moreover, all safety parameter signals including steam and feedwater flow-rate as well as steam generator water level are made available to the KF within the PSDS, i.e. ideal signal availability.

7.1.2.1 Case 1a: KF-based point-predictive shutdown

The KF-based point-PSDS design detects an abnormal condition when either the mean value of the safety parameter prediction, $\hat{y}\,[k+i|k]\,\forall i = 1, \ldots, N_p$, or the safety parameter measurement, $y\,[k]$, reach the corresponding TSP, Ξ_l. The sensor measurement is included in the proposed trip decision-making procedure of Chapter 5 to avoid a delay in trip beyond the trip that occurs due to a detection by the conventional SDS. Within the following simulations, however, the point-PSDS design of Figure 5.3 is modified to include only the predictive trip algorithm and not the conventional backup. Thus, the following simulations evaluate the effect that the various prediction algorithms have on the time-to-trip. For point-prediction, time-to-trip, Δk_p, is measured from the time-step of injecting the PIE to the time-step when a point-prediction reaches the TSP, i.e. a point-predicted down-crossing of Ξ_l.

KF-based point-predictions are plotted alongside the dynamic response of the steam generator water level in Figure 7.4a) and 7.4b) for a loss of feedwater flow PIE during SWPI and PRD power transients respectively. The point-predictions are calculated to a

prediction horizon of $N_p = 3$ time-steps or 0.3s into the future and are observed to follow the dynamic response of the water level and also the expected inverse response characteristic. The length of the selected prediction horizon allows for investigating the ability of the KF to calculate accurate prediction at short prediction horizons. More specifically, this prediction horizon is one time-step longer than the length of the regulated maximum time for decision making within CANDU SDS1. In other words, the minimal prediction horizon in order to achieve a time of trip detection that is earlier than the conventional time of detection when the safety parameter measurement reaches the TSP. The KF-based point-predictive time-to-trip results, Δk_p, are 65.5s for SWPI and 183.4s for PRD. Time-step k_d now represents the time of point-predictive trip detection rather than conventional trip detection.

KF-based point-predictions are also plotted for the trip-SPD and nontrip-SPD scenarios in Figure 7.5a) and Figure 7.5b) respectively. These point-predictions also use a horizon of $N_p = 3$. As in the case of the PRD and SWPI transients, the point-predictions are observed to follow the dynamic response of the water level. The KF-based point-predictive time-to-trip for the simulated trip occurrence is 21.0s. In contrast, there is no detection of trip within the non-trip SPD scenario plotted in Figure 7.5b). Again, these results are restated along with all other simulation and benchmark results in Table 7.3 at the end of the section after all simulation cases have been presented.

The time-steps surrounding the point-predictive trip detections of Figure 7.4 and Figure 7.5 are highlighted in the four plots of Figure 7.6. These plots focus on the time of trip detection in the same manner as for the detailed plots of the conventional results. These plots also illustrate that the KF-based prediction filters the instantaneous noise variations

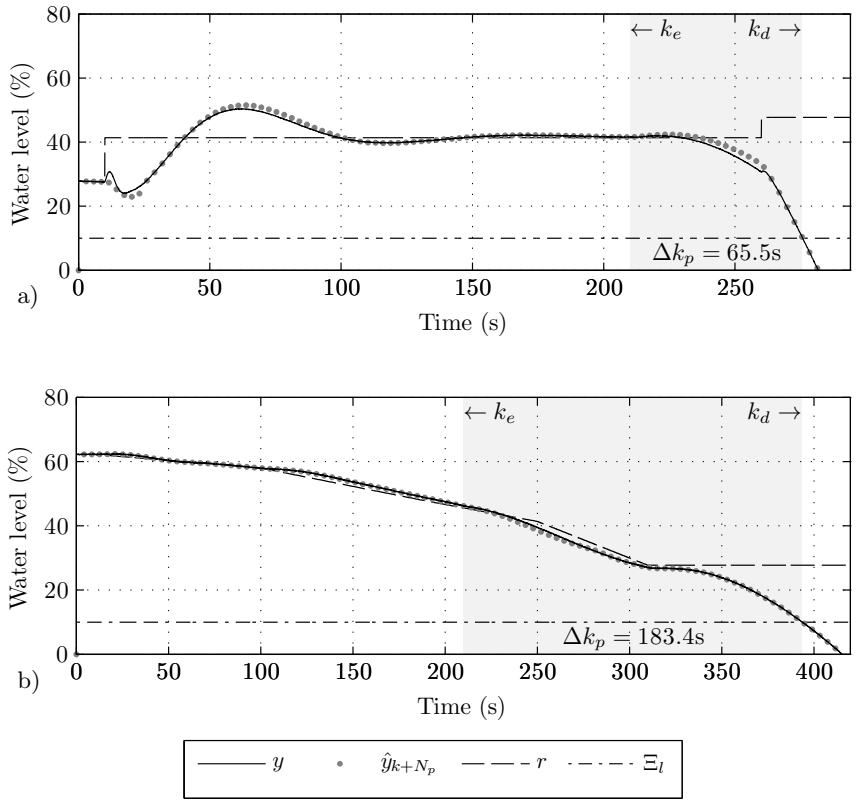

Figure 7.4: Case 1a: simulated KF-based point-predictive SGLL trip occurrences due to loss of feedwater flow PIE during a) SWPI and b) PRD power transients under multi-model matching conditions.

from the measurement signal. This filtering is a result of the predictions relying more on the provided model rather than the measured safety parameters and is a function of the state and measurement noise covariances. The covariances of these point-predictive results are calculated by the ALMF algorithm. A balance between the model and measurement uncertainty is observed in Figure 7.6b) where the predictions do not necessarily correspond with the spikes in noise values. In other words, if the model were considered to be uncertain, a large state noise covariance, the predictions would include variations that are similar to the noise within the measurement signal.

The detailed plots of Figure 7.6 include the hypothetical time-step at which the mea-

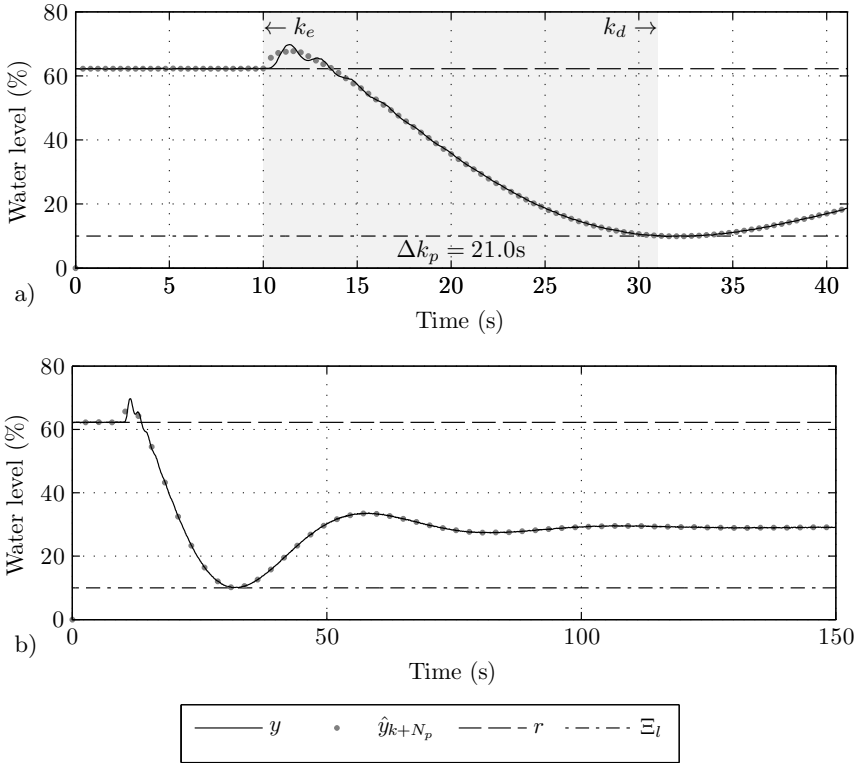

Figure 7.5: Case 1a: simulated KF-based point-predictive SGLL trip occurrences due to a disturbance in the water level set-point from a normal value of 62.24% to disturbed values of a) 29.0%, and b) 29.1% under multi-model matching conditions.

surement reaches the TSP, denoted k_c. This would be the time-step of conventional trip occurrence if the conventional trip logic was active within the PSDS. This time-step, and corresponding time-to-trip, are also the benchmarks against which the predictive shutdown activations are compared.

The point-predictions of Figure 7.6 are plotted at the prediction horizon N_p time-steps after the time-step in which the predictions are calculated. The predictive trip detections, denoted k_d, are, however, illustrated at the time-step of detection, up to $N_p = 3$ time-steps prior to the apparent trip inducing point-prediction value. The variable time-based offset of trip detection is due to the fact that any point-prediction within the prediction window may cause a predictive trip, e.g. $(k_d + 2)$.

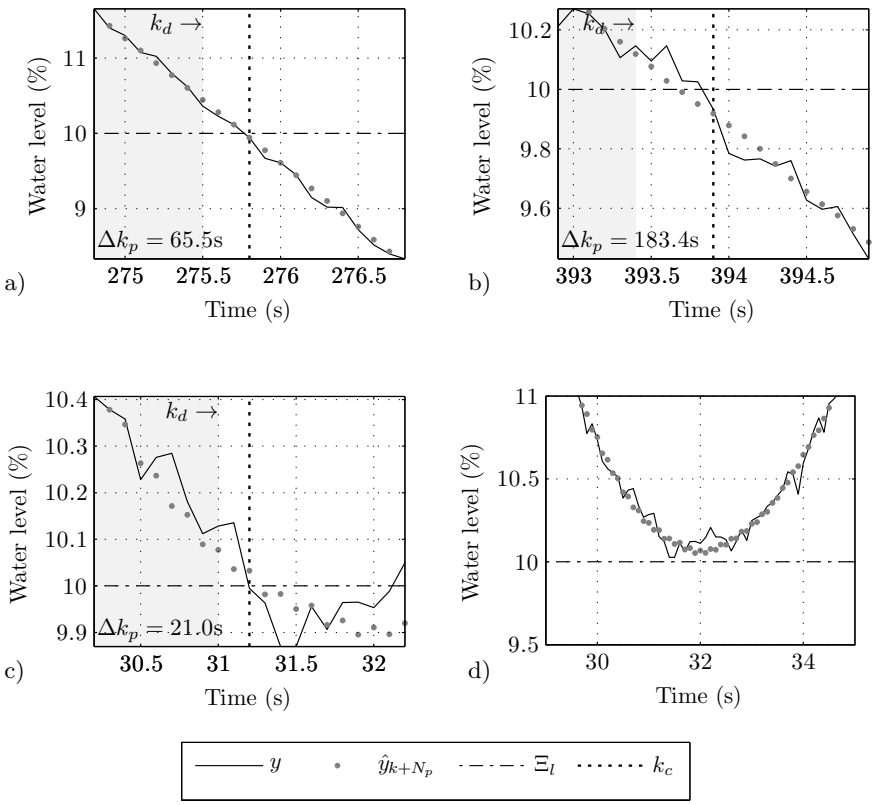

Figure 7.6: Case 1a: time-steps surrounding the simulated KF-based point-predictive SGLL trip occurrences for a) SWPI, b) PRD, c) trip-SPD, and d) nontrip-SPD under multi-model matching conditions.

For the SWPI power transient, the point-predictive trip detection occurs $N_p = 3$ time-steps prior to the down-crossing of the measurement with Ξ_l. Point-predictive trip provides a 0.3s improvement or reduction in time-to-trip for the SWPI power transient when compared against benchmark conventional shutdown. For the PRD power transient, it is also the point-prediction at the prediction horizon that first reaches the TSP, but in this case the point-prediction does not coincide with the down-crossing of the safety parameter measurement and the TSP. An improvement in time-to-trip of 0.5s is therefore observed during the PRD transient when compared against conventional SDS results. For the trip-SPD scenario, it is again the point-prediction at the prediction horizon, $(k_d + N_p)$, that first

reaches the TSP. This predictive trip event results in a 0.2s reduction in time-to-trip with respect to the conventional SDS. Finally, in the nontrip-SPD scenario of Figure 7.6d), the point-predictions correctly avoid a predictive trip occurrence.

In the case of Figure 7.6c), the point-predictive reaches the TSP prior to the time of conventional trip. In Figure 7.6c) and Figure 7.6d), however, the minimum measurement within the range of plotted measurements is observed to be less than the minimum of the point-prediction. This discrepancy indicates that an alternate value of set-point disturbance may result in a missed trip occurrence causing either a delayed trip or continued operation without a trip occurrence at all. Missed point-predictive trips may therefore occur due to the filtering of measurement noise that is performed by the KF-based predictions, i.e. the instantaneous noise values of the measurement may result in a conventional trip occurrence. Thus, given a relatively accurate model of the system, KF-based point-predictions favour continued operation over the activation of the shutdown procedure. In other words, point-predictions favour productivity over safety.

Additional plots whereby the point-predictions are propagated from the KF-based estimates of the current time-step, k, through to the prediction horizon, $(k + N_p)$, are included in Figure 7.7a), Figure 7.7b), and Figure 7.7c) for SWPI, PRD, and trip-SPD transients respectively. The sets of point-prediction propagations are plotted every $N_p + 2$ time-steps leading up to the interval-predictive trip detection, hence the spacing between the sets of marked points. The propagation follows the dynamic response of the system, indicating that the KF-based point-estimates are also accurate. The nontrip-SPD scenario is not included in this set of plots since no impending abnormal condition was detected.

The plots of Figure 7.7 emphasize the time-step of occurrence for the point-predictive

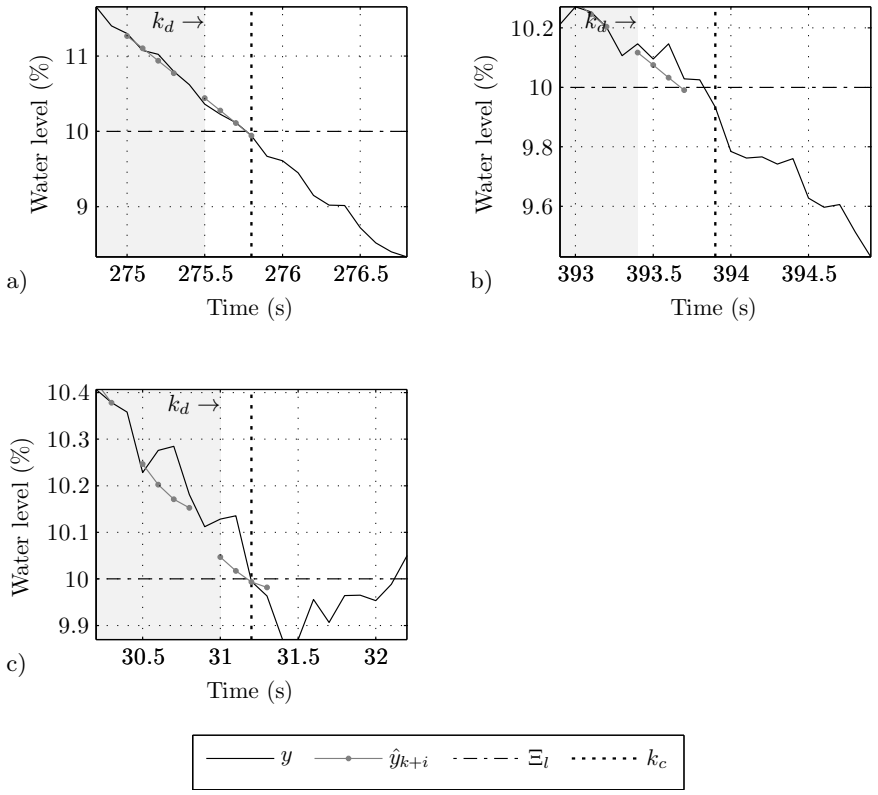

Figure 7.7: Case 1a: KF-based point-predictions being propagated over the prediction window, $i = 0, \ldots, 3$, while approaching the SGLL trip occurrence during a) SWPI, b) PRD, and c) trip-SPD transients under multi-model matching conditions.

trip detection relative to the predicted down-crossing of the TSP. More specifically, the trip inducing point-prediction of Figure 7.7c) is observed to be the two-step-ahead, $(k_d + 2)$, value within the prediction window rather than the value of the prediction horizon, N_p.

7.1.2.2 Case 1b: KF-based interval-predictive shutdown without ALMF

The KF-based interval-PSDS design detects an abnormal condition when either the upper bound of the confidence interval for a safety parameter prediction, $\hat{y}^u\left[k+i|k\right] \forall i = 1, \ldots, N_p$, or a sensor measurement, $y\left[k\right]$, reaches a low TSP, Ξ_l. While the point-predictions of the previous case are optimal with respect to the mean squared error of the estimations,

the expected value of the future measurements are defined over a probability distribution. In being defined over a probability distribution there is a percentage probability within each time-step of the prediction window that the true measurement is either greater or less than the point-predicted value. Thus, at the time-step of point-predictive trip there could be as little as 50% probability that the measurement will actually reach the TSP. The interval-PSDS design instead utilizes the confidence interval metric to attain a higher level of confidence in an impending abnormal condition.

In the following results, the bounds of the two-tailed 95% confidence interval are used, i.e. a significance level of $\underline{\alpha} = 0.05$. This is equivalent to a one-tailed confidence interval of 97.5% and significance level $\alpha = 0.025$. Thus, when the upper bound of the confidence interval reaches the low TSP there is 97.5% probability that the future safety parameter measurement will reach the TSP. As with point-prediction, the interval-PSDS design of Figure 5.4 is modified for the following simulations to include only the predictive trip action without conventional trip. Thus, interval-predictive time-to-trip, Δk_p, is measured from the time-step of injecting the PIE to the time-step when the upper bound of the interval-prediction reaches the TSP, i.e. a high confidence interval-predicted down-crossing of Ξ_l. This is in contrast to to a low confidence interval-predicted down-crossing which would potentially cause an increase in the false trip occurrences that are already experienced during point-predictive trip.

The interval-PSDS design utilized in the following results does not include the ALMF noise covariance estimation algorithm of Section 3.6. Instead, the measurement noise covariance estimate is assumed to be equal to the true covariance, $\hat{R}_y = R_y = 6.24$. The diagonal elements of the state noise covariance are assigned the values listed in Table

6.3, with the off-diagonal elements of the covariance assumed to be equal to zero, i.e. $\hat{R}_x = \text{diag}(\bullet)$. These values are chosen due to the actual uncertainty not being known, e.g. model mismatch. In this manner, the model assumed within the KF is considered less certain than the steam generator water level measurement.

The time-steps surrounding the interval-predictive trip detections are highlighted in Figure 7.8a) and Figure 7.8b) for the SWPI and PRD power transients respectively. As with the point-predictions, the interval-predictions are calculated to a prediction horizon of $N_p = 3$ time-steps or 0.3s. Moreover, the interval-predictions are plotted at the time-step for which the predictions have been calculated, i.e. the prediction horizon N_p time-steps after the predictions are calculated. The interval-predictive time-to-trip results for the simulated trip occurrences are 65.6s for SWPI and 184.0s for PRD.

The interval-predictions observed in Figure 7.8 demonstrate a 0.2s reduction in time-to-trip during the SWPI power transient. In contrast, the interval-predictions fail to detect a trip condition at an time that is earlier than that of conventional trip for the PRD power transient where the time-to-trip is instead increased by 0.1s. This missed trip occurrence is the result of the upper bound of the predicted confidence intervals not reaching the TSP prior to the down-crossing of the SGLL TSP by the steam generator water level measurement. Perhaps, if a longer prediction horizon were used, the interval would have reached the TSP prior to the conventional trip. The interval-predictions also fail to detect the trip condition for the trip-SPD transient since the upper bound of the confidence interval never reaches the TSP. Thus, missed trip events occur in both Figure 7.8b) and Figure 7.8c). These two missed trip occurrences demonstrate that the interval-PSDS favours continued operation over the activation of the shutdown procedure when compared against the point-

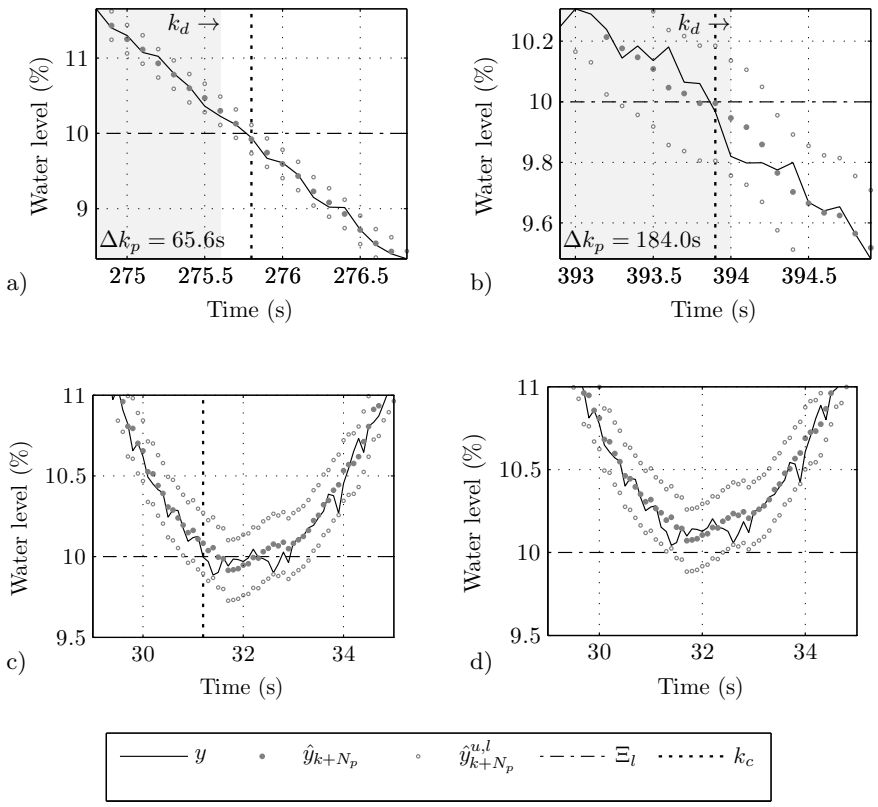

Figure 7.8: Case 1b: time-steps surrounding the simulated KF-based interval-predictive SGLL trip occurrences due to a loss of feedwater flow PIE during a) SWPI and b) PRD, c) trip-SPD, and d) nontrip-SPD transients under multi-model matching conditions without ALMF-based noise covariance estimation.

predictions. Finally, the interval-PSDS correctly avoids the detection of an impending trip condition as observed in Figure 7.8d) for the nontrip-SPD transient.

The confidence intervals are propagated from the KF-based estimates through to the prediction horizon in Figure 7.9a) and Figure 7.9b) for SWPI and PRD power transients respectively. The confidence intervals are observed to bound the measurement signal throughout the prediction window. The confidence interval is observed to expand as the predictions are propagated forward in time. This limited expansion is a result of the state noise covariance being relatively small in comparison to the admissible range of the system measurements. More precisely, the square root of the diagonal elements within

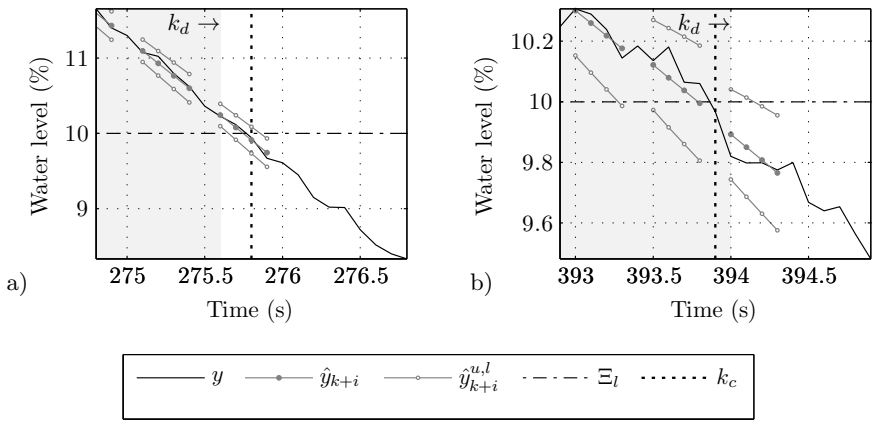

Figure 7.9: Case 1b: KF-based point-predictions being propagated over the prediction window, $i = 0, \ldots, 3$, while approaching the SGLL trip occurrence during a) SWPI, and b) PRD power transients under multi-model matching conditions without ALMF-based noise covariance estimation.

the state noise covariance matrix can be compared against the admissible range as follows; $\sqrt{96.7} = 9.83\text{mm} \ll 4000\text{mm}$ at 15% power level. The effect of the state noise, as indicated in the previous standard deviation, is also further reduced by the state-to-measurement matrix, C.

The following simulations investigate the effect of state noise covariance on the performance of KF-based interval-predictions within the current case. Confidence intervals for two alternate and fictitious values of state noise covariances are propagated from the KF-based estimates through to the prediction horizon in Figure 7.10a) and Figure 7.10b) for the SWPI power transient. The diagonal elements of the state noise covariance are assigned respective values of $\hat{R}_x = 0.1$ in the first case and $\hat{R}_x = 3120.0$ in the second case with the off-diagonal elements of the covariance set equal to zero.

In Figure 7.10a), the model that is assumed within the KF is considered to have less uncertainty than the safety parameter measurement. This lesser uncertainty is a result of

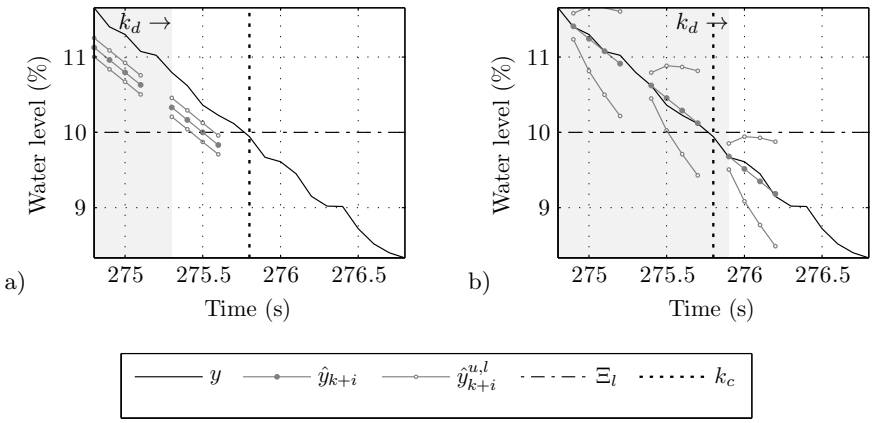

Figure 7.10: Case 1b: KF-based point-predictions being propagated over the prediction window, $i = 0, \ldots, 3$, while approaching the SGLL trip occurrence during an SWPI power transient with assumed state noise covariances of a) $\hat{R}_x = \text{diag}\,(0.1)$, and b) $\hat{R}_x = \text{diag}\,(3120.0)$.

the small value that is assumed for the state noise covariance. In contrast, the KF that is utilized in the results of Figure 7.10b) assumes that the model is more uncertain than the measurements. This increase in uncertainty is a result of the larger value that is assumed for the state noise covariance. These are the two competing filtering considerations within KF-based estimation and prediction: trust the model or trust the measurement, as discussed in Section 3.6. In the case of shutdown, where a trip occurrence is defined as the measurement reaching the TSP, it is beneficial to trust the measurement. That said, in this work the noise covariances are adapted by the ALMF so that the KF may either trust the model or measurement depending on performance of the filter.

The interval-predictive time-to-trip results for the simulated trip occurrences are 65.3s for the relatively uncertain measurement of Figure 7.10a) and 65.9s for the relatively uncertain model of Figure 7.10b). Neither of these results are particularly favourable since the interval-predictions of Figure 7.10a) are erroneous with respect to the measurement, and those of Figure 7.10b) are late with respect to the conventional SDS trip occurrence.

That said, large uncertainty in the assumed model with respect to the measurement does result in the one-step-ahead predictions following the measurement more closely.

For a shutdown system that is concerned with the measurement prediction problem, more uncertainty in the model results in short term predictions that are more accurate to the measurements. In this case, long term predictions are less likely to be accurate given that the multi-step-ahead predictions are only based on the modelled response of the system yet it has been decided that the model is uncertain. For interval-prediction, an increase in model uncertainty with respect to measurement uncertainty causes increased delay in the decision-making process. Thus, the size of the noise covariances affect the ability of the point- and interval-PSDS design differently.

7.1.2.3 Case 1c: KF-based interval-predictive shutdown with ALMF

The following interval-predictions are calculated by including the ALMF noise covariance estimation algorithm of Section 3.6 within the interval-PSDS design. The time-steps surrounding the interval-predictive trip detections are highlighted in Figure 7.11a) and Figure 7.11b) for the SWPI and PRD power transients respectively. The interval-predictive time-to-trip results for the simulated trip occurrences are 65.7s for SWPI and 183.7s for PRD.

The interval-predictions observed in Figure 7.11 demonstrate 0.1s and 0.2s reductions in time-to-trip during the SWPI and PRD power transients respectively. As in the previous case that does not utilize the ALMF algorithm, the interval-predictions again fail to detect the trip condition for the trip-SPD transient since the upper bound of the confidence interval never reaches the TSP. Thus, a missed trip event occurs in Figure 7.11c) for the trip-SPD transient. Moreover, the interval-PSDS again correctly avoids an impending trip condition

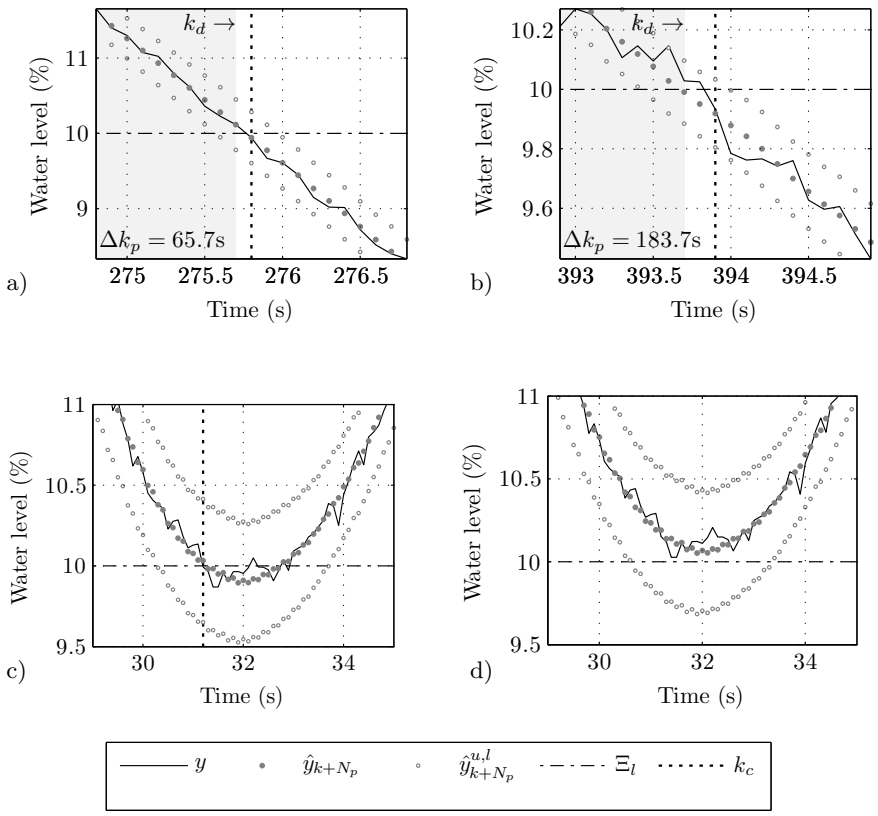

Figure 7.11: Case 1c: simulation of KF-based interval-predictive SGLL trip occurrences due to a loss of feedwater flow PIE during a) SWPI, b) PRD, c) trip-SPD, and d) nontrip-SPD transients under multi-model matching conditions with ALMF-based noise covariance estimation.

in Figure 7.11d) for the nontrip-SPD transient.

The confidence intervals are propagated from the KF-based estimates through to the prediction horizon in Figure 7.12a) and Figure 7.12b) for SWPI and PRD power transients respectively. The confidence intervals, including the predictions up to time-step $(k + N_p)$ bound the dynamic of the system in the majority of time-steps. This is especially true for the SWPI power transient of Figure 7.12a) where the bounds appear to be wide in relation to the measurement noise. This discrepancy in bounds is due, in part, to the loss of secondary side feedwater flow PIE transient causing a larger negative rate of change in the water level

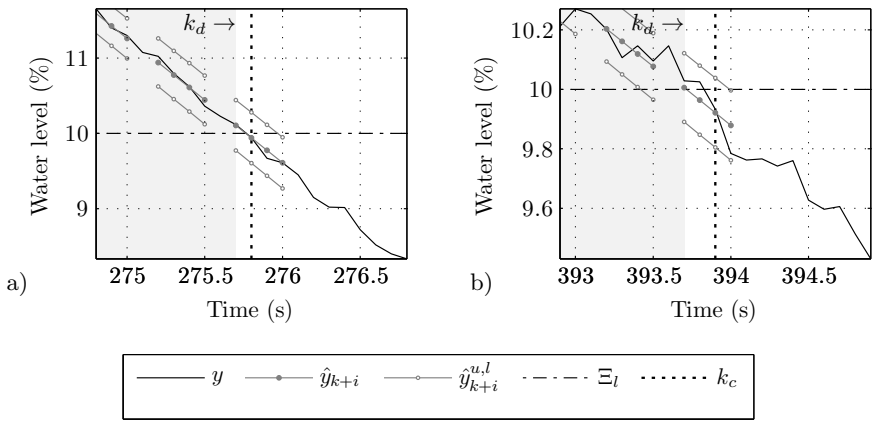

Figure 7.12: Case 1c: examples of the KF-based interval-predictions iterating over the entire prediction time-interval, $i = 0, \ldots, 3$, while approaching the SGLL trip occurrence during a) SWPI and b) PRD power transients under multi-model matching conditions with ALMF-based noise covariance estimation.

during the SWPI power transient at the time of trip. The difference in rate of change in water level is illustrated in Figure 7.4a) and 7.4b). In addition, the SWPI power transient includes discontinuous steps in water level set-point that affect the accuracy of the *a priori* KF-based measurement estimates with respect to the one-step-ahead measurement. The ALMF noise covariance estimation algorithms capture these inaccuracies as uncertainty, hence the wider bounds.

The ALMF noise covariances result in the confidence intervals of Figure 7.12 not expanding over the prediction window. This absence of expansion indicates that the state noise covariance is relatively small with respect to measurement uncertainty. The smaller value of noise covariance aids the interval-based decision-making process in reducing time-to-trip. These results can be compared directly against those of Figure 7.9 where a missed trip occurred for the PRD scenario.

Although the interval-PSDS design provides the benefit of considering a higher con-

fidence in an impending abnormal condition, the interval-based decisions tend to favour continued operation or productivity rather than safety. The interval-PSDS design also increases the rate of missed trip occurrences when compared against the point-PSDS design. The confidence intervals of the predictions do, however provide additional information about the probability, and these metrics may provide benefit to some safety-related applications given proper modelling as well as a thorough investigation regarding the selection of prediction horizon.

7.1.2.4 Case 1d: KF-based optimal-predictive shutdown

The KF-based optimal-PSDS design detects an abnormal condition by selecting an optimal prediction horizon or bias as a function of confidence in an impending measurement for a safety parameter prediction, $\hat{y}^o[k+i|k]$ where $i = 1, \ldots, N_p$, or a sensor measurement, $y[k]$, reaches the corresponding TSP, Ξ. Either an interval-prediction, upper or lower, or a point-prediction may be used, although the point-predictions are recommended since the confidence is considered through statistical testing. The selection of an optimal and effective prediction horizon or mean bias rather allows the PSDS to consider the quality of the previously calculated predictions. The optimal-PSDS then uses this information to determine the quality of the current predictions.

Although the interval-predictions allow for the confidence of an impending abnormal condition to be considered by the PSDS, the intervals are also calculated using assumed distributions, or statistics that describe the noise. The consequence of performing open-loop predictions with assumed probability distributions is that the prediction algorithm is not aware as to whether or not these distributions are accurate. Thus, at the time-step

of interval-predictive trip the PSDS could be misled into believing that the measurement belongs within the bounds of the confidence. The optimal-PSDS design instead adapts the mean bias of the confidence interval and the prediction horizon to optimal values given the past performance of the prediction algorithm.

The optimal-PSDS selects a subset of the measurement predictions from within the prediction window that are considered to be of sufficient accuracy for comparison against the TSP. If no predictions are considered of sufficient quality or accuracy, the optimal-PSDS resorts to comparing the measurement against the TSP. Thus, in this case of poor prediction quality, the optimal-PSDS design regresses to the conventional SDS design. The optimal-predictive time-to-trip is measured from the time-step of injecting the PIE to the time-step when the either the optimal-prediction or measurement reaches the TSP, i.e. the optimally predicted down-crossing of Ξ_l. The following optimal-predictions are calculated by combining the IB and NIS tests of Section 5.3.1. Predictions are considered of sufficient quality if both the IB and NIS tests are successful. In other words, if either of the tests indicates that the predictions are not accurate, the corresponding prediction is not considered within the optimal subset.

The time-steps surrounding the optimal-predictive trip detections are highlighted in Figure 7.13 for the SWPI, PRD, and SPD transients. The interval-predictive time-to-trip results for the simulated trip occurrences are 63.8s for SWPI, 181.7s for PRD, and 21.0s for trip-SPD. In addition, the non-trip condition of the nontrip-SPD scenario is correctly avoided by the optimal-PSDS design. These detailed plots illustrate the prediction that is considered to be optimal. This optimal point-prediction is connect by a horizontal line to the time-step in which the prediction was calculated. In this manner, the variations

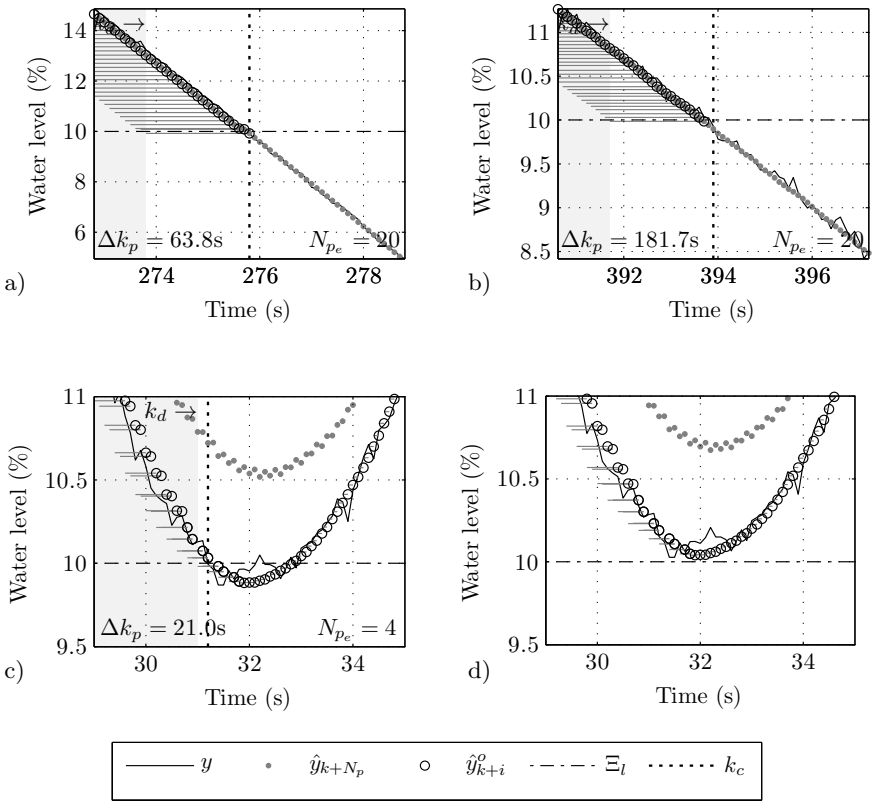

Figure 7.13: Case 1d: simulation of KF-based optimal-predictive SGLL trip occurrences due to a loss of feedwater flow PIE during a) SWPI, b) PRD, c) trip-SPD, and d) nontrip-SPD transients under multi-model matching conditions.

in effective prediction horizon is visible in the plotted results. The effective predictions horizons are also denoted in the lower right corner of the individual plots as N_{p_e}.

The optimal-predictions observed in Figure 7.13 demonstrate 2.0s and 2.2s reductions in time-to-trip during the SWPI and PRD power transients respectively. These large values for optimal prediction horizon indicate that the prediction algorithm is able to accurately predict impending measurement and potential conditions. Moreover, the model provided to the KF is likely to be accurate. The ability of the optimal-PSDS design to adapt the prediction horizon is observed in the lines that are connected to the $\hat{y}^o$ of Figure 7.13c) for the trip-SPD transient. Here, the effective prediction horizon is reduced to four time-steps

at the time of trip with only a 0.2s reduction in time-to-trip.

In utilizing point-predictions, the optimal-PSDS favours safety over continued operation. In contrast to point-prediction, however, the optimal point-prediction is not only sufficiently accurate with respect to some significance level, but this value has an upper maximum FPR or missed trip rate. The optimal-PSDS also maximizes TPR and minimizes FNR or false trip rate within the subset of selected accurate predictions. The optimal-PSDS therefore has the advantage of considering confidence in an impending measurement value without waiting for some function of the probability distribution to reach the alarm threshold or TSP.

7.1.3 PSDS Case 2: Reduced-order multi-model with parameter error

The second simulation case considers the same reduced-order multi-model matching between the simulated scaled-Irving model and the predictive models within the KFs of the PSDSs as in the first case. This case also, however, includes an erroneous parameter within the scaled-Irving model. The presence of parameter errors within the identified model simulates the real-world condition where the model of a system is inaccurate to the true system. These parameter errors are assumed to be a result of poor system identification or modelling. Parameter error may also occur under an uncertain condition whereby the parameters of the true system deviate from those that are included in the model of the PSDS. The PSDS designs are therefore modified to include the disturbance estimation and prediction error compensation algorithms of Chapter 4.

More specifically, the erroneous parameter, $G_1 = 0.029$, is assumed within the model that is provided to the KF and RLS algorithms rather than the true parameter within the steam generator system, $G_1 = 0.058$. The erroneous parameter is shared across all steam flow-rates, q_v, and is selected to be one half of the value of the nominal parameter. Parameter G_1 is the gain associated with the main integrator within the dynamic response of the system, as illustrated in (6.1). The assumed model therefore misrepresents the rate of response of the integrator component as half the rate of the true system. The modelling conditions for this case represent a relatively large uncertainty in terms of model mismatch. This uncertainty adds to the reduced-order and multi-model matching uncertainties investigated in Case 1. In regards to signal availability, all safety parameter signals including steam and feedwater flow-rate as well as steam generator water level are made available to the KF within the PSDS. This is the same signal availability assumption as for Case 1.

7.1.3.1 Case 2a: KF-based point-predictive shutdown

The time-steps surrounding the point-predictive trip detections for the uncertain case of parameter error are highlighted in the four plots of Figure 7.14 for the SWPI, PRD, trip-SPD, and nontrip-SPD transients. In the case of SWPI and PRD transients in Figure 7.14a) and Figure 7.14b) respectively, the predictions are completely erroneous. Although these results include the use of the ALMF algorithm for noise covariance estimation, the predictions do not follow the dynamic response of the measurement. This is one of the primary reasons for investigating the use of the RLS filter for disturbance input estimation.

The point-predictive trip decisions of Figure 7.14c) and Figure 7.14d) for trip-SPD and

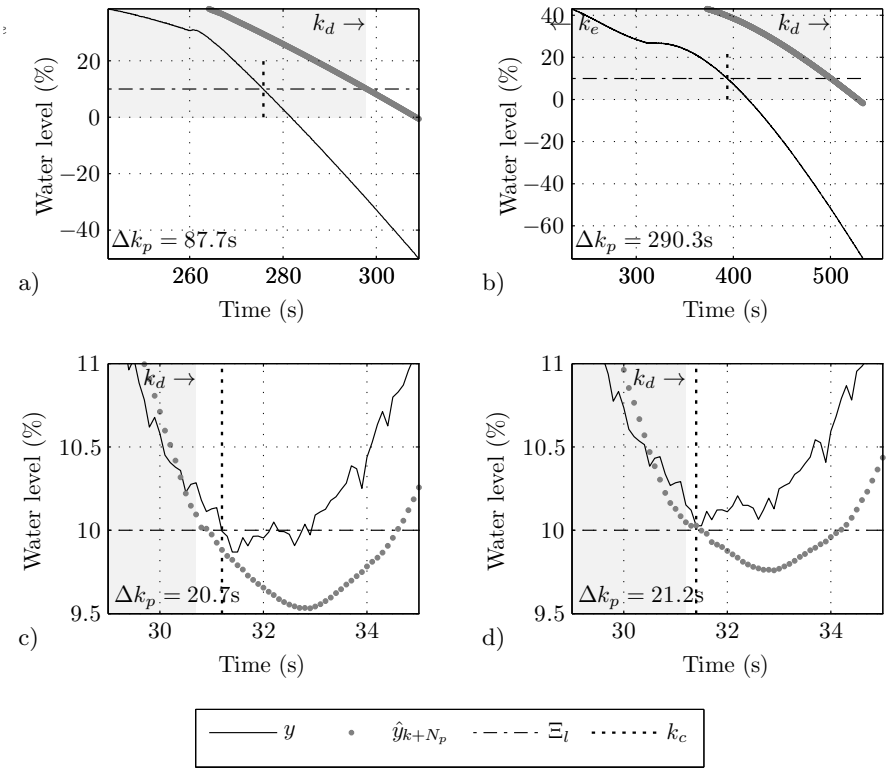

Figure 7.14: Case 2a: time-steps surrounding the simulated KF-based point-predictive SGLL trip occurrences for a) SWPI, b) PRD, c) trip-SPD, and d) nontrip-SPD under the model parameter error condition.

nontrip-SPD transients do not have as large a magnitude of error with respect to the future measurements. The point-predictive trip decision is even somewhat accurate in the case of the trip-SPD. The result is a reduction in time-to-trip equal to 0.5s. The predictive trip decision for the nontrip-SPD transient, however, results in a false or spurious trip occurrence. Thus, the point-predictions mislead the point-PSDS to activate the shutdown procedure when, in fact, the system continues to operate within the boundaries of normal operation. For accurate models and assumed statistics, it is expected that the point-predictions favour early trip conditions or safety. Under model mismatch, this property of the point-PSDS is not necessarily observed whereby the point-predictions lead to an

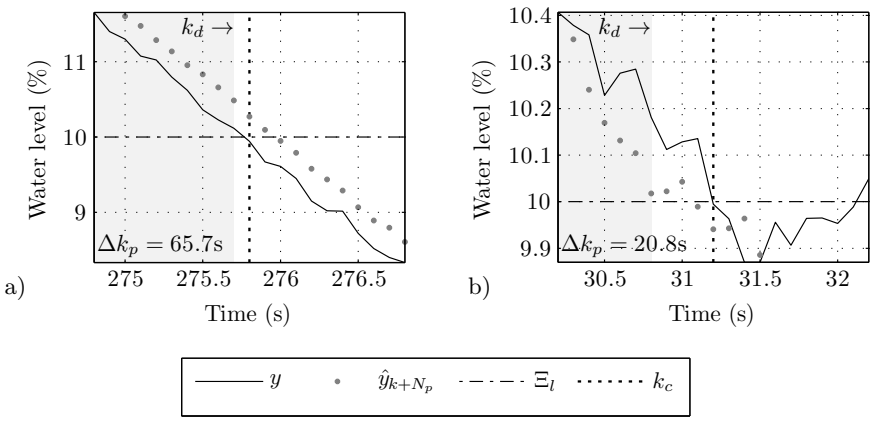

Figure 7.15: Case 2a: time-steps surrounding the simulated KF-based point-predictive SGLL trip occurrences for a) SWPI and c) trip-SPD under the model parameter error condition with only ALMF-based state noise covariance estimation and constant measurement noise covariance, $\hat{R}_y = 6.24$.

increase in either spurious or missed trip rates. Thus, under the conditions of this case, the inaccurate point predictions are detrimental to the safety critical decision making process.

One alternate idea is to force the known measurement noise covariance to be constant and to calculate the state noise covariance using the ALMF algorithm. The result is that the measurements are always considered to be of some predetermined constant uncertainty and the ALMF decides the accuracy of the assumed model as $\hat{R}_x$. The time-steps surrounding the point-predictive trip detections for the uncertain case of parameter error are highlighted in the four plots of Figure 7.15 for the SWPI and trip-SPD transients. In the case of SWPI and trip-SPD transients in Figure 7.15a) and Figure 7.15b) respectively, the measurement noise covariance remains constant, $\hat{R}_y = 6.24$, and as a result the predictions are now more accurate to the dynamic response of the measurement. In fact, the modified form of the algorithms results in time-to-trip reductions of 0.1s and 0.4s for the SWPI and trip-SPD transients respectively.

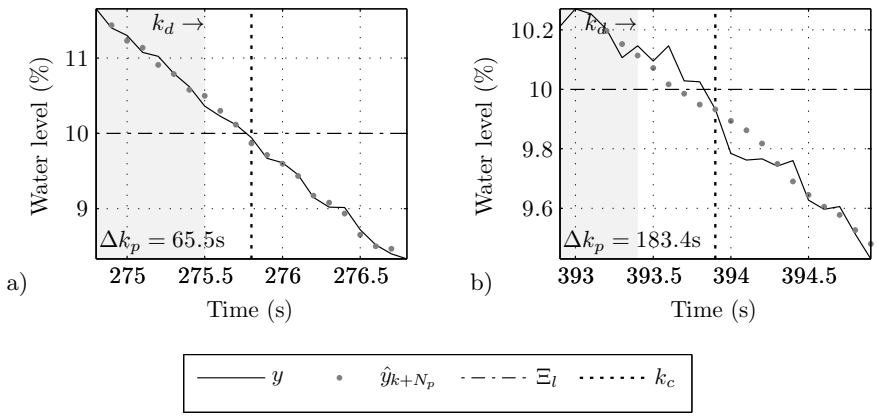

Figure 7.16: Case 2b: time-steps surrounding the simulated KF/RLS-based point-predictive SGLL trip occurrences for a) SWPI and b) PRD under the model parameter error condition.

7.1.3.2 Case 2b: KF/RLS-based point-predictive shutdown

The time-steps surrounding the point-predictive trip detections for the uncertain case of parameter error are also highlighted in the two plots of Figure 7.16 for the SWPI and PRD power transients. These point-predictions include error compensation using the RLS filter to estimate both a state and measurement disturbance input with an assumed model representing a ramp input. The prediction error compensation algorithm results in point-predictions that are more accurate than those of Figure 7.14. In fact, the KF/RLS-based point-PSDS design performs equivalently under parameter error uncertainty to the KF-based point-PSDS of Case 1. Reductions in time-to-trip of 0.3 and 0.5 are observed for SWPI and PRD transients respectively. Thus, the RLS-based disturbance estimation and prediction error compensation algorithms of Chapter 4 have been demonstrated to improve the accuracy of the multi-step-ahead predictions within these specific transients.

The time-steps surrounding the point-predictive trip detections for the uncertain case of parameter error are highlighted in Figure 7.17 for the trip-SPD transient. These point-

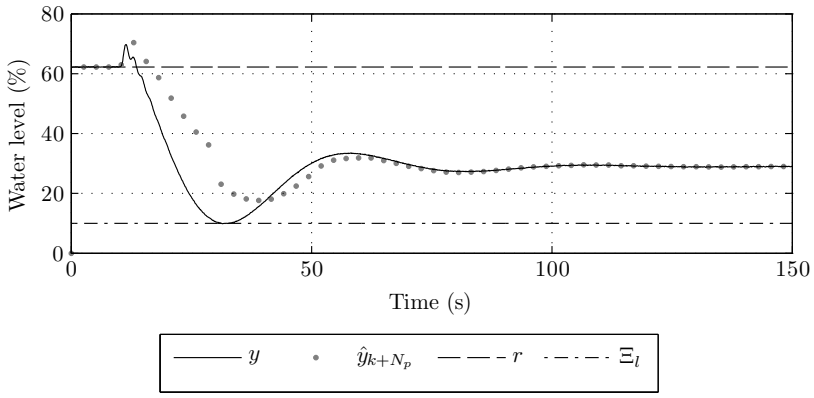

Figure 7.17: Case 2b: simulated KF/RLS-based point-predictive SGLL missed-trip occurrence during the trip-SPD transient under the model parameter error condition.

predictions also include prediction error compensation by the RLS filter to estimate both a state and measurement disturbance input with the assumed ramp input model. The RLS-based disturbance estimation algorithm is unable to compensate for both the parameter error and the disturbance in the level set-point. The result is that the point-PSDS misses the trip condition completely. In this particular case, it is not imperative that the shut-down system be activated since the system returns, relatively quickly, to normal operating conditions. This event is a missed trip occurrence, however, and reveals that there is a limit to the capabilities of the RLS-based prediction error compensation algorithm.

The RLS algorithm is only able to compensate for a subset of uncertain conditions. These are the conditions that are compatible with the predetermined disturbance model. Moreover, although the RLS algorithm provides prediction error compensation, the point-PSDS design is unaware of the predicted future measurement quality. In addition, although the RLS filter is recursive, the disturbance estimation procedure must reset periodically and therefore only considers disturbances that initiate at relatively infrequent points in time. This reset procedure is inhibited under multiple faults or failures. More specifically,

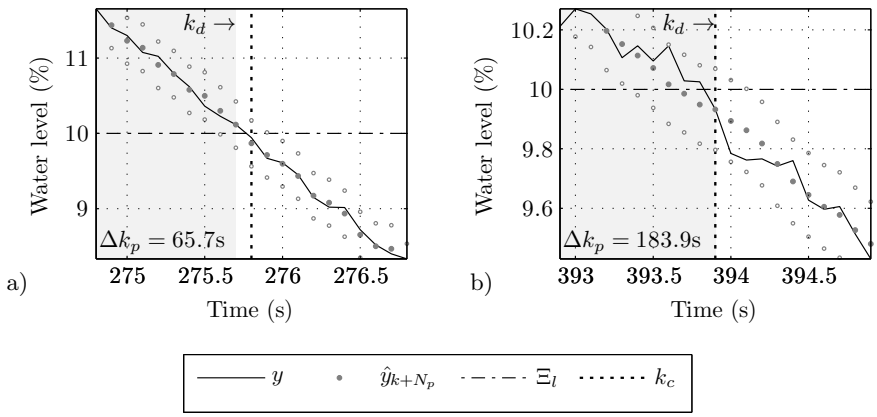

Figure 7.18: Case 2c: time-steps surrounding the simulated KF/RLS-based interval-predictive SGLL trip occurrences for a) SWPI and b) PRD under the model parameter error condition.

in the presence of multiple disturbances, or even a single incompatible disturbance, the disturbance estimates may not converge, and the assumed initial time-step of the disturbance may be prevented from being reset.

7.1.3.3 Case 2c: KF/RLS-based interval-predictive shutdown

The time-steps surrounding the interval-predictive trip detections for the uncertain case of parameter error are highlighted in the two plots of Figure 7.18 for the SWPI and PRD power transients. Simulation results for the trip- and nontrip-SPD transients are similar to those of Figure 7.17 but with the bounding confidence interval values included. These interval-predictions include error compensation using the RLS filter to estimate both a state and measurement disturbance input with assumed model. The interval-predictive decisions suffer from the same problems as the interval-predictions of Case 1. More precisely, the interval-predictions again introduce a delay in activating the shutdown procedure. The interval-predictions also therefore increase the missed trip rate.

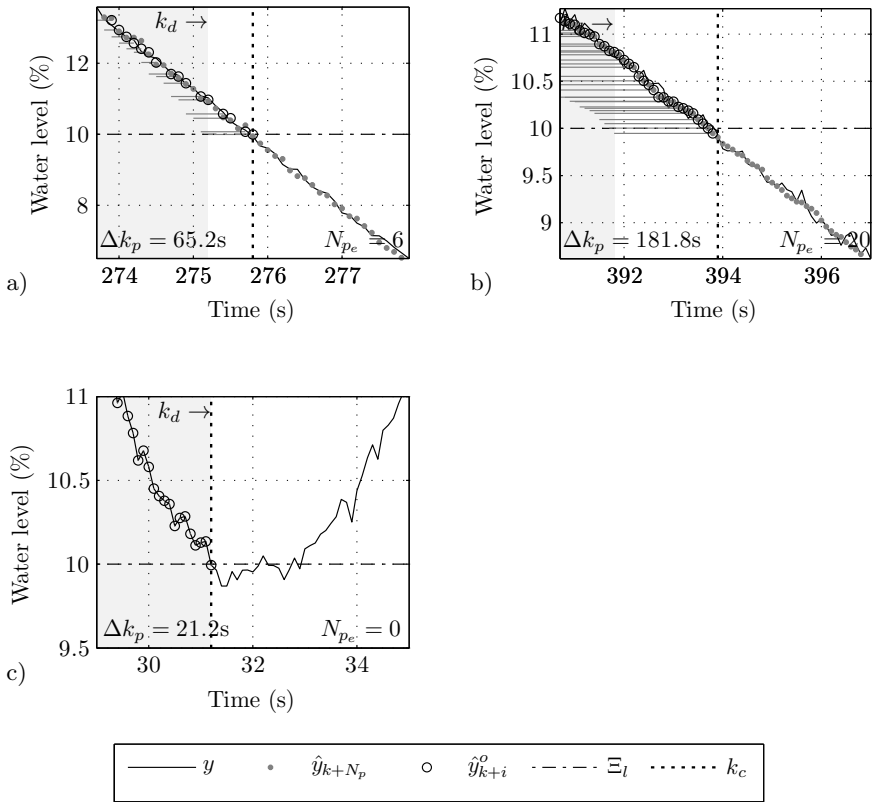

Figure 7.19: Case 2d: time-steps surrounding the simulated KF/RLS-based optimal-predictive SGLL trip occurrences for a) SWPI, b) PRD, and, c) trip-SPD under the model parameter error condition.

7.1.3.4 Case 2d: KF/RLS-based optimal-predictive shutdown

The time-steps surrounding the optimal-predictive trip detections for the uncertain case of parameter error are highlighted in the three plots of Figure 7.16 for the SWPI, PRD, and trip-SPD transients. Simulation results for the nontrip-SPD transient are similar to those of Figure 7.17. These optimal-predictions are point-predictions that have been compensated for prediction error using the RLS disturbance estimation algorithm.

In the case of the SWPI transient, the effective prediction horizon is observed to adapt from the nominal horizon of $N_p = 20$ to the effective horizon of $N_p = 6$. For the PRD

transient, the nominal horizon is maintained. Thus, each of the SWPI and PRD transients are determined to have accurate predictions within the prediction window as specified by the significance level and FPR, α. Reductions in time-to-trip of 0.7s and 2.1s are observed for the SWPI and PRD transients respectively. In contrast, the optimal-PSDS reverts to the conventional mechanism of comparing the measurement against the TSP for the trip-SPD transient. This is due to all of the predictions within the prediction window being considered of insufficient quality.

It is also possible for the optimal-predictions to include a set of possible mean biases in terms of prediction error that may satisfy the corresponding hypothesis tests. The results of Figure 7.20 consider the following set of mean biases for prediction error, $[-2, -1, 0, 1, 2]$ standard deviations from zero mean. The result is that the optimal-predictions are able to adapt an estimate of mean bias in prediction error as the result of hypothesis testing in addition to the deterministic compensation of prediction error. This is beneficial under uncertain conditions that are not able to be accurately predicted using the combination KF/RLS algorithm as well as the ALMF noise covariance estimation.

For the SWPI transient, the optimal-prediction has a mean prediction bias equal to -1 standard deviations of the prediction error at the time of optimal-predictive trip. Moreover, the optimal or effective prediction horizon for this mean prediction error is equal to the nominal full length prediction horizon, $N_p = 20$. The point-predictions are therefore determined by the statistical tests to have a mean bias that is best represented by a value other than zero. In contrast, for the PRD transient, the optimal-prediction is the nominal one of zero-mean with prediction horizon, $N_{p_e} = 20$ as included in Figure 7.19b). For the PRD transient, the mean prediction bias is observed to adapt, however, in the time-steps

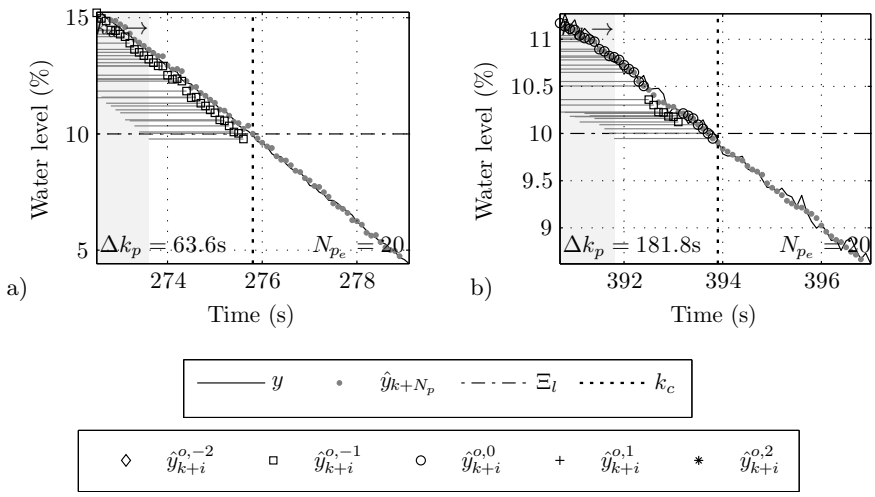

Figure 7.20: Case 2d: time-steps surrounding the simulated KF/RLS-based optimal-predictive SGLL trip occurrences for a) SWPI, b) PRD, and, c) trip-SPD under the model parameter error condition.

leading up to this optimal-predictive decision.

7.1.4 Summary

In Section 7.1.2, reduced time-to-trip is observed while utilizing the point-PSDS design and a reduced-order multi-model of the system. Reductions in time-to-trip are therefore possible given a short-term prediction horizon as well as an accurate model. The point-predictions are found to favour early trip. Under some conditions, however, the point-predictions favour continued operation when compared against conventional activation of trip. This property of the point-PSDS design is due to the filtering of noise from the measurement by the KF, hence noisy measurements may cause a trip occurrence whereas the filtered prediction may not. A comparison of the simulated time-to-trip results against benchmark conventional time-to-trip is provided in Table 7.3 for each configuration within the three simulation cases.

Table 7.3: Summary of simulation time-to-trip, k_c or k_p, and effective prediction horizon, N_{p_e}, results.
* - a false trip occurs for nontrip-SPD

	Prediction horizon, N_p (s)	Time-to-trip, $\Delta k_c \vert \Delta k_p$ $[\Delta k_p - \Delta k_c]$ (s)		
		SWPI	PRD	trip-SPD
Conventional SDS	n/a	65.8	183.9	21.2
Case 1: reduced-order multi-model				
a) KF point-PSDS	0.3	65.5 [−0.3]	183.4 [−0.5]	21.0 [−0.2]
b) KF interval-PSDS	0.3	65.6 [−0.2]	184.0 [+0.1]	no-trip
c) with ALMF	0.3	65.7 [−0.1]	183.7 [−0.2]	no-trip
d) KF optimal-PSDS	2.0	63.8 [−2.0] $N_{p_e} = 20$	181.7 [−2.2] $N_{p_e} = 20$	21.0 [−0.2] $N_{p_e} = 4$
Case 2: reduced-order multi-model with parameter error				
a) KF point-PSDS	0.3	late-trip	late-trip	20.7* [−0.5]
b) KF/RLS point-PSDS	0.3	65.5 [−0.3]	183.4 [−0.5]	no-trip
c) KF/RLS interval-PSDS	0.3	65.7 [−0.1]	183.9 [0.0]	no-trip
d) KF/RLS optimal-PSDS	2.0	65.2 [−0.7] $N_{p_e} = 6$	181.8 [−2.1] $N_{p_e} = 20$	21.2 [−0.0] $N_{p_e} = 0$

The interval-PSDS design is then investigated both with and without the ALMF noise covariance estimation algorithm. A reduction in the accuracy of the predictions with respect to the future measurements is observed for fictitious state noise covariances. In addition, expansion of the confidence interval over the prediction window is observed for larger values of state noise covariance. This expansion is in contrast to the constant width of the confidence interval for smaller covariance values. With or without the ALMF algorithm, the interval-predicted trip occurrences are observed to reduce time-to-trip by less time than the point-PSDS design. This decrease in reduction of time-to-trip is a drawback of having increased confidence in an impending abnormal condition. In some cases, the interval-predictive trip occurs after the conventional trip, i.e. an increase in time-to-trip rather than a reduction. In another case, the abnormal condition is never detected by the interval prediction. The interval-PSDS design is therefore subject to an increase in missed trip occurrences or Type I errors. Moreover, in order to reduce time-to-trip, the interval-predictions are required to be calculated further into the future than the point-predictions.

The optimal-PSDS combines the benefits of point-PSDS with the statistical assessment property of the interval-PSDS. In addition, the optimal-PSDS can consider longer prediction horizons without concern for inaccuracies to occur within the predictions of these far reaching horizons. By using the point-prediction as the metric to be compared against the TSP, the optimal-PSDS is able to match the ability of the point-PSDS to balance safety and productivity while being aware of the quality of past multi-step-ahead predictions.

The RLS disturbance estimation algorithm is able to compensate for prediction error given that the model of the disturbance is accurate. The error compensation performs best for large and consistent disturbances as mentioned in the formulation of the filter in

Chapter 4. In addition, the RLS disturbance estimation has difficulty when more than one uncertain condition is affecting the system. This problem was observed in Case 2a where the dynamic response that resulted from both parameter error and the set-point disturbance was not accurately compensated by the RLS filter.

7.2 Experimental Results

The following sections analyze the performance of a conventional SDS and the PSDS algorithms of Chapter 5 when implemented within an industry-standard safety PLC. Experiments are performed by subjecting the scaled-Irving PLS to a loss of feedwater flow PIE during each of the SWPI and PRD power transients within the experimental platform described in Chapter 6. These results provide a means for evaluating the performance of the various PSDS methods under uncertain conditions that are common to real-world prediction and forecasting problems. These results also aid in validating the simulation results of Section 7.1. The following experimental cases are investigated within this section.

- Case 1: parameter error or model mismatch, multi-model selection with ideal signal availability
- Case 2: parameter error or model mismatch, multi-model selection with unmeasured initiating event

All cases utilize the reduced-order model introduced in Section 6.6. The term unmeasured initiating event refers to a specific scenario regarding the PIE wherein the loss of feedwater flow-rate is not measured by the SDS. In Case 2, the predictive model is therefore being misled by measurements that indicate the feedwater flow-rate is either increasing or

holding steady at an erroneous flow-rate when, in actuality, the flow-rate is being reduced. The following experiments do not include the SPD transient that was investigated in the simulation results. Instead, the uncertain conditions of an unmeasured initiating event is studied in combination with the parameter error that is inherent to the experimental setup as well as most real-world applications and physical systems.

The dynamic response of the plate level is illustrated in Figure 7.21 when affected by the PIE at 200s into each of the two power transients where $\Xi_l = 10\%$ and the remaining entries are as defined in Figure 7.1. Unlike simulation, time-to-trip results for the experimental SDS include the amount of time required for signal conditioning and decision-making within the programmable electronic system. This is due to the predictions being calculated in real-time within the Tricon v9 PLC. As in the simulation, however, experimental time-to-trip results do not include the amounts of time required for relay activation and rod travel or dropping of the shut-off rods since there are no physical shutdown mechanisms included within the experimental PLS.

7.2.1 Benchmark: Conventional shutdown

Conventional SDSs trip when a safety parameter measurement, $y[k]$, reaches the corresponding TSP, Ξ_l. This is the same conventional trip procedure as for the simulations. Conventional time-to-trip is therefore measured from the time-step of injecting the PIE to the time-step when the safety parameter measurement reaches the TSP. The experimental SDS designs also utilize a hysteresis threshold to prevent deactivation of the trip sequence.

The experimental times-to-trip for conventional shutdown are 62.0s for SWPI and 86.0s

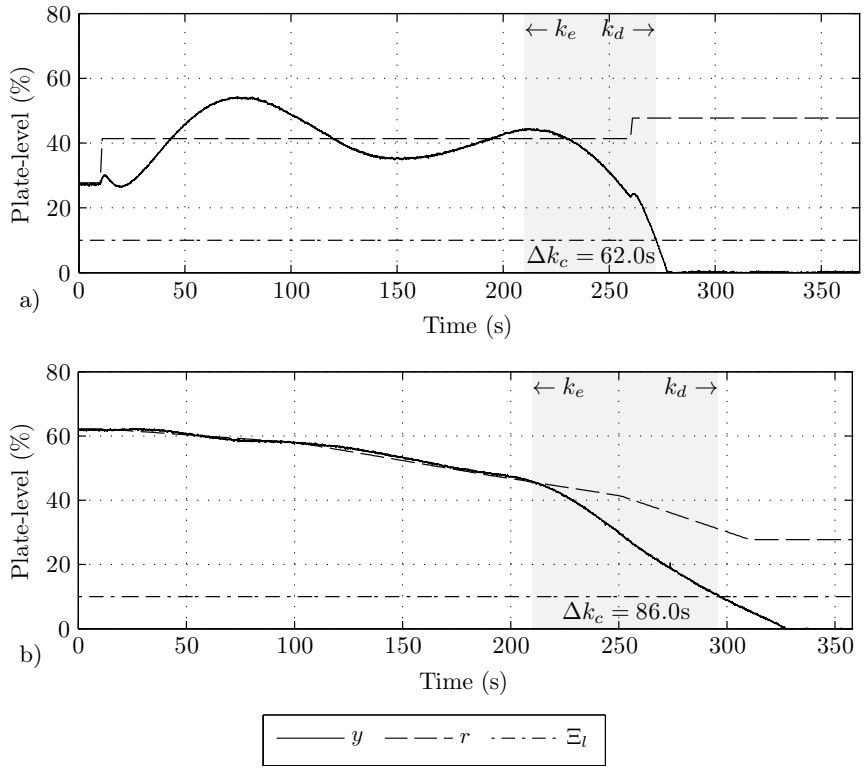

Figure 7.21: Benchmark: experimental conventional SGLL trip occurrences due to loss of feedwater flow PIE during a) SWPI and b) PRD power transients.

for PRD as plotted in Figure 7.21. These conventional time-to-trip results are the benchmarks against which the first case of experimental predictive trip detection routines are compared. Subsequent cases have similar benchmarks that are calculated for the specific instance of trip initiation as well as the dynamic response of the physical system. The reason for these separate benchmarks is the variation in the shutdown transient between successive experimental runs. In addition, it is not possible, within the current data acquisition system, to collect the decisions from each of the three PSDS designs within a single experimental iteration. The scan time for the partial SGLL implementation of conventional SDS within Tricon v9 is 22ms with a surplus of 78ms within the required 100ms interval.

7.2.2 PSDS Case 1: Reduced-order multi-model with measured PIE

This first experimental predictive shutdown case considers reduced-order multi-model matching between the simulated scaled-Irving model and the predictive models within the KFs of the various PSDS designs. As in the case of the simulations, the model parameters of the simulated system are interpolated between the operating points of Table 6.1. The modelling conditions for this case are therefore more uncertain than those of the first simulation case. This added uncertainty is the result of parameter errors in the model that is provided to the KF. These parameter errors are assumed during experimentation since the dynamic model that represents the PLS is only a mathematical abstraction of the actual system behaviour. All safety parameter signals including steam and feedwater flow-rate as well as steam generator water level are made available to the KF within the PSDS, i.e. ideal signal availability.

7.2.2.1 Case 1a: KF/RLS$_y$-based point-predictive shutdown

The KF/RLS$_y$-based point-PSDS design detects an abnormal condition when either the mean value of the safety parameter prediction, $\hat{y}\,[k+i|k]\,\forall i\,=\,1,\ldots,N_p$, or the safety parameter measurement, $y\,[k]$, reach the corresponding TSP, Ξ_l. These point-predictions include prediction error compensation using the RLS filter to estimate only a measurement disturbance input with assumed ramp input model. By only utilizing the measurement disturbance estimation algorithm, RLS$_y$, the complexity and scan times for the PSDS implementations are reduced. Point-predictive time-to-trip, Δk_p, is measured from the

time-step of injecting the PIE to the time-step when a point-prediction reaches the TSP, i.e. a point-predicted down-crossing of Ξ_l. As in the simulations, the point-PSDS design of Figure 5.3 is modified to include only predictive trip activation and not the conventional trip logic.

The time-to-trip results for experimental point-predictive shutdown are 61.4s for SWPI and 85.8s for PRD as illustrated in Figure 7.22. The point-predictions are calculated to a prediction horizon of $N_p = 5$ time-steps or 0.5s for both SWPI and PRD power transients. This prediction horizon differs from that of the simulation results in order to investigate the ability of the KF to calculate accurate prediction at various horizons. This prediction horizon is equal to two times the length of the regulated maximum time for decision making within CANDU SDS1. As in the simulation results, predictive trips occur at the time-step in that the predictions were calculated which is N_p time-steps prior to the plotted measurement predictions.

For the SWPI power transient, the point-predictive trip detection occurs two time-steps prior to the down-crossing of the measurement with Ξ_l. Point-predictive trip provides a 0.6s improvement or reduction in time-to-trip for the SWPI power transient when compared against benchmark conventional shutdown. The PRD power transient, on the other hand, provides an improvement in time-to-trip of 0.2s compared against conventional SDS results. These values of reduction are consistent with respect to the prediction horizons and also reflect the uncertainty that is inherent in the real-world experimental prediction problem.

The scan time for the SGLL implementation of predictive SDS within Tricon v9 is 67ms with a surplus of 33ms for a prediction horizon of $N_p = 5$. This scan time jumps to 85ms for the prediction horizon of $N_p = 20$. Thus, the Tricon v9 is capable of executing the KF

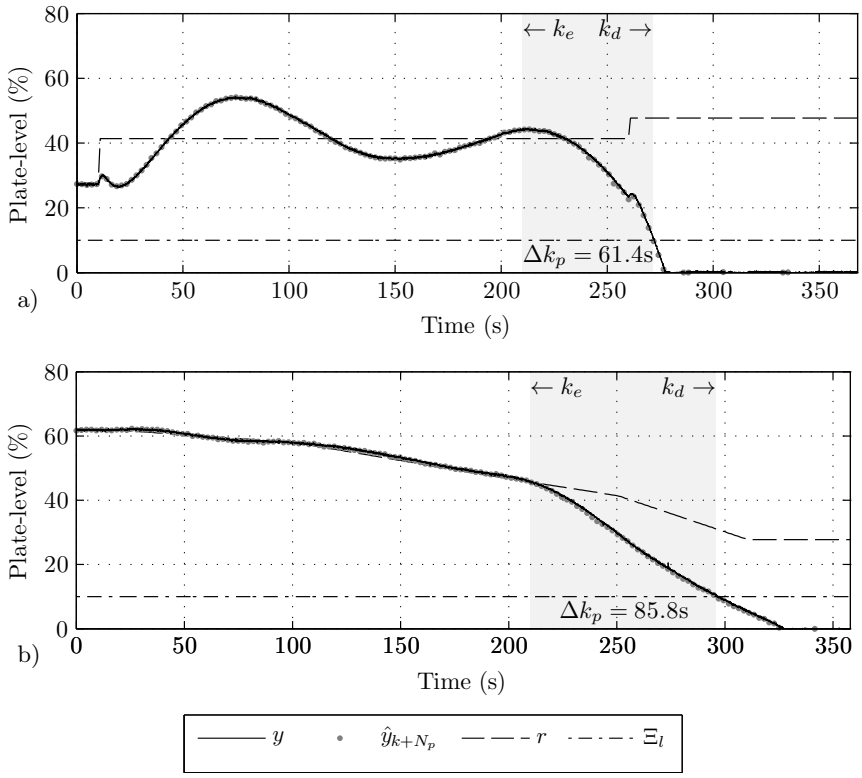

Figure 7.22: Case 1a: experimental point-predictive trip due to SGLL during power transients a) SWPI and b) PRD under model mismatch.

prediction algorithm as well as the RLS measurement disturbance estimation algorithm within the allotted 100ms time interval. Scaling this functionality up to the full set of ten or more safety parameters will, however, require a more powerful technological platform, e.g. an FPGA.

7.2.2.2 Case 1b: KF/RLS$_y$-based interval-predictive shutdown with ALMF

The KF/RLS$_y$-based interval-PSDS design incorporates the same prediction and disturbance estimation algorithms as for the point-predictive case, except that the upper bound of the interval is compared against the TSP. The time-steps surrounding the interval-predictive trip detections under the uncertain case of parameter error are highlighted in the

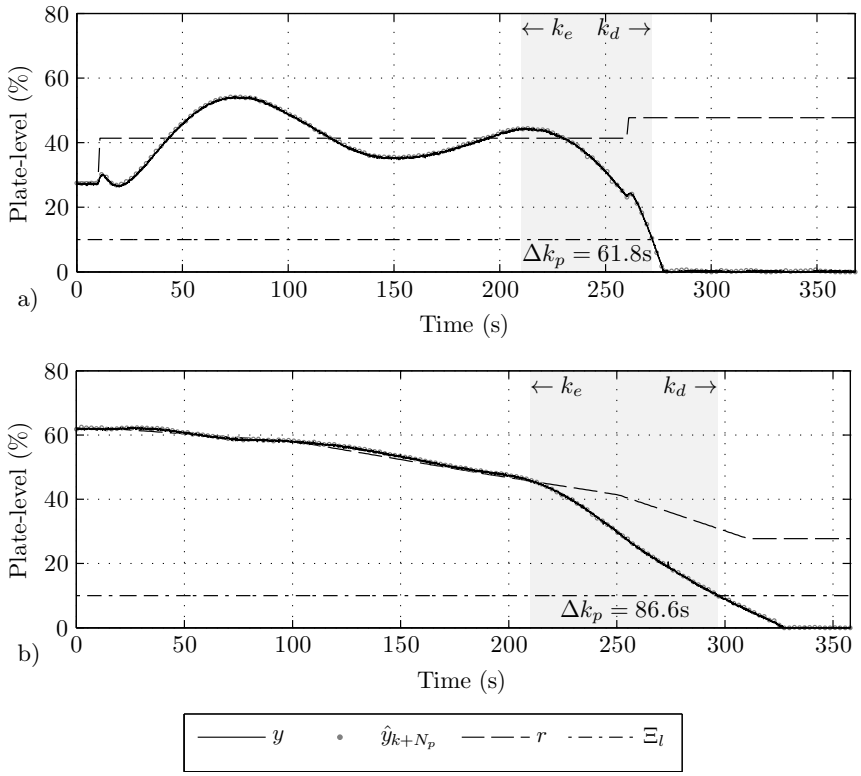

Figure 7.23: Case 1b: interval-predictive trip due to SGLL during power transients a) SWPI and b) PRD under model mismatch.

two plots of Figure 7.23 for the SWPI and PRD power transients. These interval-predictions include error compensation using the RLS filter to estimate the measurement disturbance input given an assumed model. The interval-predictions again, as in the simulation results, introduce a delay in activating the shutdown procedure. The interval-predictions also therefore increase the missed trip rate.

Interval-predictive trip provides a 0.2s improvement or reduction in time-to-trip for the SWPI power transient when compared against benchmark conventional shutdown. This time of trip is 0.4s later than for the point-predictive case. In contrast, the PRD power transient results in a missed trip occurrence with an increase in time-to-trip of 0.6s compared against conventional SDS results. In comparing this PRD result against the

point-predictive case, the error covariance for the predicted measurements is expected to be relatively wide since the change in time of trip experiences a large delay. Moreover, this large change in time-to-trip between point and interval results indicates that the error covariance for the PRD transient is also larger than that of the SWPI transient.

7.2.2.3 Case 1c: KF/RLS$_y$-based optimal-predictive shutdown

The experimental results of the optimal-PSDS design demonstrate a time-to-trip of 58.9s for SWPI and 71.3s for PRD as illustrated in Figure 7.24a) and Figure 7.24b) respectively. These are 1.3s and 0.2s less than the corresponding conventional SDS time-to-trip. The conventional SDS against which these values are compared is not the response included in Figure 7.21 but is rather another instance of the results with specific times tabulated in Table 7.4. Experimental optimal-predictions are selected using only the IB or Z test, and not the NIS test as included in the simulation results.

The effective prediction horizon, N_{p_e} for the optimal-predictions are included for SWPI and PRD transients in Figure 7.25a) and Figure 7.25b) respectively. These plots illustrate the adaptive nature of the effective prediction horizon. The predictions for the SWPI transient are accurate for large prediction horizons up to a few time-steps prior to predictive shutdown. In the case of the PRD transient, however, the effective prediction horizon is much shorter over the entire simulation.

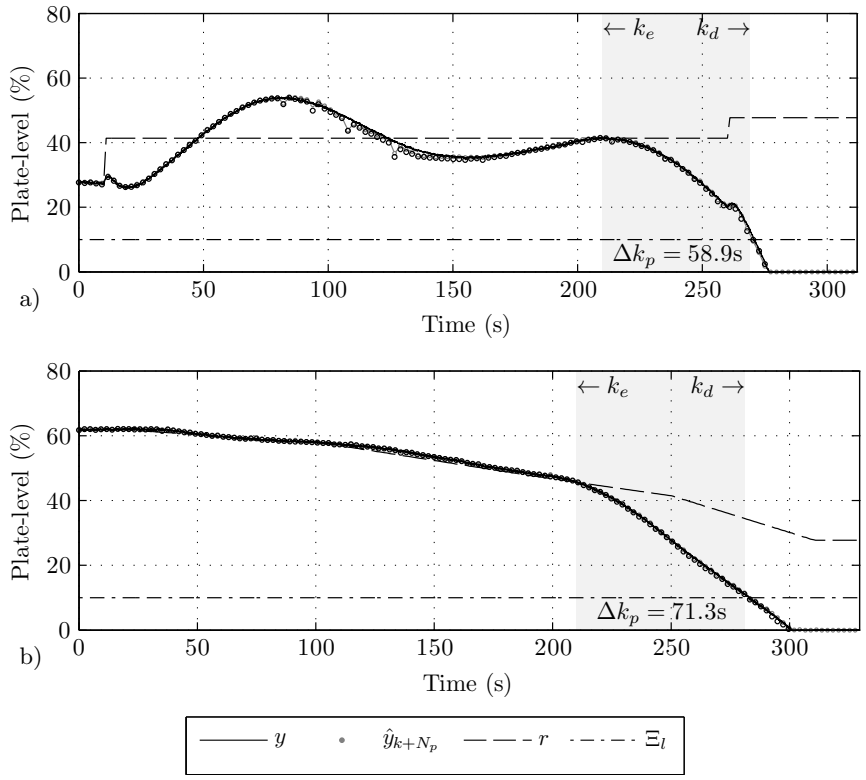

Figure 7.24: Case 1c: optimal-predictive trip due to SGLL during power transients a) SWPI and b) PRD under model mismatch.

7.2.3 PSDS Case 2: Reduced-order multi-model with unmeasured PIE

The second experimental case considers the same reduced-order multi-model matching between the simulated scaled-Irving model and the predictive models within the KFs of the PSDSs as in the first experimental case. This case also includes inaccuracies in the parameters with respect to the scaled-Irving model due to the dynamic response of the PLS not being an exact match to the scaled-Irving model. This case does not, however, include the assumption that all safety parameter signals, including steam and feedwater flow-rate as well as steam generator water level, are made available to the KF within the PSDS.

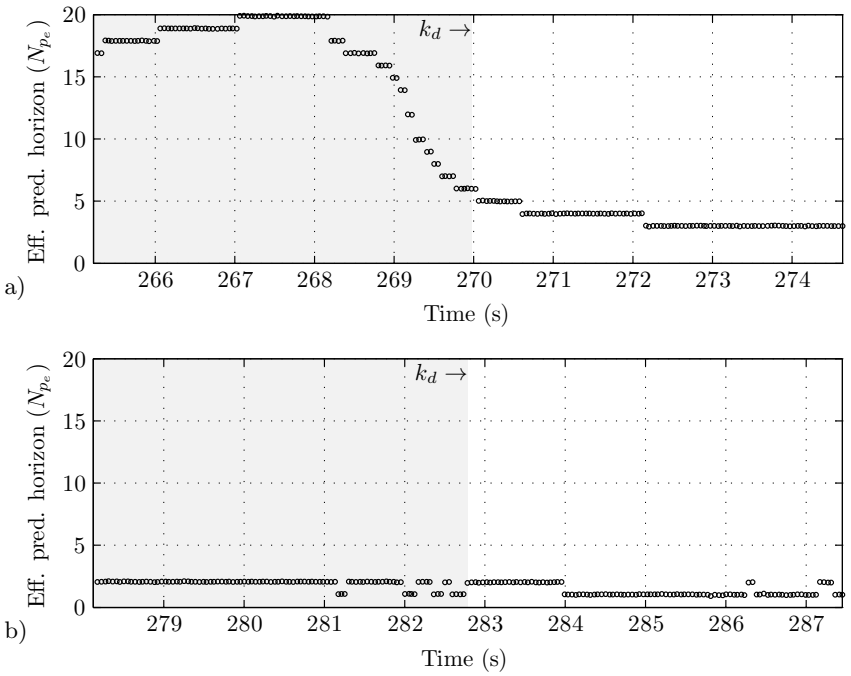

Figure 7.25: Case 1c: interval-predictive trip due to SGLL during power transients a) SWPI and b) PRD under model mismatch.

Thus, the decrease in feedwater flow-rate by 1.0%/s is an uncertain condition whereby the feedwater valve reduces flow while the manipulated variable or safety parameter for the feedwater flow-rate that is provided to the PSDS indicates that the flow is normal or increasing.

7.2.3.1 Case 2a: KF/RLS$_y$-based point-predictive shutdown

The times-to-trip for experimental point-predictive shutdown are 59.5s for SWPI and 77.3s for PRD as illustrated in Figure 7.26. These point-predictions include error compensation using the RLS filter to estimate the measurement disturbance input given an assumed model. The RLS algorithm is now compensating for both parameter error as well as the unmeasured disturbance to the system input. The point-predictions are calculated to a prediction horizon of $N_p = 5$ time-steps or 0.5s for both the SWPI and PRD power

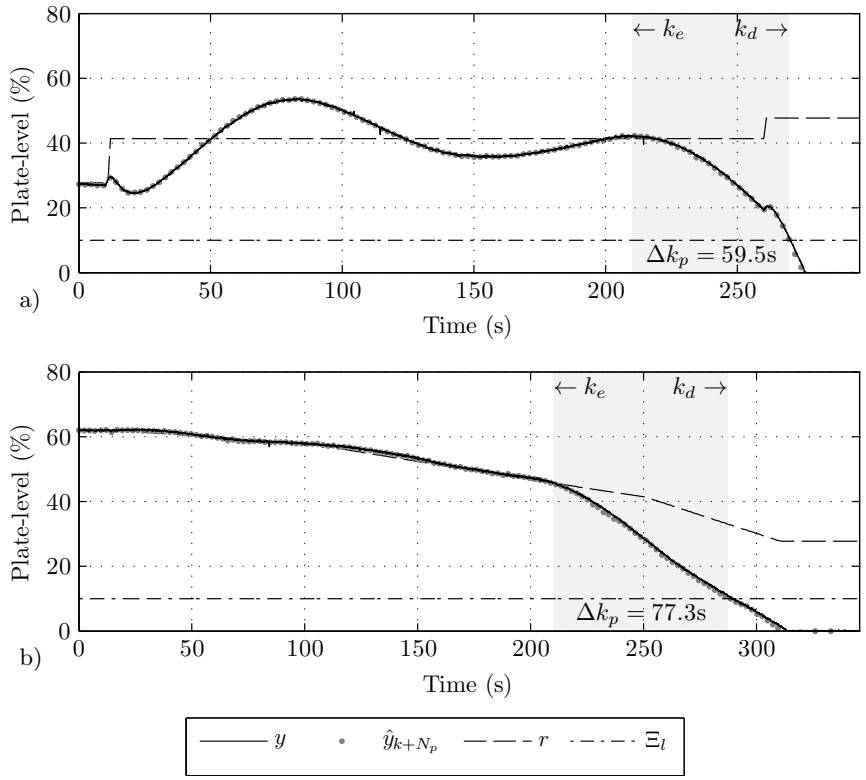

Figure 7.26: Case 2a: point-predictive trip due to SGLL during power transients a) SWPI and b) PRD under model mismatch and unmeasured initiating event.

transients. The conventional SDS against which these values are compared is also not the response included in Figure 7.21 but is rather another instance of the results as tabulated in Table 7.4.

The point-predictive trip detection occurs seven time-steps prior to the down-crossing of the measurement with Ξ_l for the SWPI power transient. Point-predictive trip therefore provides a 0.7s improvement or reduction in time-to-trip for the SWPI power transient when compared against benchmark conventional shutdown. The PRD power transient, on the other hand, provides an improvement in time-to-trip of 2.0s compared against conventional SDS results. This large value for reduction in time-to-trip for the PRD transient indicates that the KF/RLS$_y$-based point-predictions may not necessarily be accurate to

the true future measurements. The result is an early trip that may not necessarily be a true representation of the impending conditions. In other words, the RLS-based disturbance estimation overcompensates for the unmeasured disturbance in the system input.

7.2.3.2 Case 2b: KF/RLS$_y$-based interval-predictive shutdown with ALMF

The time-steps surrounding the interval-predictive trip detections for the uncertain case of parameter error are included in the two plots of Figure 7.27 for the SWPI and PRD power transients. These interval-predictions include error compensation using the RLS filter to estimate the measurement disturbance input given an assumed model. This algorithm is again compensating for both parameter error and the unmeasured initiating event, or disturbance to the system input. Moreover, the interval-predictions again introduce a delay in activating the shutdown procedure when compared against the point-predictive results. The interval-predictions also therefore increase the missed trip rate.

Interval-predictive trip provides a 0.2s improvement or reduction in time-to-trip for the SWPI power transient when compared against benchmark conventional shutdown. This time of trip occurs 0.2s later than for the point-predictive case. In contrast, the PRD power transient results in a time-to-trip that is equivalent to that of the conventional SDS case. In comparing this result against the point-predictive case, the error covariance for the predicted measurements must be relatively wide since the change in time of trip is large. Again, this large change in time-to-trip between point and interval results indicates that the error covariance for the PRD transient is also larger than that of the SWPI transient. These results demonstrate that the interval-PSDS design is able to reduce the possibility of false trip occurrences when the model provided to the KF does not necessarily represent

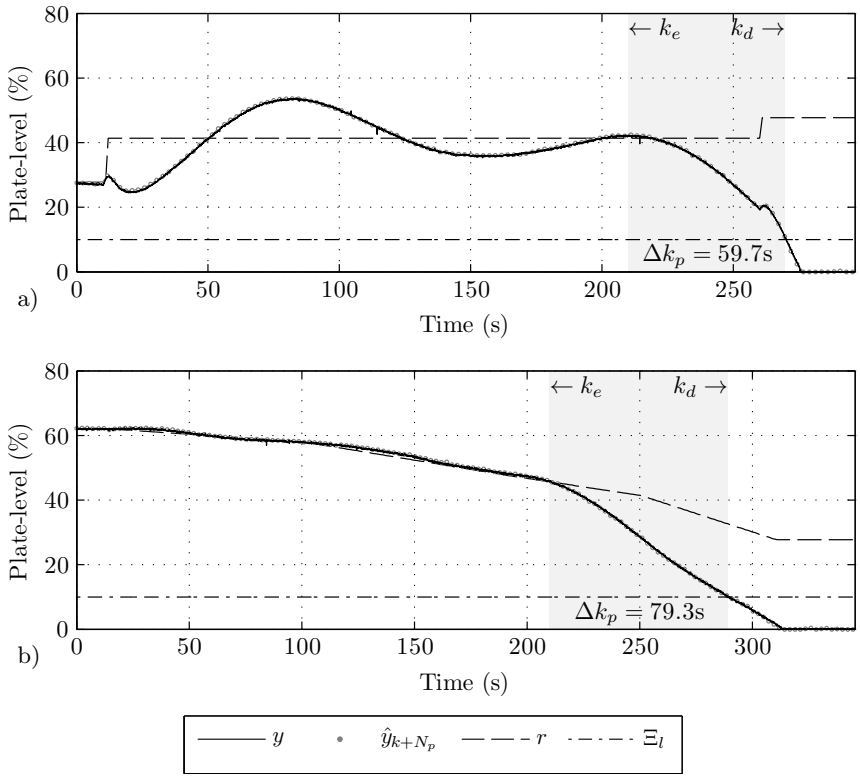

Figure 7.27: Case 2b: interval-predictive trip due to SGLL during power transients a) SWPI and b) PRD under model mismatch and unmeasured initiating event.

the true system.

7.2.3.3 Case 2c: KF/RLS$_y$-based optimal-predictive shutdown

The experimental results of the optimal-PSDS design demonstrate a time-to-trip of 60.1s for SWPI and 80.3s for PRD as illustrated in Figure 7.28a) and Figure 7.28b) respectively. For the SWPI transient, this time of trip results in a 0.3s reduction in time-to-trip in comparison to the corresponding conventional SDS time-to-trip. Moreover, the effective prediction horizon for the SWPI transient at the time of optimal-predictive shutdown is $N_{p_e} = 2$. For PRD, the time-to-trip is equivalent to that of the conventional SDS since the optimal-PSDS determines that none of the predictions are of sufficient quality to compare

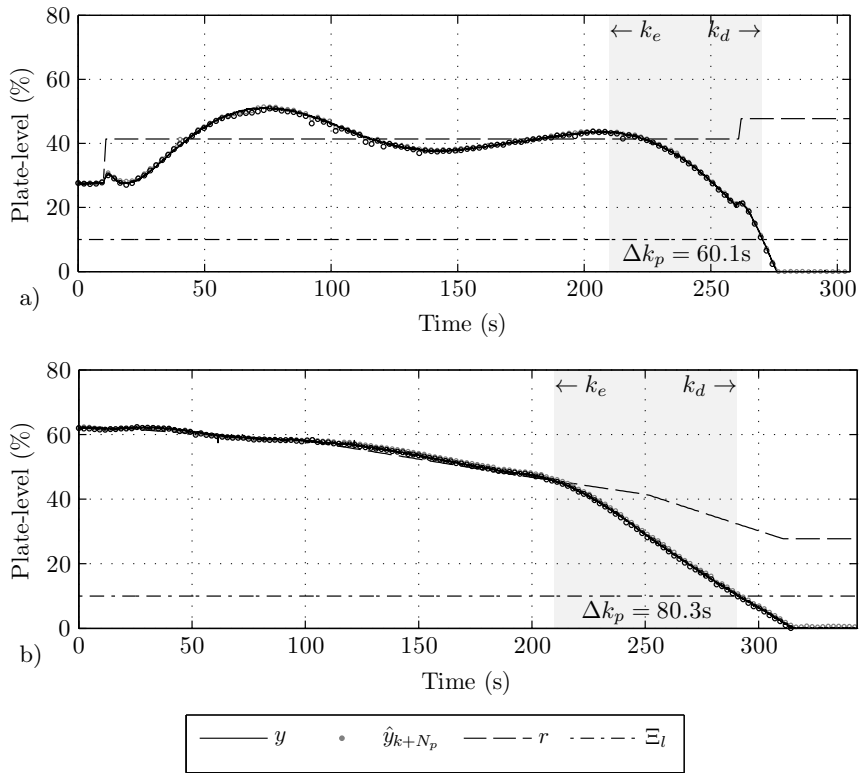

Figure 7.28: Case 2c: optimal-predictive trip due to SGLL during power transients a) SWPI and b) PRD under some model mismatch and unmeasured initiating event.

against the TSP. The conventional SDS time-to-trip results are again tabulated in Table 7.4 and are not those included in Figure 7.21.

7.2.4 Summary

The proposed PSDS designs have been successfully implemented in an industry standard safety PLC with a scan time that meets current requirements. The results of this section demonstrate through experiment that, given a short-term prediction horizon and low uncertainty in the model provided to the KF as well as low uncertainty in future system inputs, all of the proposed PSDS designs are able to achieve a reduced time-to-trip. These reductions in time-to-trip are summarized for the experimental results in Table 7.4.

Table 7.4: Summary of experimental time-to-trip and effective prediction horizon results.

	Prediction horizon,	Time-to-trip, $\Delta k_c, \Delta k_p$ $[\Delta k_p - \Delta k_c]$ (s)	
	N_p (s)	SWPI	PRD
Case 1: reduced-order multi-model			
Conventional SDS	n/a	62.0	86.0
a) KF/RLS$_y$ point-PSDS	0.5	61.4 [−0.6]	85.8 [−0.2]
b) KF/RLS$_y$ interval-PSDS	0.5	61.8 [−0.2]	86.6 [+0.6]
Case 1 continued: optimal-PSDS			
Conventional SDS	n/a	60.2	72.8
c) KF/RLS$_y$ optimal-PSDS	2.0	58.9 [−1.3] $N_{p_e} = 6$	85.8 [−0.2] $N_{p_e} = 2$
Case 2: reduced-order multi-model with unmeasured PIE			
Conventional SDS	n/a	59.9	79.3
a) KF/RLS$_y$ point-PSDS	0.5	59.5 [−0.4]	77.3 [−2.0]
b) KF/RLS$_y$ interval-PSDS	0.5	59.7 [−0.2]	79.3 [0.0]
Case 2 continued: optimal-PSDS			
Conventional SDS	n/a	60.4	80.3
c) KF/RLS$_y$ optimal-PSDS	2.0	60.1 [−0.3] $N_{p_e} = 2$	80.3 [0.0] $N_{p_e} = 2$

In Case 1, under real-world model mismatch, the point predictive algorithm achieves a reduction in time-to-trip. This is similar to the simulation case with model mismatch, except that the reductions in time-to-trip are not as consistent to the prediction horizon as in the simulation case. Moreover, the interval-PSDS is again seen to cause a delay in the trip decision-making process.

Case 2 reveals that it is necessary to asses the quality of the predictor within the PSDS. The point- and interval-PSDS designs become less capable of achieving a reduced time-to-trip as the conditions under which the system is operating deviate from the true system, environmental, and signal conditions. The optimal-PSDS, however, is able to adapt certain properties of the predictor based on the quality of the calculated predictions. It is therefore possible, through the use of the optimal-PSDS, to ensure that the predictions which are compared against an alarm threshold or TSP are, in fact, accurate to the actual impending conditions and dynamic response of the system.

Chapter 8

Conclusions and Recommendations

This dissertation presents the development of predictive shutdown logic as PSDS designs for use as an automatic protection system within an NPP. The developed prediction algorithm utilizes the update and predict stages of KF-based state estimation. In this manner, the prediction algorithm has knowledge of an assumed model of the system being protected as well as uncertainties within the modelled system parameters and signals.

The prediction algorithm is enhanced to take into consideration time-varying model parameters and noise characteristics. These two enhancements are achieved by incorporating ALMF noise covariance estimation as well as LS disturbance input estimation. A recursive solution to the LS disturbance estimation problem is also formulated within this work. The PSDS is then further enhanced to assess the quality of previously calculated multi-step-ahead predictions through the use of statistical and hypothesis testing as well as optimal alarm theory. By assessing prediction quality, the prediction algorithm is able to adapt the effective prediction horizon in order to optimize the predictive trip decisions

with respect to false and missed trip rates. The algorithm may also be extended to consider the mean bias in the prediction error and/or other statistical parameters that can be tested via statistical testing.

There are three PSDS designs developed within this work. Each design is a modular extension of the conventional logic within an existing SDS, e.g. CANDU SDS1. The first design is the point-PSDS which calculates point-predictions and then compares the predictions against an alarm threshold or TSP. Although the KF-based point-PSDS is able to reduce time-to-trip, the KF-based prediction algorithm suffers from the inability to respond to uncertain conditions during the transient to an abnormal condition. For this reason, an ALMF-based noise covariance estimation algorithm is implemented alongside the KF in order to take into consideration changes in the stochastic uncertainties that are provided to the KF. Moreover, RLS-based estimation of disturbances within both the state and measurement equations is also be implemented alongside the KF in order to compensate for prediction errors that are deterministic. The result is a KF/RLS-based PSDS that can respond to a predetermined set of deterministic and stochastic uncertainty conditions. The ultimate aim of the point-PSDS design is to calculate accurate predictions at short prediction horizons. That said, the longer the prediction horizon, the less accurate the predictions and predictive trip decisions may become.

Due to the preemptive nature of predictive trip, predictive trip decisions that are inaccurate generally result in false trip occurrences, i.e. a predicted abnormal condition does not eventually occur. Increase false trip occurrences, in turn, affect the productivity of the system being protected. The functionality of the point-PSDS design is therefore extended within the interval-PSDS design in order to counteract an increase in false trip rate.

The interval-PSDS design calculates interval-predictions and compares either the upper or lower bound of the confidence interval against a low or high TSP respectively. In this manner, predictive decisions are made when there is a predetermined and increased level of confidence in the impending abnormal conditions with respect to some predetermined alarm threshold or TSP. Although the interval-PSDS makes decisions with increased confidence, the interval-based decisions are delayed when compared against the point-predictive design. In some cases, the interval-PSDS may even miss a trip event entirely. This increase in missed trip rate is opposite to that of the point-PSDS design. The KF-based interval-PSDS suffers from the same inability to respond to uncertain conditions during transient to an abnormal condition as the point-SDS. The interval-PSDS is also, therefore, combined with the ALMF noise covariance estimation and RLS-based disturbance estimation and prediction error compensation algorithms.

The point- and interval-PSDS designs are able to make accurate predictive trip decisions given that the prior knowledge provided to the algorithm is a true representation of the actual system, environment, and signals. That said, this knowledge is often assumed, may not necessarily be accurate, and may result in an increase in false or missed trip rate Thus, PSDS functionality is again extended to consider prediction accuracy. The final optimal-PSDS design can compare either the point-predictions or the bounds of the interval-predictions against a TSP. The optimal-PSDS also, however, utilizes statistical tests to assess the quality of previously calculated safety parameter measurements. A subset of the time-steps within the prediction horizon are identified as being of sufficient quality with respect to a significance level. In addition, the optimal-PSDS may also consider a set of mean prediction error values to be compared against the TSP instead of the point-

prediction. The optimal prediction metric, either point-prediction, interval-prediction, or mean prediction error is selected by maximizing the TPR and minimizing the corresponding FNR. Thus, the optimal-PSDS design limits the maximum probability of false positive predictive trip decisions. These false positives are known as missed trip occurrences. The optimal-PSDS design also minimizes the probability of false negative trip decisions, referred to as false trip occurrences. This functionality is preferred over both of the point- and interval-PSDS designs due to the prediction algorithm being aware of prediction quality, and the predictions not being delayed to achieve a certain level of confidence.

This dissertation includes analysis simulation results as well as experiment using a Tricon v9 safety PLC. The results demonstrate that each of the proposed PSDS reduce time-to-trip when compared against a benchmark conventional SDS. This reduction in time-to-trip subsequently reduces the potential for a high power surge to cause damage to the reactor core and other critical components. In other words, predictive shutdown results in negative reactivity being inserted into the reactor core earlier than conventional SDSs under the conditions that the system model and related uncertainty descriptions are accurate to the true conditions of the system.

Through the use of KF-based measurement prediction and RLS-based disturbance estimation, the SDS now incorporates additional prior information so that the SDS can make proactive decisions prior to conventional trip decisions. Further, the proposed KF/RLS-based trip detection algorithm overcomes the fundamental limitations which restrict the potential benefits of conventional SDSs. The interval-PSDS design also provides the ability to make a trip decision given a certain level of confidence in an impending abnormal condition. Moreover, the optimal-PSDS design is able to adapt the effective prediction horizon

and mean prediction bias as a function of true and false positive and negative events. In other words, the decision-making mechanism within the optimal-PSDS selects a predictive value that is optimal with respect to minimizing false and missed trip occurrences. The optimal-PSDS design is also the only PSDS design whereby the prediction algorithm makes a predictive decision that considers the accuracy or quality of the previously predicted multi-step-ahead safety parameter measurements.

8.1 Recommended future work

This dissertation presents the foundations for enhancing a NPP SDS to make predictive decisions. These predictive decisions have been demonstrated for a single safety parameter within SDS1 of a CANDU NPP. It is expected that scaling the proposed prediction algorithms to the entire SDS1 safety parameter set will require the use of a more computationally powerful industrial controller, e.g. an FPGA. In addition, the dynamic response of the neutronics within the reactor core may require the use of nonlinear models and non-Gaussian probability distributions. It is expected that the EKF, UKF, and particle filters may be of use in predicting these increasingly complex dynamic responses. It is also recommended that the LOCA rather than the loss of secondary side feedwater PIE be investigated with respect to predictive shutdown. This recommendation is due to the fact that LOCA PIEs have the largest peak response in safety parameter measurement and therefore establish the limiting criteria for SDS response time.

This dissertation also presents a recursive solution to the LS disturbance estimation problem. The disturbance estimation is not entirely recursive, however, due to the inclu-

sion of an initiating time-step for the assumed disturbance. It is possible to formulate a fully recursive implementation that has a rolling initial time-step of disturbance for various disturbance profiles. These profiles and the fully recursive formulation of RLS-based disturbance estimation are therefore suggested for future study. In contrast, this work makes use of a dual alternating configuration for disturbance estimation. In order to switch between the two RLS filters, a switching function is established which detects the convergence of parameter error compensation to the current mean error. A complete analysis of these switching functions and the development of a more suitable approach to switching between the two estimators are recommended. Moreover, it is recommended that a future study investigate the ability of the disturbance profile for the additive disturbances to be accurate under non-additive parameter error disturbances. When implementing the RLS disturbance estimation algorithm, it is essential that the expected disturbances are compatible with the chosen disturbance profile. It is also the case that the predictive shutdown will provide various model- and data-based metrics and time-series that may be useful in alarm management and operator indication although these aspects of prediction are considered beyond the scope of this dissertation work.

Bibliography

[1] "Safety of nuclear power plants: Design," IAEA, Safety Standards SSR-2/1, 2012.

[2] US-NRC, *NRC: Glossary*, 2015.

[3] T. Wellock, "Putting the axe to the 'SCRAM' myth," http://public-blog.nrc-gateway.gov/2011/05/17/putting-the-axe-to-the-scram-myth/, May 2011.

[4] ——, "Refresh — Putting the axe to the 'SCRAM' myth," https://public-blog.nrc-gateway.gov/2016/02/18/refresh-putting-the-axe-to-the-scram-myth/, Feb. 2016.

[5] "Digital instrumentation and control systems in nuclear power plants: Safety and reliability issues," National Academy Press, Tech. Rep., 1997.

[6] L. Marshall-Libby, *The Uranium People*. New York: Crane, Russak & Co. Charles Scribner's Sons., 1979.

[7] G. Bereznai, "Nuclear power plant systems and operation," *University of Ontario Institute of Technology, Oshawa*, Jul. 2005.

[8] "Modern instrumentation and control for nuclear power plants: A guidebook," IAEA, Technical Report Series 387, 1999.

[9] "Safety related instrumentation and control systems for nuclear power plants: A safety guide," IAEA, Safety Series 50-SG-D8, 1984.

[10] "Safety Glossary: Terminology used in nuclear safety and radiation protection," IAEA, Tech. Rep. 2007 EDITION, Jun. 2007.

[11] E. Fermi, "Experimental production of a divergent chain reaction," Tech. Rep., Oct. 1952.

[12] J. Cockrell and C. Ricker, "Variation of the trip point in the ORNL type safety system," *Electrical Engineering*, vol. 78, no. 1, pp. 54–58, 1959.

[13] D. Craigen, S. Gerhart, and T. Ralston, "Case study: Darlington nuclear generating station [software-driven shutdown systems]," *IEEE Software*, vol. 11, no. 1, pp. 30–32, 1994.

[14] "Basic safety principles for nuclear power plant 75-INSAG-3 Rev. 1," IAEA, INSAG 12, Oct. 1989.

[15] J. Lisboa, "Defense-in-depth concept for nuclear power plant normal plant control systems using probability analysis," *Nuclear Science, IEEE Transactions on*, vol. 36, no. 1, pp. 1284–1290, 1989.

[16] J. She, "Investigation on the benefits of safety margin improvement in CANDU nuclear power plant using an FPGA-based shutdown system," Ph.D. dissertation, University of Western Ontario, 2012.

[17] A. Andrashov, V. Kharchenko, V. Sklyar, L. Reva, V. Dovgopolyi, and V. Golovir, "Verification of FPGA electronic designs for nuclear reactor trip systems: Test-and invariant-based methods," in *Design & Test Symposium (EWDTS), 2010 East-West*. IEEE, 2010, pp. 92–97.

[18] P. McNelles and L. Lu, "A review of the current state of FPGA Systems in nuclear instrumentation and control," in *21st International Conference on Nuclear Engineering*. American Society of Mechanical Engineers, 2013, pp. V006T16A057–V006T16A057.

[19] J. M. Harrer and J. G. Beckerley, "Nuclear power reactor instrumentation systems handbook. Volume 2," Argonne National Lab., Ill.(USA); USAEC, Washington, DC, Tech. Rep., 1974.

[20] "The role of instrumentation and control systems in power uprating projects for nuclear power plants," IAEA, Nuclear Energy Series NP-T-1.3, 2008.

[21] C. J. Lee, S. M. Baek, and S. J. Lee, "Setpoint methodology improvement considering beyond design basis events for safety-related instrumentation," *Nuclear Science, IEEE Transactions on*, vol. 61, no. 4, pp. 2120–2130, 2014, .

[22] "Implications of power uprates on safety margins of nuclear power plants," IAEA, TECDOC 1418, Sep. 2004.

[23] A. Sachs, "A classification of the Babylonian astronomical tablets of the Seleucid period," *Journal of Cuneiform Studies*, vol. 2, no. 4, pp. 271–290, 1948.

[24] S. Haykin, *Adaptive Filter Theory*, 4th ed., ser. Prentice Hall Information and System Sciences. Prentice Hall, 2002.

[25] C. F. Gauss, *Theoria Motus Corporum Coelestium in Sectionibus Conicis Solem Ambientium Auctore Carolo Friderico Gauss*. sumtibus Frid. Perthes et IH Besser, 1809.

[26] A. Legendre, "Methode de moindres quarres, pour trouver le milieu de plus probable entre les resultats des differentes obvservations," *Memoires Institute de France*, pp. 149–154, 1810.

[27] R. E. Kalman, "A new approach to linear filtering and prediction problems," *Journal of Basic Engineering*, vol. 82, no. 1, pp. 35–45, 1960, .

[28] M. V. Kothare, B. Mettler, M. Morari, P. Bendotti, and C.-M. Falinower, "Level control in the steam generator of a nuclear power plant," *Control Systems Technology, IEEE Transactions on*, vol. 8, no. 1, pp. 55–69, 2000.

[29] A. K. Jardine, D. Lin, and D. Banjevic, "A review on machinery diagnostics and prognostics implementing condition-based maintenance," *Mechanical Systems and Signal Processing*, vol. 20, no. 7, pp. 1483–1510, 2006.

[30] J. Ma and J. Jiang, "Applications of fault detection and diagnosis methods in nuclear power plants: A review," *Progress in Nuclear Energy*, vol. 53, no. 3, pp. 255–266, 2011.

[31] "Advanced surveillance, diagnostic and prognostic techniques in monitoring structures, systems and components in nuclear power plants," IAEA, Nuclear Energy Series NP-T-3.14, 2013.

[32] "Modernization of instrumentation and control in nuclear power plants," IAEA, TECDOC 1016, May 1998.

[33] "Managing modernization of nuclear power plant instrumentation and control systems," IAEA, TECDOC 1389, Feb. 2004.

[34] T. Gandhi and M. M. Trivedi, "Pedestrian collision avoidance systems: A survey of computer vision based recent studies," in *Intelligent Transportation Systems Conference*. IEEE, 2006, pp. 976–981.

[35] V. G. Snell, "Nuclear reactor safety design," 2009.

[36] "Operational limits and conditions and operating procedures for nuclear power plants," IAEA, Safety Standards Series NS-G-2.2, 2000.

[37] C. Bailey, R. Fournier, and F. Laratta, *Regional Overpower Protection in CANDU Power Reactors*. Mississauga, Ont.: Atomic Energy of Canada Limited, CANDU Operations, 1982.

[38] J. Peevers, "Bruce Power has been one of lowest-cost energy providers in Ontario in 2016," http://www.brucepower.com/low-cost-energy-in-2016/, 2016.

[39] C. J. Lee, S. Han, J. H. Yun, and S. M. Baek, "Response time evaluation for the plant protection system using a combined technique of analysis and test," in *Transactions of the Korean Nuclear Society Autumn Meeting*, Gyeongju, Korea, 2015.

[40] B. C. Juricek, D. E. Seborg, and W. E. Larimore, "Predictive monitoring for abnormal situation management," *Journal of Process Control*, vol. 11, no. 2, pp. 111–128, 2001.

[41] R. A. Martin, "A state-space approach to optimal level-crossing prediction for linear Gaussian processes," *Information Theory, IEEE Transactions on*, vol. 56, no. 10, pp. 5083–5096, 2010.

[42] N. A. Gershenfeld and A. S. Weigend, "The future of time series: Learning and understanding," in *Times Series Prediction: Forecasting the Future and Understanding the Past*, N. A. Gershenfeld and A. S. Weigend, Eds. Reading, MA: Addison-Wesley, 1993.

[43] G. C. Goodwin and K. S. Sin, *Adaptive Filtering Prediction and Control*. Englewood Cliffs, NJ: Prentice-Hall, 1984.

[44] B. D. Anderson and J. B. Moore, *Optimal Filtering*, T. Kailath, Ed. Englewood Cliffs, NJ: Prentice-Hall, Inc., 1979.

[45] A. H. Sayed, *Fundamentals of Adaptive Filtering*. John Wiley & Sons, 2003.

[46] R. G. Brown and P. Y. C. Hwang, *Introduction to Random Signals and Applied Kalman Filtering: With MATLAB Exercises and Solutions*. John Wiley & Sons, Inc, 1997.

[47] M. S. Grewal and A. P. Andrews, *Kalman Filtering Theory and Practice Using MATLAB*. John Wiley & Sons, Inc, 2008.

[48] A. Kolgomorov, "Sur l'interpolation et extrapolation des suites stationaries," *Comptes Rendus de l'académie des Sciences, Paris*, vol. 208, pp. 2043–2045, 1939.

[49] M. Krein, "On a problem of extrapolation of AN Kolmogorov," in *Dokl. Akad. Nauk SSSR*, vol. 46, 1945, p. 376.

[50] N. Wiener and E. Hopf, "On a class of singular integral equations," *Proceedings Prussian Academy Math.-Phys. Ser.*, p. 696, 1931.

[51] N. Wiener, *Extrapolation, Interpolation, and Smoothing of Stationary Time Series*. MIT Press Cambridge, 1949, vol. 2.

[52] N. Levinson, "The Wiener (root mean square) error criterion in filter design and prediction," *Journal of Mathematics and Physics*, vol. 25, no. 1, pp. 261–278, 1946.

[53] H. Wold, *A Study in the Analisys of Stationery: Time Series*. Almqvist & Wiksells Boktryckeri, 1938.

[54] R. E. Kalman and R. S. Bucy, "New results in linear filtering and prediction theory," *Journal of Basic Engineering*, vol. 83, no. 1, pp. 95–108, 1961.

[55] B. Friedland, "Treatment of bias in recursive filtering," *Automatic Control, IEEE Transactions on*, vol. 14, no. 4, pp. 359–367, 1969.

[56] T. Kailath, "An innovations approach to least-squares estimation–Part I: Linear filtering in additive white noise," *Automatic Control, IEEE Transactions on*, vol. 13, no. 6, pp. 646–655, 1968.

[57] ——, "The innovations approach to detection and estimation theory," *Proceedings of the IEEE*, vol. 58, no. 5, pp. 680–695, 1970.

[58] T. Kailath and R. Geesey, "An innovations approach to least-squares estimation–Part V: Innovations representations and recursive estimation in colored noise," *Automatic Control, IEEE Transactions on*, vol. 18, no. 5, pp. 435–453, 1973.

[59] H. W. Bode and C. E. Shannon, "A simplified derivation of linear least square smoothing and prediction theory," *Proceedings of the IRE*, vol. 38, no. 4, pp. 417–425, 1950.

[60] F. Daum, "Nonlinear filters: Beyond the Kalman filter," *IEEE Aerospace and Electronic Systems Magazine*, vol. 20, no. 8, pp. 57–69, 2005.

[61] G. L. Smith, S. F. Schmidt, and L. A. McGee, "Application of statistical filter theory to the optimal estimation of position and velocity on board a circumlunar vehicle," National Aeronautics and Space Administration, Tech. Rep., 1962.

[62] R. E. Kopp and R. J. Orford, "Linear regression applied to system identification for adaptive control systems," *AIAA Journal*, vol. 1, no. 10, pp. 2300–2306, 1963.

[63] H. Cox, "On the estimation of state variables and parameters for noisy dynamic systems," *Automatic Control, IEEE Transactions on*, vol. 9, no. 1, pp. 5–12, 1964.

[64] M. Athans, R. Wishner, and A. Bertolini, "Suboptimal state estimation for continuous-time nonlinear systems from discrete noisy measurements," *Automatic Control, IEEE Transactions on*, vol. 13, no. 5, pp. 504–514, 1968.

[65] E. A. Wan and R. Van Der Merwe, "The unscented Kalman filter for nonlinear estimation," in *IEEE Adaptive Systems for Signal Processing, Communications, and Control Symposium*, 2000, pp. 153–158.

[66] S. J. Julier and J. K. Uhlmann, "New extension of the Kalman filter to nonlinear systems," in *AeroSense'97*. International Society for Optics and Photonics, 1997, pp. 182–193.

[67] G. Evensen, "Sequential data assimilation with a nonlinear quasi-geostrophic model using Monte Carlo methods to forecast error statistics," *Journal of Geophysical Research: Oceans*, vol. 99, no. C5, pp. 10 143–10 162, 1994.

[68] G. Burgers, P. Jan van Leeuwen, and G. Evensen, "Analysis scheme in the ensemble Kalman filter," *Monthly Weather Review*, vol. 126, no. 6, pp. 1719–1724, 1998.

[69] G. Evensen, "The ensemble Kalman filter: Theoretical formulation and practical implementation," *Ocean Dynamics*, vol. 53, no. 4, pp. 343–367, 2003.

[70] H. W. Sorenson and D. L. Alspach, "Recursive Bayesian estimation using Gaussian sums," *Automatica*, vol. 7, no. 4, pp. 465–479, 1971.

[71] D. Alspach and H. Sorenson, "Nonlinear Bayesian estimation using Gaussian sum approximations," *Automatic Control, IEEE Transactions on*, vol. 17, no. 4, pp. 439–448, 1972.

[72] Z. Chen, "Bayesian filtering: From Kalman filters to particle filters, and beyond," *Statistics*, vol. 182, no. 1, pp. 1–69, 2003.

[73] N. J. Gordon, D. J. Salmond, and A. F. Smith, "Novel approach to nonlinear/non-Gaussian Bayesian state estimation," in *IEE Proceedings F - Radar and Signal Processing*, vol. 140. IET, 1993, pp. 107–113.

[74] B. Widrow, M. E. Hoff, and others, "Adaptive switching circuits," in *IRE WESCON Convention Record*, vol. 4. New York, 1960, pp. 96–104.

[75] B. Widrow, "Adaptive filters," *Aspects of Network and System Theory*, pp. 563–587, 1971.

[76] L. Griffiths, "A continuously-adaptive filter implemented as a lattice structure," in *Acoustics, Speech, and Signal Processing, IEEE International Conference On*, vol. 2. IEEE, 1977, pp. 683–686.

[77] ——, "An adaptive lattice structure for noise-cancelling applications," in *Acoustics, Speech, and Signal Processing, IEEE International Conference On*, vol. 3. IEEE, 1978, pp. 87–90.

[78] R. L. Plackett, "Some theorems in least squares," *Biometrika*, vol. 37, no. 1/2, pp. 149–157, 1950.

[79] D. Godard, "Channel equalization using a Kalman filter for fast data transmission," *IBM journal of Research and Development*, vol. 18, no. 3, pp. 267–273, 1974.

[80] M. Morf, "Fast algorithms for multivariable systems." Ph.D. dissertation, Stanford University, 1974.

[81] W. M. Gentleman and H. Kung, "Matrix triangularization by systolic arrays," in *25th Annual Technical Symposium*. International Society for Optics and Photonics, 1982, pp. 19–26.

[82] A. H. Sayed and T. Kailath, "A state-space approach to adaptive RLS filtering," *IEEE Signal Processing Magazine*, vol. 11, no. 3, pp. 18–60, 1994.

[83] J. Toyoda, M.-s. Chen, and Y. Inoue, "An application of state estimation to short-term load forecasting, Part II: Implementation," *Power Apparatus and Systems, IEEE Transactions on*, no. 7, pp. 1683–1688, 1970.

[84] H. Sorenson, "Kalman filtering techniques," *Advances in Control Systems Theory and Applications*, vol. 3, pp. 219–292, 1966.

[85] S. F. Schmidt, "Applications of state space methods to navigation problems," in *Advances in Control Systems*, 1966, vol. 3, pp. 293–340.

[86] F. D. Galiana, "An application of system identification and state prediction to electric load modelling and forecasting." Ph.D. dissertation, Massachusetts Institute of Technology, 1971.

[87] M. Sidar and B. F. Doolin, "On the feasibility of real-time prediction of aircraft carrier motion at sea," Tech. Rep., 1975.

[88] J. C. Chung, Z. Bien, and Y. S. Kim, "A note on ship-motion prediction based on wave-excitation input estimation," *IEEE Journal of Oceanic Engineering*, vol. 15, no. 3, pp. 244–250, 1990.

[89] P. G. J. ten Brummelhuis, B. d. Jong, and A. W. Heemink, "Stochastic dynamic approach to predict water levels in estuaries," *Journal of Hydraulic Engineering*, vol. 114, no. 11, pp. 1339–1358, 1988.

[90] M. Z. Chen, D. H. Zhou, and G. P. Liu, "A new particle predictor for fault prediction of nonlinear time-varying systems," *Developments in Chemical Engineering and Mineral Processing*, vol. 13, no. 3-4, pp. 379–388, 2005.

[91] H. Moradkhani, S. Sorooshian, H. V. Gupta, and P. R. Houser, "Dual state–parameter estimation of hydrological models using ensemble Kalman filter," *Advances in Water Resources*, vol. 28, no. 2, pp. 135–147, 2005.

[92] M. Mastali, J. Vazquez-Arenas, R. Fraser, M. Fowler, S. Afshar, and M. Stevens, "Battery state of the charge estimation using Kalman filtering," *Journal of Power Sources*, vol. 239, pp. 294–307, 2013.

[93] H. Sriyananda and D. R. Towill, "Prediction of human operator performance," *Reliability, IEEE Transactions on*, vol. R-22, no. 3, pp. 148–156, 1973.

[94] R. A. Heath, "Detection of change in physiological measures using an adaptive Kalman filter algorithm," *Psychological Bulletin*, vol. 96, no. 3, pp. 581–588, 1984.

[95] K. Mizumura and C.-L. Chiu, "Prediction of combined snowmelt and rainfall runoff," *Journal of Hydraulic Engineering*, vol. 111, no. 2, pp. 179–193, 1985.

[96] L. M. Hawthorne, "800 MHz mobile radio propagation prediction using Kalman filtering techniques," *Vehicular Technology, IEEE Transactions on*, vol. 38, no. 2, pp. 55–68, 1989.

[97] H. Melgaard, E. Hendricks, and H. Madsen, "Continuous identification of a four-stroke SI engine," in *American Control Conference, 1990.* IEEE, 1990, pp. 1876–1881.

[98] I. Nimmo, "Adequately address abnormal operations," *Chemical Engineering Progress*, vol. 91, no. 9, 1995.

[99] L. Wang, *Model Predictive Control System Design and Implementation Using MATLAB®*. Springer Science & Business Media, 2009.

[100] K. Roy, R. Banavar, and S. Thangasamy, "Application of fault detection and identification (FDI) techniques in power regulating systems of nuclear reactors," *Nuclear Science, IEEE Transactions on*, vol. 45, no. 6, pp. 3184–3201, 1998.

[101] J. B. Rawlings and D. Q. Mayne, *Model Predictive Control: Theory and Design*. Nob Hill Publishing, LLC, 2009.

[102] M. Basseville and I. V. Nikiforov, *Detection of Abrupt Changes: Theory and Application*. Prentice Hall Englewood Cliffs, 1993.

[103] M. Darouach and M. Zasadzinski, "Unbiased minimum variance estimation for systems with unknown exogenous inputs," *Automatica*, vol. 33, no. 4, pp. 717–719, 1997.

[104] H. Lütkepohl, *New Introduction to Multiple Time Series Analysis*. Springer Science & Business Media, 2005.

[105] E. Zamanizadeh, K. Salahshoor, and Y. Manjili, "Prediction of abnormal situation in nonlinear systems using ekf," in *Networking, Sensing and Control, IEEE International Conference On*. IEEE, 2008, pp. 681–686.

[106] J. C. Lagarias and F. Aminzadeh, "Multi-Stage Planning and the Extended Linear-Quadratic-Gaussian Control Problem," *Mathematics of Operations Research*, vol. 8, no. 1, pp. 42–63, 1983.

[107] S. K. Yang and T. S. Liu, "State estimation for predictive maintenance using Kalman filter," *Reliability Engineering and System Safety*, vol. 66, no. 1, pp. 29–39, 1999.

[108] P. Nomikos and J. F. MacGregor, "Monitoring batch processes using multiway principal component analysis," *AIChE Journal*, vol. 40, no. 8, pp. 1361–1375, 1994.

[109] G. Chen and T. J. McAvoy, "Predictive on-line monitoring of continuous processes," *Journal of Process Control*, vol. 8, no. 5, pp. 409–420, 1998.

[110] S. Butler, "Prognostic algorithms for condition monitoring and remaining useful life estimation," Ph.D. dissertation, National University of Ireland, Maynooth, 2012, .

[111] G. Vachtsevanos, F. Lewis, M. Roemer, A. Hess, and B. Wu, *Intelligent Fault Diagnosis and Prognosis for Engineering Systems*. John Wiley & Sons, Inc, 2006, vol. 13, .

[112] J. J. Sammarco, "Programmable electronic and hardwired emergency shutdown systems: A quantified safety analysis," *Industry Applications, IEEE Transactions on*, vol. 43, no. 4, pp. 1061–1068, 2007.

[113] "Best estimate safety analysis for nuclear power plants: Uncertainty evaluation," IAEA, Tech. Rep., 2008.

[114] "Safety Instrumented Functions (SIF), Safety Integrity Level (SIL), Evaluation techniques: Part 1 - introduction," ISA, Tech. Rep. ISA-TR84.00.02-2002, Jun. 2002.

[115] I. E. Commission, "IEC 61508: Functional safety of electrical/electronic/programmable electronic safety-related systems," Tech. Rep., 1999.

[116] ——, "IEC 61511: Functional safety - safety instrumented systems for the process industry," Tech. Rep., 2003.

[117] ——, "IEC 61513: Nuclear power plants - instrumentation and control for systems important to safety - general requirements for systems," 2001.

[118] ——, "IEC 62138: Nuclear power plants - instrumentation and control important for safety - software aspects for computer-based systems performing category B or C functions," 2004.

[119] ——, "IECE61131-3: Programmable controllers - part 3: Programming languages," 2003.

[120] "Safety margins of operating reactors - analysis of uncertainties and implications for decision making," IAEA, TECDOC 1332, 2003.

[121] "Instrumentation and control systems important to safety in nuclear power plants." IAEA, Safety Guide NS-G-1.3, Mar. 2002.

[122] W. Garland, *The Essential CANDU, A Textbook on the CANDU Nuclear Power Plant Technology.* University Network of Excellence in Nuclear Engineering (UNENE), 2017.

[123] C. N. S. Commission and others, "Trip parameter acceptance criteria for the safety analysis of CANDU nuclear power plants. Draft regulatory guide G-144," 2005.

[124] J. F. Miller and R. McDowell, "Significance of analog instrumentation-design philosophy of replacement dump arrest unit at Pickering Station Candu reactor," *Nuclear Science, IEEE Transactions on*, vol. 44, no. 3, pp. 1081–1083, 1997.

[125] A. Ozkaynak, "The design of a solid state trip system for nuclear power plants," *Nuclear Science, IEEE Transactions on*, vol. 26, no. 2, pp. 2933–2938, 1979.

[126] R. Reid, W., "Peach Bottom atomic power station, unit no. 2 amendment to facility operating license no. 76," United States Nuclear Regulatory Commission, Washington, D.C. 20555, Tech. Rep. Docket no. 50-277, Dec. 1980.

[127] C. Steinhardt, "Proposed amend 110 for license DPR-43," United States Nuclear Regulatory Commission, Washington, D.C. 20555, Tech. Rep. Docket no. 50-305, Aug. 1992.

[128] N. Ichiyen and W. Fieguth, "Digital computers in CANDU safety systems part I history and concepts," *Nuclear Science, IEEE Transactions on*, vol. 30, no. 3, pp. 1908–1911, 1983.

[129] R. Gilbert and C. Komorowski, "The use of digital computers in CANDU shutdown systems," in *IAEA Specialist's Meeting*, 1986.

[130] G. N. Williams and R. G. Huget, "Independence and diversity in CANDU shutdown systems," in *IAEA Specialists' Meeting*, 1992.

[131] T. Shirakawa, T. Tochigi, K. Iwaki, and T. Yokomura, "Quality assurance and quality control program for digital safety protection systems in nuclear power plants," in *IAEA Specialists' Meeting*, 1992.

[132] A. Wassyng and M. Lawford, "Lessons learned from a successful implementation of formal methods in an industrial project," in *FME 2003: Formal Methods*. Springer, 2003, pp. 133–153.

[133] I. Varga, T. Bartha, G. Szabó, and B. Kiss, "Status and actual risk monitoring in a NPP reactor protection system," in *Probabilistic Safety Assessment and Management*. Springer, 2004, pp. 2654–2659.

[134] V. Kharchenko, "Experience of RPC (Radiy) in designing, manufacturing and implementation of FPGA-based NPP I&C systems," in *1st Workshop on the Applications of Field-Programmable Gate Arrays in Nuclear Power Plants*, 2008, pp. 8–10.

[135] J. She and J. Jiang, "On the speed of response of an FPGA-based shutdown system in CANDU nuclear power plants," *Nuclear Engineering and Design*, vol. 241, no. 6, pp. 2280–2287, 2011.

[136] ——, "Potential improvement of CANDU NPP safety margins by shortening the response time of shutdown systems using FPGA based implementation," *Nuclear Engineering and Design*, vol. 244, pp. 43–51, 2012.

[137] "The Chernobyl accident: Updating of INSAG-1 : INSAG-7 : A report," IAEA, Tech. Rep., 1992.

[138] "Event Reports For 02/21/96 - 02/22/96," U.S. Nuclear Regulatory Commission Operations Center, Fitzpatrick NPP, New York, Tech. Rep. 30007, 02/22/96.

[139] "Supplement 1: Failure of a General Electric Type AK-2-25 Reactor Trip Breaker," Nuclear Regulatory Commission, Information notice 85-58, 1985.

[140] J. de Maré, "Optimal prediction of catastrophes with applications to Gaussian processes," *The Annals of Probability*, vol. 8, no. 4, pp. 841–850, 1980.

[141] A. Svensson, J. Holst, R. Lindquist, and G. Lindgren, "Optimal prediction of catastrophes in autoregressive moving-average processes," *Journal of Time Series Analysis*, vol. 17, no. 5, pp. 511–531, 1996.

[142] J. D. Zechar and T. H. Jordan, "Testing alarm-based earthquake predictions," *Geophysical Journal International*, 2008.

[143] K. Julisch, "Mining alarm clusters to improve alarm handling efficiency," in *Proceedings 17th ACSAC Conference 2001*, 2001.

[144] J. Wang, F. Yang, and T. Chen, "An overview of industrial alarm systems: Main causes for alarm overloading, research status, and open problems," *Automation Science and Engineering, IEEE Transactions on*, vol. 13, no. 2, pp. 1045–1061, 2016.

[145] W. S. Levine, *The Control Handbook*. CRC press, 1996.

[146] A. Papoulis, *Probability, Random Variables, and Stochastic Processes*, 3rd ed. McGraw Hill, Inc., 1991.

[147] I. Reid, "Course notes: Estimation II," Faculty of Engineering Science, University of Oxford, 2001.

[148] Y. Bar-Shalom, X. R. Li, and T. Kirubarajan, *Estimation with Applications to Tracking and Navigation: Theory Algorithms and Software*. John Wiley & Sons, 2004.

[149] B. Anderson and J. B. Moore, "Detectability and stabilizability of time-varying discrete-time linear systems," *SIAM Journal on Control and Optimization*, vol. 19, no. 1, pp. 20–32, 1981.

[150] N. J. Higham, *Functions of Matrices: Theory and Computation*. SIAM, 2008.

[151] B. Feng, M. Fu, H. Ma, Y. Xia, and B. Wang, "Kalman filter with recursive covariance estimation—sequentially estimating process noise covariance," *Industrial Electronics, IEEE Transactions on*, vol. 61, no. 11, pp. 6253–6263, 2014.

[152] D. G. Luenberger, "Observing the state of a linear system," *Military Electronics, IEEE Transactions on*, vol. 8, no. 2, pp. 74–80, 1964.

[153] H. Durrant-Whyte and others, "Introduction to estimation and the Kalman filter," Australian Centre for Field Robotics, 2001.

[154] J. Dimitratos, C. Georgakis, M. El-Aasser, and A. Klein, "Dynamic modeling and state estimation for an emulsion copolymerization reactor," *Computers & Chemical Engineering*, vol. 13, no. 1-2, pp. 21–33, 1989.

[155] B. J. Odelson, M. R. Rajamani, and J. B. Rawlings, "A new autocovariance least-squares method for estimating noise covariances," *Automatica*, vol. 42, no. 2, pp. 303–308, 2006.

[156] M. R. Rajamani and J. B. Rawlings, "Estimation of the disturbance structure from data using semidefinite programming and optimal weighting," *Automatica*, vol. 45, no. 1, pp. 142–148, 2009.

[157] K. Myers and B. Tapley, "Adaptive sequential estimation with unknown noise statistics," *Automatic Control, IEEE Transactions on*, vol. 21, no. 4, pp. 520–523, 1976.

[158] U. Baverstam, P. Davis, A. Garcia-Olivares, E. Henrich, and J. Koch, "Guidelines for uncertainty analysis," BIOMOVS II Technical Report No, Tech. Rep., 1993.

[159] R. Todling, *Estimation Theory and Foundations of Atmospheric Data Assimilation*, ser. Office Note Series on Global Modeling and Data Assimilation, Goddard Laboratory for Atmospheres, 1999.

[160] T. Fawcett, "An introduction to ROC analysis," *Pattern Recognition Letters*, vol. 27, no. 8, pp. 861–874, 2006.

[161] T. W. Anderson, *An Introduction to Multivariate Statistical Analysis*, 3rd ed. John Wiley & Sons, 2003.

[162] V. G. Snell, "Reactor Safety Design and Safety Analysis," in *The Essential CANDU, A Textbook on the CANDU Nuclear Power Plant Technology*, W. J. Garland, Ed. University Network of Excellence in Nuclear Engineering (UNENE), 2015, pp. 635–812.

[163] O. Glöckler, "Testing the dynamics of shutdown systems instrumentation in reactor trip measurements," *Progress in Nuclear Energy*, vol. 43, no. 1, pp. 91–96, 2003.

[164] E. Irving, C. Miossec, and J. Tassart, "Toward efficient full automatic operation of the PWR steam generator with water level adaptive control," in *2nd International Conference on Boiler Dynamics and Control in Nuclear Power Stations*, 1980, pp. 309–329.

[165] M. Akkawi and J. Jiang, "An inverse control-based set-point function for steam generator level control in nuclear power plants," *Nuclear Science, IEEE Transactions on*, vol. 58, no. 6, pp. 3291–3304, 2011.

[166] D. J. Rankin and J. Jiang, "Analytically compensated SGLC test facility," in *Proceedings of the 9th International Topical Meeting on Nuclear Power Plant Instrumentation, Control and Human-Machine Interface Technologies*. American Nuclear Society (ANS), 2015.

[167] M.-K. Kim, M. H. Shin, and M. J. Chung, "A gain-scheduled L2 control to nuclear steam generator water level," *Annals of Nuclear Energy*, vol. 26, no. 10, pp. 905–916, 1999.

[168] Q. Li and J. Jiang, "Evaluation of Foundation Fieldbus H1 networks for steam generator level control," *Control Systems Technology, IEEE Transactions on*, vol. 19, no. 5, pp. 1047–1058, 2011.

[169] D. J. Rankin and J. Jiang, "Predictive trip detection for nuclear power plants," *Nuclear Science, IEEE Transactions on*, vol. 63, no. 4, pp. 2352–2362, 2016.

Appendices

Appendix A: Copyright permissions

RightsLink®

Title:	Predictive Trip Detection for Nuclear Power Plants
Author:	Drew J. Rankin
Publication:	Nuclear Science, IEEE Transactions on
Publisher:	IEEE
Date:	Aug. 2016

Copyright © 2016, IEEE

Thesis / Dissertation Reuse

The IEEE does not require individuals working on a thesis to obtain a formal reuse license, however, you may print out this statement to be used as a permission grant:

Requirements to be followed when using any portion (e.g., figure, graph, table, or textual material) of an IEEE copyrighted paper in a thesis:

1) In the case of textual material (e.g., using short quotes or referring to the work within these papers) users must give full credit to the original source (author, paper, publication) followed by the IEEE copyright line © 2011 IEEE.
2) In the case of illustrations or tabular material, we require that the copyright line © [Year of original publication] IEEE appear prominently with each reprinted figure and/or table.
3) If a substantial portion of the original paper is to be used, and if you are not the senior author, also obtain the senior author's approval.

Requirements to be followed when using an entire IEEE copyrighted paper in a thesis:

1) The following IEEE copyright/ credit notice should be placed prominently in the references: © [year of original publication] IEEE. Reprinted, with permission, from [author names, paper title, IEEE publication title, and month/year of publication]
2) Only the accepted version of an IEEE copyrighted paper can be used when posting the paper or your thesis on-line.
3) In placing the thesis on the author's university website, please display the following message in a prominent place on the website: In reference to IEEE copyrighted material which is used with permission in this thesis, the IEEE does not endorse any of [university/educational entity's name goes here]'s products or services. Internal or personal use of this material is permitted. If interested in reprinting/republishing IEEE copyrighted material for advertising or promotional purposes or for creating new collective works for resale or redistribution, please go to http://www.ieee.org/publications_standards/publications/rights/rights_link.html to learn how to obtain a License from RightsLink.

If applicable, University Microfilms and/or ProQuest Library, or the Archives of Canada may supply single copies of the dissertation.

Copyright © 2017 Copyright Clearance Center, Inc. All Rights Reserved. Privacy statement. Terms and Conditions.
Comments? We would like to hear from you. E-mail us at customercare@copyright.com

Curriculum Vitae

Name:	Drew James Rankin
Post-Secondary Education and Degrees:	Ph.D. Electrical and Computer Engineering University of Western Ontario, London, ON 2009 – 2017
	M.Eng.Sc. Electrical and Computer Engineering University of Western Ontario, London, ON 2006 – 2008
	B.App.Sc. Electrical and Computer Engineering with Co-operative Education (Co-op) Placements University of Windsor, Windsor, ON 2002 – 2006
Honours and Awards:	Natural Science and Engineering Research Council (NSERC) Postgraduate Scholarship Doctorate (PGS D) 2010 – 2013
	Ontario Graduate Scholarship in Science and Technology (OGSST) 2009 – 2010
Related Work Experience:	Research and Teaching Assistant The University of Western Ontario 2006 – 2017

Journal Publications:

[1] D. J. Rankin, and J. Jiang, "Optimal predictive trip detection for nuclear power plants." Manuscript, Pending, 2017.

[2] D. J. Rankin, and J. Jiang, "Predictive trip detection for nuclear power plants." Nuclear Science, IEEE Transactions on, vol. 63, no. 4, pp. 2352-2362, 2016.

[3] D. J. Rankin, and J. Jiang, "A hardware-in-the-loop simulation platform for the verification and validation of safety control systems." Nuclear Science, IEEE Transactions on, vol. 58, no. 2, pp. 468-478, 2011.

[4] Q. Li, J. Jiang, and D. J. Rankin, "Evaluation of delays induced by Profibus PA networks." Instrumentation and Measurement, IEEE Transactions on, vol. 60, no. 8, pp. 2910-2917.
[5] Q. Li, D. J. Rankin, and J. Jiang, "Evaluation of delays induced by Foundation Fieldbus H1 networks." Instrumentation and Measurement, IEEE Transactions on, vol. 58, no. 10, pp. 3684-3692, 2009.

Conference Publications:

[1] D. J. Rankin, and J. Jiang, "Analytically compensated SGLC test facility." *9th International Topical Meeting on Nuclear Power Plant Instrumentation, Control, and Human-Machine Interface Technologies (NPIC & HMIT)*. Charlotte, North Carolina, USA. ANS, 2015.
[2] D. J. Rankin, and J. Jiang, "Kalman filter based predictive trip detection for nuclear power plant safety systems." *22nd International Conference on Nuclear Engineering (ICONE)*. Prague, Czech Republic. ASME, 2014.
[3] D. J. Rankin, K. P. van Hoof, and J. Jiang, "Analytically compensated physical model of a steam generator with non-minimum phase level response." *8th International Topical Meeting on Nuclear Power Plant Instrumentation, Control, and Human-Machine Interface Technologies (NPIC & HMIT)*. San Diego, California, USA. ANS, 2012.
[4] D. J. Rankin, and J. Jiang, "Effects of in-the-loop interface fidelity on the simulation of NPP processes." *7th International Topical Meeting on Nuclear Power Plant Instrumentation, Control, and Human-Machine Interface Technologies (NPIC & HMIT)*. Las Vegas, Nevada, USA. ANS, 2010.
[5] D. J. Rankin, J. She, and J. Jiang, "Evaluation of safety PLCs and FPGAs for shutdown systems in CANDU nuclear power plants." *International Symposium on Future Instrumentation and Control for Nuclear Power Plants (ISSNP/ISOFIC)*. Harbin, China. KNS, 2008.
[6] D. J. Rankin, and J. Jiang, "Hardware-in-the-loop simulation using Tricon v9 safety PLC." *16th International Conference on Nuclear Engineering (ICONE)*. Orlando, Florida, USA. ASME, 2008.
[7] D. J. Rankin, and J. Jiang, "Hardware-in-the-loop (HIL) nuclear power plant training simulation platform design and verification." *29th Annual Canadian Nuclear Society (CNS)*. Toronto, Ontario, Canada. CNS, 2007.
[8] D. J. Rankin, and J. Jiang, "Tricon and shutdown system one (SDS1)." *28th Annual Canadian Nuclear Society (CNS)*. Saint John, New Brunswick, Canada. CNS, 2007.